



**Universitat Autònoma
de Barcelona**

TESI DOCTORAL

**Expanding the scope of the
Ribonuclease A superfamily in the
host immune defense system:**

**Structural determinants of human RNases involved
in antimicrobial host defense.**

DAVID PULIDO GÓMEZ

MAIG 2013



**Universitat Autònoma
de Barcelona**

**DEPARTAMENT DE BIOQUÍMICA I BIOLOGIA
MOLECULAR**

**Expanding the scope of the Ribonuclease A
superfamily in the
host immune defense system:**

**Structural determinants of human RNases involved
in antimicrobial host defense.**

Tesi presentada per **David Pulido Gómez** per optar al grau de Doctor en
Bioquímica i Biologia Molecular sota la direcció de la **Dra. Ester Boix
Borràs** i el **Dr. Marc Torrent Burgas**.

**Unitat de Biociències del Departament de Bioquímica i Biologia
Molecular. Universitat Autònoma de Barcelona.**

Dra. Ester Boix Borràs

Dr. Marc Torrent Burgas

David Pulido Gómez

Cerdanyola del Vallès, Maig 2013

List of papers included in the thesis.

This thesis is based on the following papers which will be referred to in the text by their roman numerals.¹

I. Torrent, M., Pulido, D., de la Torre, B. G., Garcia-Mayoral, M. F., Nogues, M. V., Bruix, M., Andreu, D., and Boix, E. Refining the eosinophil cationic protein antibacterial pharmacophore by rational structure minimization, *J Med Chem* 54, 5237-5244

II. Pulido, D., Moussaoui, M., Andreu, D., Nogues, M. V., Torrent, M., and Boix, E. Antimicrobial action and cell agglutination by the eosinophil cationic protein are modulated by the cell wall lipopolysaccharide structure, *Antimicrob Agents Chemother* 56, 2378-2385

III. Torrent, M., Pulido, D., Nogues, M. V., and Boix, E. Exploring new biological functions of amyloids: bacteria cell agglutination mediated by host protein aggregation, *PLoS Pathog* 8, e1003005

IV. Torrent M, Pulido D, Valle J, Nogués M.V., Andreu D, Boix E. Ribonucleases as a host-defense family: Evidence of evolutionary conserved antimicrobial activity at the N-terminus. *Biochemical Journal* (In revision)

V. Pulido D, Moussaoui, M., Nogués M.V., Torrent M and Boix E. Towards the rational design of antimicrobial proteins: single point mutations can switch on bactericidal and agglutinating activities on the RNase A superfamily lineage. *Biochemistry* (Submitted).

VI. Pulido D, Torrent M, Andreu D, Nogués M.V. and Boix E. Two human host defense RNases against mycobacteria: the eosinophil cationic protein and the skin derived antimicrobial protein 2. *Antimicrobial Agents and Chemotherapy* (In press).

¹ Papers I, II and III are included as fundamental papers, papers IV, V and VI are included as non-fundamental papers.

Contents

Abbreviations.....	iii
Resum	v
Summary.....	vii
1. Introduction.....	3
1.2. Diversity of structural properties of antimicrobial peptides.....	3
1.2.1. Short peptides.....	3
1.2.1.1. Amphipathic α -helical peptides.	4
1.2.1.2. Amphipathic β -sheet peptides.....	6
1.2.1.3. Peptides rich in specific amino acid residues.....	8
1.2.2. Antimicrobial proteins.....	8
1.3. Biophysical determinants for antimicrobial activity	9
1.3.1. Sequence and structure.	9
1.3.2. Charge.	9
1.3.3. Hydrophobicity.....	10
1.3.4. Amphipathicity.	10
1.3.5. Polar angle.....	10
1.4. Mechanisms of action of AMPs.....	11
1.5. Immunoregulation role of Antimicrobial peptides	13
1.6. Antimicrobial peptides in drug development	14
1.7. Antimicrobial RNases.	17
1.7.1. Eosinophil ribonucleases.....	20
1.7.1.1. Eosinophil derived neurotoxin (RNase 2).....	20
1.7.1.2. Eosinophil cationic protein (RNase 3).	21
1.7.2. Non-eosinophil ribonucleases.....	22
1.7.2.1. Angiogenin (RNase 5).	22
1.7.2.2. Skin derived RNase (RNase 7).	23
1.7.2.3. Placental RNase (RNase 8).	24
2. Aims of the thesis	27
3. General discussion and future perspectives.....	31
3.1. Lipopolysaccharide binding and antimicrobial activity.	31
3.2. Antimicrobial activity and protein aggregation	32

3.3. Design of protein derived antimicrobial peptides	33
3.4. Searching for conserved antimicrobial patterns.....	34
3.5. RNases as a scaffold to design antimicrobial proteins.....	35
3.6. Testing antimicrobial RNases against mycobacteria.....	36
4. Conclusions	41
5. References	45
6. Acknowledgements.....	59
CHAPTER I	61
CHAPTER II	75
CHAPTER III	85
CHAPTER IV	102
CHAPTER V	135
CHAPTER VI	161

Abbreviations

Å Ångström

ANG Human angiogenin

APC Antigen presenting cell

APD Antimicrobial peptide database

AMPs Antimicrobial peptides

BPI Bactericidal permeability -increasing protein

Da Dalton

DCs Dendritic cells

ECP Eosinophil cationic protein

EDN Eosinophil derived neurotoxin

EGFR Epithelial growth factor

HBDS Human β -defensins

LPS Lipopolysaccharide

LTA Lipoteichoic acids

LUV Large unilamellar vesicles

MBP Major basic protein

MGD-1 *Mytilus galloprovincialis* defensin-1

MIC Minimum inhibitory concentration

MW Molecular weight

NMR Nuclear magnetic resonance

PAMPs Pathogen associated molecular patterns

PGLa Peptide-glycine-leucine amide

PGN Peptidoglycan

PGRPs Peptidoglycan recognition proteins

pI Isoelectric point

RNA Ribonucleic acid

RNase Ribonuclease

RK-1 Rabbit kidney α -defensin-1

RSV Respiratory syncytial virus

SAR Structure-activity relationships

SEM Scanning electron microscopy

TA Teichoic acid

TEM Transmission electron microscopy

TIRF Total internal reflection microscopy

TLR Toll -like receptor

Resum

El meu projecte de doctorat s'enmarca en l'estudi de l'estructura i la funció de les ribonucleases antimicrobianes humanes. Actualment, es coneixen vuit ribonucleases humanes funcionals pertanyents a la superfamília de ribonucleases secretades per vertebrats. Cal remarcar, que alhora de la seva activitat per a hidrolitzar àcids ribonucleics, també presenten altres propietats biològiques com l'activitat antimicrobiana, que suggereixen una possible funció ancestral relacionada amb el sistema immunitari.

La proteïna catiònica d'eosinòfils (ECP) és un dels components majoritaris dels grànuls secundaris dels eosinòfils. Degut al seu gran nombre d'arginines l'ECP és una proteïna molt catiònica i presenta una elevada activitat antimicrobiana vers una gran diversitat de patògens, com bacteris, helmints i protozous.

En el nostre laboratori hem estudiat extensament el mecanisme antimicrobià de diverses ribonucleases. Concretament, el treball desenvolupat en aquesta tesi ha permès:

- i. Identificar el farmacòfor de l'ECP mitjançant eines de minimització racional de l'estructura.
- ii. Analitzar els canvis que es produeixen a la superfície bacteriana com a conseqüència de l'acció de l'ECP i dels seus pèptids derivats. Principalment, en detallar com aquests interaccionen amb els lipopolisacàrids de la paret bacteriana.
- iii. Descobrir que l'agregació amiloid de l'ECP a la superfície de les bactèries és fonamental per a la seva acció antimicrobiana i, en concret, per la seva activitat d'aglutinació.
- iv. Identificar factors estructurals i de seqüència en el domini N-terminal necessaris per l'acció antimicrobiana de les ribonucleases conservats durant l'evolució.
- v. Caracteritzar els elements seqüencials de les ribonucleases que determinen les propietats antimicrobianes i d'aglutinació mitjançant el disseny de proteïnes híbrides entre les ribonucleases 2 i 3 (EDN i ECP respectivament).
- vi. Descobrir que tant l'ECP com la ribonucleasa 7 presenten activitat vers micobacteris a través d'un mecanisme similar a l'exhibit enfront de bacteris gram negatius.

En conclusió, els resultats obtinguts en aquesta tesi ens permeten conèixer millor com les ribonucleases contribueixen a l'eliminació de diferents patògens del nostre organisme i ens obren noves vies pel disseny de nous agents terapèutics per combatre microorganismes patògens.

Summary

My PhD project focuses on the structure-function analysis of human antimicrobial RNases, Currently eight functional members have been ascribed to the vertebrate secreted RNase superfamily. Together with their catalytic activity towards RNA substrates, other biological properties have been reported such as the antimicrobial activity of diverse members of the family, therefore suggesting that RNases could have an ancestral host-defence function.

The eosinophil cationic protein (ECP) is one of the major components of the secondary granules of human eosinophils. ECP is a highly cationic arginine-rich protein, which displays a high antimicrobial activity against pathogens, such as bacteria, helminths and protozoa.

In our laboratory the antimicrobial mechanism of action of several RNases has been extensively studied. In particular, this work enables us to determine:

- i. Identify the protein pharmacophore by rational structure minimization.
- ii. Explore the effects that take place at the bacterial cell wall upon protein-interaction. Concretely, highlight the crucial role of the lipopolysaccharide molecule in the mechanism of action of ECP, and their N-terminal peptides.
- iii. Determine that the amyloid formation at the bacterial surface is crucial for the antimicrobial activity of the protein, and in particular, due to the agglutinating activity.
- iv. Prove that the sequence and structural determinants of RNases are evolutionary conserved at the N-terminal domain.
- v. Characterize the sequence and structural determinants required for antimicrobial and agglutinating activities Through RNase rational mutagenesis of the homologous RNases 2 and 3 (EDN and ECP respectively)
- vi. Discover that either ECP or RNase 7 present antimycobacterial activity trough a similar mechanism as proved against Gram-negative bacteria.

In conclusion, the results presented in this thesis work enable us to better understanding of how RNases contribute on the host pathogen clearance and open a new window in order to the design and develop new therapeutic agents as alternative antibiotics.

INTRODUCTION

1. Introduction

Within the last twenty years more than 1200 antimicrobial peptides (AMPs) have been identified or predicted from a wide variety of organisms (1-3). Most of them can be compiled in the Antimicrobial Peptide Database (APD: <http://aps.unmc.edu/AP/main.php>). Generally, AMPs contain around 30 amino acids and display a wide spectrum of activity. Although they lack specific amino acid consensus sequences, most of them share certain common features, such as a high content on charged and hydrophobic residues, moderate amphipathicity and discrete conformational structures (4, 5). Likewise, larger polypeptides and proteins can also display antimicrobial activity (6). In fact, some proteins are sources of natural peptides, which are produced by proteolytic cleavage (7).

1.2. Diversity of structural properties of antimicrobial peptides

1.2.1. Short peptides

Structural classification of AMPs is still a controversial topic. AMPs are traditionally classified into four structural classes: linear α -helical peptides, cyclic β -sheet peptides, β -hairpin or looped peptides and peptides with extended structures (8). Another classification was later suggested on the basis of their amino acid composition and structure dividing the known AMPs into five sub-categories: anionic peptides, linear cationic α -helical peptides, linear peptides enriched in specific amino acids, charged peptide fragments and peptides with cysteines that form intramolecular bonding (9). However, in the present work we will use a third classification based on structure-function relationships found using Nuclear Magnetic Resonance (NMR). This classification is the most thoroughly accepted and cited by recent works. AMPs are presented into three structural groups: amphipathic α -helical peptides, amphipathic β -sheet peptides and extended peptides (Figure 1) (10, 11). In addition to this classification we should take into account other not so well known structural groups as cyclic peptides, globular peptides or other structures from engineered peptides.



Figure 1. *Examples of the three basic types of AMPs.* From left to right: The α -helical human cathelicidin LL-37 (PDB ID: 2K6O); the human β -defensin hBD-2, stabilized by three intramolecular disulfide bonds indicated in yellow (PDB ID: 1E4Q); the tryptophan-rich bovine indolicidin (PDB ID: 1G89). Taken from (11).

1.2.1.1. Amphipathic α -helical peptides.

This is the largest group of AMPs with more than 300 different peptides. These peptides in general consist in linear cationic α -helical peptide of 12 to 37 residues length. Amphipathic α -helical peptides have been isolated so far from phylogenetically distant organisms such as fungi, nematodes, insects, teleost fish, frogs and mammals (5). The most studied representatives of this group are cecropins, melittins, magainins and cathelicidins.

Cecropin was the first α -helical AMP isolated from insects. At the beginning of 80's cecropins A, B and C were isolated from the hemolymph of bacterial-challenged diapausing pupae of the giant silk moth *Hyalophora cecropia* (12). In this study, Hans Boman and coworkers set the basis of a field that nowadays comprises thousands of peptides, including more than 60 cecropin-like molecules (13). A mammalian homolog, cecropin P1, was also been found in the small intestine of guinea pig (14). Cecropin homologues consist of 29 -42 amino acid in length and present two distinctive common features; the presence of a tryptophan residue in position 1 or 2, and an amidated residue at the C-terminus. In membrane mimicking environments Cecropin A adopts an amphipathic α -helical structure with its N-terminal region connected by a flexible hinge region to the more hydrophobic C-terminal helix (15-17).

Melittin is another well-known AMP isolated from the venom gland of the European hornet (*Vespa crabro*). Melittins are peptides of 26 residues that exhibit a high antimicrobial activity and, like cecropins, adopt a structure based on two amphipathic helices linked by a hinge upon incubation with model membranes. Those results are well discussed in several works with different model membranes (18-26).

An enormous number of α -helical AMPs have been isolated from glands of the skin and mucosa of the stomach of several anurans; such as magainins, peptide-glycine-leucine amide (PGLa), bombinins, dermaseptins, adenoregulin, phylloxin and temporins (27-35). Magainins, isolated from the skin glands of *Xenopus laevis* are unambiguously the prototype of the amphibian α -helical peptides (27). Magainins are peptides of 23 residues that display a broad-spectrum antibacterial, antifungal, tumoricidal and immunogenic activities. Although unstructured in water, contact with the negatively charged membranes by positively charged amino acids in the primary structure favors the formation of an amphipathic structure, allowing the insertion of hydrophobic residues into the membrane leading to the formation of an α -helix secondary structure (36-39).

The cathelicidin family represents one of the most abundant AMP groups in mammals and most mammals store several members of this diverse family in neutrophils. The cathelicidins consist in a large and heterogeneous family of AMPs that are derived from propeptides of more than 100 members with a well-conserved N-terminal (the cathelicidin segment) of approximately 100 amino acids. After enzymatic cleavage, the C-terminal domain, which embodies the antimicrobial properties, is released (40-44).

Some examples are shown in Figure 2.


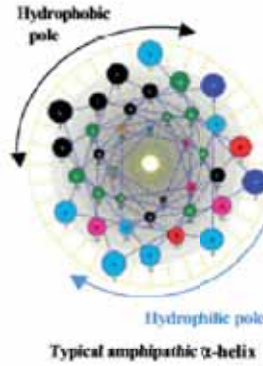

	Origin	Organism	Name	Activity	Primary structure	3D structure
Invertebrates		Silk moth <i>Hyalophora cecropia</i>	Cecropin A	B	KWLFKKIEKVGQNIIRDGIIKAGPAVAVVGGQATQIAK*	 <p>Stomoxyn</p>  <p>Hydrophobic pole</p> <p>Hydrophilic pole</p> <p>Typical amphipathic α-helix</p>  <p>Magainin</p>
		Mosquito <i>Anopheles gambiae</i>	Cecropin A	B, F, Y	GRLLKLGKKIEGAGKRVFKAALKALPVVAGVKAL*	
		Stable fly <i>Stomoxys calcitrans</i>	Stomoxyn	B, F, Y, T	RGFRKHFNKLVKKVKHTIGETAHVAKD TAVIAGSGAAVV AAT*	
	Arthropods	Fire ant <i>Pachycondylas goeldii</i>	Ponericin G1	B, H, I	GWKDKAYKAGQNLKKKGGPMKAKAALKAAMQ	
		Termite <i>Pseudacanthotermes spiniger</i>	Spinigerin	B, F, Y	HVDKKVADKVL LLLKQLRIMLLRL	
		Spider <i>Oxyopes kitabensis</i>	Oxyopinin 1	B, H, I	FRGLAKLLKIGLKS FARVLEKVLPEAAKAGKALA KSMADENAIK(QNQ)	
		Spider <i>Cupiennius salet</i>	Cupiennin 1	B, H, I	QFGALFKFLAKKVAKTVAQAAKQGAQYVYVVKQME*	
Procordates	Ascidian <i>Styela clava</i>	Clavanin A	B	VPQFLQKIIHHVGNFVHGPFHVFP*		
		Styelin D	B, H, C	QW ² LR ² K ² AAK ² GVQK ² PY ² Y ² K ² HK ⁴ Y ² Y ² IK ⁴ AAWQIGKHAL*		
Vertebrates		Sole <i>Pardachirus pavoninus</i>	Pardaxin P-I	B	QFPALIPKIISSPLFKTL LLSAVGSA LSSSSGQEQE	
		Mudfish <i>Misgurnus anguillicaudatus</i>	Misgurin	B, F, Y	RQRVEELSKFSKKGAAARRRK	
	Fishes	Flounder <i>Pleuronectes americanus</i>	Pleurocidin	B	GWGSFFKKAHVGGKRVGKAALHYL	
		Catfish <i>Parasilurus asotus</i>	Parasin I	B, Y	KGRQKQCKVRAKAKTRGG	
		Rainbow trout <i>Oncorhynchus mykiss</i>	Oncorhynchin II	B	KAVAAKKSPPKAKKPKATPKAAKSPKVKYDAAAA EKAAKSPKKATKAAKPKAAKPKAAKAKKAAAPKKK	
		White bass <i>Morone chrysops</i>	Moronecidin	B, F, Y	FFHHIFRGIVHVGKTIHKLVTG	
	Amphibians	Clawed frog <i>Xenopus laevis</i>	Magainin I	B, F	GIGKFLHSAGKFGKAFVGEIMKS	
		Common frog <i>Rana temporaria</i>	Temporin A	B, F, H	FLPLIGRVLGGIL*	
Mammals	Human <i>Homo sapiens</i>	Cathelicidin hCAT-18/LL-37	B, L	LLGDFFRKSKKIGKFKRIVQRIKDFLRNLVPRTES		
	Bovine <i>Bos taurus</i>	Indolicidin	B	ILPWKWFWDWRR*		

Figure 2. General features of some α -helical antimicrobial peptides from invertebrates and vertebrates. The activities recorded for the selected molecules are marked: B, anti-bacterial; C, cytotoxic; F, anti-fungal; H, haemolytic; I, insecticide; L, lectin-like lipopolysaccharide binding; T, trypanolytic activity; and Y, lytic effect on yeast cells. Taken from (13).

1.2.1.2. Amphipathic β -sheet peptides.

Peptides belonging to this group present an amphipathic β -sheet structure. These structures are generally stabilized by disulfide bonds, though some of them present also short α -helical segments. Depending on the number of cysteines (generally from 2 to 8) and their pairing pattern, they adopt a β -sheet amphipathic conformation with triple strands, such as defensins (45-47), a β -hairpin-like structure, like tachypleins (48, 49) and protegrin (50) or a mixed β -sheet conformation with few α -helices, as observed in plant defensins (47). Some examples are shown in Figure 3. Other β -sheet cysteine-containing peptides can also display an additional constrain by cyclization as polymyxin B (51) or arecidins (52); some examples are shown in Figure 4. In addition, within this group we found peptides with β -hairpin or looped configuration including those which contain constrained structures by single disulfide bond on the peptides chain, as in the case of thanatin (53).





	Origin	Organism	Name	Primary structure	3D structure
Invertebrates	Arthropods	Three disulfide bridges		C1 C2 C3 C4 C5 C6	 Phormia defensin-A
		Fly <i>Phormia terranovae</i>	Defensin-A	ATCDLLSGTGINHSACAARHCLLRGNRGGYCNKGVCVCRN	
		Fly <i>Glossina morsitans</i>	Defensin	VTCHIGEWVCAHCHNSKSKKSGYCSRGVVYCTH	
		Fly <i>Stomoxys calcitrans</i>	Defensin Smd1	AAKPMGITCDLLSLRWVGHAAACAHCVLVGDVGGYCTKEGLCVCKE	
		Dragonfly <i>Aeschna cyanea</i>	Defensin	GFGCPLDQMQCHRHQCQTITGRSGGYCSGPLKLTCTCYR	
		Bumblebee <i>Bombus pascuorum</i>	Defensin	VTCDLLSIKGVAEHSACAANCLSMGKAGGRCENGICLCRKTTFKELWDRKRP*	
		Tick <i>Ornithodoros moubata</i>	Defensin	GYGCFPNQYQCHSHCSGIRGYKGGYCKGTFRQTCKCY	
		Termite <i>Pseudacanthotermes spiniger</i>	Termicin	ACNFQSCWATCQAQHSIYFRFAFCDRSQCKCVFVRG*	
		Moth <i>Heliothis virescens</i>	Helioicin	DKLIGSCVWGAVNYTSDCNGECKRRGYKGGHCGSFANVNCWCET	
			Four disulfide bridges		
Fly <i>Drosophila melanogaster</i>	Drosomycin	DCLSGRYKGPCAWIDNETCFRVCCKEGRSSGHCSFSLKWCCEGC			
Molluscs	Mussel <i>Mytilus galloprovincialis</i>	MGD-1	GFGCPNNYQCHRIKCSIIPGRCGGYCGWRRLRCTCYRGG	 Mussel defensin-1	
Nematode	Fig roundworm <i>Ascaris suum</i>	ASABF	AVDFSSCARMVPEGLSKVAQGLCISSCKFQNCGTGHCEKRGGRPTCVCDRCGRGGGEMFVPMKGRSSRG	 Rabbit kidney α-defensin-1	
Vertebrates	Birds	Penguin <i>Aptenodytes patagonicus</i>	pBD-2, Sphe-2	SFGLCRLRRGFCARGRCRFFSIPIGRCSRFVQCCRRVW	 Human β-defensin-2
	Mammals	Cyclic defensins			
		Monkey <i>Macaca mulatta</i>	β -Defensin RTD-1	GFCRCLCRRGVCRICFR	
		Open-ended cyclic defensins			
		Rabbit <i>Oryctolagus cuniculus</i>	α -Defensin RK-1	MPCSCKKYCDPWEVIDGSCGLFNISKYICCREK	
Primate <i>Homo sapiens</i>	β -Defensin HBD-2	GIGDFVTCLESGAICHFVFCFRRYKQIGTCGLPGTKCKKPF			

Figure 3. Structural features of selected cyclic and open-ended cyclic peptides from invertebrates and vertebrates. The disulfide pairing is marked with black broken lines, while the head-to-tail bridging of the θ -defensin is marked with a red broken line. The ribbon drawings are (i) *Phormia* defensin-A, (ii) helioicin, (iii) *Mytilus galloprovincialis* defensin-1 (MGD-1), (iv) rabbit kidney α -defensin-1 (RK-1), and (v) human β -defensin-2 (HBD-2) and include the disulfide bridges. ASABF corresponds to *Ascaris suum* anti-bacterial factor and pBD-2/Sphe-2 to penguin β -defensin-2/spheniscin-2. Taken from (13).



	Origin	Organism	Name	Activity	Primary structure	3D structure
Invertebrates	Arthropods	Insect <i>Podisus maculiventris</i>	Thanatin	B, F, Y	GSKKPVPPIIYCNRRRTGK[CORM	 <p>Thanatin</p>
		Horseshoe crab <i>Tachyplesus tridentatus</i>	Tachyplesin-1	B, Y, V, H	KWCFRVCYRGICYRRCR*	
		Horseshoe crab <i>Limulus polyphemus</i>	Polyphemusin	B, Y	RRWCFRVCYRGFCYRKR*	
		Scorpion <i>Androctonus australis</i>	Androctonin	B, F	RSVCRQIKICRRRGGCCYYKCTNRPY	
		Spider <i>Acanthoscuria gomesiana</i>	Gomesin	B, F, Y, P, H	zCRRRLCYKQRCVITYCRGR*	
Vertebrates	Fishes	White bass <i>Morone chrysops x saxatilis</i>	Hepcidin	B, Irh	GCRFCNCCPNMSGCGVCCRF	 <p>Protegrin-1</p>
	Amphibians	Japanese frog <i>Rana brevipoda</i>	Brevinin-1	B, Y	FLPVLAGIAAKVVPALFCKIKTKC	
		Edible frog <i>Rana esculenta</i>	Esculentin-1	B, Y, H	GIFSKLGRKKIKNLLISGLKNVGRVGM	
		Indian bull frog <i>Rana tigerina</i>	Tigerinin-1	B, Y	DVVRTGIDIAGCKIKGEC	
	Mammals	Bovine <i>Bos taurus</i>	Bactenecin	B	RLCRIVVIRVCR	
	Porcine <i>Sus scrofa</i>	Protegrin-1	B, F, Y, V	RGGRLCYCRRRFCVCGR*		
	Mouse <i>Mus musculus</i>	Hepcidin	B, Irh	DTNFPICIFCCKCCNNSQCGICCKT		

Figure 4. Characteristics of selected β -hairpin-like anti-microbial peptides with one and two disulfide bridges from invertebrates and vertebrates. The disulfide pairing is marked with lines. The activities are: B, anti-bacterial; F, anti-fungal; H, haemolytic; Irh, iron-regulatory hormone; P, anti-parasitic; V, anti-viral; and Y, lytic effect on yeast cells. The gray boxes, delineated by the cysteine residues in the thanatin and brevinin-1 sequences correspond to the so-called insect box and *Rana* box, respectively. The ribbon drawing of thanatin from the insect *Podisus maculiventris* and of protegrin-1 from porcine leukocytes includes the disulfide bridges. Taken from (13).

The most studied family within this group are mammalian defensins, which are further classified into three subfamilies, namely α -, β - and θ -defensins. Both α - and β -defensins adopt a triple-stranded antiparallel β -sheet structure constrained by three sulfide bridges (45, 54). On the other hand, θ -defensins display a cyclized peptide backbone with a conserved pattern of three disulfide bridges (55).

1.2.1.3. Peptides rich in specific amino acid residues

This group is defined by linear antimicrobial peptides with an overrepresentation of specific residues that cannot be ascribed to any specific motif archetype. The tryptophan rich peptide indolicidin and the histidine-rich histatin belong to this group.

Indolicidin was the first antimicrobial peptide rich in tryptophan discovered and isolated from bovine neutrophils. It is a short peptide of 13 residues length that contains five tryptophans (56). As other AMPs it displays a broad-spectrum antimicrobial activity against bacteria, fungi and protozoa (57). The structure of indolicidin was solved by NMR in a negatively charged membrane model (58).

Histatins are a group of histidine-rich peptides with a length between 7 to 38 amino acids (59). They are constitutively synthesized by the parotid and the submandibular/sublingual salivary gland in humans and higher macaques (60). Histatins 1 and 3 are product of different genes while histatin 5 is generated by histatin 3 proteolytic cleavage (61). These peptides display a broad-spectrum of antimicrobial activity though they are also being studied for the treatment of fungal affections (62, 63).

1.2.2. Antimicrobial proteins

Besides classical short antimicrobial peptides, polypeptides and proteins also play a fundamental role in the host immune defence. In the present work we investigated the human antimicrobial RNases, which will be further analyzed in section 1.7. (Antimicrobial RNases). Two relevant examples of antimicrobial proteins are the peptidoglycan recognition proteins (PGRPs) and lactoferrin. The first was discovered in insects and constitute a family of variable sized proteins ranging from 20 to 120 KDa that specifically binds peptidoglycans, the main component of Gram-positive cell wall (64). Lactoferrin is a 80 KDa iron-binding glycoprotein mainly found in biological fluids of mammals, such as milk, saliva, tears and seminal fluid (65) but also found in the secondary granules of neutrophils. It is believed that lactoferrin is one of the first defence system of the organism against infection. Several studies suggest that lactoferrin could be the precursor of smaller antimicrobial peptides through acidic hydrolysis (66). In particular, both human and bovine lactoferrin are cationic

peptides of 50 amino acid length with one to two disulfide bonds that present an enhanced antimicrobial activity compared with its parental protein (66).

1.3. Biophysical determinants for antimicrobial activity

The discovery of shared features between AMPs is fundamental to understand how they exert their antimicrobial action. Calculation structure-activity relationships (SAR) are a powerful tool to characterize antimicrobial activity but also to assist classification of novel peptides. Several approaches have been used in order to highlight those determinants, as sequence modification methods, synthetic combinatorial libraries, template assisted methods, comparative analysis and systematic alteration of the peptide properties (9, 67).

1.3.1. Sequence and structure.

Despite AMPs tend to adopt similar secondary structure patterns upon interaction with the membrane they do not share consensus sequential motifs. Nonetheless, they present some common traits like amino acid composition. For example, glycine commonly appears to be conserved in position one protecting the peptide against aminopeptidases (68). Lysine and arginine are among the most common amino acids present in AMPs sequence that secure the interaction between positively charged AMPs with the negatively charged pathogen membranes. Finally, hydrophobic and aromatic residues (mainly leucine) are also required to anchor AMPs to the membrane (69).

It is well known that another fundamental feature common to AMPs is the acquisition of a definite three-dimensional structure upon interaction with pathogen membranes. In fact, the partition of the peptide chains into the membranes is usually accompanied by peptide secondary folding (70).

1.3.2. Charge.

Bacterial cytoplasmic membranes are rich in acidic phospholipids, such as phosphatidyl-glycerol and cardiolipin that confer an overall negative charge (71). In addition, other molecular counterparts are present on the bacterial cell envelopes. Lipopolysaccharides in Gram-negative bacteria and peptidoglycans and lipoteichoic acids in Gram-positive bacteria confer additional negative charges. On the envelopes of fungi other highly negatively charged molecules are present, such as phosphomannans, chitin and β -1,3-glucan. The electrostatic interaction between AMPs and the negatively charged pathogen surfaces seem to be crucial for their antimicrobial action. Most AMPs display a high number of lysines and arginines and contain none or few aspartic and glutamic residues, carrying a net charge from +2 to +11 (72). There is a direct correlation between peptide charge and potency though increasing the net charge beyond a threshold does not improve the

antimicrobial profile of AMPs, presumably due to an imbalance between charge and hydrophobicity (73).

1.3.3. Hydrophobicity.

Peptide hydrophobic content is defined as the fraction of hydrophobic residues within a peptide. Most AMPs display hydrophobic contents around 50%. Hydrophobicity is a crucial feature that modulates the antimicrobial efficiency and selectivity of AMPs, because it governs the partition degree of a peptide from water to the lipid bilayer. A fine balance between charge and hydrophobicity is required in AMPs. In this context, a substantial reduction of hydrophobicity is directly correlated with a low antimicrobial profile whereas a severe increase causes a loose in selectivity towards microbial membranes, inducing eukaryotic cytotoxicity (74).

1.3.4. Amphipathicity.

Amphipathicity is defined as the distribution of hydrophobic and hydrophilic residues within a peptide. A quantitative measure of amphipathicity is the hydrophobic moment, calculated as the vectorial sum of individual amino acid hydrophobicity vectors, normalized to an ideal helix (75). The archetypical conformation is the amphipathic α -helix with three to four residues per turn, which is optimal for interaction and folding upon membrane interaction. Amphipathicity is essential for antimicrobial activity, where the charged face drives the initial electrostatic interaction while the hydrophobic peptide face inserts into the membrane through Van der Waals interactions. However, an increase of the hydrophobic moment beyond a threshold causes not only the disruption of microbial membranes but also permeabilization of host cells, often referred as haemolytic values when erythrocytes are used as model host cells (76).

1.3.5. Polar angle.

Polar angle is defined as the relative proportion of polar and nonpolar faces within a peptide with α -helix conformation. A hypothetical peptide with solely hydrophobic residues in one face and hydrophilic residues on the other side will present a polar angle of 180° . Smaller polar angle leads to a better membrane permeabilization, translocation and pore formation. Also, polar angle is directly correlated with the overall stability of peptide-induced membrane pores (77). Therefore a correct balance between charge, hydrophobicity, amphipathicity and polar angle is required for optimum antimicrobial profiles.

1.4. Mechanisms of action of AMPs

The mechanism of action mainly relies on its action at the membrane level. Negatively charged microbial membranes drive the electrostatic interaction with the peptide where the correct span between charged and hydrophobic residues leads the peptide to adopt amphipathic structures with the charged side facing outward towards the phospholipid head groups and the hydrophobic side embedded into the acyl tail core. The insertion of AMPs into the membrane leads to the membrane disruption jeopardizing cell homeostasis. Many authors have explored the membranolytic activity of AMPs and several mechanisms of action have been proposed (78, 79).

One mechanism consists in the membrane permeabilization through the formation of pore structures that span the membrane. In the barrel-stave model, the pore formation is driven by the hydrophobic domains of the peptide interacting with the acyl chains, facing inwards towards the membrane core, whereas the charged face forms the pore lining. In this model peptide helices form a bundle perpendicular to the membrane plane with a central lumen, where the helical peptides are the staves of the barrel. Alamethicin is the most studied example of AMP which forms barrel-stave stable pores (80). The toroidal model differs from the barrel-stave model as the peptides may not be perpendicularly inserted in the lipid bilayer but always curving inwards the polar head groups of the membrane phospholipids by electrostatic interaction (81). In the disordered toroidal pore model lipid molecules are also curved inwards but by a more disordered process, where only one or two peptides are located at the center of the lumen pore and the others are located at the end of the pore at the external leaflet. That is the case of the AMP honey bee venom derived melittin (82) or the β -hairpin-like porcine protegrin I, which forms oligomeric transmembrane β -barrels in anionic membranes producing stable toroidal pores.

On the other hand, in the carpet model AMPs are electrostatically bound throughout the membrane covering the surface in carpet-like manner. After a critical threshold, the additional peptides that access to the membrane promote drastic changes in the membrane curvature, which is followed by the membrane disruption and micellation. Several AMPs, such as cecropins and magainins, exert their membranolytic action in a carpet-like manner (83). Other membrane perturbing effects are induced by α -helical AMPs, where lipid segregation occurs due to membrane thinning or thickening promoting a slow leakage of intracellular content or non-lytic membrane depolarization (84). Several AMPs, such as temporins B and L, target oxidized lipids. Therefore, the release of reactive oxygen species during the inflammation process could enhance the antimicrobial efficacy of some peptides (85). The extended peptide, Phe-, His- and Gly rich peptide clavanin A permeabilizes neutral

membranes as a regular α -helical peptide, but only in acidic conditions, by inhibitory interactions with proteins involved in maintaining the pH gradient across the membrane (86).

Although the permeabilization of the cell seems fundamental in order to kill microbes, not all the AMPs exert their antimicrobial function at the lipidic membrane level. Several AMPs can cross the microbe membranes and have intracellular targets. For example, pyrrolicorin when translocated intracellularly acts upon interaction with the heat shock protein DnaK and GroEL, drosomicin can inhibit DnaK and apidaecin inhibits the chaperon-assisted protein folding (83). The β -sheet AMP tachyplesin or the α -helical buforin, besides its membranolytic function can also bind to DNA, probably interfering with DNA-protein interactions (83, 87). The β -hairpin peptide lactoferricin can act by inhibitory activity of the ATP proton-motive force machinery uncoupling the ATP-dependent multidrug efflux pump (88). Finally, defensins that besides their membrane active permeabilization can bind to the peptidoglycan lipid II inhibiting the cell wall biosynthesis enzymes of *Staphylococcus* (89).

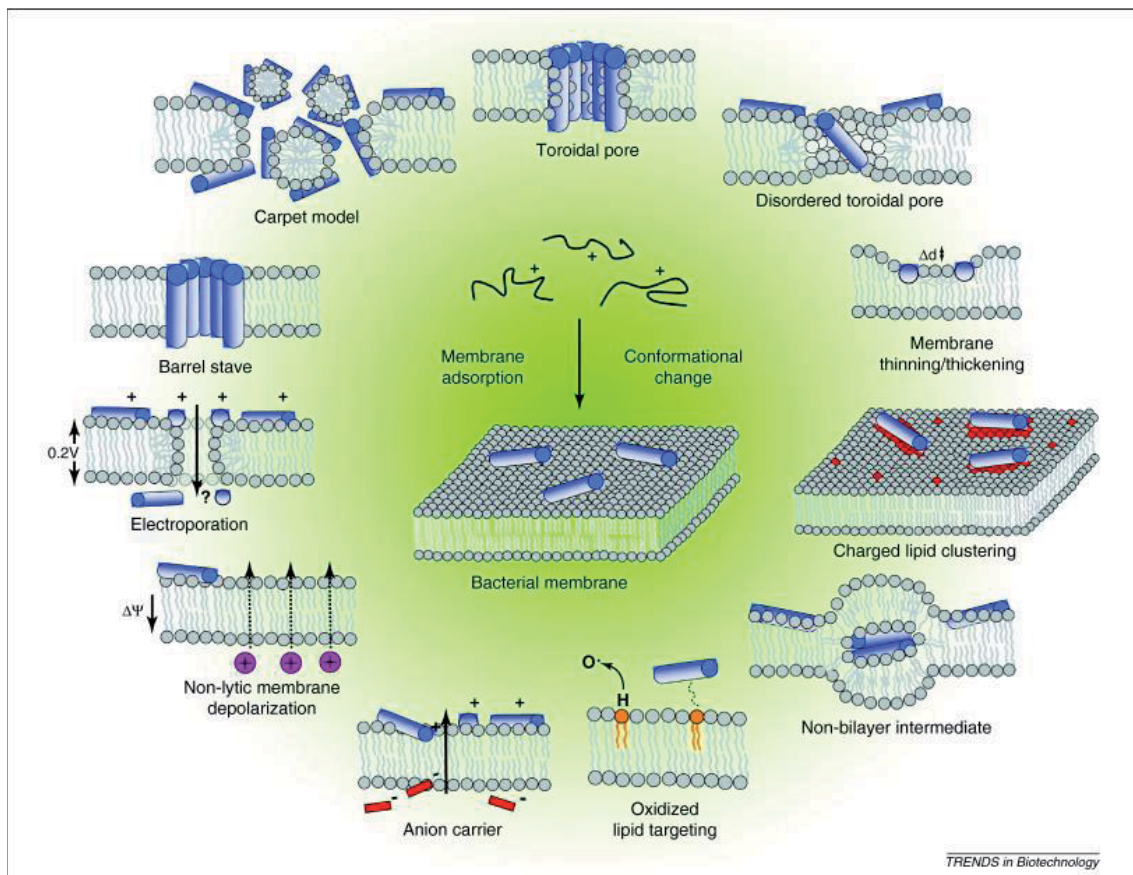


Figure 5. Events occurring at the bacterial cytoplasmic membrane following initial antimicrobial peptide (AMP) adsorption. These events are not necessarily exclusive of each other. In the classical models of membrane disruption, the peptides lying over the membrane reach a threshold concentration and insert themselves

across the membrane to form either peptide-lined pores in the barrel-stave model, micellar structures in the carpet model, or peptide-and-lipid-lined pores in the toroidal pore model. Taken from (90).

1.5. Immunoregulation role of Antimicrobial peptides

The antimicrobial properties of AMPs have been extensively described in several infection models, with a wide range of organisms, clinical fastidious isolates and reductionist systems such as model membranes (91). Besides its direct microorganisms killing activity, AMPs can help to clear infection based on their immunomodulatory properties related to cross-talking with both innate and adaptive immunity, as depicted in Figure 6. One of the modulatory properties of AMPs is the LPS neutralization activity. LPS is the mayor component of the outer membrane of Gram-negative bacteria and the mayor effector of septic shock during infection. Several AMPs can neutralize the adverse effects of LPS *in vitro* and *in vivo*, among them, the most studied may be cathelicidin, defensins, polymyxin B and bactericidal permeability-increasing protein (BPI) (92). In more detail, cathelicidins are able to i) directly interact and neutralize LPS ii) disaggregate LPS, reducing the binding affinity to the lipopolysaccharide binding protein (LBP), and iii) inhibit the production of proinflammatory cytokines through clearing of LPS from cell surfaces in monocyte- or macrophage-like cells (93). Another immunomodulatory related activity is chemotaxis. The first non-microbicidal activity described on AMPs was the chemoattraction of human monocytes by human defensins about twenty years ago (94). Later, the α -defensins human neutrophil peptide 1 and -2 were described as potent chemoattractors for several cellular types, such as CD4+, CD45RA+ and CD8+ T cells, as well as dendritic cells. Human β -defensins (HBD 1, 2 and 3) are able to recruit memory T cells, dendritic cells, monocytes and mast cells. At the same time, cathelicidins are able to recruit memory T cells, monocytes and mast cells but not dendritic cells (9). AMPs are also found to act as an epithelial growth factor (EGFR) in lung, as observed for LL-37 (95). In this context, another important immunomodulatory property is the ability of some AMPs, such as LL-37, to promote wound healing through re-epithelialization and granulation tissue formation (95). Other important findings highlight the role of AMPs in modulating proinflammatory cytokine production. Human α -defensins have been shown to promote the expression of inflammatory cytokines and co-stimulatory molecules on lymphocytes. HBD3 is responsible of dendritic cell maturation and proinflammatory cytokine modulation (96). All these novel properties of AMPs open as a new window to elucidate new approaches based on innate and adaptive immunity regulation to fight against pathogens (97).

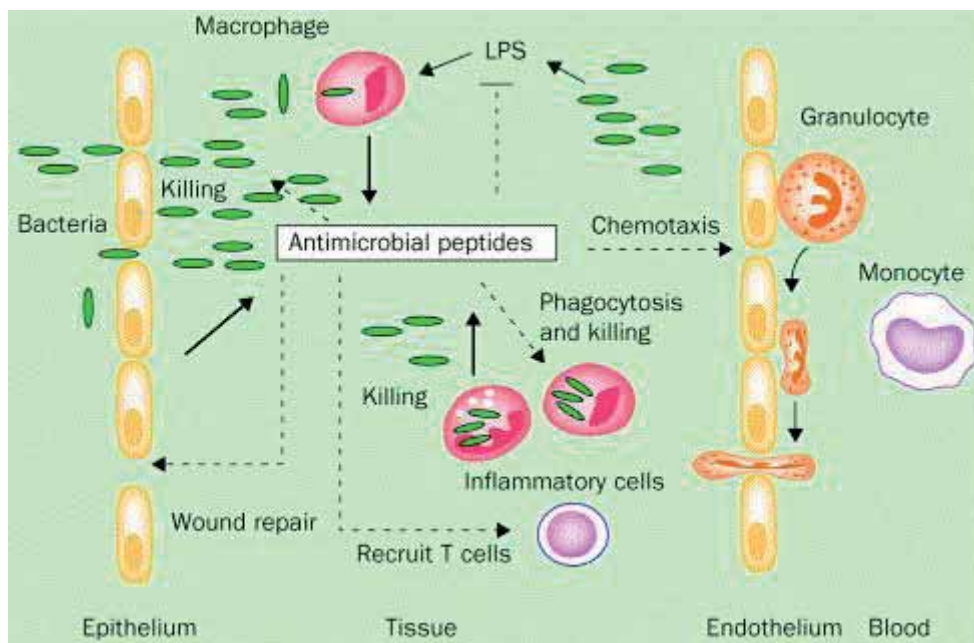


Figure 6. Schematic representation of the role of antimicrobial peptides in the complex network of innate immunity. LPS (lipopolysaccharide). Taken from (98).

1.6. Antimicrobial peptides in drug development

Currently about 40 compounds are in active clinical development, where half of them have been launched during the last ten years. Several, either natural or synthetic AMPs have entered into and/or completed clinical trials; some examples are shown in Table 1. For instance, the eleven residues AMP, derived from lactoferrin, hLF1-11, was proven to be safe when injected intravenously (99). Pexiganan, a peptide derived from magainin has demonstrated efficacy in phase III trials. Omiganan (MBI-226), a derived indolicin peptide, is also in phase III trials, and has been proven to reduce significantly microbiological catheter colonization (100). Other peptides have completed the clinical trials, that is the case of polymyxin used as the last-resort drug against acute multiresistant infection of *Pseudomonas spp.* and *Acinetobacter spp.* Gramidicin S, a cationic cyclic peptide, is extensively used as topical ointment and eye drops. Another example is the lantibiotic nisin which is currently approved as food additive in Europe (101). Another promising application of AMPs is the elaboration of AMP-coated devices. Solids supports would be AMPs tethered in order to prevent microbial surface colonization. We should take into account another promising approach which has been exploited during the last years, the usage of amyloid-forming peptides which after selective insertion of charged amino acids adopt amphipathic structures that can be converted into membrane-disrupting AMPs (102). One of the major problems that face AMPs-coated supports is the reduction of the antimicrobial capability; it has been demonstrated that tethered peptides are nearly 100 times

less active than their soluble counterparts (103). The major problems faced by AMPs into clinical development are mainly, i) host toxicity, ii) proteolytic degradation and iii) production cost. One of the crucial point on the development of AMPs as clinical drugs is their potential toxicity. Several approaches are carried out in order to overcome host toxicity, such as reduction of the hemolytic profile, animal testing or masking the peptide through inclusion into delivery vectors as liposomes (104). The half-life of a peptide within an organism, and its liability to proteolytic degradation could be addressed by using D-amino acids, non-natural amino acid analogues or mimetics with different backbones structures (105). The cost of goods could be addressed by reduction of the peptide sequence and improving the obtainment technical approaches.

Table 1. Selected host defence peptides in drug development. Taken from (100).

Name	Sequence	Company	Description	Application	Trial phase	Comments	Clinical trial identifiers and further information
Pexiganan acetate (MSI 78)	GIGKFLKK AKKFGKAF VKILKK	MacroChem	Synthetic analogue of magainin 2 derived from frog skin	Topical antibiotic	III	No advantage demonstrated over existing therapies	NCT00563433 and NCT00563394
Omiganan (MX-226/ MBI-226)	ILRWPW WPWRRK	Migenix/ BioWest therapeutics	Synthetic cationic peptide derived from indolicidin	Topical antiseptic, prevention of catheter infections	III	Missed primary end point (infections) but achieved secondary end points of microbiologically confirmed infections and catheter colonization	NCT00027248 and NCT00231153
Omiganan (CLS001)	ILRWPW WPWRRK	Cutanea Life Sciences/ Migenix	Synthetic cationic peptide derived from indolicidin	Severe acne and rosacea; anti-inflammatory	II/III	Significant efficacy in Phase II trials for both indications; in Phase III trials	NCT00608959
Iseganan (IB-367)	RGGLCY CRGRFC VCVGR	Ardea Biosciences	Synthetic 17-mer peptide derived from protegrin 1	Oral mucositis in patients undergoing radiation therapy	III	No advantage demonstrated over existing therapies	NCT00022373
hLF1-11	GRRRRS VQWCA	AM-Pharma	Cationic peptide fragment comprising amino-terminal amino acids 1-11 of human lactoferricin	Bacteraemia and fungal infections in immunocompromised haematopoietic stem cell transplant recipients	I/II	Significant efficacy observed in Phase I trials; mechanism of action appears to be immunomodulatory rather than antibiotic; Phase II trials initiated after a long delay	NCT00509938
XOMA 629	KLFR-(D-naphtho-Ala)-QAK-(D-naphtho-Ala)	Xoma	Derivative of bactericidal permeability-increasing protein	Impetigo	IIa	No Phase IIa results available (trial started in July 2008)	XOMA website
PAC-113	AKRHHG YKRKFH	Pacgen Biopharmaceuticals	Synthetic 12-mer peptide derived from histatin 3 and histatin 5	Oral candidiasis	IIb	Phase IIb results (announced June 2008): 34% increase in primary end point efficacy level; Phase III trial not initiated	NCT00659971
CZEN-002	(CKPV) ₂	Zengen	Dimeric octamer derived from α-melanocyte-stimulating hormone	Vulvovaginal candidiasis; anti-inflammatory	IIb	Positive efficacy results announced; Phase IIb trial is a dose-ranging study	US Patent application serial number 09/535066
IMX942	KSRIVPA IPVSLI	Inimex	Synthetic cationic peptide derived from IDR1 and bacteneicin	Nosocomial infection, febrile neutropenia	Ia	Phase Ia trial completed in 2009; no Phase II trial announced yet	Inimex Pharmaceuticals website
OP-145	IGKEFK RIVERIK RFLREL VRPLR	OctoPlus; Leiden University, The Netherlands	Synthetic 24-mer peptide derived from LL-37 for binding to lipopolysaccharides or lipoteichoic acid	Chronic bacterial middle ear infection	II (completed)	Clinical proof-of-efficacy in Phase II trials; no Phase III trials proposed yet	ISRCTN84220089
Ghrelin ²¹⁸	GSSFLSPE HORVQQ RKESKPP AKLQPR	University of Miyazaki, Japan; Papworth Hospital, Cambridge, UK	Endogenous host-defence peptide	Airway inflammation, chronic respiratory infection and cystic fibrosis	II	Peptide hormone that suppresses neutrophil-dominant inflammation in airways of patients with chronic respiratory infection	JPRN-UMIN000002599, JPRN-UMIN000001598 and NCT00763477
PMX-30063	Structure not disclosed	PolyMedix	Arylamide oligomer mimetic of a defensin	Acute bacterial skin infections caused by <i>Staphylococcus</i> spp.	II	Mimetic rather than peptide; currently in Phase II trials	NCT01211470; PolyMedix website
Delmitide (RDP58) ²¹¹	RXXRX XXGY (X = norleucine)	Genzyme	Semisynthetic D-amino acid decapeptide derived from HLA class I B2702	Inflammatory bowel disease	II (completed)	A protease-resistant, D-amino acid-containing peptide with similar efficacy to asacol; attempting to improve activity through formulation	Genzyme website ; ISRCTN84220089
Plectasin ²¹²	GFGC ₂ NG PWDEDD MQC ₂ HNH C ₂ KSikGYK GGYC ₂ AKG GFVC ₂ KC ₂ Y	Novozymes	Fungal defensin; candidate in development is an amino-acid substitution variant	Bacterial diseases	Pre-clinical	Excellent efficacy demonstrated in animal models	Novozymes website
HB1345	Decanoyl-KFKWPW	Helix BioMedix	Synthetic lipohexapeptide	Acne; broad-spectrum antibiotic	Pre-clinical	Looks promising as this is a very small lipopeptide	Helix BioMedix website

HLA, human leukocyte antigen; IDR1, innate defence regulator 1; LL-37, human cathelicidin antimicrobial peptide LL-37.

1.7. Antimicrobial RNases.

The RNase A superfamily takes its name from the first ribonuclease discovered, the bovine pancreatic RNase (RNase A), and groups together all the RNases homologous found in vertebrates (106, 107). Eight functional members, known as “canonical RNases” have been isolated from humans (Figure 7 and Table 2) (108). They present some common features i) the ability to hydrolyze RNA substrates, ii) a unique disulfide-bond pattern that shapes its particular tertiary structure, iii) a catalytic triad, conformed by two histidines and one lysine. It must be emphasized that, independently to their ribonuclease activity, a variety of other biological functions have been reported. A worthy effort has been applied in order to highlight the antimicrobial and immunomodulatory activities of the family; suggesting that RNases could have an ancestral host-defence function (109-112).

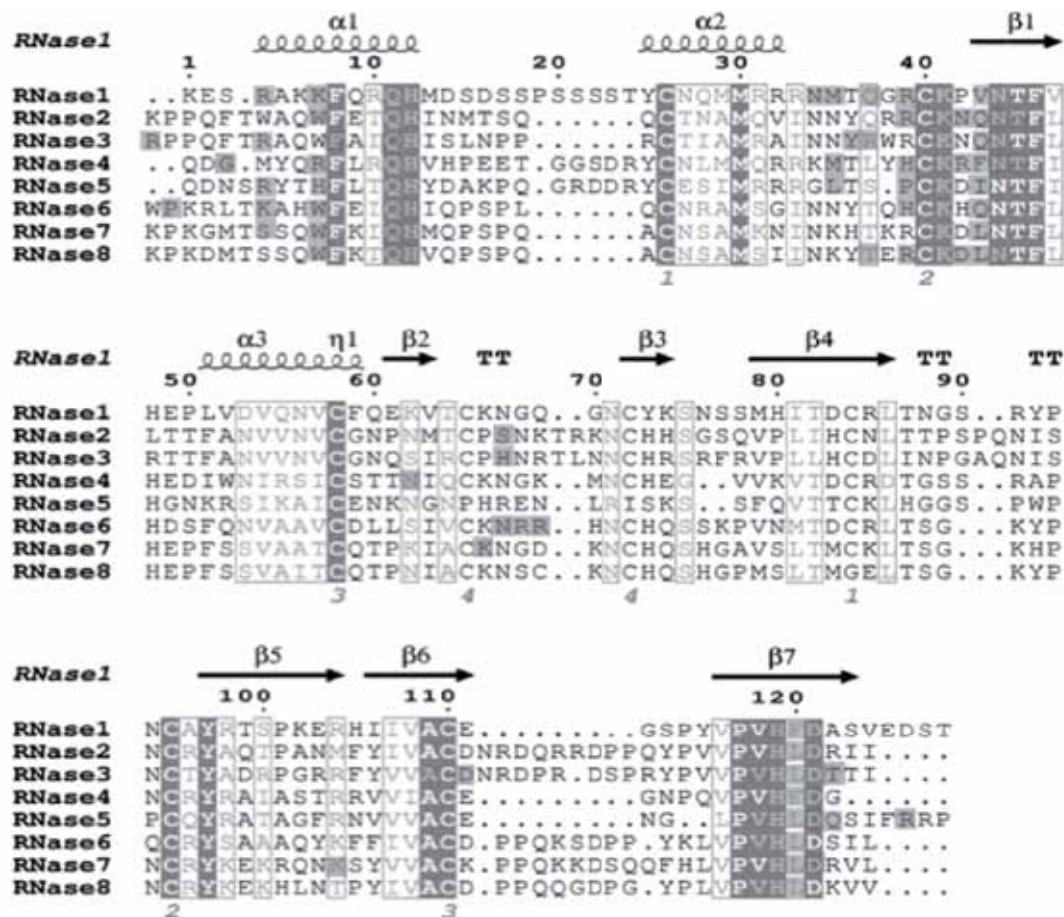


Figure 7. Primary sequence alignment of the human RNases belonging to the vertebrate-secreted RNase A family. Conserved amino acids in all sequences are boxed in black. The alignment was performed using *Clustal W*, and the picture was drawn using the *ESPrpt* program (<http://esprpt.ibcp.fr/ESPrpt/>). Modified from (113).

Table 2. Properties of human RNases from the RNase A family. Information was taken, unless indicated, from UniProt Protein Knowledgebase data (UniProtKB; <http://www.uniprot.org>). Bactericidal activity reported in the literature is indicated and classified as low, moderate or high, when a quantified reference is available. Taken from (113).

Protein name (alternative name) ₁	Main source	Reported bactericidal activity	Known natural variants ²	Postranslational modifications	Proposed role
RNase 1 (Human pancreatic RNase) [P07998] 128/28	Pancreas, human endothelial cells and other tissues and body fluids	None		3 N-linked glycosylation sites (114)	RNA digestion in ruminant homologues. Unknown non digestive physiological role for the human member (115)
RNase 2 (Eosinophil derived neurotoxin, EDN) [P10153] 134/27	Matrix of eosinophil large specific granules, liver, lung, spleen, neutrophils and monocytes	None	His73/Gln His129/Asn	5 potential N-glycosylation sites; C-linked mannose at Trp7 (116) (117); Tyr33 nitration (118)	Host defence against viral infections; chemotaxis for dendritic cells (119)
RNase 3 (Eosinophil Cationic Protein, ECP) [P12724] 133/27	Matrix of eosinophil large specific granules and also minority in neutrophils	High (nM- μ M range) MIC ₁₀₀ = 0.3-1.5 μ M (tested against several Gram negative and Gram positive species (120) (121)	Arg97/Thr (related to asthma propensity and disease induced pathologies) (122) (123) Gly103Arg	3 potential N-glycosylation sites; 10 purified variants of N-linked glycosylated forms (124); N-glycosylation processed upon secretion by activated eosinophils (125); Tyr33 nitration (118)	Host defence against parasite, viral and bacterial infections; immunomodulation (126) (112, 127) (128)
RNase 4 [P34096] 119/28	Ubiquitous, with predominance in liver and lung	None		Pyro-Glu (N-terminal Gln cyclation) (129)	Unknown. mRNA cleavage? (129)

RNase 5 (Angiogenin) [P03950] 123/24	Expressed predominantly in the liver. Also detected in endothelial cells, neurons, intestinal epithelium and keratinocytes	High-moderate (low - μ M range) Contradictory reports (130, 131)	multiple substitutions related to amyotrophic lateral sclerosis (ALS9)(132)	Pyro-Glu (N-terminal Gln cyclation) (133)	Angiogenesis; cell differentiation; host defence? (130, 134-136)
RNase 6 (RNase K6) [Q93091] 127/23	Strong expression in lung, followed by heart, placenta, kidney, pancreas, liver, brain and skeletal muscle. Also expressed in monocytes and neutrophils.	None	R66Q	2 potential N-glycosylation sites (137)	Host defence?; RNA catabolism? (137, 138)
RNase 7 (Skin derived antimicrobial protein 2, SAP-2) [Q9H1E1] 128/28	Expressed in various epithelial tissues including skin, respiratory tract, genito-urinary tract and, at a low level, in the gut. Expressed in liver, kidney, skeletal muscle and heart.	High (nM- μ M range) Broad-spectrum antimicrobial activity against many pathogenic microorganisms and remarkably potent activity (LD90 < 30 nM) against a vancomycin resistant <i>Enterococcus faecium</i> (139)	A75P Y88H (116)	1 potential N-glycosylation site	Host defence. Skin protection. Protection of respiratory, intestinal epithelium and urinary tract (139, 140) (141) (142)
RNase 8 (Placental RNase) [Q8TDE3] 127/27	Expressed in Placenta	High-moderate (low - μ M range) Contradictory reports. Tested against a wide bacteria spectra (LD90 from 0.1 to 1 μ M)(143)			Placenta protection against infection? (144) (143) Unknown role not related to secreted RNases (145)

¹[UniProtKB ID], Mature protein/ signal peptide lengths; ² Only natural variants in the mature protein reported in the UniProtKB are included.

only very moderate antiparasitical activity (157), EDN is active against several viruses in a ribonuclease dependent manner, such as rhinovirus, adenovirus and, against the respiratory syncytial virus (RSV) (158-160). EDN also acts as a modulator of the host immune system leading immature dendritic cells (DCs) chemotaxis and maturation both *in vitro* and *in vivo* (154, 161-163). In addition, EDN has been described as an endogenous ligand of toll-like receptor 2 (TL2) regulating antigen presenting cells (APC), thus connecting with adaptive immune system. EDN has been classified as an alarmin, a protein capable of activating and modulating the host immune system (163, 164).

1.7.1.2. Eosinophil cationic protein (RNase 3).

At the beginning of the 70's, a highly cationic arginine-rich protein (19 Arg out of 133 amino acids, pI of 10.3) was isolated from the secondary granules of human eosinophils. Human ECP is secreted in response to both several infectious agents and different inflammation processes (126, 165). The protein also displays an $\alpha + \beta$ conformation formed by three α -helices at the N-terminus and six β -sheet, stabilized by four disulfide bridges; a pattern conserved among the RNase A family (151, 166). ECP has a number of biological activities, including a highly antimicrobial activity against bacteria (167), and many parasites, such as helminths and protozoa (157, 168-172), cytotoxic and neurotoxic (173), antiviral (174), antitumoral (175) and immunoregulatory activities (176). However, in contrast to EDN, its antimicrobial properties are not dependent on the ribonuclease activity (174).

The antibacterial activity of the protein has been extensively studied in our laboratory. ECP displays a high antibacterial activity against both Gram-positive and Gram-negative bacteria (167). ECP is able to interact with many molecules, including the bacterial cell wall moieties, as lipopolysaccharide (LPS) and peptidoglycan (PNG) or the glycosaminoglycans present at the eukaryote cellular matrix, such as heparan sulphate (113, 177-179). It has been described that ECP is able to interact with negatively charged model membranes and subsequently produce the disruption and aggregation upon incubation of large unilamellar liposomes (LUV) (180). The suggested mechanism of action of ECP could be described by two main processes, during the first step the protein interacts with the negatively charged molecular components of the bacterial cell wall and cytoplasmic membranes; and in the second one a subsequent bacterial agglutination and membrane destabilization occurs (181). The sequence/structural determinants of the antibacterial properties of ECP have been located at its N-terminal 45 first amino acids by peptide synthesis approach (120). Specifically, two separate regions lead the process of membrane aggregation/ bacterial agglutination (8-16 residues) and membrane

disruption (33-36 residues) (120). Further results highlight that the N-terminal hydrophobic patch corresponding to 8 to 16 residues could be an amyloid-like prone region triggering the formation of protein amyloid aggregates under certain conditions (182).

Other biological activities of ECP have been determined. High concentrations of ECP were observed in the serum of patients with renal cell adenocarcinoma, suggesting that activated eosinophils are present in the tumor microenvironment, and that the protein participates in the tumor destruction (183). Further investigations demonstrated that ECP was able to suppress the growth of several tumoral human cell lines (175).

ECP has a range of immunomodulatory activities, including, the suppression of both T-cell proliferative responses and immunoglobulin synthesis by B cells, mast cell degranulation, regulation of fibroblast activities, induction of airway mucus secretion, and interaction with the coagulation and complement systems (124, 173, 184-186).

1.7.2. Non-eosinophil ribonucleases

Antimicrobial RNases are not only expressed in the secretory granules of eosinophils. Other ribonucleases such as RNase 5, 7 and 8 are expressed in multiple somatic tissues. RNase 5, for instance, is expressed predominantly in liver but also detected in endothelial cells, neurons, intestinal epithelium and keratinocytes. RNase 7, at the same time, is found in various epithelial tissues, such as skin, respiratory and urinary tracts. RNase 8 is expressed mainly in placenta where it might exert its antimicrobial action (109). Those three RNases are well studied and their antimicrobial activities are further discussed below. Other members, mainly RNases 4 and 6 are at this date poorly studied and, although there are some evidences that they could be involved in human host defence, there is still controversy.

1.7.2.1 Angiogenin (RNase 5).

Human angionenin (ANG) was firstly discovered as a tumor-derived protein with a potent agiogenic activity about 25 years ago (187). ANG adopts the overall structural conformation characteristic of the RNase A superfamily (188). Bactericidal and antifungal activities are reported in human ANG together with their homologues in mice, (ANG1 and 4) (130). It has been described that ANG may play a role in host-defence in bacterial challenged intestinal tract; presenting antimicrobial activity against several gram-positive and gram-negative bacteria (130). Recent studies highlight the antifungal activity of ANG which can suppress the growth of *C. albicans*. Both are expressed after intestinal infection (189).

1.7.2.2. Skin derived RNase (RNase 7).

At the beginning of the century a novel human epithelial ribonuclease was discovered, and named RNase 7 (139). The protein was reported as a major antimicrobial protein of healthy skin and is mainly produced by keratinocytes induced by bacterial challenge. RNase 7 is expressed by epithelial tissues; such as skin, respiratory tract, genitourinary tract and in a less amount in gastrointestinal tract (190). RNase 7 also displays the prototypical $\alpha + \beta$ RNase A superfamily fold (191). A differential feature may be the nature of its positively charged residues (18 Lysines of 128 amino acids), as shown in Figure 9.

RNase 7 exhibits a broad spectrum of antimicrobial activity against both Gram-negative bacteria (*E. coli* and *P. aeruginosa*), and Gram-positive bacteria (*Propionibacterium acnes*, *S. aureus*) and the yeast *C. Albicans* in a very low micromolar range. RNase 7 is extremely effective against *Enterococcus faecium* with a lethal dose inferior to 30 nM (the lowest value known so far for an antimicrobial RNase); suggesting that RNase 7 may be the central effector of bacteria clearance at the gut epithelia (139). Recently, studies highlight that RNase 7 is a potent antibacterial at the urinary tract participating in the clearance of several uropathogenic bacteria (192). The antibacterial properties of the protein seem to be located at the N-terminal portion (191). Later studies confirm and expand these findings determining that secondary structure appears to be crucial for RNase 7 antimicrobial activity; being its structural β -sheets 1, 3 and 4 the antimicrobial determinants (193).

The mechanism of action of RNase 7 has been studied in our laboratory using a model membrane system. The antimicrobial mechanism of action is mostly dependent on its membrane destabilization ability. RNase 7 is not able to interact and disrupt neutral membranes, but can induce the vesicle leakage in a submicromolar range against negatively charged membranes (181). Different spectroscopic and imaging techniques were leading us to dissect the membrane destabilization into three steps: vesicle content leakage, aggregation and sample precipitation (181). At the bacterial cell wall level it has been proved that RNase 7 is able to bind the heterosaccharides from Gram-negative (lipopolysaccharide) and Gram-positive (peptidoglycan). After recognition of the bacteria at both cell wall and membrane level, the protein exerts its antibacterial effect producing the leakage of the cell after destabilization of the cytoplasmic membrane without inducing the bacterial agglutination, as ECP does (194).

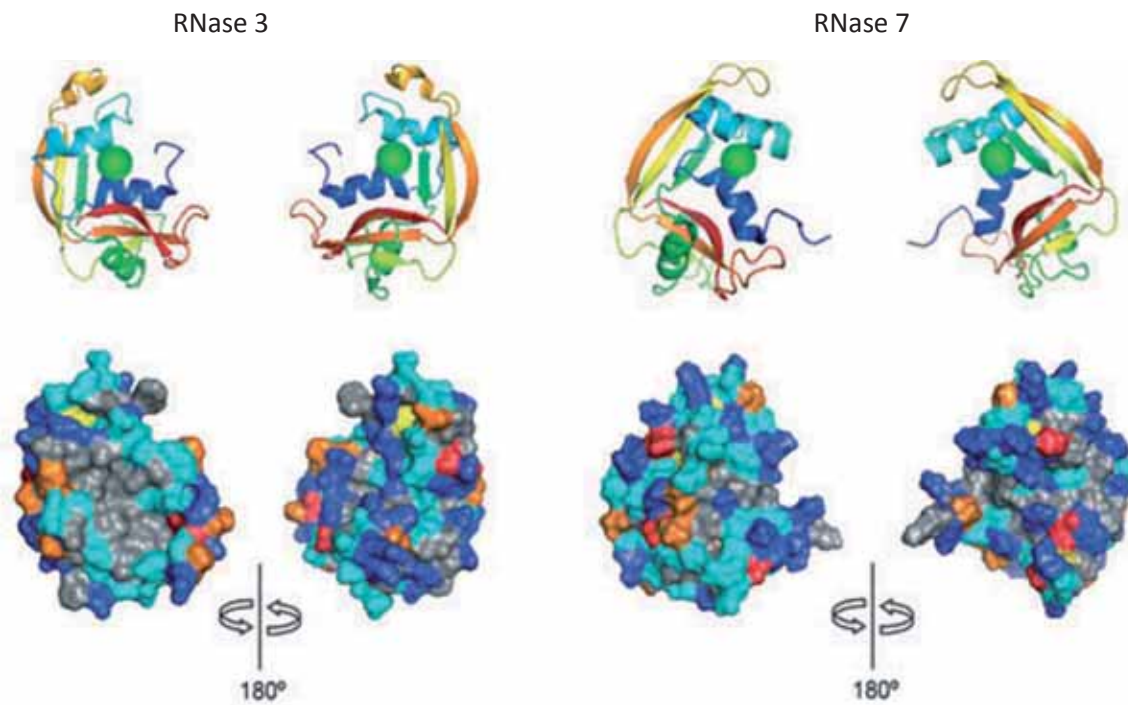


Figure 9. (A) Ribbon representation of the 3D structures of RNase 3 (1DYT.pdb) and RNase 7 (2HKY.pdb). Molecules are colored from the N- to C-terminus. A circle highlights the active site. (B) Molecular surface representation of RNase 3 and RNase 7. Hydrophobic residues are labeled in grey, cationic residues in blue, anionic residues in red, cysteine residues in yellow, proline residues in orange and non-charged polar residues in cyan. Taken from (194).

1.7.2.3. Placental RNase (RNase 8).

A decade ago a novel member of the RNase A superfamily, termed RNase 8, was discovered in human placenta (144). Afterwards RNase 8 expression was reported in several tissues, such as spleen, lung, testis, and liver (145). RNase 8 and RNase 7 share 78% sequence identity; therefore, it is reasonable to speculate that RNase 8 may play a role in host-defence. In fact, several studies do report RNase 8 antipathogenic activity against different pathogenic Gram-positive and Gram-negative bacteria and fungi, inhibiting the growth of *C. albicans* (143).

AIMS OF THE THESIS

2. Aims of the thesis

The overall aim of the present work is to characterize the mechanism of action of antimicrobial ribonucleases, focused in identifying the structural determinants required for their antimicrobial properties. In particular, the specific aims of the thesis were:

Chapter I:

- To determine the pharmacophore of the Eosinophil cationic Protein (ECP) by a rational structure minimization approach.

Chapter II:

- To understand the processes taking place at the bacterial cell wall upon interaction with ECP and, in particular, to study the role of the lipopolysaccharide molecule in the protein mechanism of action.

Chapter III:

- To determine the role of the protein amyloid aggregation and its correlation with the bacterial agglutination and killing.

Chapter IV:

- To identify the sequence and structural determinants of human antimicrobial RNases conserved along evolution at their antimicrobial N-terminal domain.

Chapter V:

- To determine the role of the key antimicrobial regions on human ECP through rational single point mutation on its homologue counterpart EDN.

Chapter VI:

- To explore the antimicrobial activity of ECP, RNase 7 and their N-terminal derived peptides towards mycobacteria.

GENERAL DISCUSSION AND FUTURE PERSPECTIVES

3. General discussion and future perspectives

Antimicrobial RNases are small cationic proteins belonging to the vertebrate-secreted RNase A family. This family comprises all the vertebrate members homologous to RNase A. In humans, eight genes encoding for functional proteins have been identified, also known as “canonical RNases”. Despite of the low sequence identity, between several members, as low as 30%, they all share three main features; i) the ability to hydrolyze RNA substrates ii) a catalytic triad composed of two histidines and one lysine iii) and a common three-dimensional structure with three to four conserved disulfide bonds. Together with the shared RNase catalytic activity, a variety of other biological activities, such as angiogenic, antitumoral, antiparasitic, antimicrobial and immunomodulatory properties are reported for human ribonucleases, suggesting their function as multifunctional proteins (113). Remarkably, several human RNases display different antimicrobial actions against a wide range of pathogens as bacteria, fungi, yeast and parasites, and play a direct role in host immune system as key modulators. In particular, our lab has extensively studied RNase 3, also known as eosinophil cationic protein (ECP). ECP is one of the major proteins in the secondary granules by eosinophils, which are secreted during infection. ECP is a highly cationic protein which has been reported to exert antimicrobial activity against helminths, protozoa, bacteria and fungi in a non RNase-dependent manner (113). The protein is able to interact and disrupt pathogenic membranes and is also able to recognize several cell wall molecules of bacteria, such as lipopolysaccharide (LPS) and peptidoglycan (PG) and glycosaminoglycans as heparin (113, 177, 178). The antimicrobial properties seem to be mostly retained on the first two α -helices corresponding to the 45 first amino acids (120). ECP can also agglutinate both model membranes and Gram-negative bacteria in a low micromolar range (181, 194). ECP would act in three different steps that define a dynamic process of bacterial killing. First, the protein interacts with the negatively charged cell wall molecules. Next, the protein promotes the agglutination of bacteria and finally induces bacterial cell leakage finally killing the pathogen.

3.1. Lipopolysaccharide binding and antimicrobial activity.

In this thesis we investigated further the antimicrobial mechanism of action of ECP. It is known that ECP is able to agglutinate Gram-negative bacteria but not Gram-positive bacteria. Also ECP displays a high affinity to the LPS polysaccharide moiety of Gram-negative bacteria. The LPS outer layer confers bacteria a hydrophobic protective barrier against much of the antimicrobials, such as antibiotics, detergents and host proteins (195). However, there are several antimicrobials that exert their antibacterial activity through direct interaction with the

LPS molecule, such as lactoferrin or lysozyme that show a decrease in their activity when tested with a progressively truncated LPS (196). Those facts encouraged us to investigate the role of LPS in the antimicrobial action of ECP. We tested the antimicrobial and agglutinating abilities of the protein against a progressively LPS truncated *E. coli* mutant strains (197) (further detailed in Chapter II). As lactoferrin or lysozyme, ECP was far more active against rough mutants (with longer LPS core) when compared with deep-rough mutants (with shorter LPS core) showing seven fold higher minimum inhibitory concentration (MIC) values. In addition, ECP displayed a slower membrane depolarization and bacterial-killing kinetics on deep-rough mutants and this strain showed a lower mortality rate. Regarding to the agglutinating activity of the protein, ECP was unable to agglutinate the deep-rough mutant. These evidences led us to suggest that the LPS polysaccharide moiety is essential to trigger Gram-negative bacterial cell agglutination, which we found directly correlated with antimicrobial activity. During agglutination the outer membrane is disrupted and causes a loss of the membrane potential, compromising cell homeostasis. Unfortunately, the molecular determinants required for LPS interaction are not elucidated yet. The LPS molecule is the main responsible of septic shock during bacterial acute infection (198), causing more than 500,000 deaths per year worldwide (92). Therefore, discovering new agents for LPS neutralization has become a goal of general scientific interest. We suggest that ECP may be a good candidate as a template for the development of new anti-LPS agents and we aim to pursue this investigation by developing new peptides based on the ECP N-terminus for septic shock treatment.

3.2. Antimicrobial activity and protein aggregation

ECP was previously reported to form amyloid-like aggregates due to a hydrophobic patch at the protein N-terminus (residues 8 to 16) (182). A single point mutation, Ile 13 to Ala, completely abolished the amyloid prone region of ECP disabling its aggregation properties. Those previous results suggested that the role of amyloid self-protein aggregation was related to the agglutinating properties of the protein. In this work we tested the wild type ECP and the mutant I13A (see Chapter III for further details). Our results directly correlated the antimicrobial action of the protein with the agglutinating activity (199). I13A mutant showed no agglutinating activity and low antibacterial action between ten to five times lower than wild type ECP. These results encouraged us to further analyze the protein agglutination mechanism at both membrane and cell level by means of fluorescent labelling and confocal microscopy. The results obtained highlighted that the agglutination process was mediated by amyloid-like protein aggregation. The presence of protein aggregates was also confirmed by Total Internal Reflection Microscopy (TIRF) and binding to amyloid diagnostic dyes. Therefore, we discovered

evidence that amyloid aggregation can be linked to bacteria clearance. Thus, we suggest that after binding to the bacterial surface a conformational rearrangement of the protein could expose the N-terminal patch triggering the amyloid self-aggregation process driving the agglutination of the bacterial cell. Additionally, during last years several reports brilliantly linked the amyloid aggregation propensity of several proteins with their antimicrobial activities. Therefore a novel and promising new approach on the development of new antimicrobials is the amyloid-based designed peptides (102). In consequence, we suggest that ECP amyloid-prone region might be used as a scaffold for the development of new amyloid based antimicrobial peptides.

3.3. Design of protein derived antimicrobial peptides

The widespread use of antibiotics as a general treatment for bacterial infections has been questioned as an alarming emergence of bacteria resistance develops. In this context, AMPs are viewed as promising candidates due to their high potency, wide spectrum of activity and vastly diverse mechanism of action. With the aim to use AMPs as therapeutic drugs against pathogens, several approaches are studied to improve the AMPs antimicrobial features. One of those approaches consists in the use of antimicrobial proteins as scaffolds to develop synthetic peptides with enhanced antimicrobial activity. That is the case of human RNases and, in particular, of ECP.

Structure-function studies of ECP showed that most of the antimicrobial activity of ECP was largely retained by its N-terminal domain (120). This domain, encompassing residues 1 to 45, is equipotent compared to the whole protein, retaining most of the biophysical properties, such as membrane agglutination and leakage. Moreover, the antimicrobial action of the N-terminal domain also depends on LPS binding as showed by the use of progressively LPS truncated strains. Therefore the antimicrobial mechanism of action of this peptide seems to be equivalent to its parental protein. With all these information and using rational structure-guided minimization of the N-terminal domain we were able to define the ECP pharmacophore, the peptide analogue ECP(6-17)~Ahx~ (23-36) (200) (where Ahx stands for aminohexanoic acid; see Chapter I). This approach lead to a peptide with a size reduction of 40% versus the lead peptide ECP(1-45) and up to 80% from ECP with the preserved α -helical structure of the native protein, as shown by NMR experiments. Despite of the high size reduction, the peptide displayed a high antimicrobial activity against both Gram-positive and – negative bacteria with a potent disruptive membrane leakage and a remarkable lipopolysaccharide (LPS) affinity. Besides, only a very small increase in haemolytic activity was

observed when compared to the ECP(1-45) analogue. Therefore, we found a correct balance between size and antimicrobial features of this analogue as further reduction of the ECP(6-17)~Ahx~(23-36) analogue strongly decreased the antimicrobial properties. Surprisingly, ECP(6-17) ~Ahx~(23-36) mechanism of action appeared to be LPS independent, showing lower agglutination propensity and remarkable activity against deep-rough mutants. Also, a higher and faster membrane depolarization activity was also observed. Those results suggest that the peptide ECP(6-17)~Ahx~(23-36) enhances lytic mechanism of action while losing the ability to interact with LPS, probably due to its enhanced hydrophobicity.

On summary, we suggest that ECP(6-17)~Ahx~(23-36) is a good template to develop ECP-based antimicrobial compounds against resistant strains. Certainly, more efforts are needed to overcome the difficulties for the drug design of ECP-based peptides. Several approaches could be tested in near future, including the synthesis of D-enantiomer variants, pegylated versions or mimetics using non-natural amino acids to elude the natural pathogen proteases and increase the half-life of these peptides. Finally, it is necessary to study the survival rate of model animals challenged with bacterial infection after treatment with ECP-derived peptides that would provide information on the toxicity, pharmacodynamics and *in vivo* potency, required for later clinical trials.

3.4. Searching for conserved antimicrobial patterns.

Human RNases are small multifunctional proteins that play a crucial role in several biologic processes, such as metabolism of RNA, angiogenesis, antitumour, immunomodulator and antimicrobial activities. Concerning to their antimicrobial activity human RNases share high isoelectric points, a common feature among AMPs that is required for interaction with negatively charged microbial surfaces. However, neither a sequential nor a structural evolutionary pattern that embodies these antimicrobial properties has been reported yet. In this context, as we highlighted before, the antimicrobial domain of ECP is comprised in the N-terminal first 45 amino acids, being the residues from 24 to 45 essential for the antimicrobial action and the residues from 8 to 16 crucial for protein aggregation and bacterial agglutination (120). Therefore, it is tempting to hypothesize the potential role of the N-terminal domain in the antimicrobial action of human RNases. To test this hypothesis, we synthesized the N-terminal domain of all human RNases and thereafter tested their antimicrobial and agglutinating activities (201) (see Chapter IV). We have found that all N-terminal domains of human RNases with described antimicrobial activity were active against all Gram-positive and negative bacteria species tested, presenting MIC values similar to the previously reported for

their parental proteins (113). We also found a strong correlation between the ability to disrupt model membranes and the antimicrobial activity. Therefore, the correlation between liposome leakage, membrane depolarization and antimicrobial activity in bacteria suggests that the mechanism of action of these peptides occurs at the membrane level and not by interaction with bacteria internal targets. It is also worth mentioning that we found a significant correlation between the peptide structure in membrane-like environments and the antimicrobial activity, suggesting that the conformational changes that occur at the membrane level are crucial to trigger membrane destabilization.

All peptides with antimicrobial activity also showed bacterial agglutinating activity and even more interestingly, we found a direct correlation between the agglutinating activity and the ability to bind LPS. This observation further supports our claim that agglutination takes place at the external membrane of Gram-negative bacteria cell wall and that bacteria agglutination is an essential feature for the antimicrobial action of ribonucleases. Therefore, it seems reasonable to suggest that the N-terminal segment of human RNases might be a successful antimicrobial template conserved along evolution to confer antimicrobial properties to antimicrobial RNases. To test our hypothesis, we extended our search to other vertebrate RNases by analyzing the antimicrobial profile of all secreted vertebrate RNases using the AMPA algorithm (202). AMPA is available as a web application to assess the antimicrobial domains of proteins, with a focus on the design of new antimicrobial drugs. The web server uses peptide sequences to predict the antimicrobial domains of proteins and polypeptides (203). This computational analysis shows that most RNases display a putative antimicrobial region overlapping the antimicrobial prone region reported for human ECP. In accordance to these results we can suggest a common evolution that took place at the N-terminal domain ascribing a host defence role to vertebrate RNases. In any case, further experimental analysis should be done in order to corroborate this hypothesis. Synthetic peptide and protein recombinant expression approach of selected vertebrate secreted RNases would help us to confirm whether the N-terminal domain of the RNase A members evolved as the antimicrobial determinant of the family.

3.5. RNases as a scaffold to design antimicrobial proteins.

To further understand the sequence and structural determinants of the antimicrobial function of human RNases at the N-terminal domain we compared ECP with its closest homologue, the eosinophil derived neurotoxin (EDN or RNase 2) (204) (see Chapter V). The ancestral precursor of EDN/ECP started to diverge about 50 million years ago by gene duplication (147). Since then

multiple mutations have accumulated in both proteins providing their different biological properties. ECP is highly cationic and displays an antimicrobial action against a wide range of pathogens independently of its RNase activity. On the other hand, EDN displays a low bactericidal activity, although it has been reported to present a high antiviral activity directly correlated to its ability to hydrolyze the viral RNA (160). When further analysing the antimicrobial N-terminal region of both eosinophil RNases we observed that EDN presented a clear segregation of charged and hydrophobic residues rather than a scrambled distribution, as is the case of ECP. We incorporated into EDN sequence two single point mutations, glutamine 34 to arginine and arginine 35 to tryptophan, building an EDN variant with a similar exposed antimicrobial region of ECP. This EDN variant displayed an antimicrobial activity similar to ECP. Then we designed a second variant where, in addition to the previous mutations, we substituted the EDN threonine 12 for isoleucine, generating a hydrophobic patch at the surface of the protein, similar to the one displayed by ECP. By enhancing the hydrophobicity of the N-terminal region of EDN we allowed EDN to agglutinate Gram-negative bacteria, though in lower levels when compared to ECP. The antimicrobial profile of this EDN variant is also increased supporting the concept that the self-aggregation process is essential in the mechanism of action of antimicrobial RNases. In this context, only few mutations were needed to change the antimicrobial profile of these proteins, evincing that ribonucleases have a suitable scaffold to display antimicrobial activity and suggesting that the host-defence function of ribonucleases is not just a collateral product of evolution.

3.6. Testing antimicrobial RNases against mycobacteria.

Human antimicrobial RNases are involved in several biologic processes in host-defence. For instance RNase 7 is expressed mainly in skin, urinary and respiratory tracts, displaying a high antimicrobial action especially against bacteria and is reported to be one of the major effectors in skin protection (205). On the other hand, recent results linked mycobacterial tuberculosis with eosinophil activation and ECP was found to contribute synergistically with α -defensins to mycobacterial growth inhibition (198). These previous results lead us to consider the role of antimicrobial RNases during mycobacterial infection. The human RNases 3 and 7, together with their N-terminal derived peptides were tested against *Mycobacterium* (206) (see Chapter VI). *M. vaccae* was chosen as rapid growing non-virulent and suitable working species model. The antimicrobial assays confirmed that both tested human RNases were able to inhibit mycobacteria in a low micromolar range and ultrastructural analysis revealed how both RNases promote a complete cell disruption, including swelling, intracellular spillage and membrane detachment. On the other hand, the N-terminal derived peptide from RNase 7 was

able to permeabilize, depolarize and displayed an antimycobacterial profile similar to the entire protein; whereas, the N-terminal peptide of ECP displayed an even enhanced antimicrobial profile than the parental protein. The ECP(1-45) peptide was able to almost inhibit the mycobacterial growth at 5 μ M, depolarizing and permeabilizing the mycobacterial membranes with an increased efficiency. Those results could be explained by the comparison of the biophysical properties of both peptides, where the ECP peptide shows a higher isoelectric point (pI=12.61 versus 10.94) a higher positive net charge (+8 versus +7) and an increased amphipathicity due to its scrambled cationic and hydrophobic residues. In addition, further computational analysis applying the AMPA algorithm showed that RNase 7 N-terminus contains an anionic residue (D39) that may disrupt the antimicrobial region.

We also observed that ECP and its N-terminal derived peptide were able to agglutinate mycobacteria. We conclude that ECP, as shown by Gram-negative bacteria, is able to recognize cell wall components at the surface of the mycobacterial cell that could drive the rearrangement of the protein leading to the self-aggregation process ensuing mycobacterial agglutination. Therefore, it is tempting to suggest that ECP self-aggregation at the bacterial surface may trigger *in vivo* the xenophagy machinery contributing to the mycobacterial clearance inside the macrophage (207).

To conclude, the results presented in this work highlight how antimicrobial RNase-derived peptides, and in particular the ECP(1-45) peptide, could be used as a template to develop new antimycobacterial agents. Given that current treatments against this mycobacterial infection are expensive and cumbersome (208), it is worth to further investigate the biological role of the antimicrobial RNases against mycobacterial diseases, such as tuberculosis. Therefore, a deeper study of the antimicrobial action of human RNases against pathogenic species, such as *M. tuberculosis* and their biological role in a macrophage infection model is required.

CONCLUSIONS

4. Conclusions

Chapter I:

- Structure-guided minimization was applied to the N-terminal antimicrobial domain of the Eosinophil Cationic Protein (ECP) to define the minimal requirements for antimicrobial activity. The ECP(1-45) parental peptide was downsized to the analogue ECP(6-17)~Ahx~(23-36), as the ECP pharmacophore.
- The results present ECP as a useful template for the development of new antimicrobial agents.

Chapter II:

- Antimicrobial and agglutinating activities of ECP are directly correlated with its interaction to the LPS moiety of the bacteria cell wall.
- Cell wall LPS is required for the agglutinating activity of either ECP or its N-terminal peptide ECP(1-45).
- ECP(6-17)~Ahx~(23-36) displays a different mechanism of action, LPS independent, with an enhanced membrane lytic activity respect to the parental protein.

Chapter III:

- Cell agglutination activity of ECP is required for the antimicrobial action of the protein and is directly correlated with bacterial mortality rates.
- Cell agglutination is mediated by protein self-aggregation at the bacteria surface.
- ECP aggregates formed on the surface of bacterial cell are of amyloid nature.

Chapter IV:

- The antimicrobial properties of human RNases are retained at their N-terminal domain.
- The antimicrobial N-terminal domain seems to be conserved in all vertebrate RNases suggesting that this region may have evolved to provide a host-defence function.
- These findings suggest that the N-terminal of antimicrobial RNases provide a suitable scaffold for the development of new antimicrobial agents.

Chapter V:

- Single point mutations on the ECP closest homologue EDN can switch on the protein bactericidal and agglutinating activities.
- Antimicrobial profile enhancement of EDN variants on bacterial killing, membrane leakage and LPS binding, reinforces the previous hypothesis on the antimicrobial role of ECP 24 to 45 N-terminal segment and the main role of W35 in the membrane destabilization process.
- Agglutinating activity determined for EDN variants reinforces the hypothesis of the key role of the hydrophobic N-terminal patch (residues 8 to 16) and, in particular, the contribution of I13 residue for the protein self-aggregation.

- The fact that antimicrobial and agglutinating properties were generated in EDN by only three point mutations highlight the potential of rational design of peptide-based antimicrobials using human RNases as a template.

Chapter VI:

- Antimycobacterial activity was determined for ECP and the skin derived RNase 7 showing that some members of the RNase A family display an effective cytotoxicity towards mycobacteria.
- The results support a putative physiological role of RNases secreted by eosinophils and epithelial tissues during mycobacterial infection
- The high potency of the antimicrobial and agglutinating profiles of the peptide ECP(1-45) offers a new perspective to develop new antimycobacterial strategies.

REFERENCES

5. References

1. Thomas S, Karnik S, Barai RS, Jayaraman VK, Idicula-Thomas S. CAMP: a useful resource for research on antimicrobial peptides. *Nucleic Acids Res.* 2010 Jan;38(Database issue):D774-80.
2. Yeung AT, Gellatly SL, Hancock RE. Multifunctional cationic host defence peptides and their clinical applications. *Cell Mol Life Sci.* 2011 Jul;68(13):2161-76.
3. Nakatsuji T, Gallo RL. Antimicrobial peptides: old molecules with new ideas. *J Invest Dermatol.* 2012 Mar;132(3 Pt 2):887-95.
4. Zasloff M. Antimicrobial peptides of multicellular organisms. *Nature.* 2002 Jan 24;415(6870):389-95.
5. Yount NY, Bayer AS, Xiong YQ, Yeaman MR. Advances in antimicrobial peptide immunobiology. *Biopolymers.* 2006;84(5):435-58.
6. Otvos L, Jr. Antibacterial peptides and proteins with multiple cellular targets. *J Pept Sci.* 2005 Nov;11(11):697-706.
7. Nibbering PH, Ravensbergen E, Welling MM, van Berkel LA, van Berkel PH, Pauwels EK, et al. Human lactoferrin and peptides derived from its N terminus are highly effective against infections with antibiotic-resistant bacteria. *Infect Immun.* 2001 Mar;69(3):1469-76.
8. Powers JP, Hancock RE. The relationship between peptide structure and antibacterial activity. *Peptides.* 2003 Nov;24(11):1681-91.
9. Diamond G, Beckloff N, Weinberg A, Kisich KO. The roles of antimicrobial peptides in innate host defense. *Curr Pharm Des.* 2009;15(21):2377-92.
10. Bhattacharjya S, Ramamoorthy A. Multifunctional host defense peptides: functional and mechanistic insights from NMR structures of potent antimicrobial peptides. *FEBS J.* 2009 Nov;276(22):6465-73.
11. Wiesner J, Vilcinskas A. Antimicrobial peptides: the ancient arm of the human immune system. *Virulence.* 2010 Sep-Oct;1(5):440-64.
12. Steiner H, Hultmark D, Engstrom A, Bennich H, Boman HG. Sequence and specificity of two antibacterial proteins involved in insect immunity. *Nature.* 1981 Jul 16;292(5820):246-8.
13. Bulet P, Stocklin R, Menin L. Anti-microbial peptides: from invertebrates to vertebrates. *Immunol Rev.* 2004 Apr;198:169-84.
14. Lee JY, Boman A, Sun CX, Andersson M, Jornvall H, Mutt V, et al. Antibacterial peptides from pig intestine: isolation of a mammalian cecropin. *Proc Natl Acad Sci U S A.* 1989 Dec;86(23):9159-62.
15. Holak TA, Engstrom A, Kraulis PJ, Lindeberg G, Bennich H, Jones TA, et al. The solution conformation of the antibacterial peptide cecropin A: a nuclear magnetic resonance and dynamical simulated annealing study. *Biochemistry.* 1988 Oct 4;27(20):7620-9.
16. Silvestro L, Axelsen PH. Membrane-induced folding of cecropin A. *Biophys J.* 2000 Sep;79(3):1465-77.
17. Bechinger B. Structure and functions of channel-forming peptides: magainins, cecropins, melittin and alamethicin. *J Membr Biol.* 1997 Apr 1;156(3):197-211.
18. Boman HG, Wade D, Boman IA, Wahlin B, Merrifield RB. Antibacterial and antimalarial properties of peptides that are cecropin-melittin hybrids. *FEBS Lett.* 1989 Dec 18;259(1):103-6.
19. Terwilliger TC, Eisenberg D. The structure of melittin. I. Structure determination and partial refinement. *J Biol Chem.* 1982 Jun 10;257(11):6010-5.
20. Frey S, Tamm LK. Orientation of melittin in phospholipid bilayers. A polarized attenuated total reflection infrared study. *Biophys J.* 1991 Oct;60(4):922-30.
21. Cornut I, Desbat B, Turlet JM, Dufourcq J. In situ study by polarization modulated Fourier transform infrared spectroscopy of the structure and orientation of lipids and amphipathic peptides at the air-water interface. *Biophys J.* 1996 Jan;70(1):305-12.

22. Yang L, Harroun TA, Weiss TM, Ding L, Huang HW. Barrel-stave model or toroidal model? A case study on melittin pores. *Biophys J*. 2001 Sep;81(3):1475-85.
23. Raghuraman H, Chattopadhyay A. Influence of lipid chain unsaturation on membrane-bound melittin: a fluorescence approach. *Biochim Biophys Acta*. 2004 Oct 11;1665(1-2):29-39.
24. Raghuraman H, Chattopadhyay A. Interaction of melittin with membrane cholesterol: a fluorescence approach. *Biophys J*. 2004 Oct;87(4):2419-32.
25. Raghuraman H, Chattopadhyay A. Effect of micellar charge on the conformation and dynamics of melittin. *Eur Biophys J*. 2004 Nov;33(7):611-22.
26. Raghuraman H, Ganguly S, Chattopadhyay A. Effect of ionic strength on the organization and dynamics of membrane-bound melittin. *Biophys Chem*. 2006 Nov 20;124(2):115-24.
27. Zasloff M. Magainins, a class of antimicrobial peptides from *Xenopus* skin: isolation, characterization of two active forms, and partial cDNA sequence of a precursor. *Proc Natl Acad Sci U S A*. 1987 Aug;84(15):5449-53.
28. Ali MF, Soto A, Knoop FC, Conlon JM. Antimicrobial peptides isolated from skin secretions of the diploid frog, *Xenopus tropicalis* (Pipidae). *Biochim Biophys Acta*. 2001 Nov 26;1550(1):81-9.
29. Pierre TN, Seon AA, Amiche M, Nicolas P. Phylloxin, a novel peptide antibiotic of the dermaseptin family of antimicrobial/opioid peptide precursors. *Eur J Biochem*. 2000 Jan;267(2):370-8.
30. Mignogna G, Simmaco M, Kreil G, Barra D. Antibacterial and haemolytic peptides containing D-alloisoleucine from the skin of *Bombina variegata*. *EMBO J*. 1993 Dec;12(12):4829-32.
31. Novkovic M, Simunic J, Bojovic V, Tossi A, Juretic D. DADP: the database of anuran defense peptides. *Bioinformatics*. 2012 May 15;28(10):1406-7.
32. Conlon JM. Structural diversity and species distribution of host-defense peptides in frog skin secretions. *Cell Mol Life Sci*. 2011 Jul;68(13):2303-15.
33. Conlon JM. The contribution of skin antimicrobial peptides to the system of innate immunity in anurans. *Cell Tissue Res*. 2010 Jan;343(1):201-12.
34. Nascimento AC, Fontes W, Sebben A, Castro MS. Antimicrobial peptides from anurans skin secretions. *Protein Pept Lett*. 2003 Jun;10(3):227-38.
35. Mangoni ML. Temporins, anti-infective peptides with expanding properties. *Cell Mol Life Sci*. 2006 May;63(9):1060-9.
36. Shai Y. Mechanism of the binding, insertion and destabilization of phospholipid bilayer membranes by alpha-helical antimicrobial and cell non-selective membrane-lytic peptides. *Biochim Biophys Acta*. 1999 Dec 15;1462(1-2):55-70.
37. Nascimento JM, Franco OL, Oliveira MD, Andrade CA. Evaluation of Magainin I interactions with lipid membranes: an optical and electrochemical study. *Chem Phys Lipids*. 2012 Jul;165(5):537-44.
38. Nguyen KT, Le Clair SV, Ye S, Chen Z. Molecular interactions between magainin 2 and model membranes in situ. *J Phys Chem B*. 2009 Sep 10;113(36):12358-63.
39. Davis RW, Arango DC, Jones HD, Van Benthem MH, Haaland DM, Brozik SM, et al. Antimicrobial peptide interactions with silica bead supported bilayers and *E. coli*: buforin II, magainin II, and arenicin. *J Pept Sci*. 2009 Aug;15(8):511-22.
40. Nijnik A, Hancock R. Host defence peptides: antimicrobial and immunomodulatory activity and potential applications for tackling antibiotic-resistant infections. *Emerg Health Threats J*. 2009;2:e1.
41. Bucki R, Leszczynska K, Namiot A, Sokolowski W. Cathelicidin LL-37: a multitask antimicrobial peptide. *Arch Immunol Ther Exp (Warsz)*. 2010 Feb;58(1):15-25.
42. Huttner KM, Bevins CL. Antimicrobial peptides as mediators of epithelial host defense. *Pediatr Res*. 1999 Jun;45(6):785-94.

43. Gennaro R, Zanetti M. Structural features and biological activities of the cathelicidin-derived antimicrobial peptides. *Biopolymers*. 2000;55(1):31-49.
44. Pasupuleti M, Schmidtchen A, Malmsten M. Antimicrobial peptides: key components of the innate immune system. *Crit Rev Biotechnol*. 2011 Jun;32(2):143-71.
45. Ganz T. Defensins: antimicrobial peptides of innate immunity. *Nat Rev Immunol*. 2003 Sep;3(9):710-20.
46. Yamaguchi Y, Ouchi Y. Antimicrobial peptide defensin: identification of novel isoforms and the characterization of their physiological roles and their significance in the pathogenesis of diseases. *Proc Jpn Acad Ser B Phys Biol Sci*. 2012;88(4):152-66.
47. Stotz HU, Thomson JG, Wang Y. Plant defensins: defense, development and application. *Plant Signal Behav*. 2009 Nov;4(11):1010-2.
48. Matsuzaki K, Sugishita K, Miyajima K. Interactions of an antimicrobial peptide, magainin 2, with lipopolysaccharide-containing liposomes as a model for outer membranes of gram-negative bacteria. *FEBS Lett*. 1999 Apr 23;449(2-3):221-4.
49. Doherty T, Waring AJ, Hong M. Peptide-lipid interactions of the beta-hairpin antimicrobial peptide tachyplesin and its linear derivatives from solid-state NMR. *Biochim Biophys Acta*. 2006 Sep;1758(9):1285-91.
50. Ostberg N, Kaznessis Y. Protegrin structure-activity relationships: using homology models of synthetic sequences to determine structural characteristics important for activity. *Peptides*. 2005 Feb;26(2):197-206.
51. Tsubery H, Ofek I, Cohen S, Fridkin M. Structure activity relationship study of polymyxin B nonapeptide. *Adv Exp Med Biol*. 2000;479:219-22.
52. Ovchinnikova TV, Aleshina GM, Balandin SV, Krasnosdembkaya AD, Markelov ML, Frolova EI, et al. Purification and primary structure of two isoforms of arenicin, a novel antimicrobial peptide from marine polychaeta *Arenicola marina*. *FEBS Lett*. 2004 Nov 5;577(1-2):209-14.
53. Imamura T, Yasuda M, Kusano H, Nakashita H, Ohno Y, Kamakura T, et al. Acquired resistance to the rice blast in transgenic rice accumulating the antimicrobial peptide thanatin. *Transgenic Res*. 2009 Jun;19(3):415-24.
54. Pazgier M, Prah A, Hoover DM, Lubkowski J. Studies of the biological properties of human beta-defensin 1. *J Biol Chem*. 2007 Jan 19;282(3):1819-29.
55. Wilmes M, Cammue BP, Sahl HG, Thevissen K. Antibiotic activities of host defense peptides: more to it than lipid bilayer perturbation. *Nat Prod Rep*. 2011 Aug;28(8):1350-8.
56. Selsted ME, Novotny MJ, Morris WL, Tang YQ, Smith W, Cullor JS. Indolicidin, a novel bactericidal tridecapeptide amide from neutrophils. *J Biol Chem*. 1992 Mar 5;267(7):4292-5.
57. Hsu CH, Chen C, Jou ML, Lee AY, Lin YC, Yu YP, et al. Structural and DNA-binding studies on the bovine antimicrobial peptide, indolicidin: evidence for multiple conformations involved in binding to membranes and DNA. *Nucleic Acids Res*. 2005;33(13):4053-64.
58. Rozek A, Friedrich CL, Hancock RE. Structure of the bovine antimicrobial peptide indolicidin bound to dodecylphosphocholine and sodium dodecyl sulfate micelles. *Biochemistry*. 2000 Dec 26;39(51):15765-74.
59. Devine DA, Hancock RE. Cationic peptides: distribution and mechanisms of resistance. *Curr Pharm Des*. 2002;8(9):703-14.
60. Rijnkels M, Elnitski L, Miller W, Rosen JM. Multispecies comparative analysis of a mammalian-specific genomic domain encoding secretory proteins. *Genomics*. 2003 Oct;82(4):417-32.
61. Campese M, Sun X, Bosch JA, Oppenheim FG, Helmerhorst EJ. Concentration and fate of histatins and acidic proline-rich proteins in the oral environment. *Arch Oral Biol*. 2009 Apr;54(4):345-53.
62. De Smet K, Contreras R. Human antimicrobial peptides: defensins, cathelicidins and histatins. *Biotechnol Lett*. 2005 Sep;27(18):1337-47.

63. Bechinger B. Insights into the mechanisms of action of host defence peptides from biophysical and structural investigations. *J Pept Sci.* 2011 May;17(5):306-14.
64. Dziarski R. Peptidoglycan recognition proteins (PGRPs). *Mol Immunol.* 2004 Feb;40(12):877-86.
65. Yen CC, Shen CJ, Hsu WH, Chang YH, Lin HT, Chen HL, et al. Lactoferrin: an iron-binding antimicrobial protein against *Escherichia coli* infection. *Biometals.* 2011 Aug;24(4):585-94.
66. Wakabayashi H, Takase M, Tomita M. Lactoferricin derived from milk protein lactoferrin. *Curr Pharm Des.* 2003;9(16):1277-87.
67. Teixeira V, Feio MJ, Bastos M. Role of lipids in the interaction of antimicrobial peptides with membranes. *Prog Lipid Res.* 2012 Apr;51(2):149-77.
68. Giangaspero A, Sandri L, Tossi A. Amphipathic alpha helical antimicrobial peptides. *Eur J Biochem.* 2001 Nov;268(21):5589-600.
69. Chan DI, Prenner EJ, Vogel HJ. Tryptophan- and arginine-rich antimicrobial peptides: structures and mechanisms of action. *Biochim Biophys Acta.* 2006 Sep;1758(9):1184-202.
70. Seelig J. Thermodynamics of lipid-peptide interactions. *Biochim Biophys Acta.* 2004 Nov 3;1666(1-2):40-50.
71. Lugtenberg EJ, Peters R. Distribution of lipids in cytoplasmic and outer membranes of *Escherichia coli* K12. *Biochim Biophys Acta.* 1976 Jul 20;441(1):38-47.
72. Niyonsaba F, Nagaoka I, Ogawa H. Human defensins and cathelicidins in the skin: beyond direct antimicrobial properties. *Crit Rev Immunol.* 2006;26(6):545-76.
73. Papanastasiou EA, Hua Q, Sandouk A, Son UH, Christenson AJ, Van Hoek ML, et al. Role of acetylation and charge in antimicrobial peptides based on human beta-defensin-3. *APMIS.* 2009 Jul;117(7):492-9.
74. Pasupuleti M, Walse B, Svensson B, Malmsten M, Schmidtchen A. Rational design of antimicrobial C3a analogues with enhanced effects against *Staphylococci* using an integrated structure and function-based approach. *Biochemistry.* 2008 Sep 2;47(35):9057-70.
75. Watson JL, Gillies ER. Amphipathic beta-strand mimics as potential membrane disruptive antibiotics. *J Org Chem.* 2009 Aug 21;74(16):5953-60.
76. Jiang Z, Vasil AI, Hale JD, Hancock RE, Vasil ML, Hodges RS. Effects of net charge and the number of positively charged residues on the biological activity of amphipathic alpha-helical cationic antimicrobial peptides. *Biopolymers.* 2008;90(3):369-83.
77. Uematsu N, Matsuzaki K. Polar angle as a determinant of amphipathic alpha-helix-lipid interactions: a model peptide study. *Biophys J.* 2000 Oct;79(4):2075-83.
78. Wimley WC. Describing the mechanism of antimicrobial peptide action with the interfacial activity model. *ACS Chem Biol.* 2010 Oct 15;5(10):905-17.
79. Rahnamaeian M. Antimicrobial peptides: modes of mechanism, modulation of defense responses. *Plant Signal Behav.* 2011 Sep;6(9):1325-32.
80. Vedovato N, Rispoli G. A novel technique to study pore-forming peptides in a natural membrane. *Eur Biophys J.* 2007 Sep;36(7):771-8.
81. Tang M, Hong M. Structure and mechanism of beta-hairpin antimicrobial peptides in lipid bilayers from solid-state NMR spectroscopy. *Mol Biosyst.* 2009 Apr;5(4):317-22.
82. Sengupta D, Leontiadou H, Mark AE, Marrink SJ. Toroidal pores formed by antimicrobial peptides show significant disorder. *Biochim Biophys Acta.* 2008 Oct;1778(10):2308-17.
83. Brogden KA. Antimicrobial peptides: pore formers or metabolic inhibitors in bacteria? *Nat Rev Microbiol.* 2005 Mar;3(3):238-50.
84. Epanand RM, Epanand RF. Bacterial membrane lipids in the action of antimicrobial agents. *J Pept Sci.* 2011 May;17(5):298-305.
85. Mattila JP, Sabatini K, Kinnunen PK. Oxidized phospholipids as potential molecular targets for antimicrobial peptides. *Biochim Biophys Acta.* 2008 Oct;1778(10):2041-50.

86. van Kan EJ, Demel RA, Breukink E, van der Bent A, de Kruijff B. Clavanin permeabilizes target membranes via two distinctly different pH-dependent mechanisms. *Biochemistry*. 2002 Jun 18;41(24):7529-39.
87. Lan Y, Ye Y, Kozłowska J, Lam JK, Drake AF, Mason AJ. Structural contributions to the intracellular targeting strategies of antimicrobial peptides. *Biochim Biophys Acta*. 2010 Oct;1798(10):1934-43.
88. Gifford JL, Hunter HN, Vogel HJ. Lactoferricin: a lactoferrin-derived peptide with antimicrobial, antiviral, antitumor and immunological properties. *Cell Mol Life Sci*. 2005 Nov;62(22):2588-98.
89. Sass V, Schneider T, Wilmes M, Korner C, Tossi A, Novikova N, et al. Human beta-defensin 3 inhibits cell wall biosynthesis in Staphylococci. *Infect Immun*. 2010 Jun;78(6):2793-800.
90. Nguyen LT, Haney EF, Vogel HJ. The expanding scope of antimicrobial peptide structures and their modes of action. *Trends Biotechnol*. 2011 Sep;29(9):464-72.
91. Hancock RE, Nijnik A, Philpott DJ. Modulating immunity as a therapy for bacterial infections. *Nat Rev Microbiol*. 2012 Apr;10(4):243-54.
92. Pulido D, Nogues MV, Boix E, Torrent M. Lipopolysaccharide neutralization by antimicrobial peptides: a gambit in the innate host defense strategy. *J Innate Immun*. 2012;4(4):327-36.
93. Bowdish DM, Davidson DJ, Lau YE, Lee K, Scott MG, Hancock RE. Impact of LL-37 on anti-infective immunity. *J Leukoc Biol*. 2005 Apr;77(4):451-9.
94. Territo MC, Ganz T, Selsted ME, Lehrer R. Monocyte-chemotactic activity of defensins from human neutrophils. *J Clin Invest*. 1989 Dec;84(6):2017-20.
95. Carretero M, Escamez MJ, Garcia M, Duarte B, Holguin A, Retamosa L, et al. In vitro and in vivo wound healing-promoting activities of human cathelicidin LL-37. *J Invest Dermatol*. 2008 Jan;128(1):223-36.
96. Funderburg N, Lederman MM, Feng Z, Drage MG, Jadowsky J, Harding CV, et al. Human - defensin-3 activates professional antigen-presenting cells via Toll-like receptors 1 and 2. *Proc Natl Acad Sci U S A*. 2007 Nov 20;104(47):18631-5.
97. Pasupuleti M, Schmidtchen A, Malmsten M. Antimicrobial peptides: key components of the innate immune system. *Crit Rev Biotechnol*. 2012 Jun;32(2):143-71.
98. Lupetti A, Welling MM, Pauwels EK, Nibbering PH. Radiolabelled antimicrobial peptides for infection detection. *Lancet Infect Dis*. 2003 Apr;3(4):223-9.
99. Velden WJ, van Iersel TM, Blijlevens NM, Donnelly JP. Safety and tolerability of the antimicrobial peptide human lactoferrin 1-11 (hLF1-11). *BMC Med*. 2009;7:44.
100. Fjell CD, Hiss JA, Hancock RE, Schneider G. Designing antimicrobial peptides: form follows function. *Nat Rev Drug Discov*. 2011 Jan;11(1):37-51.
101. Hancock RE. Cationic antimicrobial peptides: towards clinical applications. *Expert Opin Investig Drugs*. 2000 Aug;9(8):1723-9.
102. Kagan BL, Jang H, Capone R, Teran Arce F, Ramachandran S, Lal R, et al. Antimicrobial properties of amyloid peptides. *Mol Pharm*. 2011 Apr 2;9(4):708-17.
103. Hilpert K, Elliott M, Jenssen H, Kindrachuk J, Fjell CD, Korner J, et al. Screening and characterization of surface-tethered cationic peptides for antimicrobial activity. *Chem Biol*. 2009 Jan 30;16(1):58-69.
104. Desai TR, Wong JP, Hancock RE, Finlay WH. A novel approach to the pulmonary delivery of liposomes in dry powder form to eliminate the deleterious effects of milling. *J Pharm Sci*. 2002 Feb;91(2):482-91.
105. Choudhary A, Raines RT. An evaluation of peptide-bond isosteres. *Chembiochem*. 2011 Aug 16;12(12):1801-7.
106. Beintema JJ, Kleineidam RG. The ribonuclease A superfamily: general discussion. *Cell Mol Life Sci*. 1998 Aug;54(8):825-32.
107. Cuchillo CM, Nogues MV, Raines RT. Bovine pancreatic ribonuclease: fifty years of the first enzymatic reaction mechanism. *Biochemistry*. Sep 20;50(37):7835-41.

108. Sorrentino S. The eight human "canonical" ribonucleases: molecular diversity, catalytic properties, and special biological actions of the enzyme proteins. *FEBS Lett.* Jun 3;584(11):2194-200.
109. Boix E, Salazar VA, Torrent M, Pulido D, Nogues MV, Moussaoui M. Structural determinants of the eosinophil cationic protein antimicrobial activity. *Biol Chem.* Aug;393(8):801-15.
110. Cho S, Zhang J. Zebrafish ribonucleases are bactericidal: implications for the origin of the vertebrate RNase A superfamily. *Molecular biology and evolution.* [Research Support, N.I.H., Extramural]. 2007 May;24(5):1259-68.
111. Pizzo E, D'Alessio G. The success of the RNase scaffold in the advance of biosciences and in evolution. *Gene.* 2007 Dec 30;406(1-2):8-12.
112. Rosenberg HF. RNase A ribonucleases and host defense: an evolving story. *J Leukoc Biol.* 2008 May;83(5):1079-87.
113. Boix E, Salazar VA, Torrent M, Pulido D, Nogues MV, Moussaoui M. Structural determinants of the eosinophil cationic protein antimicrobial activity. *Biol Chem.* 2012 Aug;393(8):801-15.
114. Beintema JJ, Blank A, Schieven GL, Dekker CA, Sorrentino S, Libonati M. Differences in glycosylation pattern of human secretory ribonucleases. *Biochem J.* 1988 Oct 15;255(2):501-5.
115. Sorrentino S. The eight human "canonical" ribonucleases: Molecular diversity, catalytic properties, and special biological actions of the enzyme proteins. *Febs Letters.* 2010 Jun 3;584(11):2194-200.
116. Clark HF, Gurney AL, Abaya E, Baker K, Baldwin D, Brush J, et al. The Secreted Protein Discovery Initiative (SPDI), a large-scale effort to identify novel human secreted and transmembrane proteins: A bioinformatics assessment. *Genome Research.* 2003 Oct;13(10):2265-70.
117. Krieg J, Hartmann S, Vicentini A, Glasner W, Hess D, Hofsteenge J. Recognition signal for C-mannosylation of Trp-7 in RNase 2 consists of sequence Trp-x-x-Trp. *Molecular Biology of the Cell.* 1998 Feb;9(2):301-9.
118. Ulrich M, Petre A, Youhnovski N, Promm F, Schirle M, Schumm M, et al. Post-translational tyrosine nitration of eosinophil granule toxins mediated by eosinophil peroxidase. *J Biol Chem.* 2008 Oct 17;283(42):28629-40.
119. Rosenberg HF. Eosinophil-derived neurotoxin/ RNase 2: connecting the Past, the Present and the Future. *Current Pharm Biotec.* 2008;9:135-40.
120. Torrent M, de la Torre BG, Nogues VM, Andreu D, Boix E. Bactericidal and membrane disruption activities of the eosinophil cationic protein are largely retained in an N-terminal fragment. *Biochem J.* 2009 Aug 1;421(3):425-34.
121. Torrent M, Pulido D, De la Torre BG, Garcia de la Torre J, Nogues MV, Bruix M, et al. Refining the Eosinophil Cationic Protein Antibacterial Pharmacophore by Rational Structure Minimization. *Journal of Medicinal Chemistry.* 2011;54:7.
122. Eriksson J, Reimert CM, Kabatereine NB, Kazibwe F, Ileri E, Kadzo H, et al. The 434(G>C) polymorphism within the coding sequence of Eosinophil Cationic Protein (ECP) correlates with the natural course of *Schistosoma mansoni* infection. *Int J Parasitol.* 2007 Oct;37(12):1359-66.
123. Adu B, Doodoo D, Adukpo S, Gyan BA, Hedley PL, Goka B, et al. Polymorphisms in the RNASE3 gene are associated with susceptibility to cerebral malaria in Ghanaian children. *PLoS One.* 2011;6:e29465.
124. Eriksson J, Woschnagg C, Fernvik E, Venge P. A SELDI-TOF MS study of the genetic and post-translational molecular heterogeneity of eosinophil cationic protein. *J Leukoc Biol.* 2007 Dec;82(6):1491-500.
125. Woschnagg C, Rubin J, Venge P. Eosinophil cationic protein (ECP) is processed during secretion. *J Immunol.* 2009 Sep 15;183(6):3949-54.

126. Venge P, Bystrom J, Carlson M, Hakansson L, Karawaczyk M, Peterson C, et al. Eosinophil cationic protein (ECP): molecular and biological properties and the use of ECP as a marker of eosinophil activation in disease. *Clin Exp Allergy*. 1999 Sep;29(9):1172-86.
127. Boix E, Torrent M, Sánchez D, Nogués MV. The Antipathogen Activities of Eosinophil Cationic Protein. *Current Pharm Biotec*. 2008;9:141-52.
128. Bystrom J, Amin K, Bishop-Bailey D. Analysing the eosinophil cationic protein - a clue to the function of the eosinophil granulocyte. *Respiratory Research*. 2011 Jan 14;12.
129. Hofsteenge J, Vicentini A, Zelenko O. Ribonuclease 4, an evolutionarily highly conserved member of the superfamily. *Cellular and Molecular Life Sciences*. 1998 Aug;54(8):804-10.
130. Hooper LV, Stappenbeck TS, Hong CV, Gordon JI. Angiogenins: a new class of microbicidal proteins involved in innate immunity. *Nat Immunol*. 2003 Mar;4(3):269-73.
131. Abtin A, Eckhart L, Mildner M, Ghannadan M, Harder J, Schroder JM, et al. Degradation by Stratum Corneum Proteases Prevents Endogenous RNase Inhibitor from Blocking Antimicrobial Activities of RNase 5 and RNase 7. *Journal of Investigative Dermatology*. 2009 Sep;129(9):2193-201.
132. Greenway MJ, Andersen PM, Russ C, Ennis S, Cashman S, Donaghy C, et al. ANG mutations segregate with familial and 'sporadic' amyotrophic lateral sclerosis. *Nature Genetics*. 2006 Apr;38(4):411-3.
133. Strydom DJ, Fett JW, Lobb RR, Alderman EM, Bethune JL, Riordan JF, et al. Amino-Acid Sequence of Human-Tumor Derived Angiogenin. *Biochemistry*. 1985;24(20):5486-94.
134. Moenner M, Gusse M, Hatzi E, Badet J. The widespread expression of angiogenin in different human cells suggests a biological function not only related to angiogenesis. *Eur J Biochem*. 1994 Dec 1;226(2):483-90.
135. Strydom DJ. The angiogenins. *Cell Mol Life Sci*. 1998 Aug;54(8):811-24.
136. Gao XW, Xu ZP. Mechanisms of action of angiogenin. *Acta Biochimica Et Biophysica Sinica*. 2008 Jul;40(7):619-24.
137. Rosenberg HF, Dyer KD. Molecular cloning and characterization of a novel human ribonuclease (RNase k6): Increasing diversity in the enlarging ribonuclease gene family. *Nucleic Acids Research*. 1996 Sep 15;24(18):3507-13.
138. Dyer KD, Rosenberg HF, Zhang JZ. Isolation, characterization, and evolutionary divergence of mouse RNase 6: Evidence for unusual evolution in rodents. *Journal of Molecular Evolution*. 2004 Nov;59(5):657-65.
139. Harder J, Schroder JM. RNase 7, a novel innate immune defense antimicrobial protein of healthy human skin. *J Biol Chem*. 2002 Nov 29;277(48):46779-84.
140. Zhang J, Dyer KD, Rosenberg HF. Human RNase 7: a new cationic ribonuclease of the RNase A superfamily. *Nucleic Acids Res*. 2003 Jan 15;31(2):602-7.
141. Simanski M, Köten B, Schröder JM, Gläser R, Harder J. Antimicrobial RNases in Cutaneous Defense. *Journal of Innate Immunity*. 2012;4:241-7.
142. Spencer JD, Schwaderer AL, DiRosario JD, McHugh KM, McGillivray G, Justice SS, et al. Ribonuclease 7 is a potent antimicrobial peptide within the human urinary tract. *Kidney International*. 2011 Jul;80(2):175-81.
143. Rudolph B, Podschun R, Sahly H, Schubert S, Schroder JM, Harder J. Identification of RNase 8 as a novel human antimicrobial protein. *Antimicrob Agents Chemother*. 2006 Sep;50(9):3194-6.
144. Zhang J, Dyer KD, Rosenberg HF. RNase 8, a novel RNase A superfamily ribonuclease expressed uniquely in placenta. *Nucleic Acids Res*. 2002 Mar 1;30(5):1169-75.
145. Chan CC, Moser JM, Dyer KD, Percopo CM, Rosenberg HF. Genetic diversity of human RNase 8. *BMC Genomics*. 2012;13:40.
146. Rosenberg HF, Dyer KD, Tiffany HL, Gonzalez M. Rapid evolution of a unique family of primate ribonuclease genes. *Nat Genet*. 1995 Jun;10(2):219-23.
147. Zhang J, Rosenberg HF, Nei M. Positive Darwinian selection after gene duplication in primate ribonuclease genes. *Proc Natl Acad Sci U S A*. 1998 Mar 31;95(7):3708-13.

148. Hamann KJ, Ten RM, Loegering DA, Jenkins RB, Heise MT, Schad CR, et al. Structure and chromosome localization of the human eosinophil-derived neurotoxin and eosinophil cationic protein genes: evidence for intronless coding sequences in the ribonuclease gene superfamily. *Genomics*. 1990 Aug;7(4):535-46.
149. Zhang J, Rosenberg HF. Complementary advantageous substitutions in the evolution of an antiviral RNase of higher primates. *Proc Natl Acad Sci U S A*. 2002 Apr 16;99(8):5486-91.
150. Dyer KD, Rosenberg HF. The RNase a superfamily: generation of diversity and innate host defense. *Molecular diversity*. [Research Support, N.I.H., Intramural Review]. 2006 Nov;10(4):585-97.
151. Boix E, Leonidas DD, Nikolovski Z, Nogues MV, Cuchillo CM, Acharya KR. Crystal structure of eosinophil cationic protein at 2.4 Å resolution. *Biochemistry*. 1999 Dec 21;38(51):16794-801.
152. Durack DT, Ackerman SJ, Loegering DA, Gleich GJ. Purification of human eosinophil-derived neurotoxin. *Proc Natl Acad Sci U S A*. 1981 Aug;78(8):5165-9.
153. Leonidas DD, Boix E, Prill R, Suzuki M, Turton R, Minson K, et al. Mapping the ribonucleolytic active site of eosinophil-derived neurotoxin (EDN). High resolution crystal structures of EDN complexes with adenylic nucleotide inhibitors. *J Biol Chem*. 2001 May 4;276(18):15009-17.
154. Yang D, Rosenberg HF, Chen Q, Dyer KD, Kurosaka K, Oppenheim JJ. Eosinophil-derived neurotoxin (EDN), an antimicrobial protein with chemotactic activities for dendritic cells. *Blood*. 2003 Nov 1;102(9):3396-403.
155. Lehrer RI, Szklarek D, Barton A, Ganz T, Hamann KJ, Gleich GJ. Antibacterial properties of eosinophil major basic protein and eosinophil cationic protein. *J Immunol*. 1989 Jun 15;142(12):4428-34.
156. Rosenberg HF, Dyer KD. Eosinophil cationic protein and eosinophil-derived neurotoxin. Evolution of novel function in a primate ribonuclease gene family. *J Biol Chem*. 1995 Dec 15;270(50):30234.
157. Hamann KJ, Gleich GJ, Checkel JL, Loegering DA, McCall JW, Barker RL. In vitro killing of microfilariae of *Brugia pahangi* and *Brugia malayi* by eosinophil granule proteins. *J Immunol*. 1990 Apr 15;144(8):3166-73.
158. Garofalo R, Kimpen JL, Welliver RC, Ogra PL. Eosinophil degranulation in the respiratory tract during naturally acquired respiratory syncytial virus infection. *J Pediatr*. 1992 Jan;120(1):28-32.
159. Harrison AM, Bonville CA, Rosenberg HF, Domachowske JB. Respiratory syncytial virus-induced chemokine expression in the lower airways: eosinophil recruitment and degranulation. *Am J Respir Crit Care Med*. 1999 Jun;159(6):1918-24.
160. Domachowske JB, Dyer KD, Bonville CA, Rosenberg HF. Recombinant human eosinophil-derived neurotoxin/RNase 2 functions as an effective antiviral agent against respiratory syncytial virus. *J Infect Dis*. 1998 Jun;177(6):1458-64.
161. Rosenberg HF. Eosinophil-derived neurotoxin / RNase 2: connecting the past, the present and the future. *Curr Pharm Biotechnol*. 2008 Jun;9(3):135-40.
162. Yang D, Chen Q, Rosenberg HF, Rybak SM, Newton DL, Wang ZY, et al. Human ribonuclease A superfamily members, eosinophil-derived neurotoxin and pancreatic ribonuclease, induce dendritic cell maturation and activation. *J Immunol*. 2004 Nov 15;173(10):6134-42.
163. Yang D, Chen Q, Su SB, Zhang P, Kurosaka K, Caspi RR, et al. Eosinophil-derived neurotoxin acts as an alarmin to activate the TLR2-MyD88 signal pathway in dendritic cells and enhances Th2 immune responses. *J Exp Med*. 2008 Jan 21;205(1):79-90.
164. Oppenheim JJ, Tewary P, de la Rosa G, Yang D. Alarmins initiate host defense. *Adv Exp Med Biol*. 2007;601:185-94.
165. Bystrom J, Amin K, Bishop-Bailey D. Analysing the eosinophil cationic protein--a clue to the function of the eosinophil granulocyte. *Respir Res*.12:10.

166. Laurents DV, Bruix M, Jimenez MA, Santoro J, Boix E, Moussaoui M, et al. The (1)H, (13)C, (15)N resonance assignment, solution structure, and residue level stability of eosinophil cationic protein/RNase 3 determined by NMR spectroscopy. *Biopolymers*. 2009 Dec;91(12):1018-28.
167. Carreras E, Boix E, Rosenberg HF, Cuchillo CM, Nogues MV. Both aromatic and cationic residues contribute to the membrane-lytic and bactericidal activity of eosinophil cationic protein. *Biochemistry*. 2003 Jun 10;42(22):6636-44.
168. McLaren DJ, Peterson CG, Venge P. *Schistosoma mansoni*: further studies of the interaction between schistosomula and granulocyte-derived cationic proteins in vitro. *Parasitology*. 1984 Jun;88 (Pt 3):491-503.
169. Singh A, Batra JK. Role of unique basic residues in cytotoxic, antibacterial and antiparasitic activities of human eosinophil cationic protein. *Biol Chem*. Apr;392(4):337-46.
170. Elshafie AI, Hlin E, Hakansson LD, Elghazali G, Safi SH, Ronnelid J, et al. Activity and turnover of eosinophil and neutrophil granulocytes are altered in visceral leishmaniasis. *Int J Parasitol*. Mar;41(3-4):463-9.
171. Kierszenbaum F, Villalta F, Tai PC. Role of inflammatory cells in Chagas' disease. III. Kinetics of human eosinophil activation upon interaction with parasites (*Trypanosoma cruzi*). *J Immunol*. 1986 Jan;136(2):662-6.
172. Waters LS, Taverne J, Tai PC, Spry CJ, Targett GA, Playfair JH. Killing of *Plasmodium falciparum* by eosinophil secretory products. *Infect Immun*. 1987 Apr;55(4):877-81.
173. Venge P, Bystrom J. Eosinophil cationic protein (ECP). *Int J Biochem Cell Biol*. 1998 Apr;30(4):433-7.
174. Rosenberg HF. Recombinant human eosinophil cationic protein. Ribonuclease activity is not essential for cytotoxicity. *The Journal of biological chemistry*. 1995 Apr 7;270(14):7876-81.
175. Maeda T, Kitazoe M, Tada H, de Llorens R, Salomon DS, Ueda M, et al. Growth inhibition of mammalian cells by eosinophil cationic protein. *Eur J Biochem*. 2002 Jan;269(1):307-16.
176. de Oliveira PC, de Lima PO, Oliveira DT, Pereira MC. Eosinophil cationic protein: overview of biological and genetic features. *DNA Cell Biol*. 2012 Sep;31(9):1442-6.
177. Torrent M, Navarro S, Moussaoui M, Nogues MV, Boix E. Eosinophil cationic protein high-affinity binding to bacteria-wall lipopolysaccharides and peptidoglycans. *Biochemistry*. 2008 Mar 18;47(11):3544-55.
178. Torrent M, Nogues MV, Boix E. Eosinophil cationic protein (ECP) can bind heparin and other glycosaminoglycans through its RNase active site. *J Mol Recognit*. 2010 Jan-Feb;24(1):90-100.
179. Hung SC, Lu XA, Lee JC, Chang MD, Fang SL, Fan TC, et al. Synthesis of heparin oligosaccharides and their interaction with eosinophil-derived neurotoxin. *Org Biomol Chem*. 2011 Jan 28;10(4):760-72.
180. Torrent M, Cuyas E, Carreras E, Navarro S, Lopez O, de la Maza A, et al. Topography studies on the membrane interaction mechanism of the eosinophil cationic protein. *Biochemistry*. 2007 Jan 23;46(3):720-33.
181. Torrent M, Sanchez D, Buzon V, Nogues MV, Cladera J, Boix E. Comparison of the membrane interaction mechanism of two antimicrobial RNases: RNase 3/ECP and RNase 7. *Biochim Biophys Acta*. 2009 May;1788(5):1116-25.
182. Torrent M, Odorizzi F, Nogues MV, Boix E. Eosinophil cationic protein aggregation: identification of an N-terminus amyloid prone region. *Biomacromolecules*. 2010 Aug 9;11(8):1983-90.
183. Trulsson A, Nilsson S, Venge P. The eosinophil granule proteins in serum, but not the oxidative metabolism of the blood eosinophils, are increased in cancer. *Br J Haematol*. 1997 Aug;98(2):312-4.

184. Bystrom J, Garcia RC, Hakansson L, Karawajczyk M, Moberg L, Soukka J, et al. Eosinophil cationic protein is stored in, but not produced by, peripheral blood neutrophils. *Clin Exp Allergy*. 2002 Jul;32(7):1082-91.
185. Jonsson UB, Bystrom J, Stalenheim G, Venge P. Polymorphism of the eosinophil cationic protein-gene is related to the expression of allergic symptoms. *Clin Exp Allergy*. 2002 Jul;32(7):1092-5.
186. Legrand F, Driss V, Delbeke M, Loiseau S, Hermann E, Dombrowicz D, et al. Human eosinophils exert TNF-alpha and granzyme A-mediated tumoricidal activity toward colon carcinoma cells. *J Immunol*. 2010 Dec 15;185(12):7443-51.
187. Fett JW, Strydom DJ, Lobb RR, Alderman EM, Bethune JL, Riordan JF, et al. Isolation and characterization of angiogenin, an angiogenic protein from human carcinoma cells. *Biochemistry*. 1985 Sep 24;24(20):5480-6.
188. Chavali GB, Papageorgiou AC, Olson KA, Fett JW, Hu G, Shapiro R, et al. The crystal structure of human angiogenin in complex with an antitumor neutralizing antibody. *Structure*. 2003 Jul;11(7):875-85.
189. Forman RA, deSchoolmeester ML, Hurst RJ, Wright SH, Pemberton AD, Else KJ. The goblet cell is the cellular source of the anti-microbial angiogenin 4 in the large intestine post *Trichuris muris* infection. *PLoS One*. 2012;7(9):e42248.
190. Schroder JM, Harder J. Antimicrobial skin peptides and proteins. *Cell Mol Life Sci*. 2006 Feb;63(4):469-86.
191. Huang YC, Lin YM, Chang TW, Wu SJ, Lee YS, Chang MD, et al. The flexible and clustered lysine residues of human ribonuclease 7 are critical for membrane permeability and antimicrobial activity. *J Biol Chem*. 2007 Feb 16;282(7):4626-33.
192. Spencer JD, Schwaderer AL, Dirosario JD, McHugh KM, McGillivray G, Justice SS, et al. Ribonuclease 7 is a potent antimicrobial peptide within the human urinary tract. *Kidney Int*. 2011 Jul;80(2):174-80.
193. Wang H, Schwaderer AL, Kline J, Spencer JD, Kline D, Hains DS. Contribution of structural domains to the activity of ribonuclease 7 against uropathogenic bacteria. *Antimicrob Agents Chemother*. 2012 Feb;57(2):766-74.
194. Torrent M, Badia M, Moussaoui M, Sanchez D, Nogues MV, Boix E. Comparison of human RNase 3 and RNase 7 bactericidal action at the Gram-negative and Gram-positive bacterial cell wall. *FEBS J*. 2010 Apr;277(7):1713-25.
195. Nikaido H. Molecular basis of bacterial outer membrane permeability revisited. *Microbiol Mol Biol Rev*. 2003 Dec;67(4):593-656.
196. Prokhorenko IR, Zubova SV, Ivanov AY, Grachev SV. Interaction of Gram-negative bacteria with cationic proteins: Dependence on the surface characteristics of the bacterial cell. *Int J Gen Med*. 2009;2:33-8.
197. Pulido D, Moussaoui M, Andreu D, Nogues MV, Torrent M, Boix E. Antimicrobial action and cell agglutination by the eosinophil cationic protein are modulated by the cell wall lipopolysaccharide structure. *Antimicrob Agents Chemother*. 2012 May;56(5):2378-85.
198. Cohen J. The immunopathogenesis of sepsis. *Nature*. 2002 Dec 19-26;420(6917):885-91.
199. Torrent M, Pulido D, Nogues MV, Boix E. Exploring new biological functions of amyloids: bacteria cell agglutination mediated by host protein aggregation. *PLoS Pathog*. 2012;8(11):e1003005.
200. Torrent M, Pulido D, de la Torre BG, Garcia-Mayoral MF, Nogues MV, Bruix M, et al. Refining the eosinophil cationic protein antibacterial pharmacophore by rational structure minimization. *J Med Chem*. 2011 Jul 28;54(14):5237-44.
201. Torrent M, Pulido D, V J, Nogues MV, Andreu D, Boix E. Ribonucleases as a host-defense family: Evidence of evolutionary conserved antimicrobial activity at the N-terminus. *Biochemical Journal*. 2013;In revision.

202. Torrent M, Di Tommaso P, Pulido D, Nogues MV, Notredame C, Boix E, et al. AMPA: an automated web server for prediction of protein antimicrobial regions. *Bioinformatics*. Jan 1;28(1):130-1.
203. Torrent M, Di Tommaso P, Pulido D, Nogues MV, Notredame C, Boix E, et al. AMPA: an automated web server for prediction of protein antimicrobial regions. *Bioinformatics*. 2011 Jan 1;28(1):130-1.
204. Pulido D, Moussaoui M, Nogues MV, Torrent M, Boix E. Towards the rational design of antimicrobial proteins: single point mutations can switch on bactericidal and agglutinating activities on the RNase A superfamily lineage. *Biochemistry*. 2013;Submitted.
205. Bernard JJ, Gallo RL. Protecting the boundary: the sentinel role of host defense peptides in the skin. *Cell Mol Life Sci*. 2011 Jul;68(13):2189-99.
206. Pulido D, Torrent M, Nogues MV, Andreu D, Boix E. Two human host defense RNases against mycobacteria: the eosinophil cationic protein and the skin derived antimicrobial protein 2. *Antimicrob Agents Chemother*. 2013;In press.
207. Cemma M, Brumell JH. Interactions of pathogenic bacteria with autophagy systems. *Curr Biol*. 2012 Jul 10;22(13):R540-5.
208. Dye C, Glaziou P, Floyd K, Raviglione M. Prospects for tuberculosis elimination. *Annu Rev Public Health*. 2012 Mar 18;34:271-86.

ACKNOWLEDGEMENTS

6. Acknowledgements.

To better express my gratitude to all the people who have contributed to this work, I have written this section in catalan.

A la Dra. M. Victòria Nogués, a la Dra. Ester Boix, al Dr. Mohammed Moussaoui, al Dr. Marc Torrent i per últim a la Dra. Susanna Navarro per acollir-me al seu grup d'investigació i permetre'm iniciar una carrera investigadora; pel recolzament rebut, per la seva confiança durant tot aquest temps i pel seu interès en aquest treball. I especialment a la Dra. Ester Boix i al Dr. Marc Torrent per les tasques de direcció d'aquest treball. Sense ells res d'això no hagués estat possible.

Al Dr. David Andreu, a la Dra. Marta Bruix i a la Dra. M^a Flor García per tot l'ajut i la inestimable col·laboració que m'han brindat durant tot el procés de producció d'aquest treball.

Al meus companys de laboratori Vivian Salazar i José Blanco per ajudar-me i "aguantar-me" cada dia durant aquests quatre anys.

A tots el companys i companyes del departament per tot el suport que m'han donat fent més amenes tant les tasques experimentals com docents. I en especial a la "Colla del Tupper" per les magnífiques converses sobre "això i allò" i "com arreglar el món-en el temps de fer un cafè+piti"; i també per suposat a les "RMN-nenes" per animar-me els dies amb el seu bon humor i fent alguna que altre "xelita".

A la meva família, pares i avis per tot l'amor, suport i ajuda que m'han ofert durant tot el procés d'elaboració d'aquest treball. I en especial a la meva parella per haver aguantat cada dia les "alegries" i "penes" d'aquesta tesi.

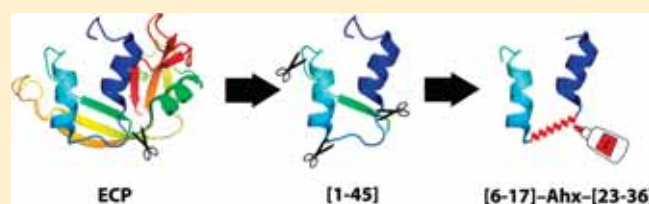
CHAPTER I

Refining the Eosinophil Cationic Protein Antibacterial Pharmacophore by Rational Structure Minimization

Marc Torrent,^{†,‡} David Pulido,[†] Beatriz G. de la Torre,[‡] M. Flor García-Mayoral,[§] M. Victòria Nogués,[†] Marta Bruix,[§] David Andreu,^{*,‡} and Ester Boix^{*,†}[†]Department of Biochemistry and Molecular Biology, Universitat Autònoma de Barcelona, E-08193 Cerdanyola del Vallès, Spain[‡]Department of Experimental and Health Sciences, Pompeu Fabra University, Barcelona Biomedical Research Park, Dr. Aiguader, 88, E-08003 Barcelona, Spain[§]Rocasolano Institute of Physical Chemistry, CSIC, Serrano 119, 28006 Madrid, Spain

S Supporting Information

ABSTRACT: Sequence analysis of eosinophil cationic protein (ECP), a ribonuclease of broad antimicrobial activity, allowed identification of residues 1–45 as the antimicrobial domain. We have further dissected ECP(1–45) with a view to defining the minimal requirements for antimicrobial activity. Structure-based downsizing has focused on both α -helices of ECP(1–45) and yielded analogues with substantial potency against Gram-negative and -positive strains. Analogues ECP(8–36) and ECP(6–17)-Ahx-(23–36) (Ahx, 6-aminohexanoic acid) involve 36% and 40% size reduction relative to (1–45), respectively, and display a remarkably ECP-like antimicrobial profile. Both retain segments required for self-aggregation and lipopolysaccharide binding, as well as the bacterial agglutination ability of parent ECP. Analogue (6–17)-Ahx-(23–36), in particular, is shown by NMR to preserve the helical traits of the native 8–16 (α 1) and 33–36 (α 2) regions and can be proposed as the minimal structure capable of reproducing the activity of the entire protein.



INTRODUCTION

An alarming increase in bacterial resistance to classical antibiotics has become a serious concern among health professionals and spurred intense efforts toward the development of new antimicrobial leads. In this context, antimicrobial peptides (AMPs) are viewed as promising candidates because of their substantial potency, broad spectrum, and distinct mechanism of action.¹ AMPs target bacterial membranes to which they are driven by mainly electrostatic interactions and which upon binding they disrupt, collapsing transmembrane gradients and eventually causing cell death.² Bacterial strategies for resisting AMPs require substantial membrane (phospholipid and protein) remodeling, a demanding task that explains the very low incidence of AMP resistance in bacteria.³

A number of AMPs are fragments of larger proteins, either naturally derived by proteolysis (e.g., the cathelicidins⁴) or derived by peptide synthesis approaches.⁵ In the latter case, educated deconstruction of complex antimicrobial proteins has allowed the identification of structural features essential for bioactivity.^{6,7} Although this pharmacophore dissection process is not straightforward and still requires a substantial amount of trial-and-error, it is worthwhile in that defining such minimal structural motifs provides helpful clues for developing therapeutically useful AMP templates.⁸

Eosinophil cationic protein (ECP, RNase 3) is a secretion ribonuclease used as a model for the potential involvement of

mammalian RNases in the host defense system.^{9,10} Expressed mainly in eosinophils and selectively released at the inflammation area,^{11,12} ECP is reportedly involved in immunoregulation and tissue remodeling processes.^{13,14} Its broad antibacterial spectrum includes both Gram-negative and -positive strains at a low micromolar range.¹⁵ Although its mechanism of action is not completely understood, ECP has been described to act through a carpet-like mechanism, causing membrane destabilization and subsequent vesiculation.¹⁶ ECP also has high affinity for bacterial cell wall components, such as lipopolysaccharide and peptidoglycans,¹⁷ and a strong tendency to aggregate *Escherichia coli* cells.¹⁸

A previous attempt to delineate the antibacterial domain of ECP led to the identification of the N-terminus (residues 1–45) as the main antibacterial domain of the protein.¹⁹ We have probed deeper into this region and in this paper describe how antimicrobially equipotent analogues of substantially reduced size (and consequently synthetic difficulty and costs) can be successfully derived from ECP by a structural minimization approach.

RESULTS AND DISCUSSION

Peptide Design and Synthesis. The starting point for a simplified ECP-derived antimicrobial lead candidate was the

Received: June 2, 2011

Published: June 22, 2011

Table 1. Sequence Information^a and Chemical Properties of ECP Analogues

Peptide	ECP residues	Sequence	HPLC retention time (min) ^b	[M+H] ⁺	
				Theory	Found
1	1-45	RPPQFTRAQWF ^{α1} AIQHISLNPPRSTIAMRAIN ^{α2} NYRWR ^{β1} SKNQNTFLR	5.05 (20-40%)	5479.91	5483.50 ^c
2	24-45	TIAMRAIN ^{α2} NYRWR ^{β1} SKNQNTFLR	6.13 (10-45%)	2752.46	2753.28
3	1-19	RPPQFTRAQWF ^{α1} AIQHISLN	6.19 (15-50%)	2310.22	2311.73
4	8-45	AQWF ^{α1} AIQHISLNPPRSTIAMRAIN ^{α2} NYRWR ^{β1} SKNQNTFLR	5.72 (15-60%)	4598.43	4598.88
5	8-36	AQWF ^{α1} AIQHISLNPPRSTIAMRAIN ^{α2} NYRWR	6.66 (15-50%)	3509.85	3510.54
6	16-45	ISLNPPRSTIAMRAIN ^{α2} NYRWR ^{β1} SKNQNTFLR	5.80 (10-60%)	3616.94	3617.87
7	(6-17)-(23-36)	TRAQWF ^{α1} AIQHIS-Ahx-STIAMRAIN ^{α2} NYRWR	6.79 (10-60%)	3302.75	3303.29
8	(8-15)-(23-36)	AQWF ^{α1} AIQH-Ahx-STIAMRAIN ^{α2} NYRWR	5.60 (15-60%)	2845.49	2845.26
9	(8-15)-(23-31)	AQWF ^{α1} AIQH-Ahx-STIAMRAIN	5.28 (15-60%)	2070.10	2070.00

^aSecondary structure elements (based on ECP structure) shown above peptide 1 sequence. ^bIn parentheses, linear gradient (solvent B into A over 15 min; see Experimental Section for details) used for optimal separation. ^cMALDI TOF mass spectrum acquired in the linear mode.

previously defined ECP N-terminal domain comprising the first 45 residues.¹⁹ ECP(1-45) (**1**, Table 1) preserved the antimicrobial properties of native ECP, bound LPS with high affinity, and could permeabilize lipid vesicles at submicromolar concentration. Dissection of this domain into two peptides containing respectively the α 1 and α 2 helices, namely, ECP(1-19) and ECP(24-45) (**2**, **3**; Table 1), met with only partial success, as antimicrobial activity was substantially reduced in both analogues, particularly in **2**.¹⁹ Recent NMR work on peptide **1**,²⁰ on the other hand, showed it to be partially unstructured in water and yet with two incipient α -helices closely matching α 1 and α 2 of native ECP, respectively, the latter expanding all the way down to the C-terminus of **1**. The α -helical trend was significantly enhanced in the presence of lipid vesicles, as is often the case. In light of these structural data, in our next attempt to define an ECP antimicrobial pharmacophore we have sought to keep together, albeit minimalistically, both α 1 and α 2 helical regions which, as usual in AMPs, are expected to be involved in membrane interaction. This hypothesis has led to a new set of analogues (**4-9**, Table 1) displaying various levels of ECP(1-45) sequence coverage and allowing outlining of a substantially simplified pharmacophore.

Three of the six new analogues entail various levels of trimming of the **1** sequence (Table 1), from moderate (**4**, first 7 N-terminal residues) to more drastic (**5**, first 7 N-terminal plus nine C-terminal; **6**, first 15 N-terminal residues), but all maintaining both α 1 and α 2 helical segments and an unsplit (internal) sequence. For the other three analogues (**7-9**), even more reductionistic criteria were applied, namely, dissecting out the 5-7 intervening loop residues (ISLNPPR) between α 1 and α 2 and replacing them by a flexible 6-aminohexanoic acid (Ahx) connector, an approach proven successful in linking discontinuous bioactive segments of polypeptide neurotransmitters.^{21,22}

All analogues were successfully prepared by Fmoc-based, solid phase peptide synthesis protocols,²³ purified to homogeneity by HPLC, and identified by MALDI-TOF mass spectrometry. As in our earlier ECP dissection exercise,¹⁹ the Cys23 and Cys37 residues, disulfide-bonded respectively to Cys83 and Cys96 and

keeping the N-terminus tied to the rest of the ECP structure, were mutated to Ser in all analogues to prevent formation of unwanted intra- or intermolecular disulfide-linked species.

Activity and Structure of ECP Analogues. The six new analogues (**4-9**) were tested for antimicrobial activity against three Gram-negative and three Gram-positive species (Table 2). As a broader panel of bacteria than in a previous study¹⁹ was available, both ECP and ECP(1-45) (**1**), the latter closely matching the former in antimicrobial spectrum,¹⁹ were retested as reference compounds, as were single-helix analogues **2** and **3**. Antimicrobial profiles were complemented by a hemolysis assay (Table 2) as a measure of toxicity toward eukaryotic cells and by CD spectroscopy to evaluate peptide structure in the presence of either SDS or bacterial lipopolysaccharide (LPS) (Figure 1, Table 3), two micelle-promoting, membrane-like environments, the latter being the fundamental component of the Gram-negative bacterial cell wall. In addition, assays for liposome leakage, LPS binding, and *E. coli* agglutination (Table 4) were performed, the last two regarded as descriptive parameters of AMP activity against Gram-negative bacteria.¹⁷ The goal of such an exhaustive comparison on both bacterial and artificial membrane systems was to outline the minimal sequence conferring antimicrobial properties to native ECP.

For analogues **1-3**, the above assays corroborated previous data,¹⁹ namely, (i) the practical equipotency of **1** and native ECP on a representative set of bacteria, with a certain preference for Gram-negatives and MIC values slightly in the submicromolar range, the only exception being *M. luteus* (Table 2), (ii) the decrease (1 log unit on average) of antimicrobial activity in **2** and its virtually complete loss in analogue **3**, indicative of the crucial role of both the α 2 and α 1 helical segments, especially the former one, (iii) a slight increase in hemolytic activity of peptides **1-3** relative to the native protein (Table 2), and (iv) a correlation between the level of peptide structuration (representative CD spectra in Table 3), on the one hand, and membrane lytic and LPS binding activities (Table 4).

Among the six new analogues, the first three (**4-6**) displayed various levels of sequence shortening at the N- or C-terminus or

Table 2. Bactericidal (MIC₁₀₀ in μM) and Hemolytic Activity (HC₅₀ in μM) of ECP and Analogues

peptide	size reduction vs 1 (%)	bactericidal activity						hemolytic activity
		<i>Escherichia coli</i>	<i>Pseudomonas</i> sp.	<i>Acinetobacter baumannii</i>	<i>Staphylococcus aureus</i>	<i>Micrococcus luteus</i>	<i>Enterococcus faecium</i>	
ECP		0.4 ± 0.1	0.62 ± 0.07	0.6 ± 0.1	0.40 ± 0.06	1.5 ± 0.3	0.87 ± 0.07	>25
1	100	0.62 ± 0.07	0.6 ± 0.1	0.6 ± 0.1	0.62 ± 0.07	1.5 ± 0.3	0.87 ± 0.07	11.7 ± 0.2
2	51	7 ± 1	7 ± 1	1.1 ± 0.2	1.5 ± 0.3	7 ± 1	7 ± 1	18.7 ± 0.1
3	48	>10	>10	>10	>10	>10	>10	11.2 ± 0.1
4	16	0.45 ± 0.09	1.5 ± 0.3	0.88 ± 0.07	0.7 ± 0.1	1.5 ± 0.3	1.5 ± 0.3	10.5 ± 0.2
5	36	1.5 ± 0.3	3.5 ± 0.9	1.5 ± 0.3	0.7 ± 0.1	3.5 ± 0.9	1.5 ± 0.3	10.3 ± 0.1
6	33	1.5 ± 0.3	1.5 ± 0.3	3.5 ± 0.9	1.5 ± 0.3	3.5 ± 0.9	3.5 ± 0.9	10.5 ± 0.2
7	40	0.6 ± 0.1	1.5 ± 0.3	0.88 ± 0.07	0.87 ± 0.07	1.5 ± 0.3	1.5 ± 0.3	7.3 ± 0.1
8	49	1.5 ± 0.3	3.5 ± 0.9	7 ± 1	1.1 ± 0.2	>10	>10	14.4 ± 0.1
9	60	>10	>10	>10	>10	>10	>10	15.2 ± 0.1
CA(1–8)M(1–18)		1.1 ± 0.2	0.6 ± 0.1	0.88 ± 0.07	0.4 ± 0.1	1.5 ± 0.3	1.5 ± 0.3	7.8 ± 0.2

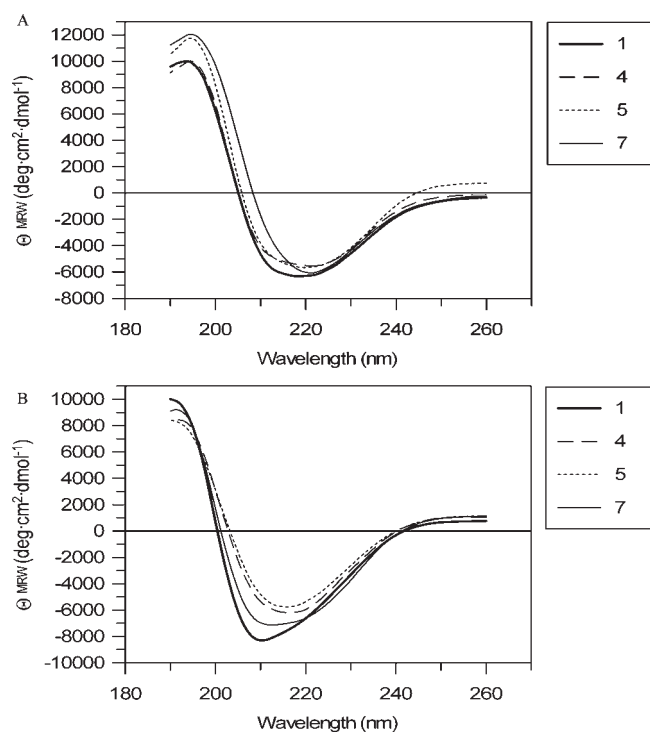


Figure 1. CD spectra of representative peptides in the presence of SDS (A) and LPS (B) micelles, as described in the Experimental Section.

both, in all cases less drastic (16–36% size reduction vs 1) than 2 or 3 above but nonetheless quite informative. Thus, N-terminally truncated 4 underwent a minor loss in antimicrobial activity with respect to 1 (Table 2) while maintaining comparable levels of α -helix structure in the presence of SDS and LPS micelles (Figure 1, Table 3) as well as similar liposome leakage activities (Table 4). The lower affinity of 4 for LPS (ED_{50} of 1.58 vs 0.78 μM for 1) appeared consistent with its reduced though still significant *E. coli* agglutination activity. Further trimming of 4 at the C-terminus, as in analogue 5, entailed a loss in activity, mainly (2- to 5-fold vs 1) against Gram-negatives and less pronounced against Gram-positives (Table 2). This loss of activity correlated with a decrease in both liposome leakage and LPS binding abilities

Table 3. α -Helix Content (in %) in the Presence of SDS and LPS Micelles As Determined by CD

peptide	SDS	LPS
1	73.1	35.9
2	60.8	16.8
3	68.4	3.8
4	69.1	27.8
5	69.1	26.4
6	64.2	15.2
7	73.0	35.5
8	55.3	29.5
9	60.7	29.7

Table 4. Liposome Leakage, LPS Binding, and *E. coli* Agglutination of Analogues 1–9

peptide	ED_{50} (μM)		
	liposome leakage	LPS binding	<i>E. coli</i> agglutination
1	0.41 ± 0.06	0.78 ± 0.05	++ ^b
2	1.25 ± 0.06	1.52 ± 0.03	–
3	ND ^a	ND ^a	–
4	0.40 ± 0.05	1.58 ± 0.06	+ ^c
5	0.74 ± 0.07	2.43 ± 0.05	+ ^c
6	0.76 ± 0.10	6.13 ± 0.09	–
7	0.82 ± 0.10	1.60 ± 0.08	+ ^c
8	1.63 ± 0.09	1.95 ± 0.03	–
9	ND ^a	5.13 ± 0.09	–

^a No activity detected below 10 μM peptide concentration. ^b Minimal agglutinating concentration (MAC) below 0.5 μM . ^c MAC below 1 μM .

(Table 4), while in contrast the α -helical content of the peptide in the presence of SDS and LPS micelles was practically indistinguishable from that found for 4. However, further truncation of 4 by eight extra residues at the N-terminus to give the analogue 6 not only caused a general deterioration of the antimicrobial profile relative to 4 (Table 2) but also diminished structuration in micelle environment (particularly LPS), a sharp loss in LPS binding ability, and the practical disappearance of agglutination

ability (Table 4). This last deficiency is consistent with the fact that, in contrast to 4 and 5, analogue 6 lacks the region (residues 8–16) with the highest aggregation potential, as predicted by the Aggrescan²⁴ software and confirmed by site-directed mutagenesis,²⁵ while analogues 4 and 5 retain such a region and also show significant agglutinating behavior. Further comparative insights into the binding of the peptides may be obtained by the shifts observed in Trp fluorescence upon binding to liposomes or bacterial wall components such as LPS and lipoteichoic acid (LTA). Thus, analogues 4–6 displayed substantial red shifts in front of lipid vesicles (Table S1, Supporting Information), while in LPS and LTA environments, significant shifts were observed, respectively, for 4 and 5 and for 4 alone. Therefore, LTA binding would not seem to correlate with antimicrobial activity on Gram-positive strains for these peptides, whereas a good correlation between LPS binding and antimicrobial activity can be drawn for the Gram-negative strains.

Taking then peptide 5 as the smallest analogue retaining most of the antimicrobial activity, we attempted a more radical minimization that might eventually allow the outlining of an antimicrobial pharmacophore. To this end, a single spacer residue of recognized flexibility (6-aminohexanoic acid, Ahx)²² was used to replace the loop connecting the $\alpha 1$ and $\alpha 2$ helices, with three new analogues (7–9) being designed and tested on such basis. Remarkably, the antimicrobial profile of analogue 7 not just preserved (Table 2) but indeed distinctly enhanced that of 5 against 4 out of the 6 test organisms. The superior performance was supported by findings such as an LPS binding capacity in the same range compared with much larger analogue 2 or 4 or an agglutinating ability parallel to 4 and 5 (Table 4) and was also fully consistent with structural data from CD, indicating an α -helix content similar to that of peptide 5 in both SDS and LPS micelles (Table 3) and especially with NMR data showing a remarkable preservation of native structure (see below).

Attempts at further size reduction by removal of two residues at each end of the N-terminal $\alpha 1$ helix to give analogue 8 met with a clear deterioration in antimicrobial properties, e.g., inactivity toward two of the Gram-positive test organisms as well as an abrupt drop in the activity against *Acinetobacter*. In tune with this, liposome leakage activity of 8 was about 2-fold reduced relative to any of the previous analogues, and its *E. coli* agglutinating ability was again lost, as also found for the poorly performing analogue 5 above. All these observations underscore the important contribution of the four removed residues, particularly of Arg7, recently shown to be involved in the binding of ECP to heparin and glycosaminoglycan structures,²⁰ an ability that might be similarly relevant in the interaction with the Gram-negative bacteria cell wall. Finally, the attempt to dispense with the $\alpha 2$ helix at the C-terminal section led to an analogue (9) totally unable to cause microbial cell death below 10 μM (Table 2). These adverse results correlated rather well with the substantial loss in helical structure for both 8 and 9 (Table 3), with their pronounced decrease in LPS binding (Table 4), or with the smaller red shifts in Trp fluorescence found for 8 upon incubation with LTA or for 9 with both LPS and LTA (Table S1, Supporting Information), the latter suggesting that binding to the cell wall envelope is determinant in the antimicrobial action of these peptides. The inactivity of analogue 9, C-terminally truncated from residue 31 onward, is expected on the basis of a sequence scanning algorithm²⁶ that predicts for positions downstream from Ile30, an antimicrobial region that would logically be missing in 9. Equally or more eloquent for the inactivity of 9 are structural factors such

as the absence of Trp35, a residue known to be required for membrane binding and lysis,¹⁶ or the similar lack of Arg36, which together with Trp35 has been related to glycosaminoglycan binding in biophysical studies^{17,18,27} and to antimicrobial activity in mutagenesis studies.^{15,28} Also, a chimera recently constructed by inserting the ECP(33–36) sequence (which 9 lacks) into a nontoxic RNase was shown to endow it with some bactericidal activity.²⁹

NMR Solution Structure of Analogue 7. Further support for the suitability of analogue 7 was obtained from NMR structural studies. Although the ¹H NMR spectra of 7 in aqueous solution (pH 4.4, 25 °C) showed limited chemical shift dispersion, indicating that no preferred stable secondary structure was adopted, analysis of the conformational shifts ($\Delta\delta_{\text{H}\alpha}$) showed some helical tendency between Ala8-Gln14 and Ile25-Arg36, with ~28% and ~24% helix populations in these segments estimated from the chemical shift data,³³ respectively. In dodecylphosphocoline (DPC) micelles the spectra showed more disperse chemical shifts compared to the water solution (Table S2, Supporting Information), allowing for helical regions at each end of the Ahx linker to be clearly delineated: an N-terminal segment spanning Arg7-His15 (population 51%) and a C-terminal segment spanning Ser23-Arg36 (population 64%).

As is often the case with isolated peptides, conformational equilibria preclude the interpretation of the NMR data of 7 in terms of a single structure. Nonetheless, calculation of a limited number of structures compatible with the experimental data is a general and useful way to visualize the structural features of the favored family of structures present in the conformational ensemble of the peptide. Such a model structure is shown in Figure 2A for analogue 7 in DPC micelles. The calculations were done as described in Experimental Section, and statistics are summarized in Table S3, Supporting Information. The model structures are quite well-defined within the helical peptide segments previously determined on the basis of $\Delta\delta_{\text{H}\alpha}$. The N-terminal α -helical stretch approximately coincides with that previously reported for the native α_1 helix of ECP (Arg7-Ile16)³⁴ and 1,²⁰ and the C-terminal α -helical stretch similarly matches the native α_2 helix of ECP (Cys23-Asn31)³⁴ (Figure 2B). While the Ahx residue is too flexible to induce a preferred relative orientation of both helical regions and thus a clear-cut segregation of polar/hydrophobic residues, it is interesting that in most conformers residues Trp10 and Ile13 of the N-terminal and Ile30 and Tyr33 of the C-terminal helices are oriented toward the concave face of the structure, in a disposition similar to that adopted by these side chains in the native ECP structure.

Final Remarks. In this work we have shown how structure-guided minimization of the ECP(1–45) antimicrobial domain leads to analogues such as 4–7, with substantial size reduction [for 7, 40% vs ECP(1–45) or 80% vs native ECP] and yet displaying a broad, potent antimicrobial spectrum not dissimilar to that of either ECP(1–45) or native ECP. On the basis of the present data, analogue 7 displays an optimal balance between antimicrobial efficacy and structural simplicity, and the NMR evidence that it preserves to a substantial degree the α -helical features of ECP confirms our previous proposal^{34,20} of the $\alpha 1$ and $\alpha 2$ helices as the antimicrobially relevant pharmacophore of ECP and hence a useful template for the development of ECP-based AMPs. A slight increase in hemolytic activity of 7 ($\text{HC}_{50} = 7.3 \pm 0.1 \mu\text{M}$) relative to other analogues ($\text{HC}_{50} \approx 10 \mu\text{M}$, Table 2) is of minor concern; indeed, 7 parallels in both antimicrobial and hemolytic activity as well as in size, a recognized

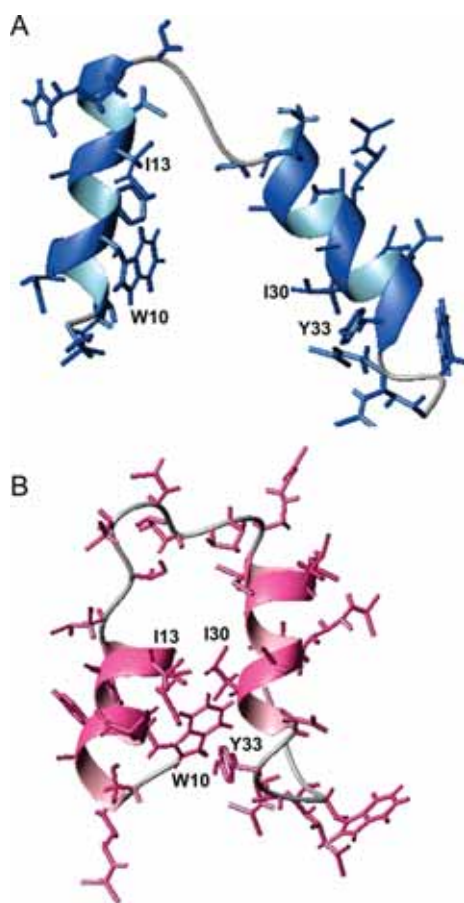


Figure 2. (A) Molecular model of peptide 7 as determined by NMR spectroscopy. (B) Helices $\alpha 1$ and $\alpha 2$ of native ECP (PDB code 2KB5). Residues W10, I13, I30, and Y33 pointing to the helical interface are labeled.

AMP standard such as the cecropin–melittin hybrid CA(1–8)-M(1–18) (Table 2).^{30–32} In conclusion, our data allow us to propose 7 as an ideally downsized version of ECP and hence a valuable antimicrobial lead structure.

EXPERIMENTAL SECTION

Materials. DOPC (dioleoyl phosphatidylcholine) and DOPG (dioleoyl phosphatidylglycerol) were from Avanti Polar Lipids (Alabaster, AL). ANTS (8-aminonaphthalene-1,3,6-trisulfonic acid disodium salt), DPX (*p*-xylenebispyridinium bromide), and BC (BODIPY TR cadaverine, where BODIPY is boron dipyrromethane (4,4-difluoro-4-bora-3a,4a-diaza-*s*-indacene) were purchased from Invitrogen (Carlsbad, CA). LT (lipoteichoic acids) from *Staphylococcus aureus* and LPS (lipopolysaccharides) from *Escherichia coli* serotype 0111:B4 were purchased from Sigma-Aldrich (St. Louis, MO). PD-10 desalting columns with Sephadex G-25 were from GE Healthcare (Waukesha, WI). Strains used were *Escherichia coli* (BL2, Novagen), *Staphylococcus aureus* (ATCC 502A), *Acinetobacter baumannii* (ATCC 15308), *Pseudomonas sp* (ATCC 15915), *Micrococcus luteus* (ATCC 7468), and *Enterococcus faecium* (ATCC 19434).

Peptides. Fmoc-protected amino acids and 2-(1*H*-benzotriazol-1-yl)-1,1,3,3-tetramethyluronium hexafluorophosphate (HBTU) were obtained from Iris Biotech (Marktredwitz, Germany). Fmoc-Rink-amide (MBHA) resin was from Novabiochem (Läufelfingen, Switzerland). HPLC-grade acetonitrile (ACN) and peptide synthesis-grade *N*,

N-dimethylformamide (DMF), *N,N*-diisopropylethylamine (DIEA), and trifluoroacetic acid (TFA) were from Carlo Erba-SDS (Peypin, France).

Solid phase peptide synthesis was done by Fmoc-based chemistry on Fmoc-Rink-amide (MBHA) resin (0.1 mmol) in a model 433 synthesizer (Applied Biosystems, Foster City, CA) running FastMoc protocols. Couplings used 8-fold molar excess each of Fmoc-amino acid and HBTU and 16-fold molar excess of DIEA. Side chains of trifunctional residues were protected with *tert*-butyl (Ser, Thr, Tyr), *tert*-butyloxycarbonyl (Lys, Trp), 2,2,4,6,7-pentamethylidihydrobenzofuran-5-sulfonyl (Arg), and trityl (Asn, Gln, His) groups. After chain assembly, full deprotection and cleavage were carried out with TFA–water–triisopropylsilane (95:2.5:2.5 v/v, 90 min, room temperature). Peptides were isolated by precipitation with cold diethyl ether and separated by centrifugation, dissolved in 0.1 M acetic acid, and lyophilized. Analytical reversed-phase HPLC was performed on a Luna C₁₈ column (4.6 mm × 50 mm, 3 μ m; Phenomenex, CA). Linear gradients of solvent B (0.036% TFA in ACN) into A (0.045% TFA in H₂O) were used for elution at a flow rate of 1 mL/min and with UV detection at 220 nm. Preparative HPLC runs were performed on a Luna C₁₈ column (21.2 mm × 250 mm, 10 μ m; Phenomenex, CA), using linear gradients of solvent B (0.1% in ACN) into A (0.1% TFA in H₂O), as required, with a flow rate of 25 mL/min. MALDI-TOF mass spectra were recorded in the reflector or linear mode in a Voyager DE-STR workstation (Applied Biosystems, Foster City, CA) using α -hydroxycinnamic acid matrix. Fractions of adequate (>90%) HPLC homogeneity and with the expected mass were pooled, lyophilized, and used in subsequent experiments.

Expression and Purification of ECP. Wild-type ECP was obtained from a human ECP synthetic gene. Protein expression in the *E. coli* BL21DE3 strain, folding of the protein from inclusion bodies, and purification were carried out as previously described.³⁵

MIC (Minimal Inhibitory Concentration) Determination.

Antimicrobial activity was expressed as the MIC, defined as the lowest peptide concentration that completely inhibits microbial growth. MIC of each peptide was determined from two independent experiments performed in triplicate for each concentration. Peptides were dissolved in 10 mM sodium phosphate buffer, pH 7.5, and serially diluted from 10 to 0.2 μ M. Bacteria were incubated at 37 °C overnight in Luria–Bertani broth and diluted to give approximately 5×10^5 CFU/mL. In each assay peptide solutions were added to each bacteria dilution and incubated for 4 h, and samples were plated onto Petri dishes and incubated at 37 °C overnight.

Minimal Agglutination Activity. *E. coli* cells were grown at 37 °C to mid-exponential phase (OD₆₀₀ = 0.6), centrifuged at 5000g for 2 min, and resuspended in Tris-HCl buffer, 0.15 M NaCl, pH 7.5, in order to give an absorbance of 10 at 600 nm. A 200 μ L aliquot of the bacterial suspension was incubated with peptide at various (0.1–10 μ M) concentrations at 25 °C overnight. Aggregation behavior was observed by visual inspection and minimal agglutinating concentration expressed as previously described³⁶

Hemolytic Activity. Fresh human red blood cells (RBCs) were washed 3 times with PBS (35 mM phosphate buffer, 0.15 M NaCl, pH 7.4) by centrifugation for 5 min at 3000g and resuspended in PBS at 2×10^7 cells/mL. RBCs were incubated with peptides at 37 °C for 4 h and centrifuged at 13000g for 5 min. The supernatant was separated from the pellet and its absorbance measured at 570 nm. The 100% hemolysis was defined as the absorbance obtained by sonicating RBCs for 10 s. HC₅₀ was calculated by fitting the data to a sigmoidal function.

Liposome Preparation. LUVs (large unilamellar vesicles) of ~100 nm diameter were prepared from a chloroform solution of DOPC/DOPG (3:2 molar ratio). After vacuum-drying, the lipid film was suspended in 10 mM Tris/HCl, 0.1 M NaCl, pH 7.4 buffer to give a 1 mM solution, then frozen and thawed several times prior to extrusion through polycarbonate membranes as previously described.¹⁸

Fluorescence Measurements. Tryptophan fluorescence emission spectra were recorded using a 280 nm excitation wavelength. Slits were set at 2 nm for excitation and 5–10 nm for emission. Emission spectra were recorded from 300–400 nm at a scan rate of 60 nm/min in a 10 mm × 10 mm cuvette, with stirring immediately after sample mixing. Protein and peptide spectra at 0.5 μM in 10 mM Hepes buffer, pH 7.4, were obtained at 25 °C in the absence or presence of 200 μM liposome suspension, 200 μM LPS (assuming a 90 000 g/mol molecular mass), or 200 μM LTA, as calculated from a 2200 molecular mass reference value. Fluorescence measurements were performed on a Cary Eclipse spectrofluorimeter. Spectra in the presence of liposomes were corrected for light scattering by subtracting the corresponding LUV background. For each condition three spectra were averaged. The fluorescence spectra were also calculated as a function of the frequency scale (wavenumber) and adjusted using a log normal function as detailed previously.¹⁶

LPS Binding Assay. LPS binding was assessed using the fluorescent probe Bodipy TR cadaverine (BC) as described.¹⁷ Briefly, the displacement assay was performed by the addition of 1–2 μL aliquots of ECP or peptide solution to 1 mL of a continuously stirred mixture of LPS (10 μg · mL⁻¹) and BC (10 μM) in 5 mM Hepes buffer at pH 7.5. Fluorescence measurements were performed on a Cary Eclipse spectrofluorimeter. The BC excitation wavelength was 580 nm, and the emission wavelength was 620 nm. The excitation slit was set at 2.5 nm, and the emission slit was set at 20 nm. Final values correspond to an average of four replicates and were the mean of a 0.3 s continuous measurement. Quantitative effective displacement values (ED₅₀) were calculated.

ANTS/DPX Liposome Leakage Assay. The ANTS/DPX liposome leakage fluorescence assay was performed as described.¹⁸ Briefly, a unique population of LUVs of DOPC/DOPG (3:2 molar ratio) lipids was obtained containing 12.5 mM ANTS, 45 mM DPX, 20 mM NaCl, and 10 mM Tris/HCl, pH 7.5. The ANTS/DPX liposome suspension was diluted to 30 μM and incubated at 25 °C in the presence of ECP or peptides. The percentage of leakage (%L) was determined by monitoring the release of liposome content at peptide concentrations up to 10 μM after 1 h of incubation, as follows: %L = 100(F_p - F₀)/(F₁₀₀ - F₀), where F_p is the final fluorescence intensity after peptide addition (1 h) and F₀ and F₁₀₀ are the fluorescence intensities before peptide addition and after addition of 0.5% Triton X100. ED₅₀ was calculated by fitting the data to a sigmoidal function.

CD Spectroscopy. Far-UV CD spectra were obtained from a Jasco J-715 spectropolarimeter as described.¹⁹ Mean-residue ellipticity [θ] (deg · cm² · dmol⁻¹) was calculated as

$$[\theta] = \frac{\theta(\text{MRW})}{10cl}$$

where θ is the experimental ellipticity (deg), MRW is the mean residue molecular mass of the peptide, c is the molar concentration of peptide, and l is the cell path length. Data from four consecutive scans were averaged. Spectra of ECP and peptides (4–8 μM in 5 mM sodium phosphate, pH 7.5) in the absence and presence (1 mM) of SDS and LPS (1 mM, nominal MW = 90 kDa) were recorded. Samples were centrifuged for 5 min at 10000g before use. Percentage of secondary structure was estimated with the Jasco software, as described by Yang et al.³⁷ and by the Selcon software.³⁸

NMR Spectroscopy. Peptide 7 samples for NMR were prepared at ~1 mM in 90% H₂O/10% D₂O or ~50 mM [²H₃₈]dodecylphosphocholine (DPC, Cambridge Isotope Laboratories) in 90% H₂O/10% D₂O. The pH was adjusted to 4.4 at 25 °C with no correction for isotope effects. NMR experiments were performed in a Bruker AV-800 instrument equipped with a cryoprobe and field gradients. All data were acquired and processed with TOPSPIN (version 1.3) (Bruker, Germany) at two temperatures, 25 and 35 °C. COSY, TOCSY, NOESY, and ¹H–¹³C HSQC spectra were acquired with standard pulse

sequences. Water suppression was accomplished with presaturation or by using the WATERGATE module.³⁹ Mixing times were 60 and 150 ms for the TOCSY and NOESY experiments, respectively. The spectral assignment of the peptide in the different solvents was performed by following the well-established sequential-specific methodology based on homonuclear spectra.⁴⁰

Helix population in the peptide segments was quantified from ¹H_α conformational chemical shift values, Δδ_{H_α}.³³ To obtain the helix percentage, the Δδ_{H_α}Δδ_{H_α} = δ_{H_α}^{observed} - δ_{H_α}^{random coil} values for all the residues were averaged, divided by the Δδ_{H_α} value corresponding to 100% helix, -0.39 ppm,⁴¹ and multiplied by 100. The random coil values were from Wishart et al.⁴²

The 3D structure of the peptide in DPC was obtained from distance constraints derived from a NOESY spectrum at 25 °C with 150 ms mixing time. The NOE cross-peaks were integrated with the automatic subroutine of the SPARKY program⁴³ and then calibrated and converted into upper limit distance constraints. Structures were calculated using the CYANA (version 2.1) program⁴⁴ with the distance constraints and backbone dihedral angle ranges obtained from TALOS.⁴⁵ Finally, the structures were energy-minimized and refined. Families of 50 structures satisfactorily reproducing the experimental constraints were generated; the best 20 of such structures on the basis of energies and Ramachandran plot quality were selected for further analysis. All structures were visualized and analyzed with MOLMOL.⁴⁶

■ ASSOCIATED CONTENT

S Supporting Information. Characterization of the peptide tryptophan spectra in the presence of lipid vesicles, LPS micelles, and LTA micelles; HN and H_α chemical shifts of analogue 7 in water and DPC micelles; statistics of structural restraints and violations. This material is available free of charge via the Internet at <http://pubs.acs.org>.

■ AUTHOR INFORMATION

Corresponding Author

*For D.A.: phone, +34-933160868; fax, +34-933161901; e-mail, david.andreu@upf.edu. For E.B.: phone, +34-935814147; e-mail, ester.boix@uab.cat.

■ ACKNOWLEDGMENT

M.T. is a recipient of an Alianza Cuatro Universidades fellowship. Work was supported by the Spanish Ministry of Science and Innovation [Grants BFU2009-09371 to E.B., BIO2008-04487-CO3-02 to D.A., and CTQ2008-00080 to M.B.], Generalitat of Catalonia [Grants SGR2009-795 and SGR2009-494], and the European Union [Grant HEALTH-F3-2008-223414 (LEISHDRUG) to D.A.].

■ ABBREVIATIONS USED

Ahx, aminohexanoic acid; AMP, antimicrobial peptide; COSY, correlation spectroscopy; DOPC, dioleoyl phosphatidylcholine; DOPG, dioleoyl phosphatidylglycerol; DPC, [²H₃₈]dodecylphosphocholine; ECP, eosinophil cationic protein; HSQC, heteronuclear single quantum coherence; LPS, lipopolysaccharide; LTA, lipoteichoic acid; LUV, large unilamellar vesicle; MIC, minimum inhibitory concentration; NOE, nuclear Overhauser effect; NOESY, nuclear Overhauser effect spectroscopy; SDS, sodium dodecyl sulfate; TOCSY, total correlation spectroscopy

REFERENCES

- (1) Hadley, E. B.; Hancock, R. E. Strategies for the discovery and advancement of novel cationic antimicrobial peptides. *Curr. Top. Med. Chem.* **2010**, 1872–1881.
- (2) Shai, Y. Mode of action of membrane active antimicrobial peptides. *Biopolymers* **2002**, 66, 236–248.
- (3) Yeaman, M. R.; Yount, N. Y. Mechanisms of antimicrobial peptide action and resistance. *Pharmacol. Rev.* **2003**, 55, 27–55.
- (4) Ramanathan, B.; Davis, E. G.; Ross, C. R.; Blecha, F. Cathelicidins: microbicidal activity, mechanisms of action, and roles in innate immunity. *Microbes Infect.* **2002**, 4, 361–372.
- (5) Rathinakumar, R.; Walkenhorst, W. F.; Wimley, W. C. Broad-spectrum antimicrobial peptides by rational combinatorial design and high-throughput screening: the importance of interfacial activity. *J. Am. Chem. Soc.* **2009**, 131, 7609–7617.
- (6) Romestand, B.; Molina, F.; Richard, V.; Roch, P.; Granier, C. Key role of the loop connecting the two beta strands of mussel defensin in its antimicrobial activity. *Eur. J. Biochem.* **2003**, 270, 2805–2813.
- (7) Vila-Perello, M.; Sanchez-Vallet, A.; Garcia-Olmedo, F.; Molina, A.; Andreu, D. Structural dissection of a highly knotted peptide reveals minimal motif with antimicrobial activity. *J. Biol. Chem.* **2005**, 280, 1661–1668.
- (8) Vila-Perello, M.; Tognon, S.; Sanchez-Vallet, A.; Garcia-Olmedo, F.; Molina, A.; Andreu, D. A minimalist design approach to antimicrobial agents based on a thionin template. *J. Med. Chem.* **2006**, 49, 448–451.
- (9) Cho, S.; Beintema, J. J.; Zhang, J. The ribonuclease A superfamily of mammals and birds: identifying new members and tracing evolutionary histories. *Genomics* **2005**, 85, 208–220.
- (10) Dyer, K. D.; Rosenberg, H. F. The RNase A superfamily: generation of diversity and innate host defense. *Mol. Diversity* **2006**, 10, 585–597.
- (11) Boix, E.; Nogues, M. V. Mammalian antimicrobial proteins and peptides: overview on the RNase A superfamily members involved in innate host defence. *Mol. Biosyst.* **2007**, 3, 317–335.
- (12) Boix, E.; Torrent, M.; Sanchez, D.; Nogues, M. V. The antipathogen activities of eosinophil cationic protein. *Curr. Pharm. Biotechnol.* **2008**, 9, 141–152.
- (13) Rubin, J.; Zagai, U.; Blom, K.; Trulson, A.; Engstrom, A.; Venge, P. The coding ECP 434(G>C) gene polymorphism determines the cytotoxicity of ECP but has minor effects on fibroblast-mediated gel contraction and no effect on RNase activity. *J. Immunol.* **2009**, 183, 445–451.
- (14) Zagai, U.; Skold, C. M.; Trulson, A.; Venge, P.; Lundahl, J. The effect of eosinophils on collagen gel contraction and implications for tissue remodelling. *Clin. Exp. Immunol.* **2004**, 135, 427–433.
- (15) Carreras, E.; Boix, E.; Rosenberg, H. F.; Cuchillo, C. M.; Nogues, M. V. Both aromatic and cationic residues contribute to the membrane-lytic and bactericidal activity of eosinophil cationic protein. *Biochemistry* **2003**, 42, 6636–6644.
- (16) Torrent, M.; Cuyas, E.; Carreras, E.; Navarro, S.; Lopez, O.; de la Maza, A.; Nogues, M. V.; Reshetnyak, Y. K.; Boix, E. Topography studies on the membrane interaction mechanism of the eosinophil cationic protein. *Biochemistry* **2007**, 46, 720–733.
- (17) Torrent, M.; Navarro, S.; Moussaoui, M.; Nogues, M. V.; Boix, E. Eosinophil cationic protein high-affinity binding to bacterial-wall lipopolysaccharides and peptidoglycans. *Biochemistry* **2008**, 47, 3544–3555.
- (18) Torrent, M.; Nogues, M. V.; Boix, E. Eosinophil cationic protein (ECP) can bind heparin and other glycosaminoglycans through its RNase active site. *J. Mol. Recognit.* **2011**, 24, 90–100.
- (19) Torrent, M.; de la Torre, B. G.; Nogues, V. M.; Andreu, D.; Boix, E. Bactericidal and membrane disruption activities of the eosinophil cationic protein are largely retained in an N-terminal fragment. *Biochem. J.* **2009**, 421, 425–434.
- (20) Garcia-Mayoral, M. F.; Moussaoui, M.; de la Torre, B. G.; Andreu, D.; Boix, E.; Nogues, M. V.; Rico, M.; Laurents, D. V.; Bruix, M. NMR structural determinants of eosinophil cationic protein binding to membrane and heparin mimetics. *Biophys. J.* **2010**, 98, 2702–2711.
- (21) Beck-Sickinger, A. G.; Grouzmann, E.; Hoffmann, E.; Gaida, W.; van Meir, E. G.; Waeber, B.; Jung, G. A novel cyclic analog of neuropeptide Y specific for the Y2 receptor. *Eur. J. Biochem.* **1992**, 206, 957–964.
- (22) Beck-Sickinger, A. G.; Jung, G. Structure–activity relationships of neuropeptide Y analogues with respect to Y1 and Y2 receptors. *Biopolymers* **1995**, 37, 123–142.
- (23) Fields, G. B.; Noble, R. L. Solid phase peptide synthesis utilizing 9-fluorenylmethoxycarbonyl amino acids. *Int. J. Pept. Protein Res.* **1990**, 35, 161–214.
- (24) Conchillo-Sole, O.; de Groot, N. S.; Aviles, F. X.; Vendrell, J.; Daura, X.; Ventura, S. AGGRESCAN: a server for the prediction and evaluation of “hot spots” of aggregation in polypeptides. *BMC Bioinf.* **2007**, 8, 65.
- (25) Torrent, M.; Odorizzi, F.; Nogues, M. V.; Boix, E. Eosinophil cationic protein aggregation: identification of an N-terminus amyloid prone region. *Biomacromolecules* **2010**, 11, 1983–1990.
- (26) Torrent, M.; Nogues, M. V.; Boix, E. A theoretical approach to spot active regions in antimicrobial proteins. *BMC Bioinf.* **2009**, 10, 373.
- (27) Fan, T. C.; Fang, S. L.; Hwang, C. S.; Hsu, C. Y.; Lu, X. A.; Hung, S. C.; Lin, S. C.; Chang, M. D. Characterization of molecular interactions between eosinophil cationic protein and heparin. *J. Biol. Chem.* **2008**, 283, 25468–25474.
- (28) Carreras, E.; Boix, E.; Navarro, S.; Rosenberg, H. F.; Cuchillo, C. M.; Nogues, M. V. Surface-exposed amino acids of eosinophil cationic protein play a critical role in the inhibition of mammalian cell proliferation. *Mol. Cell. Biochem.* **2005**, 272, 1–7.
- (29) Torrent, M.; Ribo, M.; Benito, A.; Vilanova, M. Bactericidal activity engineered on human pancreatic ribonuclease and onconase. *Mol. Pharmacol.* **2009**, 6, 531–542.
- (30) Andreu, D.; Ubach, J.; Boman, A.; Wahlin, B.; Wade, D.; Merrifield, R. B.; Boman, H. G. Shortened cecropin A-melittin hybrids. Significant size reduction retains potent antibiotic activity. *FEBS Lett.* **1992**, 296, 190–194.
- (31) Piers, K. L.; Brown, M. H.; Hancock, R. E. Improvement of outer membrane-permeabilizing and lipopolysaccharide-binding activities of an antimicrobial cationic peptide by C-terminal modification. *Antimicrob. Agents Chemother.* **1994**, 38, 2311–2316.
- (32) Piers, K. L.; Hancock, R. E. The interaction of a recombinant cecropin/melittin hybrid peptide with the outer membrane of *Pseudomonas aeruginosa*. *Mol. Microbiol.* **1994**, 12, 951–958.
- (33) Jimenez, M. A.; Bruix, M.; Gonzalez, C.; Blanco, F. J.; Nieto, J. L.; Herranz, J.; Rico, M. CD and ¹H-NMR studies on the conformational properties of peptide fragments from the C-terminal domain of thermolysin. *Eur. J. Biochem.* **1993**, 211, 569–581.
- (34) Laurents, D. V.; Bruix, M.; Jimenez, M. A.; Santoro, J.; Boix, E.; Moussaoui, M.; Nogues, M. V.; Rico, M. The ¹H, ¹³C, ¹⁵N resonance assignment, solution structure, and residue level stability of eosinophil cationic protein/RNase 3 determined by NMR spectroscopy. *Biopolymers* **2009**, 91, 1018–1028.
- (35) Boix, E.; Nikolovski, Z.; Moiseyev, G. P.; Rosenberg, H. F.; Cuchillo, C. M.; Nogues, M. V. Kinetic and product distribution analysis of human eosinophil cationic protein indicates a subsite arrangement that favors exonuclease-type activity. *J. Biol. Chem.* **1999**, 274, 15605–15614.
- (36) Torrent, M.; Badia, M.; Moussaoui, M.; Sanchez, D.; Nogues, M. V.; Boix, E. Comparison of human RNase 3 and RNase 7 bactericidal action at the Gram-negative and Gram-positive bacterial cell wall. *FEBS J.* **2010**, 277, 1713–1725.
- (37) Yang, J. T.; Wu, C. S.; Martinez, H. M. Calculation of protein conformation from circular dichroism. *Methods Enzymol.* **1986**, 130, 208–269.
- (38) Sreerama, N.; Woody, R. W. A self-consistent method for the analysis of protein secondary structure from circular dichroism. *Anal. Biochem.* **1993**, 209, 32–44.
- (39) Piotto, M.; Saudek, V.; Sklenar, V. Gradient-tailored excitation for single-quantum NMR spectroscopy of aqueous solutions. *J. Biomol. NMR* **1992**, 2, 661–665.

(40) Wüthrich, K. *NMR of Proteins and Nucleic Acids*; Wiley-Interscience: New York, 1986.

(41) Wishart, D. S.; Sykes, B. D.; Richards, F. M. Relationship between nuclear magnetic resonance chemical shift and protein secondary structure. *J. Mol. Biol.* **1991**, *222*, 311–333.

(42) Wishart, D. S.; Bigam, C. G.; Holm, A.; Hodges, R. S.; Sykes, B. D. ^1H , ^{13}C and ^{15}N random coil NMR chemical shifts of the common amino acids. I. Investigations of nearest-neighbor effects. *J. Biomol. NMR* **1995**, *5*, 67–81.

(43) Goddard, T. D.; Kneller, D. G. *SPARKY*, version 3; University of California: San Francisco, CA, 2005.

(44) Guntert, P. Automated NMR structure calculation with CYANA. *Methods Mol. Biol.* **2004**, *278*, 353–378.

(45) Cornilescu, G.; Delaglio, F.; Bax, A. Protein backbone angle restraints from searching a database for chemical shift and sequence homology. *J. Biomol. NMR* **1999**, *13*, 289–302.

(46) Koradi, R.; Billeter, M.; Wuthrich, K. MOLMOL: a program for display and analysis of macromolecular structures. *J. Mol. Graphics* **1996**, *14* (51–55), 29–32.

Refining the ECP antibacterial pharmacophore by rational structure minimization

*Marc Torrent^{‡§}, David Pulido[‡], Beatriz G. de la Torre[§], M. Victòria Nogués[‡],
David Andreu^{§*} and Ester Boix^{‡*}.*

Table S1. Tryptophan fluorescence of peptides in the presence of lipid vesicles, LPS micelles and LTA micelles.

Table S2. HN and H_α chemical shifts of analog **7** in water and DPC micelles.

Table S3. Statistics of structural restraints and violations

Table S1. Tryptophan fluorescence of peptides in the presence of lipid vesicles, LPS micelles and LTA micelles.

Peptide	Buffer	DOPC:DOPG 3:2		LPS		LTA	
	λ max (nm)	λ max (nm)	λ shift (nm)	λ max (nm)	λ shift (nm)	λ max (nm)	λ shift (nm)
1	352	342	10	344	8	342	10
2	355	341	14	346	9	344	11
3	339	336	3	337	2	337	2
4	355	341	14	346	9	344	11
5	355	342	13	345	10	350	5
6	355	341	14	350	5	352	3
7	357	342	15	345	12	348	9
8	355	342	13	346	9	350	5
9	356	349	7	354	2	352	4

Table S2. HN and H_α chemical shifts of analog **7** in water and DPC micelles.

Residue	water		DPC	
	<u>HN</u>	<u>H_α</u>	<u>HN</u>	<u>H_α</u>
Thr6	---	3.92	---	4.03
Arg7	8.81	4.32	9.14	4.21
Ala8	8.46	4.22	8.58	4.14
Gln9	8.27	4.19	8.05	4.15
Trp10	8.02	4.54	8.06	4.38
Phe11	7.71	4.39	7.82	4.31
Ala12	7.96	4.16	7.87	4.22
Ile13	7.92	4.06	7.80	3.97
Gln14	8.25	4.24	8.04	4.06
His15	8.50	4.69	8.05	4.63
Ile16	8.21	4.21	7.86	4.18
Ser17	8.40	4.39	8.26	4.43
Ahx	7.98	2.32, 2.32	7.94	2.47, 2.23
Ser23	8.29	4.48	8.77	4.02
Thr24	8.18	4.36	8.30	4.05
Ile25	8.04	4.07	7.51	3.82
Ala26	8.24	4.28	8.04	4.02
Met27	8.17	4.38	8.31	4.28
Arg28	8.16	4.29	7.80	4.10
Ala29	8.17	4.31	7.93	4.18
Ile30	8.01	4.10	8.15	3.79
Asn31	8.38	4.67	8.23	4.50
Asn32	8.29	4.63	7.99	4.61
Tyr33	8.08	4.43	7.89	4.31
Arg34	7.99	4.17	7.89	4.11
Trp35	7.95	4.60	7.96	4.59
Arg36	7.90	4.13	7.93	4.14

Table S3. Statistics of structural restraints and violations

Number of restraints:

Total distance restraints	301
Intra-residue, (i-j)=0	109
Short-range, (i-j)=1	115
Medium-range, 1<(i-j)<5	77
Long-range, (i-j)≥5	0
Angular restraints (φ , ψ)	34

Structure calculation:

Average target function value	0.31
Average maximum distance violation (Å)	0.23
Maximum dihedral angle violation (°)	1.19

RMSD values (20 conformers):

Backbone (superposition helix α 1: 7-15)	0.24
Backbone (superposition helix α 2: 23-36)	1.31
Heavy atoms (superposition helix α 1: 7-15)	1.22
Heavy atoms (superposition helix α 2: 23-36)	2.88

CHAPTER II

Antimicrobial Action and Cell Agglutination by the Eosinophil Cationic Protein Are Modulated by the Cell Wall Lipopolysaccharide Structure

David Pulido,^a Mohammed Moussaoui,^a David Andreu,^b M. Victòria Nogués,^a Marc Torrent,^{a,b} and Ester Boix^a

Department of Biochemistry and Molecular Biology, Universitat Autònoma de Barcelona, Cerdanyola del Vallès, Spain,^a and Department of Experimental and Health Sciences, Pompeu Fabra University, Barcelona, Spain^b

Antimicrobial proteins and peptides (AMPs) are essential effectors of innate immunity, acting as a first line of defense against bacterial infections. Many AMPs exhibit high affinity for cell wall structures such as lipopolysaccharide (LPS), a potent endotoxin able to induce sepsis. Hence, understanding how AMPs can interact with and neutralize LPS endotoxin is of special relevance for human health. Eosinophil cationic protein (ECP) is an eosinophil secreted protein with high activity against both Gram-negative and Gram-positive bacteria. ECP has a remarkable affinity for LPS and a distinctive agglutinating activity. By using a battery of LPS-truncated *E. coli* mutant strains, we demonstrate that the polysaccharide moiety of LPS is essential for ECP-mediated bacterial agglutination, thereby modulating its antimicrobial action. The mechanism of action of ECP at the bacterial surface is drastically affected by the LPS structure and in particular by its polysaccharide moiety. We have also analyzed an N-terminal fragment that retains the whole protein activity and displays similar cell agglutination behavior. Conversely, a fragment with further minimization of the antimicrobial domain, though retaining the antimicrobial capacity, significantly loses its agglutinating activity, exhibiting a different mechanism of action which is not dependent on the LPS composition. The results highlight the correlation between the protein's antimicrobial activity and its ability to interact with the LPS outer layer and promote bacterial agglutination.

Lipopolysaccharide (LPS) is the main outer membrane component of Gram-negative bacteria. The LPS molecule is a phosphorylated glycolipid composed of lipid A, also known as endotoxin, and a polysaccharide moiety. In turn, the latter is composed of the inner core (comprising three heptose residues and a 3-deoxy-D-manno-octulosonic acid residue), the outer core (comprising two glucose residues, two galactose residues, and one N-acetylglucosamine residue), and the antigenic “O” region composed of several repeats of different oligosaccharide units (Fig. 1A and B) (2, 9, 25, 27).

LPS serves as a first barrier against antibiotics by hampering the diffusion of chemicals through the outer membrane (12). In fact, some modifications targeting the LPS structure in Gram-negative bacteria have been reported to confer resistant phenotypes against antibiotics and particularly against antimicrobial proteins and peptides (AMPs) (29). LPS, and in particular the lipid A portion, is released during bacterial infection, inducing inflammation and ultimately septic shock (4, 11). Unraveling the structural determinants for LPS interaction can assist in the design of new antibiotics with endotoxin-neutralizing properties (5, 15, 17).

AMPs interact with LPS competitively, displacing the divalent cations, breaking LPS compactness, and thus furthering the transport of peptides across the outer membrane (18). This process is modulated by the LPS charge, structure, and packing of lipid acyl chains in the outer layer (6, 24, 26). Several studies have determined that many AMPs require crossing of the outer membrane in order to reach the inner phospholipid bilayer, where they exert their action (7, 8, 23).

Eosinophil cationic protein (ECP) is an antimicrobial protein stored in the secondary granules of eosinophils that has an active role in infection control, immunomodulation, and tissue-remodelling processes (3, 37). ECP displays high antimicrobial activity

and is able to specifically agglutinate Gram-negative bacteria before cell permeation occurs (30). Interestingly, in model membrane studies, ECP also promotes vesicle aggregation previous to any leakage event (36). Our previous results highlighted the correlation between ECP activity and its affinity to LPS (33).

Further experimental work evidenced that the antimicrobial domain of the protein lies in its N terminus (10, 28, 31). Indeed, a peptide containing the first 45 N-terminal residues (peptide [1-45]) (Fig. 1C) has been shown to retain the antimicrobial activity of the whole protein (32). A refinement of the antimicrobial domain by rational structure minimization led us to the synthesis of a shorter peptide ([6-17]-Ahx-[23-36]) that links the two first α -helical segments (Fig. 1C) and embodies the protein pharmacophore (35). However, though the shortest construct can agglutinate bacterial cells, its affinity for LPS is significantly reduced compared with that of the whole protein (35).

In order to study the role of LPS in the bactericidal properties of ECP and its derivative peptides, a wide battery of *Escherichia coli* K-12 mutant strains have been tested. These mutant strains, presenting distinctive chemotypes, are defective in genes involved in the biosynthesis and assembly of LPS (20, 29). From the results presented here, we conclude that for ECP and its N-terminal do-

Received 10 November 2011 Returned for modification 24 December 2011

Accepted 5 February 2012

Published ahead of print 13 February 2012

Address correspondence to Ester Boix, ester.boix@uab.cat, or Marc Torrent, marc.torrent@uab.cat.

Copyright © 2012, American Society for Microbiology. All Rights Reserved.

doi:10.1128/AAC.06107-11

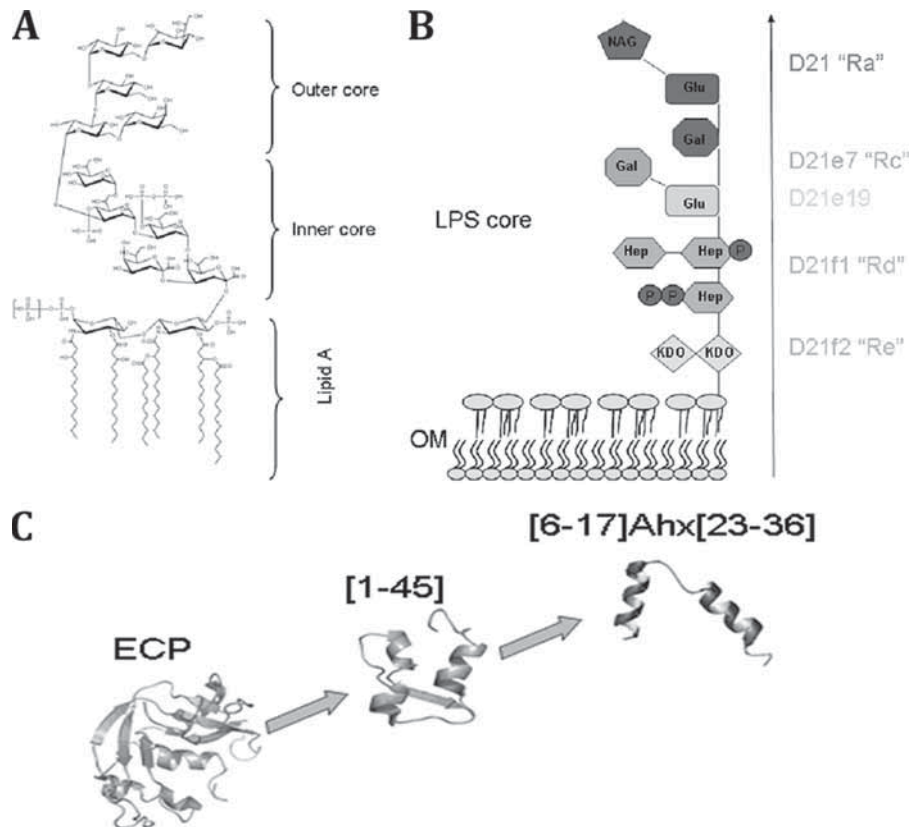


FIG 1 (A and B) Chemical structure of LPS core (A) and chemotype scheme for the strains used (B). The Ra chemotype (strain D21) possesses the entire LPS core, the Rc chemotype includes the heptose chain and a Glu residue (strain D21e7) and an additional Gal residue (strain D21e19), the Rd chemotype contains the heptose and Kdo (strain D21f1), and the Re chemotype (strain D21f2) contains uniquely the Kdo portion. Only the D21 strain contains the phosphate residues associated with the heptose residues. (C) Structure scheme for ECP and derived peptides showing [6-17]-Ahx-[23-36] structure based on nuclear magnetic resonance (NMR) information (16, 21, 35).

main, both bacterial agglutination and antimicrobial activities are correlated with the LPS structure. A peptide with a further trimming of the N-terminal domain, though retaining the antimicrobial action, displays a different mechanism of action that is not dependent on the LPS layer. Therefore, the protein and the N-terminal antimicrobial domain can induce bacterial cell death by action at the cell outer layer without any active transport into the cytoplasm.

MATERIALS AND METHODS

Strains and chemicals. *Escherichia coli* K-12 mutants deficient in lipopolysaccharide (LPS) synthesis were obtained from the *E. coli* Genetic Stock Center (Department of Biology, Yale University, New Haven, CT). The Alexa Fluor 488 protein labeling kit and the LIVE/DEAD bacterial viability kit were purchased from Molecular Probes (Eugene, OR). The BacTiter-Glo assay kit was from Promega (Madison, WI).

Expression and purification of recombinant ECP. Wild-type ECP was expressed using a synthetic gene for the human ECP-coding sequence. Protein expression in *E. coli* strain BL21(DE3) (Novagen, Madison, WI), folding of the protein from inclusion bodies, and purification were carried out as previously described (1).

Peptides. Peptides [1-45] and [6-17]-Ahx-[23-36] were prepared by fluorenyl-methoxycarbonyl (Fmoc) solid-phase peptide synthesis methods (14). All peptides were purified by high-pressure liquid chromatography (HPLC) to ~95% homogeneity and satisfactorily characterized by matrix-assisted laser desorption/ionization–time of flight mass spectrometry (MALDI-TOF-MS).

Bacterial viability assays. Bacterial viability was assayed using the BacTiter-Glo microbial cell viability kit (Promega). Briefly, ECP or peptide [1-45] or [6-17]-Ahx-[23-36] was dissolved in 10 mM sodium phosphate buffer (pH 7.5), serially diluted from 10 to 0.1 μ M, and tested against *E. coli* strains (optical density at 600 nm [OD₆₀₀] = 0.2) for 4 h of incubation time. Fifty microliters of culture was mixed with 50 μ l of BacTiter-Glo reagent in a microtiter plate according to the manufacturer's instructions and incubated at room temperature for 10 min. Luminescence was read on a Victor3 plate reader (Perkin-Elmer, Waltham, MA) with a 1-s integration time. Fifty percent inhibitory concentrations (IC₅₀s) were calculated by fitting the data to a dose-response curve.

Kinetics of bacterial survival were determined using the LIVE/DEAD bacterial viability kit (Molecular Probes, Invitrogen) in accordance with the manufacturer's instructions. *E. coli* K-12 mutant strains were grown at 37°C to an OD₆₀₀ of 0.2, centrifuged at 5,000 \times g for 5 min, and stained in a 0.75% NaCl solution. Fluorescence intensity was continuously measured after protein or peptide addition (5 μ M) using a Cary Eclipse spectrofluorimeter (Varian Inc., Palo Alto, CA) as described previously (30). To calculate bacterial viability, the signal in the range of 510 to 540 nm was integrated to obtain the Syto 9 signal (live bacteria) and that in the range of 620 to 650 nm was integrated to obtain the propidium iodide (PI) signal (dead bacteria). The percentage of live bacteria was represented as a function of time, and t_{50} values were calculated by fitting the data to a simple exponential decay function.

Minimal agglutination concentration (MAC). *E. coli* cells were grown at 37°C to an OD₆₀₀ of 0.2, centrifuged at 5,000 \times g for 2 min, and resuspended in Tris-HCl buffer–0.1 M NaCl (pH 7.5) in order to give an

absorbance at 600 nm of 10. An aliquot of 200 μ l of the bacterial suspension was treated with increasing protein or peptide concentrations (from 0.01 to 10 μ M) and incubated at room temperature for 1 h. The aggregation behavior was observed by visual inspection, and the agglutinating activity is expressed as the minimum agglutinating concentration of the sample tested, as previously described (35).

Bacterial cytoplasmic membrane depolarization assay. Membrane depolarization was followed using a method described earlier (30). Briefly, *E. coli* K 12 strains were grown at 37°C to an OD₆₀₀ of 0.2, centrifuged at 5,000 \times g for 7 min, washed with 5 mM HEPES (pH 7.2) containing 20 mM glucose, and resuspended in 5 mM HEPES-KOH, 20 mM glucose, and 100 mM KCl at pH 7.2 to an OD₆₀₀ of 0.05. DiSC3(5) was added to a final concentration of 0.4 μ M, and changes in the fluorescence were continuously recorded after addition of protein or peptide (5 μ M). The time required to achieve half of total membrane depolarization was estimated from nonlinear regression analysis. The same assays were performed in the presence of 2 mM EDTA to perturb the LPS organization by chelation of divalent cations.

SEM. Briefly, *E. coli* K-12 strain cell cultures of 1 ml were grown at 37°C to mid-exponential phase (OD₆₀₀ of 0.2) and incubated with 5 μ M protein or peptides in phosphate-buffered saline (PBS) at room temperature. Sample aliquots were taken for up to 4 h of incubation and were prepared for analysis by scanning electron microscopy (SEM), as previously described (33).

Transmission electron microscopy (TEM). *E. coli* K-12 strains were grown to an OD₆₀₀ of 0.2 and incubated with 5 μ M ECP or peptides for 4 h. After treatment, bacterial pellets were prefixed with 2.5% glutaraldehyde and 2% paraformaldehyde in 0.1 M cacodylate buffer at pH 7.4 for 2 h at 4°C and postfixed in 1% osmium tetroxide buffered in 0.1 M cacodylate at pH 7.4 for 2 h at 4°C. The samples were dehydrated in acetone (50, 70, 90, 95, and 100%). The cells were immersed in Epon resin, and ultrathin sections were examined in a Jeol JEM 2011 instrument (Jeol Ltd., Tokyo, Japan).

Docking. Docking simulations were conducted with AutoDock 4.0 (Scripps Research Institute, La Jolla, CA). ECP structure 1DYT.pdb (22) was used as receptor molecule, and LPS ligand was obtained from 1FI1.pdb (13). Water molecules were removed from the structure; hydrogen atoms and atomic partial charges were added using Autodock Tools. In the first docking approach, receptor and ligand were kept rigid. The interaction of a probe group, corresponding to each type of atom found in the ligand, with the protein structure was computed at 0.5-Å grid positions in a 90-Å cubic box centered in the protein. The docking was accomplished using 150 Lamarckian genetic algorithm (LGA) runs, and the initial position of the ligand was random. The number of individuals in populations was set to 150. The maximum number of energy evaluations that the genetic algorithm should make was 2,500,000. The maximum number of generations was 27,000. The number of top individuals that are guaranteed to survive into the next generation was 1. Rates of gene mutation and crossover were 0.02 and 0.80, respectively. Following docking, all structures generated for the same compound were subjected to cluster analysis, with cluster families being based on a tolerance of 2 Å for an all-atom root mean square (RMS) deviation from a lower-energy structure.

For the second stage, the global minimum structure was subjected to redocking under the same conditions but allowing 8 rotatable bonds (see Fig. 7) and to cluster analysis using a box centered in the ligand with a 0.250-Å grid spacing.

RESULTS

In order to study the role of LPS in the antimicrobial action of ECP, we have evaluated four LPS-defective strains derived from *E. coli* K-12 D21 lacking the O-antigen portion, the latter being used as a control (Fig. 1A and B). The Ra chemotype (strain D21) possesses the entire LPS core, the Rc chemotype (strains D21e7 and D21e19) does not display any further sugar moiety after the hep-

TABLE 1 Antimicrobial activities of ECP and derived peptides with *E. coli* K-12 D21 and defective strains D21e7, D21e19, D21f1, and D21f2^a

Strain	IC ₅₀ , μ M (mean \pm SD)		
	ECP	[1-45]	[6-17]-Ahx-[23-36]
D21	0.4 \pm 0.1	0.9 \pm 0.4	2.5 \pm 0.1
D21e7	0.6 \pm 0.1	0.9 \pm 0.2	2.9 \pm 0.5
D21e19	0.8 \pm 0.1	1.2 \pm 0.3	3.5 \pm 0.3
D21f1	1.3 \pm 0.4	1.4 \pm 0.3	1.8 \pm 0.6
D21f2	2.9 \pm 0.4	1.4 \pm 0.2	1.8 \pm 0.1

^a Antimicrobial activity was calculated by following the bacterial viability as described in Materials and Methods.

tose portion (with only a Glu and/or Gal residue attached), the Rd chemotype (D21f1) contains the 3-deoxy-D-manno-octulosonic acid (Kdo) and heptose residues, while the D21f2 retains only the Kdo. The D21 strain is the only one that contains the phosphate residues associated with the LPS heptoses.

Bactericidal activity studies. At a first approach, we examined bacterial viability at different protein concentrations using the luminescent BacTiter Pro reagent (Promega). Viable, metabolically active cells are measured by ATP quantification using a coupled luminescence detection assay. Thus, the luminescent signal is proportional to the amount of ATP required for the conversion of luciferin into oxyluciferin in the presence of luciferase. From 0.1 to 10 μ M protein or peptide, IC₅₀s, defined as the concentration at which cell viability is reduced to 50%, were determined. The results show that ECP antimicrobial activity is dependent on both LPS length and charge (Table 1). For strains D21 to D21e19, the antimicrobial activity is only slightly reduced, but a more severe decrease is observed for strain D21f2, having the fully truncated LPS. A comparison with the two representative ECP N-terminal peptides (Fig. 1C) provided complementary data on the bactericidal activity modulation by the LPS outer layer. For peptide [1-45], a modest increase in IC₅₀s is detected when the LPS complexity is reduced. In turn, peptide [6-17]-Ahx-[23-36] displays an opposite trend compared with ECP, with strains D21f1 and D21f2 being the most sensitive to the peptide action (Table 1). Thus, LPS polysaccharide hinders peptide [6-17]-Ahx-[23-36] action rather than assisting it, contrary to what is observed for ECP and, to a lesser extent, for peptide [1-45].

To further understand the role of LPS in the antimicrobial action of ECP, we followed the time course of the bactericidal process using the LIVE/DEAD bacterial viability kit, consisting of a 1:1 mixture of Syto 9 and propidium iodide (PI) nucleic acid dyes. Syto 9 can cross the cytoplasmic membrane and label all bacterial cells, while PI can access only the content of membrane-damaged cells, competing with and displacing bound Syto 9. The integration of Syto 9 and PI fluorescence provides an estimation of the viability percentage for monitoring the kinetics of the bactericidal process. On one hand, the values obtained for the cell viability percentage after 4 h of incubation (Fig. 2A) are consistent with the IC₅₀s described above (Table 1). On the other hand, the time of half viability (*t*₅₀), defined as the time needed to reduce cell viability to 50%, particularly increases for strain D21f2 with both ECP and peptide [1-45] (Fig. 2B). However, for [6-17]-Ahx-[23-36], *t*₅₀ values are similar for all strains tested, suggesting that the bactericidal kinetics for the latter peptide are independent of LPS structure.

To examine the influence of LPS structure on ECP action at the

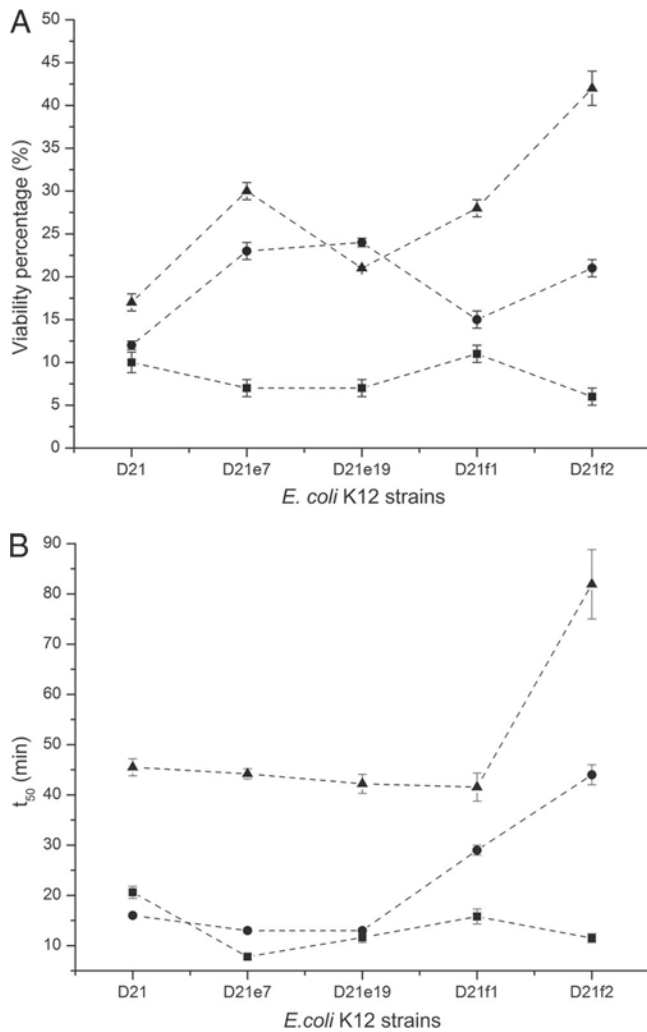


FIG 2 Viability percentage and half time were determined with the LIVE/DEAD kit after 4 h of incubation of mid-log-phase-grown *E. coli* K-12 D21, D21e7, D21e19, D21f1, and D21f2 cultures with 5 μ M protein and peptides. The percent viability (A) and half time of viability (B) after incubation with ECP (\blacktriangle), [1-45] (\bullet), or [6-17]-Ahx[23-36] (\blacksquare) are depicted. The order of the strains on the x axis denotes increasing degrees of LPS truncation.

bacterial cell membrane, we used the DiSC3(5) fluorescent probe, which is sensitive to membrane potential. The DiSC3(5) fluorescence is quenched upon interaction with intact cell membranes. When the membrane potential is lost, the probe is released to the medium, resulting in an increase of fluorescence that can be recorded as a function of time. Thus, we have measured the half-depolarization time (t_{50}), defined as the time needed to achieve a half-depolarization effect. For ECP, the depolarization is delayed as a function of the LPS truncation grade (Fig. 3). However, peptide [6-17]-Ahx-[23-36] shows similar t_{50} values for all the strains tested, suggesting that depolarization is not affected by LPS composition. Furthermore, the presence or absence of EDTA in the incubation medium has no effect on membrane depolarization (data not shown). EDTA is a chelating agent that disrupts LPS structure by sequestering divalent cations that tightly pack the polysaccharide moiety of LPS. These results suggest that both ECP and peptides by themselves may efficiently displace the divalent cations from the outer layer.

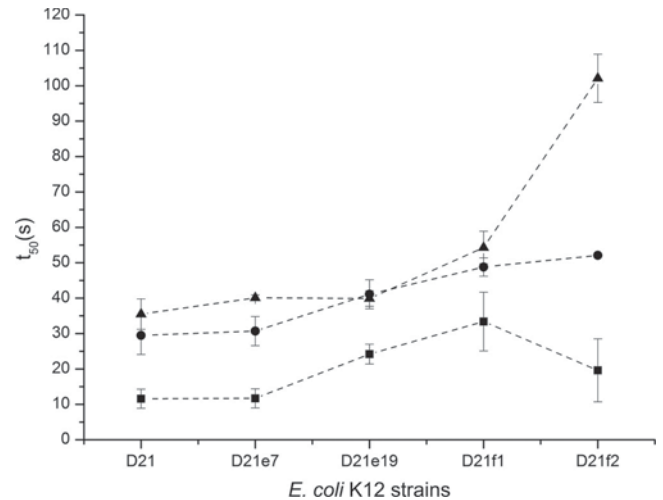


FIG 3 Depolarization activity on *E. coli* K-12 D21, D21e7, D21e19, D21f1, and D21f2 cells was followed using the DiSC3(5) dye depolarization assay with a 5 μ M protein concentration. The time needed to achieve a half-depolarizing effect is depicted for ECP (\blacktriangle), [1-45] (\bullet), and [6-17]-Ahx[23-36] (\blacksquare). The order of the strains on the x axis denotes increasing degrees of LPS truncation.

Finally, *E. coli* K-12 mutants were visualized by transmission electron microscopy (TEM) after incubation (Fig. 4). For ECP a complete disruption of cell integrity was observed. Outer bacterial layers were detached, and the cell shape was considerably altered, suggesting that ECP induces a mechanical disruption of the cell. Material condensation appears as electron-dense granular areas inside the cell, even in the D21f2 mutant strain. For peptide [1-45], a similar behavior is observed, though the outer layers seem to suffer less from mechanical disruption. Mutant strains D21f1 and D21f2 appear to be less condensed, and, particularly in strain D21f2, the outer layers seem to be well preserved. In contrast, for peptide [6-17]-Ahx-[23-36], the outer layer morphology is not significantly altered compared with that of control cells, and neither condensation nor material spillage outside the cell is observed. It is important to highlight that no bacterial agglutination can be observed by TEM due to sample preparation.

These results together suggest that ECP and peptide [1-45] display similar mechanisms of action, needing the entire LPS structure to ensure bacterial killing. In contrast, the action of peptide [6-17]-Ahx-[23-36] action is hindered by complex LPS structures, suggesting a different mechanism of action.

Studies of agglutinating activity. It has been described that ECP shows high LPS affinity and can agglutinate *E. coli* cells in the micromolar range (30). To quantify the agglutinating activity, we determined the minimal agglutination concentration (MAC), defined as the minimal peptide concentration able to induce agglutination in bacteria (35). Again, a correlation can be observed between LPS core complexity and agglutinating activity (Fig. 5). Strain D21f2, with the shortest LPS, shows no agglutination even after 12 h of incubation with 5 μ M ECP. This behavior was observed for both ECP and peptides. However, peptide [6-17]-Ahx-[23-36] needed a much higher concentration to promote bacterial cell agglutination, perhaps due to its lower affinity for LPS (35).

With the aim of studying cell surface morphology, we examined bacterial cultures by scanning electron microscopy (SEM). For all *E. coli* K-12 mutants, consistent cell damage was observed

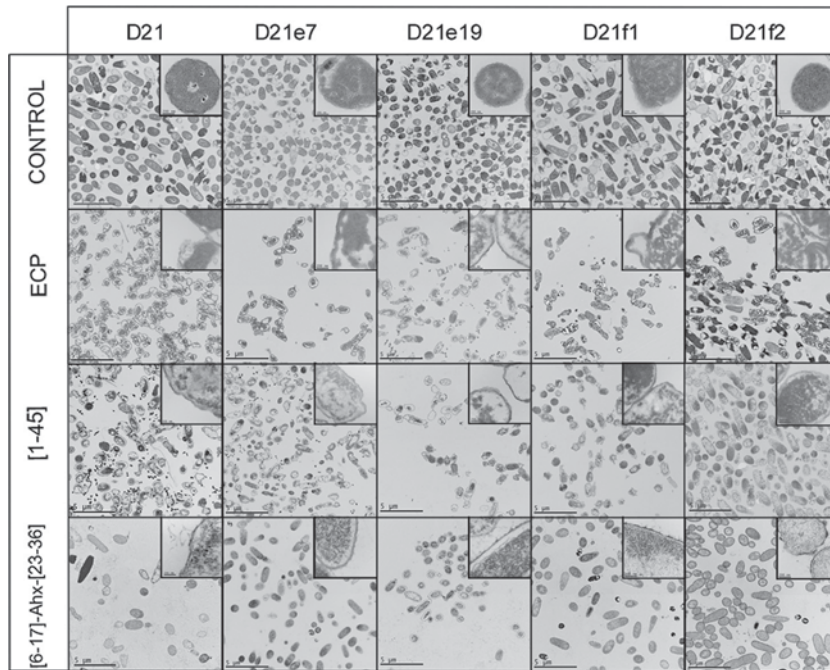


FIG 4 Transmission electron micrographs of *E. coli* K-12 strains (D21, D21e7, D21e19, D21f1, and D21f2) incubated in the presence of 5 μ M ECP, [1-45], or [6-17]-Ahx[23-36] for 4 h. The magnification scale is indicated at the bottom of each micrograph.

after incubation with both ECP and peptides (Fig. 6). For ECP, a high degree of cell agglutination, for strains D21 to D21f1, is observed. While the characteristic baton-shaped cell morphology is maintained, the bacterial cell wall appears to be considerably damaged and only strain D21f2 displays a low degree of agglutination, in agreement with the MAC experiments described above. For

peptide [1-45], similar agglutination levels are observed, also showing a high level of damage at the cell surface, except for strain D21f2. However, for peptide [6-17]-Ahx-[23-36], only small clusters of bacteria were observed, with the cell wall being only locally damaged. These observations agree with the TEM images, where neither material spillage nor material condensation was found.

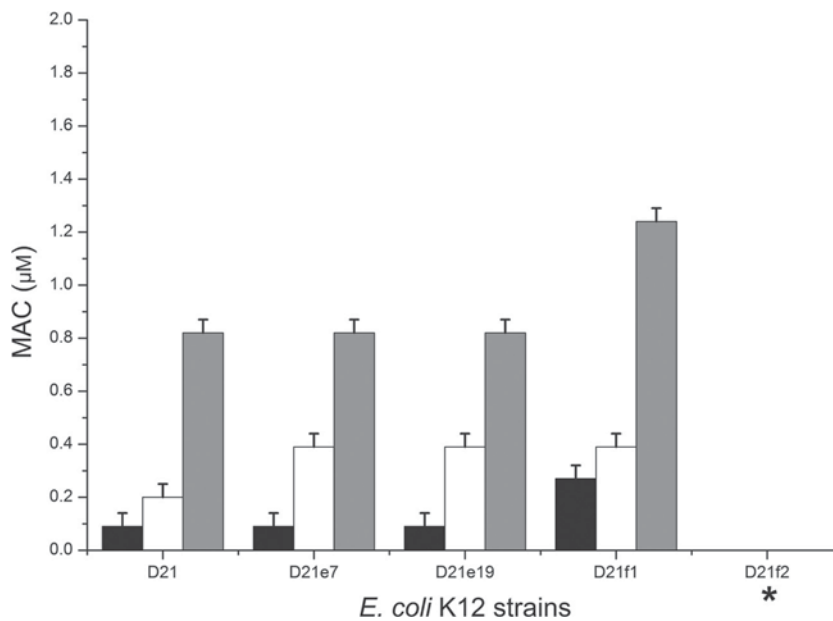


FIG 5 The agglutination activity was evaluated by the calculation of the minimal agglutination concentration (MAC) of the sample tested, corresponding to the first condition where bacterial aggregates are visible to the naked eye. The results for ECP (black bars), [1-45] (white bars), and [6-17]-Ahx[23-36] (gray bars) are shown. *, strain D21f2 does not show agglutination up to a concentration of 10 μ M. The order of the strains on the x axis denotes increasing degrees of LPS truncation.

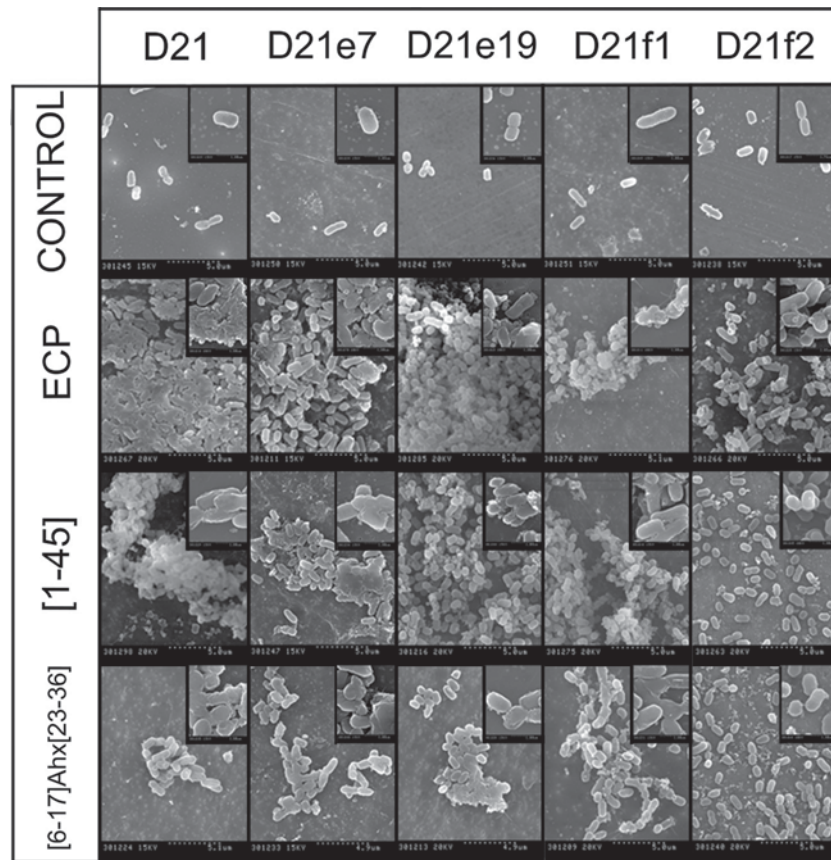


FIG 6 Scanning electron micrographs of *E. coli* K-12 strains (D21, D21e7, D21e19, D21f1, and D21f2) incubated in the presence of 5 μ M ECP, [1-45], or [6-17]-Ahx[23-36] for 4 h. The magnification scale is shown at the bottom of each micrograph.

DISCUSSION

LPS is thought to act as a permeability barrier for antibiotics, detergents, and host proteins (25). It has been described that Gram-positive bacteria are more susceptible to specific antibiotics than Gram-negative, less permeable bacteria (29). Several hypotheses can explain how LPS modulates Gram-negative outer envelope permeability. Nikaido and coworkers have suggested that the carbohydrate moiety would act as a barrier against hydrophobic molecules (25), thus explaining why the permeability of some antibiotics (e.g., cephalosporins) is proportional to their hydrophobicity (19). In fact, X-ray diffraction studies suggest that LPS thickness (i.e., its polysaccharide content) is inversely proportional to outer membrane permeability (29), supporting the aforementioned hypothesis (25).

On the other hand, some AMPs (e.g., lactoferrin or lysozyme) seem to decrease their antimicrobial activity with a progressively truncated LPS core (26), similarly to what was observed for ECP in the present study (Table 1). Additionally, ECP can induce the agglutination of Gram-negative bacteria, a behavior that is not shared with many other AMPs. Indeed, the agglutinating activity of ECP seems to be crucial for its antimicrobial action, suggesting that agglutination is required for bacterial killing (35).

The agglutinating activity is evidenced by SEM micrographs showing that rough mutants, but not the D21f2 deep-rough mutant, become clumped after treatment with ECP (Fig. 6). We thus suggest that the LPS polysaccharide moiety is essential to trigger

Gram-negative bacterial cell agglutination, which is directly correlated with antimicrobial activity (Table 1; Fig. 5). For the D21f2 deep-rough mutant, agglutination is almost insignificant, which is translated to high MIC values, increased times to reduce cell culture viability, and slow depolarization kinetics (Table 1 and Fig. 2 and 3). We conclude from these data that ECP needs to first interact with the polysaccharide moiety of LPS, triggering cell agglutination. This process will mechanically disrupt the bacterial outer layer (Fig. 4), thus disturbing the membrane potential and bacterial homeostasis. Binding affinity to LPS was previously confirmed for the whole protein (33) and for the [1-45] peptide (32).

Simulations of docking of ECP to LPS show a high affinity for the complex (-16.53 kcal/mol). LPS is docked on the N-terminal cationic patch of ECP (Fig. 7A), with the protein interacting in the interface between lipid A and the polysaccharide moiety of LPS (Fig. 7B). Specific hydrogen-bonding contacts are observed for Arg1, Trp10, Gln14, Lys38, and Gln40 (Fig. 7C). These results may explain the severe decrease in the antimicrobial and agglutinating activities observed for the D21f2 mutant, which lacks the sugar molecules shown to bind to ECP.

The results were then compared with those for the ECP [1-45] peptide, which corresponds to the ECP antimicrobial domain located at the N terminus (32). We have observed here that the agglutinating activity is maintained, though it is slightly reduced (Fig. 5). The antimicrobial activity and the mechanical disruption of bacterial cells are also conserved (Table 1; Fig. 4). In fact, pep-

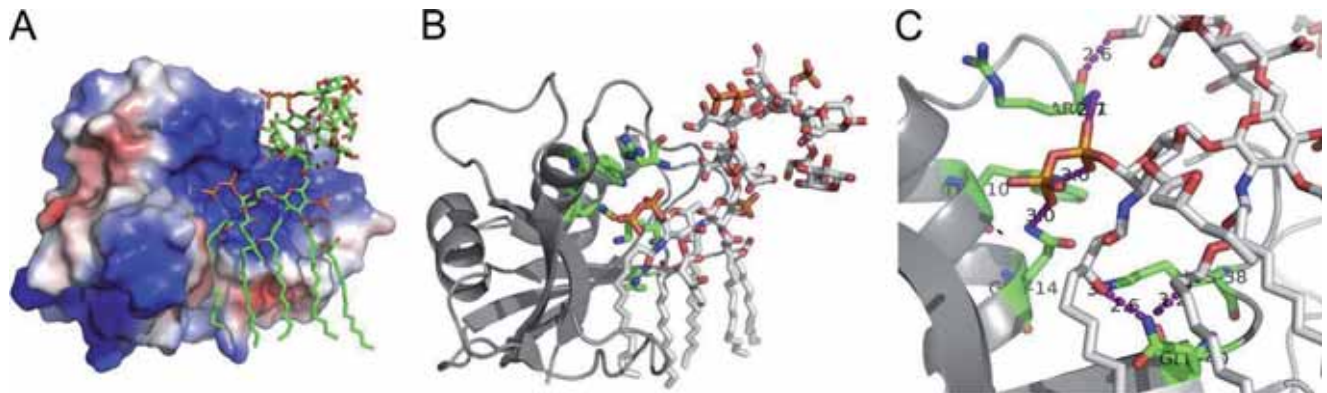


FIG 7 Complex of ECP and LPS calculated by molecular docking. (A) Electrostatic potential map of ECP in complex with LPS. Cationic residues are colored in blue and anionic residues in red. (B and C) Detail of the complex between ECP and LPS. Interactions are highlighted in purple. Docking simulations were conducted with Autodock 4. Protein Data Bank (PDB) codes are 1DYT for ECP (22) and 1F11 for LPS (13). The figure was constructed using PyMOL.

tide [1-45] conserves the residues described to be crucial to bind sulfate anions (E. Boix et al., unpublished results), as well as phosphorylated and sulfated polysaccharides (16, 34), which also correspond to the domain identified by molecular docking (Fig. 7).

In the search for the minimum template that retains the antimicrobial action of ECP, peptide [6-17]-Ahx-[23-36] was designed and shown to conserve the antimicrobial activity against a wide battery of bacterial strains (35). Nonetheless, we find here that the mechanism of action is not conserved despite its equal activity. Indeed, the shorter peptide construct has limited LPS affinity (35). Peptide [6-17]-Ahx-[23-36] displays a significant reduction of bacterial agglutination and does not cause notable mechanical cell disruption (Fig. 4 and 5). Peptide [6-17]-Ahx-[23-36] is more efficient in membrane depolarization (Fig. 3), which is not affected by LPS composition, a behavior that seems to correlate with cell viability kinetics (Fig. 2). In this case, LPS length is inversely correlated with MIC values (Table 1) suggesting that the polysaccharide LPS moiety would act as a permeation barrier. Indeed, peptide [6-17]-Ahx-[23-36] is the most hydrophobic compound, with a hydrophobic-to-hydrophilic ratio of 0.9 (ratios of 0.6 and 0.8 were calculated for ECP and peptide [1-45], respectively), in agreement with the hypothesis that LPS would act as a barrier for more-hydrophobic compounds. The mechanism of action displayed by peptide [6-17]-Ahx-[23-36] is also more lytic, though it turns out to be less selective for bacterial membranes, increasing the hemolytic activity compared with that of ECP (35). Thus, ECP and its N-terminal domain show a higher selectivity for bacterial structures, favoring agglutination and cell wall damage instead of having a mere cell membrane-lytic mechanism.

In summary, we show that both ECP and its N terminus display antimicrobial and agglutinating activities that are dependent on LPS structure. However, the shorter peptide [6-17]-Ahx-[23-36] displays lower agglutinating activity though retaining the antimicrobial activity, suggesting a different mechanism of action. We conclude that the antimicrobial domain of ECP exerts a global action on bacteria by mechanically disrupting the outer layer, whereas shorter derived peptides have a more unspecific action directly at the inner membrane level.

ACKNOWLEDGMENTS

The work was supported by the Ministerio de Educación y Cultura (grant number BFU2009-09371), cofinanced by FEDER funds and by the Gen-

eralitat de Catalunya (2009 SGR 795). D.P is a recipient of a UAB predoctoral fellowship, and M.T. is a recipient of an Alianza Cuatro Universidades postdoctoral fellowship.

Spectrofluorescence measurements were performed at the Laboratori d'Anàlisi i Fotodocumentació, UAB. We thank Alejandro Sánchez-Chardi for his assistance with the electron microscopy samples at the Servei de Microscopia, UAB.

REFERENCES

- Boix E, et al. 1999. Kinetic and product distribution analysis of human eosinophil cationic protein indicates a subsite arrangement that favors exonuclease-type activity. *J. Biol. Chem.* 274:15605–15614.
- Boix E, Nogues MV. 2007. Mammalian antimicrobial proteins and peptides: overview on the RNase A superfamily members involved in innate host defence. *Mol. Biosyst.* 3:317–335.
- Boix E, Torrent M, Sanchez D, Nogues MV. 2008. The antipathogen activities of eosinophil cationic protein. *Curr. Pharm. Biotechnol.* 9:141–152.
- Brandenburg K, Andra J, Garidel P, Gutschmann T. 2011. Peptide-based treatment of sepsis. *Appl. Microbiol. Biotechnol.* 90:799–808.
- Brandenburg K, et al. 2010. Molecular basis for endotoxin neutralization by amphipathic peptides derived from the alpha-helical cationic core-region of NK-lysin. *Biophys. Chem.* 150:80–87.
- Brandenburg K, et al. 1993. Influence of the supramolecular structure of free lipid A on its biological activity. *Eur. J. Biochem.* 218:555–563.
- Brogden KA. 2005. Antimicrobial peptides: pore formers or metabolic inhibitors in bacteria? *Nat. Rev. Microbiol.* 3:238–250.
- Brown KL, Hancock RE. 2006. Cationic host defense (antimicrobial) peptides. *Curr. Opin. Immunol.* 18:24–30.
- Caroff M, Karibian D. 2003. Structure of bacterial lipopolysaccharides. *Carbohydr Res.* 338:2431–2447.
- Carreras E, Boix E, Rosenberg HF, Cuchillo CM, Nogues MV. 2003. Both aromatic and cationic residues contribute to the membrane-lytic and bactericidal activity of eosinophil cationic protein. *Biochemistry* 42:6636–6644.
- Cohen J. 2002. The immunopathogenesis of sepsis. *Nature* 420:885–891.
- Delcour AH. 2009. Outer membrane permeability and antibiotic resistance. *Biochim. Biophys. Acta* 1794:808–816.
- Ferguson AD, et al. 2001. Active transport of an antibiotic rifamycin derivative by the outer-membrane protein FhuA. *Structure* 9:707–716.
- Fields GB, Noble RL. 1990. Solid phase peptide synthesis utilizing 9-fluorenylmethoxycarbonyl amino acids. *Int. J. Pept Protein Res.* 35:161–214.
- Freder V, Ho B, Ding JL. 2004. De novo design of potent antimicrobial peptides. *Antimicrob. Agents Chemother.* 48:3349–3357.
- García-Mayoral MF, et al. 2010. NMR structural determinants of eosinophil cationic protein binding to membrane and heparin mimetics. *Biophys. J.* 98:2702–2711.
- Gutschmann T, et al. 2010. New antiseptic peptides to protect against endotoxin-mediated shock. *Antimicrob. Agents Chemother.* 54:3817–3824.

18. Hancock RE. 1997. Peptide antibiotics. *Lancet* 349:418–422.
19. Hiruma R, Yamaguchi A, Sawai T. 1984. The effect of lipopolysaccharide on lipid bilayer permeability of beta-lactam antibiotics. *FEBS Lett.* 170: 268–272.
20. Jeong H, et al. 2009. Genome sequences of *Escherichia coli* B strains REL606 and BL21(DE3). *J. Mol. Biol.* 394:644–652.
21. Laurents DV, et al. 2009. The (1)H, (13)C, (15)N resonance assignment, solution structure, and residue level stability of eosinophil cationic protein/RNase 3 determined by NMR spectroscopy. *Biopolymers* 91: 1018–1028.
22. Mallorqui-Fernandez G, et al. 2000. Three-dimensional crystal structure of human eosinophil cationic protein (RNase 3) at 1.75 Å resolution. *J. Mol. Biol.* 300:1297–1307.
23. Mangoni ML. 2011. Host-defense peptides: from biology to therapeutic strategies. *Cell. Mol. Life Sci.* 68:2157–2159.
24. Matsuzaki K, Sugishita K, Miyajima K. 1999. Interactions of an antimicrobial peptide, magainin 2, with lipopolysaccharide-containing liposomes as a model for outer membranes of gram-negative bacteria. *FEBS Lett.* 449:221–224.
25. Nikaido H. 2003. Molecular basis of bacterial outer membrane permeability revisited. *Microbiol. Mol. Biol. Rev.* 67:593–656.
26. Prokhorenko IR, Zubova SV, Ivanov AY, Grachev SV. 2009. Interaction of Gram-negative bacteria with cationic proteins: dependence on the surface characteristics of the bacterial cell. *Int. J. Gen. Med.* 2:33–38.
27. Raetz CR. 1990. Biochemistry of endotoxins. *Annu. Rev. Biochem.* 59: 129–170.
28. Sanchez D, et al. 2011. Mapping the eosinophil cationic protein antimicrobial activity by chemical and enzymatic cleavage. *Biochimie* 93:331–338.
29. Snyder DS, McIntosh TJ. 2000. The lipopolysaccharide barrier: correlation of antibiotic susceptibility with antibiotic permeability and fluorescent probe binding kinetics. *Biochemistry* 39:11777–11787.
30. Torrent M, et al. 2010. Comparison of human RNase 3 and RNase 7 bactericidal action at the Gram-negative and Gram-positive bacterial cell wall. *FEBS J.* 277:1713–1725.
31. Torrent M, et al. 2007. Topography studies on the membrane interaction mechanism of the eosinophil cationic protein. *Biochemistry* 46:720–733.
32. Torrent M, de la Torre BG, Nogues VM, Andreu D, Boix E. 2009. Bactericidal and membrane disruption activities of the eosinophil cationic protein are largely retained in an N-terminal fragment. *Biochem. J.* 421: 425–434.
33. Torrent M, Navarro S, Moussaoui M, Nogues MV, Boix E. 2008. Eosinophil cationic protein high-affinity binding to bacteria-wall lipopolysaccharides and peptidoglycans. *Biochemistry* 47:3544–3555.
34. Torrent M, Nogues MV, Boix E. 2011. Eosinophil cationic protein (ECP) can bind heparin and other glycosaminoglycans through its RNase active site. *J. Mol. Recognit.* 24:90–100.
35. Torrent M, et al. 2011. Refining the eosinophil cationic protein antibacterial pharmacophore by rational structure minimization. *J. Med. Chem.* 54:5237–5244.
36. Torrent M, et al. 2009. Comparison of the membrane interaction mechanism of two antimicrobial RNases: RNase 3/ECP and RNase 7. *Biochim. Biophys. Acta* 1788:1116–1125.
37. Venge P. 2010. The eosinophil and airway remodelling in asthma. *Clin. Respir. J.* 4(Suppl 1):15–19.

CHAPTER III

Exploring New Biological Functions of Amyloids: Bacteria Cell Agglutination Mediated by Host Protein Aggregation

Marc Torrent^{1,2*}, David Pulido¹, M. Victòria Nogués¹, Ester Boix^{1*}

¹ Department of Biochemistry and Molecular Biology, Biosciences Faculty, Universitat Autònoma de Barcelona, Cerdanyola del Vallès, Spain, ² Department of Experimental and Health Sciences, Universitat Pompeu Fabra, Barcelona Biomedical Research Park, Barcelona, Spain

Abstract

Antimicrobial proteins and peptides (AMPs) are important effectors of the innate immune system that play a vital role in the prevention of infections. Recent advances have highlighted the similarity between AMPs and amyloid proteins. Using the Eosinophil Cationic Protein as a model, we have rationalized the structure-activity relationships between amyloid aggregation and antimicrobial activity. Our results show how protein aggregation can induce bacteria agglutination and cell death. Using confocal and total internal reflection fluorescence microscopy we have tracked the formation *in situ* of protein amyloid-like aggregates at the bacteria surface and on membrane models. In both cases, fibrillar aggregates able to bind to amyloid diagnostic dyes were detected. Additionally, a single point mutation (Ile13 to Ala) can suppress the protein amyloid behavior, abolishing the agglutinating activity and impairing the antimicrobial action. The mutant is also defective in triggering both leakage and lipid vesicle aggregation. We conclude that ECP aggregation at the bacterial surface is essential for its cytotoxicity. Hence, we propose here a new prospective biological function for amyloid-like aggregates with potential biological relevance.

Citation: Torrent M, Pulido D, Nogués MV, Boix E (2012) Exploring New Biological Functions of Amyloids: Bacteria Cell Agglutination Mediated by Host Protein Aggregation. *PLoS Pathog* 8(11): e1003005. doi:10.1371/journal.ppat.1003005

Editor: H. Steven Seifert, Northwestern University Feinberg School of Medicine, United States of America

Received: May 28, 2012; **Accepted:** September 17, 2012; **Published:** November 1, 2012

Copyright: © 2012 Torrent et al. This is an open-access article distributed under the terms of the Creative Commons Attribution License, which permits unrestricted use, distribution, and reproduction in any medium, provided the original author and source are credited.

Funding: M.T. is a recipient of an Alianza Cuatro Universidades fellowship. D.P. is a recipient of a FPU fellowship (MICINN). Microscopy experiments were carried at the Servei de Microscòpia (UAB) and fluorescence measurements at Servei d'Anàlisi i Fotodocumentació (UAB). The work was funded by MICINN (BFU2009-09371), FEDER funds and Generalitat de Catalunya (2009 SGR 795). The funders had no role in study design, data collection and analysis, decision to publish, or preparation of the manuscript.

Competing Interests: The authors have declared that no competing interests exist.

* E-mail: marc.torrent@uab.cat (MT); ester.boix@uab.cat (EB)

Introduction

Antimicrobial proteins and peptides (AMPs) represent a wide family that contributes to the host defense system with multiple pathogen killing strategies [1–3]. Their fast and multitarget mechanism of action reduces the emergence of bacteria resistance and represents a valuable alternative for common antibiotics [4,5].

The mechanism of action of AMPs has been systematically investigated, suggesting that AMPs bind to bacteria cell membranes and disrupt cell homeostasis. However, more investigations are needed to completely understand how different structures determine the function of AMPs [6–12]. Membrane damage is a multifaceted mechanism that can involve different peptide assemblies and ultimately promotes membrane permeabilization when achieving a critical concentration [13,14]. Several authors have highlighted the striking resemblance of membrane disrupting mechanisms with those observed for amyloid peptides and proteins [15–17]. In both cases, membrane composition (e.g. cholesterol content) and biophysical properties (e.g. membrane fluidity and curvature) were found critical for the peptide action [13,15,18–26]. Furthermore, we have recently suggested that antimicrobial activity could have arisen through cationization of amyloid-prone regions [27]. In this light, some AMPs have been described to form amyloid structures *in vitro* [28,29] and some amyloid peptides have also been considered as putative AMPs [30,31]. In fact, we have

proposed that inherent AMP aggregation properties can modulate antimicrobial activity [32].

Interestingly, some antimicrobial proteins and peptides have been found to agglutinate bacteria cells. In this sense, bacteria agglutination has been ascribed to unspecific adhesion through hydrophobic interactions, as observed for synthetic peptides derived from the parotid secretory protein [33]. Comparative analysis on those peptides highlighted the contributions of both hydrophobic and cationic residues in the agglutination activity [33]. These results suggest that some AMPs could exploit their intrinsic aggregation properties, by triggering bacteria agglutination as part of its mechanism of action as observed for a wealth source of AMPs in saliva, which provides a first barrier to bacteria adherence in the oral cavity [34]. Agglutinating activity has been reported crucial for the antimicrobial function of Eosinophil Cationic Protein (ECP) [35], a small cationic protein specifically secreted by eosinophil granules during inflammation processes with diverse antipathogen activities [36–38]. ECP displays high antimicrobial action, with a specific bacteria agglutination activity reported for Gram-negative bacteria, at a concentration range close to the minimal inhibitory concentration, a behavior that may represent an effective bactericidal mechanism *in vivo* [39].

In order to characterize the relation between AMPs, bacteria agglutination and amyloid aggregation, we have used ECP as a model of study. We present here a detailed characterization of

Author Summary

Microbial infections are reported among the worst human diseases and cause millions of deaths per year over the world. Antibiotics are used to treat infections and have saved more lives than any other drug in human history. However, due to extended use, many strains are becoming refractive to common antibiotics. In this light, new promising compounds, like antimicrobial proteins and peptides (AMPs) are being investigated. Some AMPs also show agglutinating activity; this is the ability to clump bacteria after treatment. This feature is particularly appealing because agglutinating peptides could be used to keep bacteria to the infection focus, helping microbe clearance by host immune cells. In this study, we propose a novel mechanism to explain agglutinating activity at a molecular level using Eosinophil Cationic Protein. We show that the agglutinating mechanism is driven by the protein amyloid-like aggregation at the bacteria cell surface. Accordingly, elimination of the amyloid behavior abolishes both the agglutinating and the antimicrobial activities. This study provides a new concept on how Nature could exploit amyloid-like aggregates to fight bacterial infections. Moreover, these results could also add new insights in understanding the relation between infection and inflammation with dementia and amyloid-related diseases like Alzheimer.

protein-mediated bacteria agglutination and prove the contribution of an aggregation prone domain to the protein antimicrobial action. Complementary studies on model membranes provide a further understanding of the membrane damage process promoted by protein aggregation.

Results/Discussion

ECP was previously reported to aggregate *in vivo* on both bacterial and eukaryotic cell surface without detectable internalization [39,40]. Though these findings were essential to explain the antimicrobial and cytotoxic properties of ECP, the real nature of the aggregation process remained unknown. Besides, the protein has a high affinity towards lipopolysaccharides (LPS) [41] and agglutinates all tested Gram-negative strains [42]. On the other hand, ECP has been reported to form amyloid-like aggregates *in vitro* at specific conditions due to a hydrophobic patch located at the N-terminus. Remarkably, protein amyloid-like aggregation was efficiently abolished by mutating Ile 13 to Ala [28]. The screening of the protein primary structure [43–45] and the design of derived peptides [42,46] also allocated the antimicrobial region at the N-terminus. As the antimicrobial and amyloid active

segments of the protein colocalize [28,35,42,46], it is tempting to hypothesize that bacteria agglutination by ECP could be directly dependent on an amyloid-like aggregation process. This hypothesis raises some exciting questions: (i) Is cell agglutination required for antimicrobial activity? (ii) Is cell agglutination mediated by protein aggregation at the bacteria surface? (iii) Are aggregates formed on the surface of bacteria of amyloid nature?

Bacteria cell agglutination and antimicrobial activities

To address the first question we compared the antimicrobial action of wild type ECP (wtECP) with the I13A mutant, previously described to be unable to form aggregates *in vitro* [28]. The antimicrobial assays reveal that, while wtECP has an average minimal inhibitory concentration (MIC) value around 0.5–1 μM , the I13A mutant is unable to kill bacteria even at 5 μM concentration (Table 1). To further correlate ECP antimicrobial and agglutination activities we studied bacteria cell cultures by confocal microscopy using the SYTO9/Propidium iodide nucleic acid fluorescent labels that allow registering both cell agglutination and viability over time. Interestingly, wtECP can agglutinate Gram-negative bacteria before a viability decrease is observed (Figure 1A), however no cell agglutination takes place when bacteria are incubated with the I13A variant, even after 4 hours (Supporting Information Figure S1). These results are also supported by minimal agglutination concentrations (MAC) close to the MIC values (Table 1) and by FACS experiments showing that wtECP but not I13A mutant is able to agglutinate *E. coli* cells (Figure 1B). Thus, ECP antimicrobial activity on Gram-negative strains is strongly affected when abolishing the agglutination behavior (Ile13 to Ala mutation).

Protein aggregation on membrane models

To further analyze the protein agglutination mechanism, we tested the wtECP and I13A mutant action on a simpler biophysical system such as phospholipid membranes where liposome agglutination is registered as a function of protein concentration. In contrast to wtECP, I13A mutant completely loses the ability to agglutinate membranes (Figure 2A). In particular, when following wtECP agglutinating activity as a function of ionic strength, we observe that liposome agglutination is enhanced at high NaCl concentration (Supporting Information, Figure S2). These results suggest that vesicle agglutination is promoted by hydrophobic interactions. Even more, leakage activity in model membranes is also lost for I13A mutant (Figure 2B), meaning that protein aggregation on the membrane surface is important not only for agglutination but also for later membrane permeabilization. These results are entirely consistent with those described above for bacteria cell cultures where the Ile to Ala mutation not only

Table 1. Antimicrobial (MIC₁₀₀) and agglutinating (MAC) activities of wtECP and I13A mutant in Gram-negative strains.

	MIC ₁₀₀ (μM)		MIC ₁₀₀ (μM)		MAC (μM)		MAC (μM)	
	Phosphate buffer ^a		MH medium ^b		Phosphate buffer ^a		MH medium ^b	
	ECP	I13A	ECP	I13A	ECP	I13A	ECP	I13A
<i>E. coli</i>	0.40±0.10	>5	0.45±0.10	>5	0.25±0.1	>5	0.25±0.1	>5
<i>P. aeruginosa</i>	0.60±0.15	>5	0.90±0.20	>5	0.5±0.1	>5	0.5±0.1	>5
<i>A. baumannii</i>	0.75±0.15	>5	1.25±0.20	>5	1.0±0.2	>5	1.0±0.2	>5

^aBacteria were grown in LB medium and incubated with proteins in 10 mM NaH₂PO₄, 100 mM NaCl pH 7.4.

^bBacteria were grown and incubated with proteins in Mueller–Hinton II broth.

doi:10.1371/journal.ppat.1003005.t001

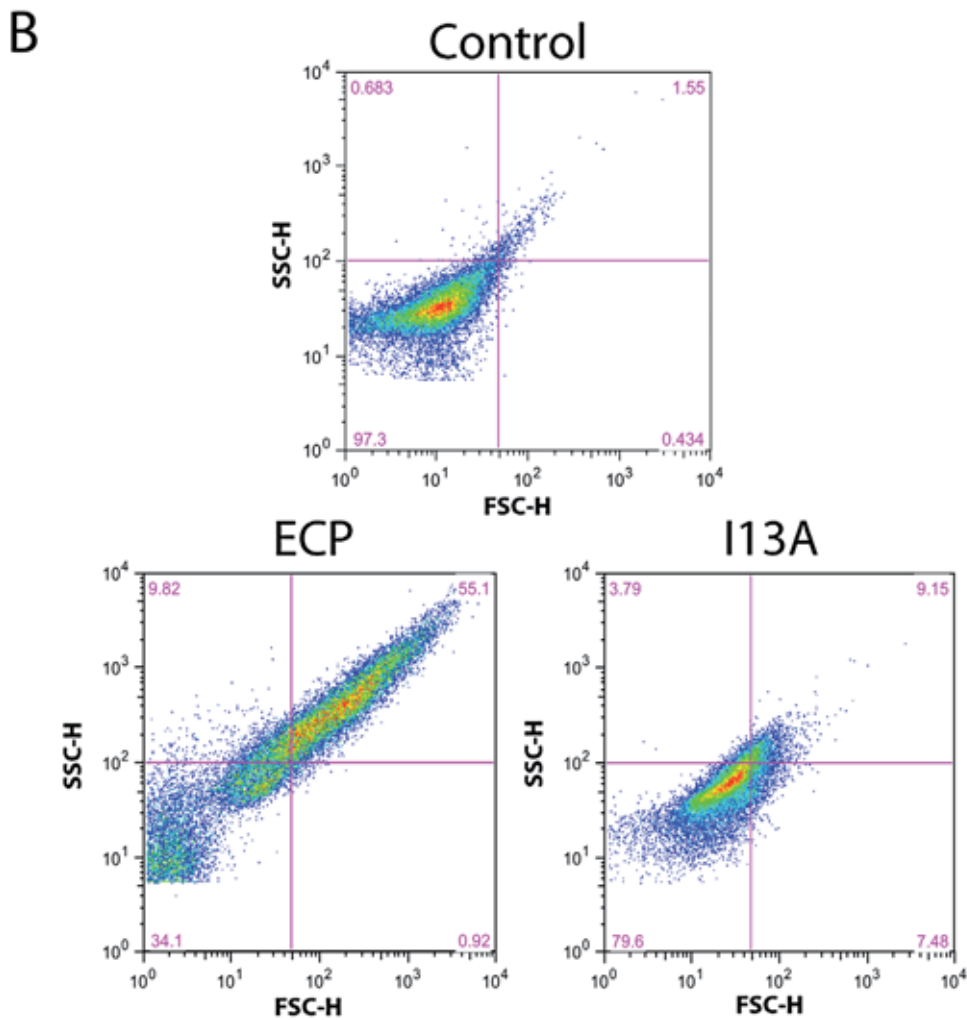
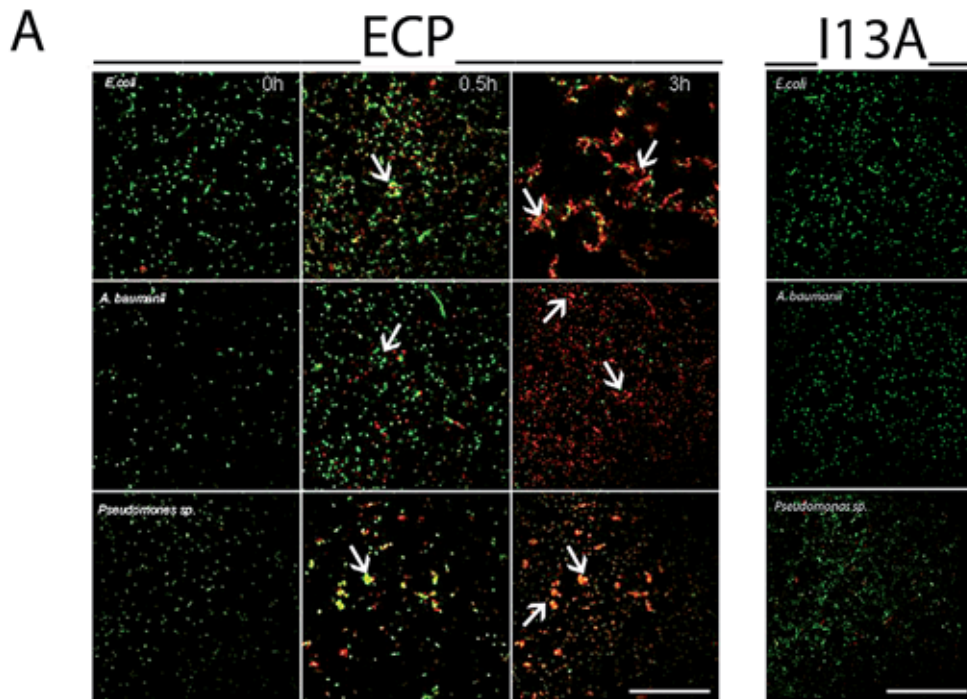


Figure 1. ECP but not I13A is able to agglutinate bacteria. (A) *E. coli*, *P. aeruginosa* and *A. baumannii* cells were incubated with 5 μ M of ECP or I13A mutant in microscopy plates during 4 h and stained with syto9 (live cells, green) and propidium iodide (dead cells, red). Images were taken at 0, 0.5 and 3 h using a Leica SP2 confocal microscopy as described in the *Materials and Methods* section. Scale bar represents 50 μ m. Arrows were depicted to show cell agglutination. Images depicted are representative from two independent experiments. (B) *E. coli* cells were incubated with 5 μ M of ECP or I13A mutant during 4 h and samples were analyzed using a FACSCalibur cytometer. FSC-H is the low-angle forward scattering, which is roughly proportional to the diameter of the cell and SSC-H is the orthogonal or side scattering, which is proportional to cell granularity or complexity. Agglutination is registered as an increase in both scattering measures. In all experiments cell cultures were grown at exponential phase ($OD_{600}=0.2$) and incubated with proteins in 10 mM sodium phosphate buffer, 100 mM NaCl, pH 7.4. The plots are representative of three independent experiments.
doi:10.1371/journal.ppat.1003005.g001

abolishes the cell agglutinating activity of ECP but also its bactericidal action.

Agglutination mediated by protein aggregation

Next, to address the question whether cell agglutination is consistently driven by protein aggregation at the bacteria surface, we incubated bacteria cultures with ECP and visualized the samples using confocal microscopy. Our results show that wtECP binds to the bacteria surface and a strong protein signal is registered at the aggregation zones (Figure 3A). On the contrary, though cell interaction is maintained for the I13A mutant, agglutination is observed neither in bacteria cell cultures nor in model membranes (Figures 3A and 3B). As expected, for model membranes we show that only wtECP is able to promote agglutination (Figure 3B). Therefore, we conclude that protein aggregation on the cellular surface is required for bacteria agglutination, which turns to be essential for the antimicrobial action. Agglutination is also observed in the presence of 20% plasma in a similar extent, suggesting that ECP agglutination is likely to take place in the physiological context (Supplementary Information Figure S3). As previously mentioned, ECP binding to bacteria is favored by interactions with the LPS outer membrane [35,41,47]. Consistently, we show here that LPS binding activity is lost for the I13A mutant, when compared with wtECP (Supplementary Information Figure S4).

In situ follow-up of amyloid aggregates

At this point however, the nature of the protein aggregates remained unknown. Thus, having previously shown that ECP is able to form amyloid-like aggregates *in vitro*, we decided to test if the observed aggregates have an amyloid-like structure using the amyloid-diagnostic dyes Thioflavin-T and Congo Red. When bacteria cultures are incubated with non-labeled wtECP, stained with ThT and visualized by total internal reflection fluorescence (TIRF) microscopy, we show that wtECP amyloid-like aggregates are located also at the cell surface (Figure 4A) similarly as what we observe for Alexa labeled wtECP (Figure 3A). Consistently, no staining is observed for non-incubated cultures and for the I13A mutant (Figure 4A). Moreover, upon bacteria incubation with wtECP, a red shift in the Congo Red spectrum is observed (Supplementary Information Figure S5A), revealing that the protein amyloid-like aggregation is triggered upon incubation with bacteria cultures.

Though ECP was previously shown to form amyloid-like aggregates *in vitro* only at low pH after a long incubation time (1–2 weeks), amyloid-like structures observed here are detected after only 4 hours of incubation. However, it is well known that some proteins can accelerate its aggregation kinetics in the presence of membrane-like environments [48–50]. Our results show that wtECP is able to form fibrillar-like aggregates on model membranes with an average size of 845 ± 150 nm (Figure 4B), comparable in size with the wtECP aggregates observed *in vitro* in the absence of lipid membranes (~ 150 nm) [28]. In fact, when tested for ThT binding, we observe aggregates with similar size

(Figure 4B). When wtECP is incubated with model membranes and tested for Congo Red binding, we obtain again a noticeable spectral shift (Supplementary Information Figure S5B). To complete these results we have also performed all the experiments detailed above using the I13A mutant and found it to be unable to form amyloid-like aggregates (Figure 4).

Conclusions

The results presented here for ECP reinforce the hypothesis that an amyloid-like aggregation process is taking place in the bacteria surface that drives bacteria cell agglutination, which is essential for the antimicrobial activity of the protein. In summary, after binding to the bacteria surface, a rearrangement of the protein could take place, exposing the hydrophobic N-terminal patch of the protein. Following, the aggregation process would start promoting the agglutination of the bacteria cells through the aggregation of the surface-attached protein molecules. The formation of aggregates on the bacteria surface will disrupt the lipopolysaccharide bilayer of Gram-negative cells exposing the internal cytoplasmic membrane to the protein action, promoting the membrane disruption and eventually the bacteria killing.

Cell agglutinating activity provides a particularly appealing feature that may contribute to the clearance of bacteria at the infectious focus. In this sense, bacteria agglutination would prepare the field before host phagocytic cells enter in the scene [33]. However, despite the interest in the pharmaceutical industry to identify the structural determinants for bacteria cell agglutination, bibliography on that subject is scarce and only few agglutinating antimicrobial proteins are described in the literature. Excitingly, there may be other proteins and peptides with similar characteristics that also follow the proposed model. Hence, the agglutinating mechanism may represent a more generalized process that may derivate in amyloid deposit formation at bacterial infection foci.

Besides, it has been reported that systematic exposure to inflammation may represent a risk factor on developing Alzheimer's disease [51,52] and other types of dementia [53]. Some studies have also demonstrated that the release of inflammatory mediators can also cause generalized cytotoxicity. In particular, ECP has been discovered to be cytotoxic [40,54] and neurotoxic, causing the Gordon phenomenon after injection intratechally in rabbits [55]. Therefore, our results suggest that the release of inflammatory mediators after infection (like AMPs) may either seed the aggregation processes in the brain and/or influence the membrane biophysical properties to trigger neurotoxicity and aggregation events.

Materials and Methods

MIC (Minimal Inhibitory Concentration) and MAC (Minimal Agglutination Concentration) determination

Antimicrobial activity was expressed as the MIC_{100} , defined as the lowest protein concentration that completely inhibits microbial growth. MIC of each protein was determined from two

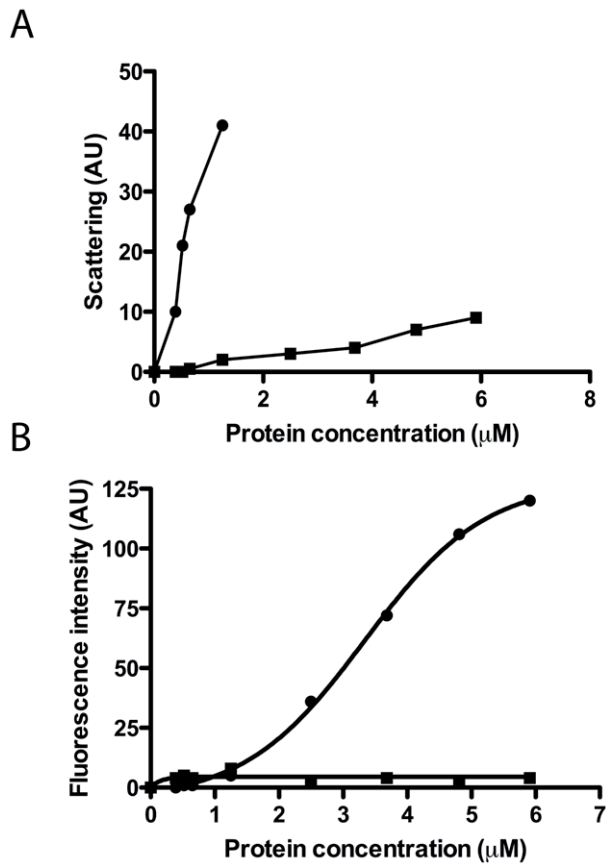


Figure 2. Liposome agglutination and leakage activity. wtECP (circles) and I13A mutant (squares) were incubated with liposomes and the agglutination (A) and leakage (B) were followed at increasing protein concentrations (1–6 μM). Agglutination was measured as light scattering (470 nm) at 90° from the beam source in a 10 mM Tris-HCl, 100 mM NaCl, pH 7.4 buffer and leakage was followed using the ANTS/DPX assay in the same buffer as described in the *Materials and Methods* section.

doi:10.1371/journal.ppat.1003005.g002

independent experiments performed in triplicate for each concentration. Bacteria were incubated at 37°C overnight in Mueller-Hinton II (MHII) broth and diluted to give approximately $5 \cdot 10^5$ CFU/mL. Bacterial suspension was incubated with proteins at various concentrations (0.1–5 μM) at 37°C for 4 h either in MHII or 10 mM sodium phosphate buffer, 100 mM NaCl, pH 7.4. Samples were plated onto Petri dishes and incubated at 37°C overnight.

For MAC determination, bacteria cells were grown at 37°C to mid-exponential phase ($OD_{600} = 0.6$), centrifuged at $5000 \times g$ for 2 min, and resuspended in 10 mM sodium phosphate buffer, 100 mM NaCl, pH 7.4, in order to give an absorbance of 0.2 at 600 nm. A 200 μL aliquot of the bacterial suspension was incubated with proteins at various (0.1–10 μM) concentrations at 25°C for 4 h. Aggregation behavior was observed by visual inspection and minimal agglutinating concentration expressed as previously described [42].

Fluorescence-Assisted Cell Sorting (FACS) assay

Bacteria cells were grown at 37°C to mid-exponential phase ($OD_{600} = 0.6$), centrifuged at $5000 \times g$ for 2 min, resuspended in 10 mM sodium phosphate buffer, 100 mM NaCl, pH 7.4 or the same buffer supplemented with 20% plasma to give a final

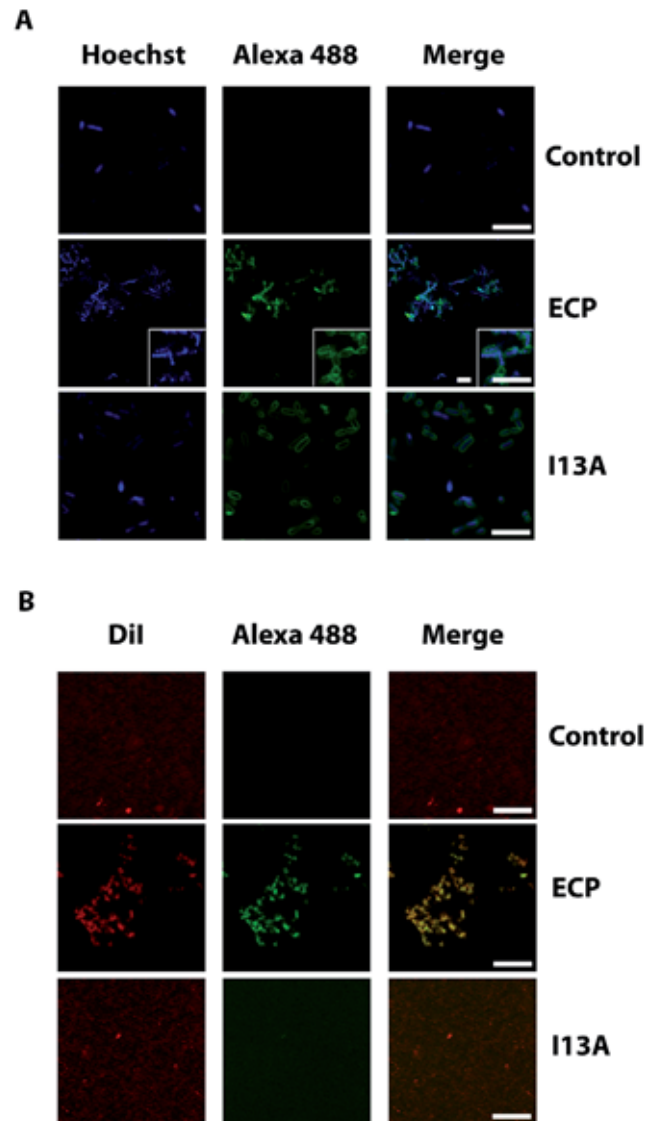


Figure 3. ECP and I13A mutant bind to the surface of bacteria and membranes. (A) *E. coli* bacteria cells stained with Hoechst (blue signal) were incubated with 5 μM of either wtECP or I13A mutant (both labeled with Alexa Fluor 488; green signal) for 4 h and visualized by confocal microscopy. In all experiments cell cultures were grown at exponential phase ($OD_{600} = 0.2$) and incubated with proteins in 10 mM sodium phosphate buffer, 100 mM NaCl, pH 7.4. (B) 500 μL of 200 μM LUV liposomes stained with Dil (red signal) were incubated with 5 μM of either wtECP or I13A mutant (both labeled with Alexa Fluor 488; green signal) for 4 h and visualized using a Leica SP2 confocal microscope. Scale bars are 5 μm length in all images and insight captions. Images depicted are representative from two independent experiments.

doi:10.1371/journal.ppat.1003005.g003

$OD_{600} = 0.2$ and preincubated for 20 min. A 500 μL aliquot of the bacterial suspension was incubated with 5 μM of wtECP or I13A mutant during 4 h. After incubation, 25000 cells were subjected to FACS analysis using a FACSCalibur cytometer (BD Biosciences, New Jersey) and a dot-plot was generated by representing the low-angle forward scattering (FSC-H) in the x-axis and the side scattering (SSC-H) in the y-axis to analyze the size and complexity of the cell cultures. Results were analyzed using FlowJo (Tree Star, Ashland, OR).

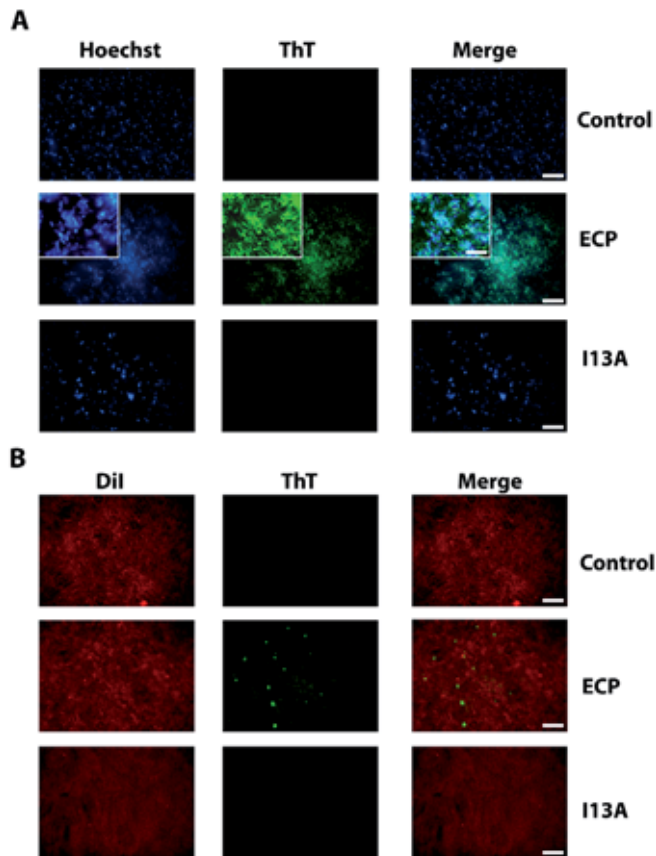


Figure 4. ECP but not I13A form amyloid-like aggregates on the surface of bacteria and membranes. (A) *E. coli* bacteria cells stained with Hoechst (blue signal) were incubated with unlabeled wtECP or I13A mutant for 4 h, stained with ThT (green signal) and visualized by TIRF microscopy. In all experiments cell cultures were grown at exponential phase ($OD_{600}=0.2$) and incubated with proteins in 10 mM sodium phosphate buffer, 100 mM NaCl, pH 7.4. (B) Planar lipid bilayers prepared as described in the *Materials and Methods* section (stained with Dil; red signal) were incubated with 5 μ M of either unlabeled wtECP or I13A mutant for 4 h, stained with 25 μ M ThT (green signal) and visualized using a Olympus FluoView 1000 TIRF microscope. Scale bar represents 20 μ m (5 μ m in the insight caption). Images depicted are representative from two independent experiments.

doi:10.1371/journal.ppat.1003005.g004

Bacteria viability assay

Bacteria viability assays were performed as described before [39]. Briefly, bacteria were incubated in 10 mM sodium phosphate buffer, 100 mM NaCl, pH 7.4 with 5 μ M of wtECP or I13A mutant and then stained using a syto 9/propidium iodide 1:1 mixture. The viability kinetics were monitored using a Cary Eclipse Spectrofluorimeter (Varian Inc., Palo Alto, CA, USA). To calculate bacterial viability, the signal in the range 510–540 nm was integrated to obtain the syto 9 signal (live bacteria) and from 620–650 nm to obtain the propidium iodide signal (dead bacteria). Then, the percentage of live bacteria was represented as a function of time.

Liposome agglutination and leakage assay

The ANTS/DPX liposome leakage fluorescence assay was performed as previously described [56]. Briefly, a unique population of LUVs of DOPC/DOPG (3:2 molar ratio) lipids was obtained containing 12.5 mM ANTS, 45 mM DPX, 20 mM NaCl, and 10 mM Tris/HCl, pH 7.4. The ANTS/DPX liposome suspension was diluted to 30 μ M concentration and incubated at 25°C in the presence of wtECP or I13A mutant. Leakage activity was followed by monitoring the increase of the fluorescence at 535 nm.

For liposome agglutination, 200 μ M LUV liposomes were incubated in 10 mM phosphate buffer, pH 7.4, containing 5 to 100 mM NaCl, in the presence of 5 μ M wtECP or I13A mutant

and the scattering signal at 470 nm was collected at 90° from the beam source using a Cary Eclipse Spectrofluorimeter (Varian Inc., Palo Alto, CA, USA) [57].

Confocal microscopy

Experiments were carried out in 35 cm² plates with a glass coverslip. For phospholipid membranes, 500 μ l of 200 μ M LUV liposomes (prepared as described in Supplementary Information) were incubated with 5 μ M wtECP or I13A mutant for 4 h in 10 mM sodium phosphate buffer, 100 mM NaCl, pH 7.4. For bacteria, 500 μ l of *E. coli* cells ($OD_{600}=0.2$) were incubated with 5 μ M wtECP or I13A mutant for 4 h in 10 mM sodium phosphate buffer, 100 mM NaCl, pH 7.4. RNase A was used always as a negative control. Samples of both liposomes and bacteria were imaged using a laser scanning confocal microscope (Olympus FluoView 1000 equipped with a UPlansApo 60 \times objective in 1.4 oil immersion objective, United Kingdom). wtECP and I13A mutant labeled with Alexa Fluor 488 were excited using a 488-nm argon laser (515–540 nm emission collected) and Vibrant Dil was excited using an orange diode (588–715 nm emission collected).

TIRF microscopy

To study the interaction of proteins with lipid membranes, planar supported lipid bilayers were used (Supplementary

Information). When using bacteria, glass coverslips were previously treated with 0.1% poly-L-lysine to ensure that samples will adhere to the surface. 500 μ l of *E. coli* cells ($OD_{600}=0.2$) were incubated with 5 μ M wtECP or I13A mutant for 4 h and then transferred to poly-L-lysine treated microscopy plates and incubated for 15 minutes. To remove unattached cells, plates were washed twice with 10 mM sodium phosphate, 100 mM NaCl, pH 7.4 buffer. RNase A was used always as a negative control. Images were captured using a laser scanning confocal microscope (Olympus FluoView 1000 equipped with a PlansApo 60 \times TIRF objective in 1.4 oil immersion objective, United Kingdom) using the same conditions as described for confocal microscopy experiments. Thioflavin T (ThT) was used to detect amyloid aggregates. In this case, samples were incubated for 4 h with unlabeled proteins as described before and then incubated with ThT at 25 μ M final concentration for 15 minutes. Then, plates were washed twice with 10 mM sodium phosphate, 100 mM NaCl buffer, pH 7.4 to remove unattached cells and ThT excess.

Supporting Information

Figure S1 Bacteria agglutination mediated by wtECP and the I13A mutant. *E. coli* bacteria cells were grown at exponential phase ($OD_{600}=0.2$) and incubated with 0.5 μ M wtECP (A) or I13A (B) in 10 mM phosphate buffer, 100 mM NaCl, pH 7.5 for 4 h. Images were taken using a Leica magnifier. wtECP incubated bacteria samples were also observed under 40 \times (C) and 100 \times (D) magnification to reveal more details on bacteria aggregates. Images were taken using a Leica optical microscope.
(TIF)

Figure S2 Liposome agglutination mediated by wtECP and I13A mutant at increasing ionic strength. Liposomes prepared as described in the *Materials and Methods* section were incubated with increasing concentrations of wtECP (circles) or I13A mutant (squares) at 5 mM (A), 50 mM (B) and 100 mM (C) NaCl in a 10 mM phosphate buffer, pH 7.5. The formation of liposome aggregates was followed as an increase in the light scattering signal at 90 $^\circ$ from the beam.
(TIF)

Figure S3 ECP is able to agglutinate bacteria cells in plasma. *E. coli* cells were incubated with 5 μ M of ECP during 4 h and samples were analyzed using a FACSCalibur cytometer. FSC-H is the low-angle forward scattering, which is roughly proportional to the diameter of the cell and SSC-H is the orthogonal or side scattering, which is proportional to cell

granularity or complexity. Agglutination is registered as an increase in both scattering measures. In all experiments, cell cultures were grown at exponential phase ($OD_{600}=0.2$) and incubated with proteins in 20% plasma diluted in 10 mM sodium phosphate buffer, 100 mM NaCl, pH 7.5. The plots are representative of three independent experiments.

(TIF)

Figure S4 wtECP and I13A mutant binding to bacteria LPS. LPS were incubated with increasing concentrations of wtECP (circles) or I13A mutant (squares) in a 10 mM phosphate buffer, 100 mM NaCl, pH 7.5. Binding to bacteria LPS was registered as a fluorescence increase of the BODIPY-cadaverine reporter as described in the *Materials and Methods* section. The occupancy factor denotes the decrease of the LPS-bound dye fraction after protein addition.

(TIF)

Figure S5 Protein aggregates bind to Congo Red dye. (A) *E. coli* (circles) and *P. aeruginosa* (triangles) bacteria cells were incubated 4 h with wtECP and assayed for Congo Red binding as described in the *Materials and Methods* section. (B) Liposomes at 10 μ M (black circles), 200 μ M (grey circles) and 1 mM (white squares) lipid concentration were incubated with wtECP and assayed for Congo Red binding as described in the *Materials and Methods* section. Congo Red differential spectra were obtained by subtracting both the signal corresponding to the protein and the lipid/bacteria in the presence of the dye. The vertical line at 480 nm represents the spectrum of Congo Red alone. Incubation of I13A mutant with both bacteria and membranes did not display any significant spectral shift.

(TIF)

Protocol S1 This file contains additional details for the *Materials and Methods* section.

(DOCX)

Acknowledgments

Microscopy experiments were carried at the Servei de Microscòpia (UAB) and fluorescence measurements at Servei d'Anàlisi i Fotodocumentació (UAB). We thank Natalia Sánchez de Groot for her assistance in the FACS analysis.

Author Contributions

Conceived and designed the experiments: MT EB. Performed the experiments: MT DP. Analyzed the data: MT DP MVN EB. Contributed reagents/materials/analysis tools: MVN EB. Wrote the paper: MT EB.

References

- Otvos L, Jr. (2005) Antibacterial peptides and proteins with multiple cellular targets. *J Pept Sci* 11: 697–706.
- Yount NY, Bayer AS, Xiong YQ, Yeaman MR (2006) Advances in antimicrobial peptide immunobiology. *Biopolymers* 84: 435–458.
- Zaslouf M (2002) Antimicrobial peptides of multicellular organisms. *Nature* 415: 389–395.
- Hancock RE, Sahl HG (2006) Antimicrobial and host-defense peptides as new anti-infective therapeutic strategies. *Nat Biotechnol* 24: 1551–1557.
- Zhang L, Falla TJ (2010) Potential therapeutic application of host defense peptides. *Methods Mol Biol* 618: 303–327.
- Brogden KA (2005) Antimicrobial peptides: pore formers or metabolic inhibitors in bacteria? *Nat Rev Microbiol* 3: 238–250.
- Gottler LM, Ramamoorthy A (2009) Structure, membrane orientation, mechanism, and function of pexiganan—a highly potent antimicrobial peptide designed from magainin. *Biochim Biophys Acta* 1788: 1680–1686.
- Marsh EN, Buer BC, Ramamoorthy A (2009) Fluorine—a new element in the design of membrane-active peptides. *Mol Biosyst* 5: 1143–1147.
- Ramamoorthy A (2009) Beyond NMR spectra of antimicrobial peptides: dynamical images at atomic resolution and functional insights. *Solid State Nucl Magn Reson* 35: 201–207.
- Thennarasu S, Huang R, Lee DK, Yang P, Maloy L, et al. (2010) Limiting an antimicrobial peptide to the lipid-water interface enhances its bacterial membrane selectivity: a case study of MSI-367. *Biochemistry* 49: 10595–10605.
- Pulido D, Nogues MV, Boix E, Torrent M (2012) Lipopolysaccharide neutralization by antimicrobial peptides: a gambit in the innate host defense strategy. *J Innate Immun* 4: 327–336.
- Torrent M, Nogues MV, Boix E (2012) Discovering new in silico tools for antimicrobial peptide prediction. *Curr Drug Targets* 13: 1148–1157.
- Wimley WC (2010) Describing the mechanism of antimicrobial peptide action with the interfacial activity model. *ACS Chem Biol* 5: 905–917.
- Nguyen LT, Hancy EF, Vogel HJ (2011) The expanding scope of antimicrobial peptide structures and their modes of action. *Trends Biotechnol* 29: 464–472.
- Butterfield SM, Lashuel HA (2010) Amyloidogenic protein-membrane interactions: mechanistic insight from model systems. *Angew Chem Int Ed Engl* 49: 5628–5654.

16. Mahalka AK, Kinnunen PK (2009) Binding of amphipathic alpha-helical antimicrobial peptides to lipid membranes: lessons from temporins B and L. *Biochim Biophys Acta* 1788: 1600–1609.
17. Kagan BL, Jang H, Capone R, Teran Arce F, Ramachandran S, et al. (2011) Antimicrobial Properties of Amyloid Peptides. *Mol Pharm* 9:708–717.
18. Brender JR, Durr UH, Heyl D, Budarapu MB, Ramamoorthy A (2007) Membrane fragmentation by an amyloidogenic fragment of human Iset Amyloid Polypeptide detected by solid-state NMR spectroscopy of membrane nanotubes. *Biochim Biophys Acta* 1768: 2026–2029.
19. Brender JR, Hartman K, Gottler LM, Cavitt ME, Youngstrom DW, et al. (2009) Helical conformation of the SEVI precursor peptide PAP248–286, a dramatic enhancer of HIV infectivity, promotes lipid aggregation and fusion. *Biophys J* 97: 2474–2483.
20. Brender JR, Hartman K, Reid KR, Kennedy RT, Ramamoorthy A (2008) A single mutation in the nonamyloidogenic region of islet amyloid polypeptide greatly reduces toxicity. *Biochemistry* 47: 12680–12688.
21. Brender JR, Lee EL, Cavitt MA, Gafni A, Steel DG, et al. (2008) Amyloid fiber formation and membrane disruption are separate processes localized in two distinct regions of IAPP, the type-2-diabetes-related peptide. *J Am Chem Soc* 130: 6424–6429.
22. Nanga RP, Brender JR, Vivekanandan S, Popovych N, Ramamoorthy A (2009) NMR structure in a membrane environment reveals putative amyloidogenic regions of the SEVI precursor peptide PAP(248–286). *J Am Chem Soc* 131: 17972–17979.
23. Nanga RP, Brender JR, Xu J, Hartman K, Subramanian V, et al. (2009) Three-dimensional structure and orientation of rat islet amyloid polypeptide protein in a membrane environment by solution NMR spectroscopy. *J Am Chem Soc* 131: 8252–8261.
24. Popovych N, Brender JR, Soong R, Vivekanandan S, Hartman K, et al. (2012) Site specific interaction of the polyphenol EGCG with the SEVI amyloid precursor peptide PAP(248–286). *J Phys Chem B* 116: 3650–3658.
25. Jelinek R, Kolesheva S (2005) Membrane interactions of host-defense peptides studied in model systems. *Curr Protein Pept Sci* 6: 103–114.
26. Tang M, Hong M (2009) Structure and mechanism of beta-hairpin antimicrobial peptides in lipid bilayers from solid-state NMR spectroscopy. *Mol Biosyst* 5: 317–322.
27. Torrent M, Valle J, Nogues MV, Boix E, Andreu D (2011) The generation of antimicrobial peptide activity: a trade-off between charge and aggregation? *Angew Chem Int Ed Engl* 50: 10686–10689.
28. Torrent M, Odorizzi F, Nogues MV, Boix E (2010) Eosinophil cationic protein aggregation: identification of an N-terminus amyloid prone region. *Biomacromolecules* 11: 1983–1990.
29. Jang H, Arce FT, Mustata M, Ramachandran S, Capone R, et al. (2011) Antimicrobial protegrin-1 forms amyloid-like fibrils with rapid kinetics suggesting a functional link. *Biophys J* 100: 1775–1783.
30. Socia SJ, Kirby JE, Washicosky KJ, Tucker SM, Ingelsson M, et al. (2010) The Alzheimer's disease-associated amyloid beta-protein is an antimicrobial peptide. *PLoS One* 5: e9505.
31. Harris F, Dennison SR, Phoenix DA (2012) Aberrant action of amyloidogenic host defense peptides: a new paradigm to investigate neurodegenerative disorders? *FASEB J* 26: 1776–1781.
32. Torrent M, Andreu D, Nogues VM, Boix E (2011) Connecting peptide physicochemical and antimicrobial properties by a rational prediction model. *PLoS One* 6: e16968.
33. Gorr SU, Sotsky JB, Shelar AP, Demuth DR (2008) Design of bacteria-agglutinating peptides derived from parotid secretory protein, a member of the bactericidal/permeability increasing-like protein family. *Peptides* 29: 2118–2127.
34. Van Nieuw Amerongen A, Bolscher JG, Veerman EC (2004) Salivary proteins: protective and diagnostic value in cariology? *Caries Res* 38: 247–253.
35. Pulido D, Moussaoui M, Andreu D, Nogues MV, Torrent M, et al. (2012) Antimicrobial Action and Cell Agglutination by Eosinophil Cationic Protein Is Modulated by the Cell Wall Lipopolysaccharide Structure. *Antimicrob Agents Chemother* 56: 2378–2385.
36. Boix E, Torrent M, Sánchez D, Nogués MV (2008) The Antipathogen Activities of Eosinophil Cationic Protein. *Current Pharm Biotec* 9: 141–152.
37. Venge P, Byström J, Carlsson M, Hakansson L, Karawacjzyk M, et al. (1999) Eosinophil cationic protein (ECP): molecular and biological properties and the use of ECP as a marker of eosinophil activation in disease. *Clin Exp Allergy* 29: 1172–1186.
38. Boix E, Salazar VA, Torrent M, Pulido D, Nogues MV, et al. (2012) Structural determinants of the eosinophil cationic protein antimicrobial activity. *Biol Chem* 393: 801–815.
39. Torrent M, Badia M, Moussaoui M, Sanchez D, Nogues MV, et al. (2010) Comparison of human RNase 3 and RNase 7 bactericidal action at the Gram-negative and Gram-positive bacterial cell wall. *FEBS J* 277: 1713–1725.
40. Navarro S, Aleu J, Jimenez M, Boix E, Cuchillo CM, et al. (2008) The cytotoxicity of eosinophil cationic protein/ribonuclease 3 on eukaryotic cell lines takes place through its aggregation on the cell membrane. *Cell Mol Life Sci* 65: 324–337.
41. Torrent M, Navarro S, Moussaoui M, Nogues MV, Boix E (2008) Eosinophil cationic protein high-affinity binding to bacteria-wall lipopolysaccharides and peptidoglycans. *Biochemistry* 47: 3544–3555.
42. Torrent M, Pulido D, de la Torre BG, Garcia-Mayoral MF, Nogues MV, et al. (2011) Refining the eosinophil cationic protein antibacterial pharmacophore by rational structure minimization. *J Med Chem* 54: 5237–5244.
43. Sanchez D, Moussaoui M, Carreras E, Torrent M, Nogues V, et al. (2011) Mapping the eosinophil cationic protein antimicrobial activity by chemical and enzymatic cleavage. *Biochimie* 93: 331–338.
44. Torrent M, Di Tommaso P, Pulido D, Nogues MV, Notredame C, et al. (2012) AMPA: an automated web server for prediction of protein antimicrobial regions. *Bioinformatics* 28: 130–131.
45. Torrent M, Nogues VM, Boix E (2009) A theoretical approach to spot active regions in antimicrobial proteins. *BMC Bioinformatics* 10: 373.
46. Torrent M, de la Torre BG, Nogues VM, Andreu D, Boix E (2009) Bactericidal and membrane disruption activities of the eosinophil cationic protein are largely retained in an N-terminal fragment. *Biochem J* 421: 425–434.
47. Torrent M, Nogues MV, Boix E (2011) Eosinophil cationic protein (ECP) can bind heparin and other glycosaminoglycans through its RNase active site. *J Mol Recognit* 24: 90–100.
48. Kayced R, Sokolov Y, Edmonds B, McIntire TM, Milton SC, et al. (2004) Permeabilization of lipid bilayers is a common conformation-dependent activity of soluble amyloid oligomers in protein misfolding diseases. *J Biol Chem* 279: 46363–46366.
49. Ambroggio EE, Kim DH, Separovic F, Barrow CJ, Barnham KJ, et al. (2005) Surface behavior and lipid interaction of Alzheimer beta-amyloid peptide 1–42: a membrane-disrupting peptide. *Biophys J* 88: 2706–2713.
50. Auvynet C, El Amri C, Lacombe C, Bruston F, Bourdais J, et al. (2008) Structural requirements for antimicrobial versus chemoattractant activities for dermaseptin S9. *FEBS J* 275: 4134–4151.
51. Krstić D, Madhusudan A, Doehner J, Vogel P, Notter T, et al. (2012) Systemic immune challenges trigger and drive Alzheimer-like neuropathology in mice. *J Neuroinflammation* 9: 151.
52. Miklossy J (2011) Emerging roles of pathogens in Alzheimer disease. *Expert Rev Mol Med* 13: e30.
53. Almeida OP, Lautenschlager NT (2005) Dementia associated with infectious diseases. *Int Psychogeriatr* 17 Suppl 1: S65–77.
54. Navarro S, Boix E, Cuchillo CM, Nogues MV (2010) Eosinophil-induced neurotoxicity: the role of eosinophil cationic protein/RNase 3. *J Neuroimmunol* 227: 60–70.
55. Fredens K, Dahl R, Venge P (1982) The Gordon phenomenon induced by the eosinophil cationic protein and eosinophil protein X. *J Allergy Clin Immunol* 70: 361–366.
56. Torrent M, Cuyas E, Carreras E, Navarro S, Lopez O, et al. (2007) Topography studies on the membrane interaction mechanism of the eosinophil cationic protein. *Biochemistry* 46: 720–733.
57. Torrent M, Sanchez D, Buzon V, Nogues MV, Cladera J, et al. (2009) Comparison of the membrane interaction mechanism of two antimicrobial RNases: RNase 3/ECP and RNase 7. *Biochim Biophys Acta* 1788: 1116–1125.

Supporting Information

Figure S1 Bacteria agglutination mediated by wtECP and the I13A mutant

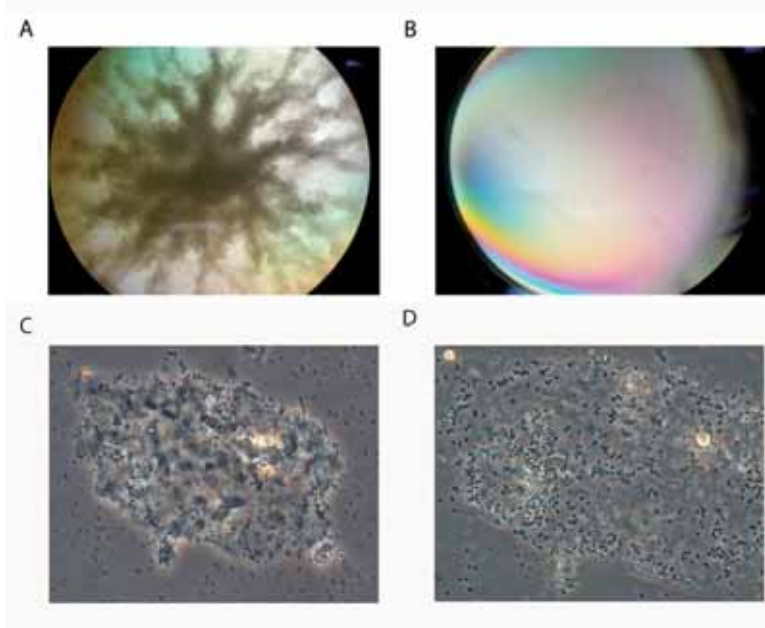


Figure S2 Liposome agglutination mediated by wtECP and I13A mutant at increasing ionic strength

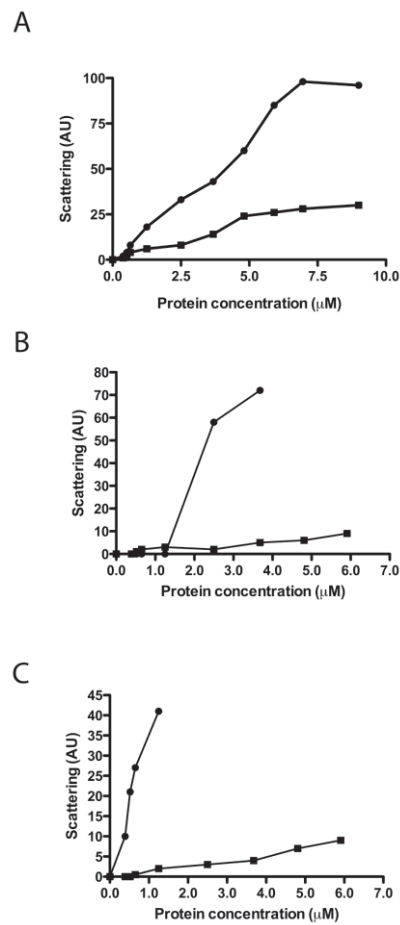


Figure S3 ECP is able to agglutinate bacteria cells in plasma.

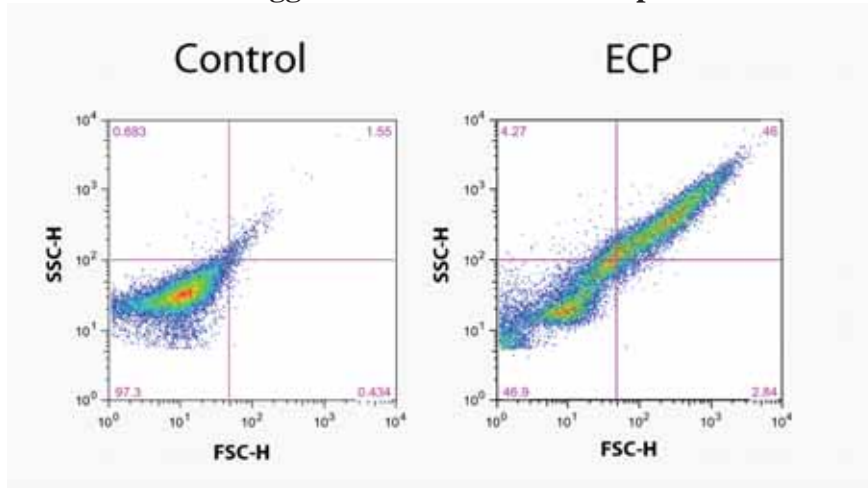


Figure S4 wtECP and I13A mutant binding to bacteria LPS.

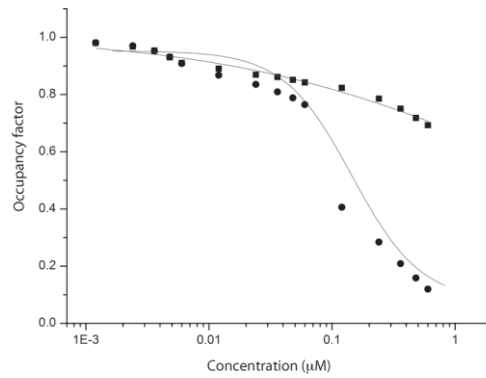
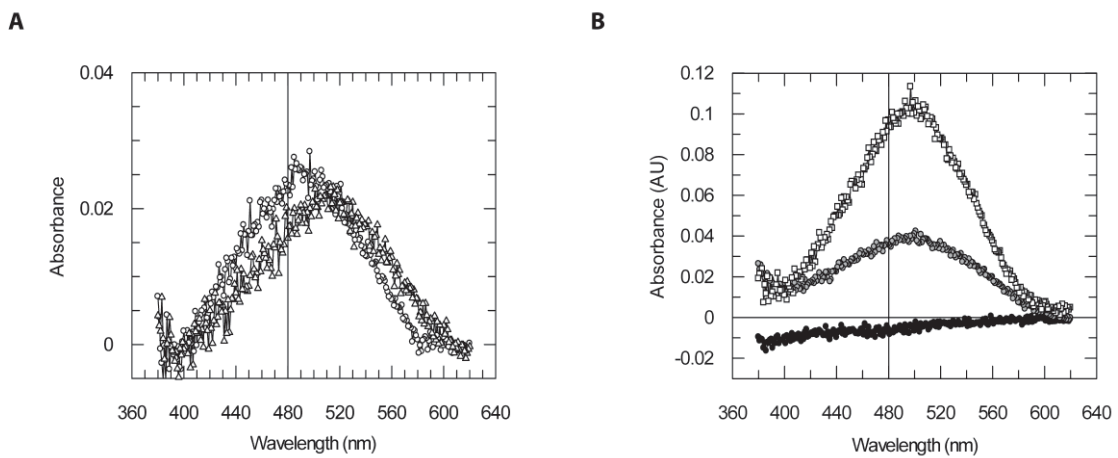


Figure S5 Protein aggregates bind to Congo Red dye



PROTOCOL S1

Materials and Methods

Materials and Strains

1,2-Dioleoyl-sn-glycero-3-phosphocholine (DOPC), 1,2-dioleoyl-sn-glycero-3-[phospho-rac-(1-glycerol)] (DOPG), Dipalmitoyl-sn-glycero-3-phosphocholine (DPPC) and Dimiristoil-sn-glycero-3--[phospho-rac-(1-glycerol)] (DMPG) were from Avanti Polar Lipids, Birmingham, AL. LPS from *E. coli* was purchased from Sigma Aldrich. 8-Aminonaphthalene-1,3,6-trisulfonic acid disodium salt (ANTS), p-xylene-bispyridiniumbromide (DPX), BC (BODIPY TR cadaverine, where BODIPY is boron dipyrromethane (4,4-difluoro-4-bora-3a,4a-diaza-s-indacene) were purchased from Invitrogen (Carlsbad, CA). Alexa Fluor 488 Protein Labelling kit and Vibrant DiI cell-labeling solution were from Molecular Probes (Invitrogen, Carlsbad, CA). pET11 expression vector and *E. coli* BL21(DE3) cells were from Novagen, Madison, WI. Strains used were *Escherichia coli* (BL21, Novagen), *Acinetobacter baumannii* (ATCC 15308) and *Pseudomonas sp* (ATCC 15915). Human plasma was extracted from a pool of healthy donor's blood.

Preparation of recombinant proteins

I13A ECP mutation was incorporated using the Quick-change mutagenesis kit from Invitrogen (Carlsbad, CA). Recombinant ECP and I13A mutant were obtained as previously described (1, 2). I13A ECP mutant was sequenced before expression and protein identity was checked by MALDI-TOF mass spectrometry.

Protein fluorescent labeling

ECP and I13A mutant were labeled with the Alexa Fluor 488 fluorophor, following the manufacturer's instructions, as previously described (3). To 0.5 mL of a 2 mg/mL protein solution in phosphate saline buffer (PBS), 50 μ L of 1 M sodium bicarbonate, pH 8.3, were added. The protein is incubated for 1 h at room temperature, with the reactive dye, with stirring, following the manufacturer's conditions. The labeled protein was separated from the free dye by a PD10-desalting column.

LUV liposome preparation

Large unilamellar vesicles (LUVs) containing DOPC/DOPG (3:2 molar ratio) of a defined size (about 100 nm) were prepared as previously described (4). LUVs were obtained from a vacuum-drying lipid chloroform solution by extrusion through 100 nm polycarbonate membranes. The lipid suspension was frozen and thawed ten times prior to extrusion. A 1 mM stock solution of liposome suspension in 10 mM phosphate buffer, 100 mM NaCl, pH 7.4 was prepared.

Formation of supported lipid bilayers (SLBs).

Supported lipid bilayers were prepared as described (5). Briefly, we dissolved DMPG and DPPC in CHCl₃/methanol 2/1(v/v) to obtain a 5 mM stock solution of each lipid. 80 µl of DMPG stock solution and 120 µl of DPPC stock solution were mixed in a glass tube to obtain a 3:2 DPPC/DOPG mixture. Then the lipid mixture was evaporated under nitrogen and dried in a desiccator under vacuum for 2 h. The dried lipid film was resuspended in 1 ml of a 10 mM Tris, 100 mM NaCl, 3 mM CaCl₂ buffer adjusted at pH 7.4 with HCl to give a 1 mM final lipid concentration of multilamellar large vesicles (MLVs) suspension. In order to obtain small unilamellar vesicles (SUVs), the lipid suspension was sonicated to clarity (five cycles of 2 min) using a water bath sonicator at 60°C. Then, 500 µl of the SUV suspension was placed in contact with the glass coverslip of a 35 cm² microscopy plate and heated for 45 min at 60 °C. After slowly cooling down the system to room temperature, the samples were rinsed carefully with a 10 mM phosphate buffer, 100 mM NaCl buffer adjusted at pH 7.4 to remove the SUV excess.

LPS Binding Assay

LPS binding was assessed using the fluorescent probe Bodipy TR cadaverine (BC) as described (6). Briefly, the displacement assay was performed by the addition of 1-2 µL aliquots of wtECP or I13A mutant solution to 1 mL of a continuously stirred mixture of LPS (10 µg/mL) and BC (10 µM) in 10 mM phosphate buffer, 100 mM NaCl, pH 7.5. Fluorescence measurements were performed on a Cary Eclipse spectrofluorimeter. The BC excitation wavelength was 580 nm, and the emission wavelength was 620 nm. The excitation slit was set at 2.5 nm, and the emission slit was set at 20 nm. Final values correspond to an average of four replicates and were the mean of a 0.3 s continuous measurement. Occupancy factor was calculated as described previously (6).

Binding to Congo Red

Binding of ECP to Congo red was tested using a Varian CARY- 100 spectrophotometer (Palo Alto, CA) to perform the spectroscopic band-shift assay. A total of 5 μL of 10 mg/mL protein solution was diluted in 45 μL of 10 mM sodium phosphate, 100 mM NaCl, and pH 7.5 buffer containing 15 μM Congo red for recording the spectra of the protein alone. For recording the shift after binding to liposomes, increasing concentration of liposomes, prepared as described previously, were added to the buffer. For recording the shift after binding to bacteria, a sufficient amount of cells was added to the buffer to reach an $\text{OD}_{600} = 0.2$. Samples were maintained 5 min at 25 $^{\circ}\text{C}$ before analysis. Congo Red differential spectra were obtained by subtracting both the signal corresponding to the protein and the lipid/bacteria in the presence of the dye. Samples incubated with the I13A mutant or lysed bacteria do not show a significant increase of Congo Red spectral shift.

REFERENCES

1. Boix E, *et al.* (1999) Kinetic and product distribution analysis of human eosinophil cationic protein indicates a subsite arrangement that favors exonuclease-type activity. *J Biol Chem* 274(22):15605-15614.
2. Torrent M, Odorizzi F, Nogues MV, & Boix E (2010) Eosinophil cationic protein aggregation: identification of an N-terminus amyloid prone region. *Biomacromolecules* 11(8):1983-1990.
3. Torrent M, *et al.* (2009) Comparison of the membrane interaction mechanism of two antimicrobial RNases: RNase 3/ECP and RNase 7. *Biochim Biophys Acta* 1788(5):1116-1125.
4. Torrent M, *et al.* (2007) Topography studies on the membrane interaction mechanism of the eosinophil cationic protein. *Biochemistry* 46(3):720-733.
5. Mingeot-Leclercq MP, Deleu M, Brasseur R, & Dufrene YF (2008) Atomic force microscopy of supported lipid bilayers. *Nature protocols* 3(10):1654-1659.
6. Torrent M, Navarro S, Moussaoui M, Nogues MV, & Boix E (2008) Eosinophil cationic protein high-affinity binding to bacteria-wall lipopolysaccharides and peptidoglycans. *Biochemistry* 47(11):3544-3555.

CHAPTER IV

Ribonucleases as a host-defense family: Evidence of evolutionary conserved antimicrobial activity at the N-terminus.

Marc Torrent^{1,2,*}, David Pulido^{1,§}, Javier Valle², M. Victòria Nogués¹, David Andreu^{2,*}
and Ester Boix^{1,*}

¹*Department of Biochemistry and Molecular Biology, Universitat Autònoma de Barcelona, Cerdanyola del Vallès, 08193, Barcelona, Spain*

²*Department of Experimental and Health Sciences, Universitat Pompeu Fabra, Dr. Aiguader 88, Barcelona, Spain*

[§] *Both authors contributed equally to this work*

^{*} *Corresponding authors:*

Marc Torrent: marc.torrent@uab.cat

David Andreu: david.andreu@upf.edu

Ester Boix: ester.boix@uab.cat

Abstract

Vertebrate secreted ribonucleases (RNases) are small proteins that play important roles in RNA metabolism, angiogenesis or host defense.

In the present study we describe the antimicrobial properties of the N-terminal domain of the human canonical RNases (hcRNases) and show that its antimicrobial activity is well conserved among their lineage. Furthermore, all domains display a similar antimicrobial mechanism, characterized by bacteria agglutination followed by membrane permeabilization.

The results presented here show that, for all antimicrobial hcRNases, (i) activity is retained at the N-terminus; (ii) the antimicrobial mechanism is conserved. Moreover, using computational analysis we show that antimicrobial propensity may be conserved at the N-terminus for all vertebrate RNases, thereby suggesting that a defense mechanism could be a primary function in vertebrate RNases and that the N-terminus was selected to ensure this property. In a broader context, from the overall comparison of the peptides' physicochemical and biological properties, general correlation rules could be drawn to assist in the structure-based development of antimicrobial agents.

Keywords: antimicrobial peptide, ribonuclease, evolution, innate immunity and drug discovery.

Introduction

RNase A-homologues comprise a vertebrate-specific superfamily that includes a wide network of diverse gene lineages (Dyer, Rosenberg 2006). Eight human members (known as canonical RNases) belong to the RNase A-like family (Cho, Beintema, Zhang 2005; Sorrentino 2010). They are all small secreted proteins (around 15 kDa), sharing a typical fold, with six or eight cysteines arranged in three or four disulfide bonds (Acharya et al. 1994; Mosimann et al. 1996; Terzyan et al. 1999; Huang et al. 2007; Kover et al. 2008; Laurents et al. 2009). All RNases include a conserved catalytic triad comprised by two histidines and one lysine, the latter located inside the characteristic RNase signature (CKXXNTF) (Sorrentino 2010) (Supporting Information, Figure S1).

All human canonical RNases (hcRNases) are catalytically active in a variable degree (Sorrentino, Libonati 1997) and some of them share relevant antimicrobial properties (Boix, Nogues 2007). However, antimicrobial and catalytic activities of hcRNases are apparently unrelated (Rosenberg 1995; Boix, Nogues 2007; Huang et al. 2007). In particular, studies in zebrafish (Pizzo et al. 2008) and chicken RNases (Nitto et al. 2006) show they display antimicrobial properties independent of a catalytic activity. Interestingly, vertebrate RNases have high isoelectric points, a common feature in antimicrobial proteins, required for interaction with the negatively charged membranes of pathogens (Boix, Nogues 2007; Torrent, Nogues, Boix 2009).

In summary, the presence of antimicrobial activity in diverse lineages of vertebrate RNases suggests that host defense might be a relevant physiological role of the superfamily (Cho, Zhang 2007). However, a sequential or structural evolutionarily selected pattern that embodies the antimicrobial activity has not yet been reported.

In this context, we recently described that, for RNase 3, a functional antimicrobial domain is located at the N-terminus of the protein (Torrent et al. 2010b; Sanchez et al. 2011; Torrent et al. 2011b; Boix et al. 2012). This domain can be further dissected into two active regions: (i) residues 24 to 45 are essential for the antimicrobial action, and (ii) residues 8 to 16 contribute to agglutination and membrane destabilization (Boix et al. 2012).

Given that many RNases display antimicrobial properties unrelated to their ribonuclease activity, it is appealing to hypothesize that an N-terminal antimicrobial domain could be preserved and/or refined along evolution to embody the antimicrobial activity. To test this hypothesis, we have synthesized the N-terminal domains of all hcRNases and

studied their antimicrobial properties. The results presented here reveal that (i) antimicrobial activity is largely confined at the N-terminus, and that (ii) the mechanism of action of the N-terminal domains is similar to that of the original proteins. Moreover, complementary computational analyses suggest that the N-terminal domain in the protein might have been selected by evolution to provide a host-defense function.

Results

Design of hcRNase-derived peptides

As the reference 1-45 segment in hcRNase 3 has been found to be the minimal domain retaining full antimicrobial properties (Torrent et al. 2009a; Torrent et al. 2011b), in a search for similar antimicrobial properties, peptides **1-8**, comprising equivalent regions of other RNase N-termini (residues 1-45 of hRNases 2, 6, 7 and 8; residues 1-48 of hRNases 1 and 4; residues 1-47 of RNase 5, Table 1) were selected for synthesis. In all cases, the peptides included the first two α -helices as well as the first β -strand from the parental protein. As before¹², the two Cys residues in the N-terminal region, disulfide-linked to distant Cys in the native protein, were replaced by isosteric Ser residues. Peptides of satisfactory quality, with the expected molecular mass, were obtained after Fmoc solid phase synthesis and HPLC purification (Table 1). Their CD secondary structures in the presence of structuring agents (TFE and DPC micelles) were found to be similar to those of the cognate proteins (Torrent et al. 2009a; Garcia-Mayoral et al. 2010).

Antimicrobial activity of hcRNases is retained at the N-terminus

To assess the antimicrobial activity of peptides **1-8** we determined their minimal inhibitory concentration (MIC) for three representative Gram-negative and Gram-positive bacteria (Table 2). Five peptides (**1, 3, 4, 6** and **7**) tested active against all strains, with MIC values between 0.2 and 10 μ M, a range close to that observed for several hcRNases (Huang et al. 2007; Torrent et al. 2009a) (Boix et al. 2012). In contrast, peptides **2, 5** and **8** were inactive against all strains. When these results are compared with available literature data on hcRNases, a good agreement between the two sets of data is observed (Table 2), with only peptide **8** differing from previously reported results (Rudolph et al. 2006). As we suspected that the discrepancy observed could be due to the inoculum size ($5 \cdot 10^5$ cells/mL in our case, $5 \cdot 10^4$ cells/mL in Rudolph et al. (Rudolph et al. 2006)), peptide **8** was reassayed using a $5 \cdot 10^4$ cells/mL inoculum and MIC values in

the 1-10 μM range, compatible with the previous reports, were determined. Thus, we conclude that the antimicrobial activity of hcRNases is consistently preserved at the N-terminus.

To characterize the cell selectivity of peptides **1-8**, their hemolytic activity was tested on sheep red blood cells. For antimicrobially active peptides (**1, 3, 4, 6-8**), hemolytic activities (measured as HC_{50}) between 10 and 20 μM were found (Table 2), while no hemolysis ($\text{HC}_{50} > 100 \mu\text{M}$) was detected for antimicrobially inert peptides **2** and **5**. For the most antimicrobially active peptides (**3, 4, 6** and **7**) MICs were 1-2 orders of magnitude lower than HCs, suggesting that hcRNase-derived peptides are good candidates for drug development, as already shown for RNase3 (Torrent et al. 2011b).

The antimicrobial mechanism of hcRNases primarily involves the N-terminus

To characterize the antimicrobial mechanism of hcRNase-derived peptides **1-8**, we first assessed their ability to depolarize and permeabilize bacterial cytoplasmic membranes. Results with representative Gram-negative and -positive organisms (Table 3) show that only the peptides with high bactericidal activity (**3, 4, 6, 7**) can cause significant membrane depolarization and permeabilization, in agreement with the antimicrobial values (Table 2).

Another specific characteristic of antimicrobial proteins, already demonstrated for the N-terminal domain of hcRNase 3 (peptide **3**)^{12, 15}, is the ability to agglutinate Gram-negative bacteria, judged as important in holding pathogens at bay at the infection focus. To test whether other hcRNase-derived peptides shared this property, their minimal agglutinating activities (MAC) were determined (Table 4). Interestingly, all antimicrobially active peptides (**1, 3, 4, 6, 7**) showed agglutinating properties to a certain degree, suggesting that this antimicrobial feature is conserved for all hcRNases. Furthermore, MAC values correlated well too with LPS binding affinities (Table 4, Supporting Information Table S1), suggesting that binding to the Gram-negative bacterial cell wall would trigger the agglutinating mechanism, as previously reported. In tune with this, no agglutination was observed for Gram-positive *S. aureus*, confirming the fact that an LPS external layer is necessary for bacterial agglutination. To further explore these agglutinating properties, we used fluorescence-assisted cell sorting (FACS). After incubation of *E. coli* cell cultures with the hcRNase-derived peptides, significant agglutination was only observed for active peptides **1, 3, 4, 6** and **7** (Figure 1A), with peptide **3**, followed by **6**, displaying the highest activity. Additionally, bacterial cells were

incubated with SYTO9 and propidium iodide (PI) to assess their viability simultaneously with agglutination (Figure 1B). Results showed dead bacteria to be present only when significant agglutinating activity was also detected, suggesting that both activities are part of a sole mechanism. One may therefore generalize the behavior of all active hcRNase-derived peptides as having the ability to dock onto external LPS layers and promote Gram-negative bacteria agglutination, triggering in turn membrane depolarization and lipid bilayer leakage, eventually resulting in cell death. For Gram-positive cells, peptides would probably diffuse across the permeable cell wall and exert their lytic action onto the cell membrane (Torrent et al. 2010a).

Previously we showed that the hcRNase 3 N-terminal domain (peptide **3**) retains the ability of the cognate protein to bind and disrupt model membranes (Torrent et al. 2009a; Torrent et al. 2011b). To determine whether all hcRNase-derived peptides behave similarly, we studied the effect of the peptides on lipid bilayer models. Changes in the tryptophan spectrum upon incubation with liposomes, a usual readout for membrane interaction, could only be assessed for peptides bearing this residue (**2**, **3**, **6**, **7** and **8**; Supplementary Information Table S1) but in all cases showed a good correspondence with antimicrobial activity. As reported for many other antimicrobial peptides, hcRNase-derived peptides were able to bind anionic liposomes, whereas no significant binding was observed for neutral ones, suggesting that electrostatic interactions are indispensable for peptide binding to lipid vesicles.

Next, the ability of the peptides to perturb bilayer stability was tested in a liposome leakage assay (Table 4). As expected, only active peptides displayed high leakage activity, and values observed for liposome content release were in good agreement with those observed for depolarization activity in bacteria (Table 3).

For a better characterization of the mechanism, the ability of hcRNase-derived peptides to agglutinate liposomes was studied by dynamic light scattering (DLS), which allows monitoring the vesicle size. All peptides were tested against both neutral and negatively charged vesicles (Figure 2), but only the latter agglutinated upon peptide interaction, again highlighting the role of electrostatic interactions in promoting agglutination. More interestingly, the only peptides capable of promoting agglutination in this assay with model membranes were those previously found to be active in either MAC or FACS experiments (Table 3, Figure 1).

In summary, results obtained using model membranes correlated well with those using bacterial cultures, hence reinforcing our claim that bactericidal mechanisms are consistently conserved at the N-termini of antimicrobially active hcRNases.

Vertebrate RNases share a conserved N-terminal antimicrobial domain

A next, logical step was to analyze the antimicrobial activity of the N-terminus across vertebrate RNases. To this end, we analyzed all RNase A homologues deposited at the Uniprot (www.uniprot.org) database using AMPA, an algorithm that scans proteins in search of potential antimicrobial regions (<http://tcoffee.crg.cat/apps/ampa/>) (Torrent, Nogues, Boix 2009; Torrent et al. 2012). Results are summarized in Figure 3, in the form of a phylogenetic tree of vertebrate RNases together with AMPA-identified putative antimicrobial regions at the N-termini of these proteins. It can be seen that most of these N-termini are potentially antimicrobial, in congruence with the experimental data in this study (Table 1). Results in Fig. 3, particularly the evolutionary distances among different hcRNases, suggest that N-terminal regions endowed with antimicrobial properties have been central in the function of RNases since their early origins and have accordingly been conserved along evolution.

Discussion

RNases are widely distributed in most vertebrate organs and tissues and can exert many different functions. Interestingly, many members of the RNase A superfamily, not only in mammals but also in other vertebrates, like fish and amphibians (Dyer, Rosenberg 2006; Nitto et al. 2006; Cho, Zhang 2007), show antimicrobial properties apparently unrelated to their nuclease activity. It has indeed been suggested that RNases might have emerged as a host-defense family in vertebrate evolution (Cho, Zhang 2007).

Although the three-dimensional structure of RNase A-like proteins is highly conserved, their amino acid sequence is quite diverse and a defined antimicrobial signature cannot be easily delineated. This is indeed the case for most antimicrobial peptides and proteins, sharing microbicidal properties despite low sequence similarity. Poor sequence homology has in practice prevented the development of robust methods for predicting antimicrobial motifs in proteins and peptides (Torrent, Nogues, Boix 2009; Torrent et al. 2012; Torrent, Nogues, Boix 2012). However, despite the lack of sequential or structural

patterns, similar physicochemical characteristics are shared among AMPs, like a net positive charge or the high content in hydrophobic amino acids (Torrent et al. 2011a). Recently, we described that the antimicrobial properties of hRNase 3 are highly retained in its N-terminal domain (Torrent et al. 2009a; Torrent et al. 2011b). This domain is equipotent compared to the whole protein, killing both Gram-negative and Gram-positive bacteria and retains its biophysical properties, including membrane agglutination and leakage (Torrent et al. 2009a; Torrent et al. 2011b). More interestingly, the chemically synthesized antimicrobial domain has a similar structure compared to its counterpart in the native protein in membrane-like environments (Garcia-Mayoral et al. 2010). However, as pointed below, there is no significant sequence similarity between the antimicrobial N-terminus of hRNase 3 and those of other antimicrobial RNases (Supplementary information text and Figures S1 and S2). For instance, the residues reported to be critical for antimicrobial activity in hRNases 3 and 7 are not significantly conserved (Supplementary information, Figure S1) (Boix et al. 2012). Nonetheless, all hcRNase N-termini have a high isoelectric point and similar hydrophobicity (Table 1).

In the present study, we have shown that all N-terminal antimicrobial domains of hcRNases with described antimicrobial activity are active against both Gram-positive and Gram-negative bacteria (Table 2). Even more interesting, in the cases where enough experimental information on the antimicrobial activity of the proteins is available, the peptides tested have similar activity (Table 2). We have also analyzed the biophysical characteristics of the peptides and evaluated the correlation between their ability to disrupt model membranes and their inherent antimicrobial activity (Tables 2 and 3). Liposome leakage shows a good correlation with both antimicrobial activity and membrane depolarization (Supplementary Information, Figure S7). The correspondence between leakage and depolarization is particularly interesting as it suggests that the antimicrobial peptides will eventually promote a disruptive action at the membrane level, rather than interacting with internal targets in the microbes. Interestingly, there is a significant correlation between the ability to acquire a defined structure in membrane-like environments (e.g. SDS micelles) and the antimicrobial activity (Supplementary Information, Figures S6 and S8), suggesting that peptides would adopt α -helical structure to perturb the bacteria membrane integrity.

All hcRNase N-terminal peptides with antimicrobial activity also show significant agglutination activity, suggesting that this trait might be inherent to antimicrobial

RNases. The agglutinating activity of hcRNase 3 has been previously attributed to a high aggregation-prone region at the N-terminus (residues 8-16) (Torrent et al. 2010a; Torrent et al. 2010b). Removal of this corresponding hydrophobic patch inside the antimicrobial domain drastically reduces hcRNase 3 antimicrobial activity, particularly in Gram-negative species. A comparison of the computed aggregation propensity profiles of all RNases shows a significant correlation between the aggregation propensity in this particular region and the observed agglutinating activity (Supplementary Information, Figures S3, S4 and S5), strengthening the conclusion that bacteria agglutination may be a characteristic trait of the antimicrobial mechanism of action.

Bacterial agglutination activity is also associated with the ability to bind LPS (Table 4). In fact, agglutination has been shown to take place in the external layers of the Gram-negative bacterial cell wall (Torrent et al. 2008; Torrent et al. 2010a). Accordingly, we suggested that following RNase binding to the external layers of Gram-negative bacteria, a slight conformational change in the protein would expose the N-terminal hydrophobic patch to the surface, thereby triggering agglutination by protein-protein interaction. Bacterial agglutination would therefore correlate with the hydrophobic nature of the aggregation-prone region (Supplementary Information, Figure S5). A side-by-side comparison of the two best studied antimicrobial hcRNases, 3 and 7, corroborate this behavior, showing that the agglutination potency is far more intense for RNase 3 than for RNase 7 (Torrent et al. 2010a). In this light, it is reasonable to conclude that both hcRNases and their derived peptides will act by a membrane perturbation mechanism, which supports the hypothesis that ribonuclease activity is not required for the antimicrobial action. Notwithstanding, we should also consider that within the context of the whole RNase A family the distinct members would combine their diverse abilities, and among them their catalytic activity, providing a fast and effective multifaceted mechanism to combat pathogens simultaneously at several cellular targets. Indeed, the most recent reviews on AMPs point at such a multifunctional working mode (Nguyen, Haney, Vogel 2011; Yeung, Gellatly, Hancock 2011)

Other literature reports also suggest that the N-terminus of RNases might be the main region responsible for their cytotoxicity. For example, Picone et al. have found that increasing the positive charge at the N-terminus of bovine seminal RNase enhances membrane interaction and antitumor activity (D'Errico et al. 2011). Interestingly, we have also found comparable behaviors in other cytotoxic RNase families, such as the

contribution of the N-terminus of ribotoxin in the interaction with lipid bilayers (Alvarez-Garcia, Martinez-del-Pozo, Gavilanes 2009).

The present experimental findings suggest that RNase N-termini might have been selected in evolution to execute host-defense related functions, particularly those dependent on a cytotoxic action. To strengthen this conclusion, we have analyzed the antimicrobial profile of all secreted vertebrate RNases using the AMPA algorithm. The analysis output (Figure 3) shows that most RNases have putative antimicrobial domains at the N-terminal region whose sequences overlap with the antimicrobial-prone region described for hcRNase 3. It is thus reasonable to suggest that both antimicrobial and catalytic activities in the RNase A-like superfamily have evolved independently and that evolution has used the N-terminal domain of RNases to develop anti-pathogen properties. Hence, the results presented here support the hypothesis that RNases might have emerged as a host-defense family.

In conclusion, we have shown that the antimicrobial properties of human RNases are retained in their N-terminal domain. Despite the low sequence conservation, the latent antimicrobial properties of this N-terminal domain in many RNase homologues suggest that this region might have evolved to provide host-defense functions for the protein. In this regard, antimicrobial RNases, and more specifically their N-terminal domains, would therefore constitute suitable scaffolds useful as lead templates for the development of wide spectrum antibiotics.

Materials and Methods

Materials and Strains

1,2-Dioleoyl-sn-glycero-3-phosphocholine (DOPC) and 1,2-dioleoyl-sn-glycero-3-[phospho-rac-(1-glycerol)] (DOPG), were from Avanti Polar Lipids, Birmingham, AL. LPS from *E. coli* was purchased from Sigma Aldrich.

8-Aminonaphthalene-1,3,6-trisulfonic acid disodium salt (ANTS), p-xylene-bispyridiniumbromide (DPX), BC (BODIPY TR cadaverine, where BODIPY is boron dipyrromethane (4,4-difluoro-4-bora-3a,4a-diaza-s-indacene) and SYTOX were purchased from Invitrogen (Carlsbad, CA). pET11 expression vector and *E. coli* BL21(DE3) cells were from Novagen, Madison, WI.

Strains used were *Escherichia coli* (BL2, Novagen), *Staphylococcus aureus* (ATCC 502A), *Acinetobacter baumannii* (ATCC 15308), *Pseudomonas sp* (ATCC 15915), *Micrococcus luteus* (ATCC 7468), and *Enterococcus faecium* (ATCC 19434).

Peptide synthesis

Fmoc-protected amino acids and 2-(1H-benzotriazol-1-yl)-1,1,3,3-tetramethyluronium hexafluorophosphate (HBTU) were obtained from Iris Biotech (Marktredwitz, Germany). Fmoc-Rink-amide (MBHA) resin was from Novabiochem (Läufelfingen, Switzerland). HPLC-grade acetonitrile (ACN) and peptide synthesis-grade N,N-dimethylformamide (DMF), N,N-diisopropylethylamine (DIEA), and trifluoroacetic acid (TFA) were from Carlo Erba-SDS (Peypin, France).

Solid phase peptide synthesis was done by Fmoc-based chemistry on Fmoc-Rink-amide (MBHA) resin (0.1 mmol) in a model 433 synthesizer (Applied Biosystems, Foster City, CA) running FastMoc protocols. Couplings used 8-fold molar excess each of Fmoc-amino acid and HBTU and 16-fold molar excess of DIEA. Side chains of trifunctional residues were protected with tert-butyl (Asp, Glu, Ser, Thr, Tyr), tert-butyloxycarbonyl (Lys, Trp), 2,2,4,6,7-pentamethyldihydrobenzofuran-5-sulfonyl (Arg), and trityl (Asn, Gln, His) groups. After chain assembly, full deprotection and cleavage were carried out with TFA–water–triisopropylsilane (95:2.5:2.5 v/v, 90 min, room temperature). Peptides were isolated by precipitation with cold diethyl ether and separated by centrifugation, dissolved in 0.1 M acetic acid, and lyophilized. Analytical reversed-phase HPLC was performed on a Luna C18 column (4.6 mm × 50 mm, 3 μm; Phenomenex, Torrance, CA). Linear 5-60% gradients of solvent B (0.036% TFA in ACN) into A (0.045% TFA in H₂O) were used for elution at a flow rate of 1 mL/min and with UV detection at 220 nm. Preparative HPLC runs were performed on a Luna C18 column (21.2 mm × 250 mm, 10 μm; Phenomenex), using linear gradients of solvent B (0.1% in ACN) into A (0.1% TFA in H₂O), as required, with a flow rate of 25 mL/min. MALDI-TOF mass spectra were recorded in the reflector or linear mode in a Voyager DE-STR workstation (Applied Biosystems, Foster City, CA) using α-hydroxycinnamic acid matrix. Fractions of adequate (>90%) HPLC homogeneity and with the expected mass were pooled, lyophilized, and used in subsequent experiments.

MIC (Minimal Inhibitory Concentration) and MAC (Minimal Agglutination Concentration) determinations

Antimicrobial activity was expressed as the MIC₁₀₀, defined as the lowest protein concentration that completely inhibits microbial growth. MIC of each peptide was determined from two independent experiments performed in triplicate for each concentration. Bacteria were incubated at 37 °C overnight in Luria-Bertani (LB) broth and diluted to give approximately 5·10⁵ CFU/mL. Bacterial suspension was incubated with peptides at various concentrations (0.1-10 μM) at 37 °C for 4 h in phosphate buffer. Samples were plated onto Petri dishes and incubated at 37 °C overnight.

For MAC determination, bacteria cells were grown at 37 °C to mid-exponential phase (OD₆₀₀ = 0.6), centrifuged at 5000×g for 2 min, and resuspended in LB to give an absorbance of 0.2 at 600 nm. A 200 μL aliquot of the bacterial suspension was incubated with peptides at various (0.1-10 μM) concentrations at 25°C for 4 h. Aggregation behavior was observed by visual inspection and minimal agglutinating concentration was expressed as previously described (Torrent et al. 2011b).

Hemolytic Activity

Fresh human red blood cells (RBCs) were washed 3 times with PBS (35 mM phosphate buffer, 0.15 M NaCl, pH 7.4) by centrifugation for 5 min at 3000×g and resuspended in PBS at 2 × 10⁷ cells/mL. RBCs were incubated with peptides at 37 °C for 4 h and centrifuged at 13000×g for 5 min. The supernatant was separated from the pellet and its absorbance measured at 570 nm. T100% hemolysis was defined as the absorbance obtained by sonicating RBCs for 10 s. HC₅₀ was calculated by fitting the data to a sigmoidal function.

Fluorescence-Assisted Cell Sorting (FACS) assay

Bacteria cells were grown at 37 °C to mid-exponential phase (OD₆₀₀ = 0.6), centrifuged at 5000×g for 2 min, resuspended in 10 mM sodium phosphate buffer, 100 mM NaCl, pH 7.4 to give a final OD₆₀₀ = 0.2 and preincubated for 20 min. A 500 μL aliquot of the bacterial suspension was incubated with 5 μM peptide for 4 h. After incubation, 25000 cells were subjected to FACS analysis using a FACSCalibur cytometer (BD Biosciences, Franklin Lakes, New Jersey) and a dot-plot was generated by representing the low-angle forward scattering (FSC-H) in the x-axis and the side scattering (SSC-H) in the y-axis to analyze the size and complexity of the cell cultures. Results were analyzed using FlowJo (Tree Star, Ashland, OR).

LUV liposome preparation

Large unilamellar vesicles (LUVs) containing DOPC, DOPG or DOPC/DOPG (3:2 molar ratio) of a defined size (about 100 nm) were prepared as previously described (Torrent et al. 2007). LUVs were obtained from a vacuum-drying lipid chloroform solution by extrusion through 100 nm polycarbonate membranes. The lipid suspension was frozen and thawed ten times prior to extrusion. A 1 mM stock solution of liposome suspension in 10 mM phosphate buffer, 100 mM NaCl, pH 7.4 was prepared.

Liposome leakage assay.

The ANTS/DPX liposome leakage fluorescence assay was performed as previously described (Torrent et al. 2007). Briefly, a unique population of LUVs of DOPC/DOPG (3:2 molar ratio) lipids was obtained containing 12.5 mM ANTS, 45 mM DPX, 20 mM NaCl, and 10 mM Tris/HCl, pH 7.4. The ANTS/DPX liposome suspension was diluted to 30 μ M concentration and incubated at 25 °C in the presence of peptide. Leakage activity was followed by monitoring the increase of fluorescence at 535 nm. (Torrent et al. 2009b).

Liposome agglutination assay

Liposome agglutination was analyzed by dynamic light scattering (DLS) using a Malvern 4700 photon correlation spectrometer (Malvern Instruments, Malvern, U.K.). An argon laser ($\lambda = 488$ nm) was used to cover the wide size range involved. Hydrodynamic radius measurements were always carried out at a reading scattering angle of 90°. From the intensity measurements recorded, data were processed by the CONTIN software (Malvern) and the hydrodynamic diameter (HD), the polydispersity index (PI), and the total number of counts were calculated. The incubation buffer was 10 mM Tris-HCl and 100 mM NaCl at pH 7.4. Measurements were performed at 25 °C, a 200 μ M final liposome concentration, and a 5 μ M peptide concentration.

LPS binding assay

LPS binding was assessed using the fluorescent probe Bodipy TR cadaverine (BC) as described (Torrent et al. 2008). Briefly, the displacement assay was performed by adding 1-2 μ L aliquots of peptide to 1 mL of a continuously stirred mixture of LPS (10 μ g/mL)

and BC (10 μ M) in 10 mM phosphate buffer, 100 mM NaCl, pH 7.5. Fluorescence measurements were performed on a Cary Eclipse spectrofluorimeter, with 580 and 620 nm as BC excitation and emission wavelengths, respectively. The excitation slit was set at 2.5 nm, and the emission slit was set at 20 nm. Final values correspond to an average of four replicates and were the mean of a 0.3 s continuous measurement. Occupancy factor was calculated as described previously (Torrent et al. 2008).

CD spectroscopy

Far-UV CD spectra were recorded in a Jasco J-715 spectropolarimeter as described (Torrent et al. 2009a). Mean-residue ellipticity $[\theta]$ ($\text{deg} \cdot \text{cm}^2 \cdot \text{dmol}^{-1}$) was calculated as

$$[\theta] = \frac{\theta(MRW)}{10cl}$$

where θ is the experimental ellipticity (deg), MRW is the mean residue molecular mass of the peptide, c is the molar concentration of peptide, and l is the cell path length. Data from four consecutive scans were averaged. Spectra of peptides (4–8 μ M in 5 mM sodium phosphate, pH 7.5) in the absence and presence (1 mM) of SDS and LPS (1 mM, nominal MW = 90 kDa) were recorded. Samples were centrifuged for 5 min at 10000 \times g before use.

SYTOX Green uptake

For SYTOX Green assays, bacterial *E. coli* and *S. aureus* cells were grown to mid-exponential growth phase ($\text{OD}_{600} \sim 0.6$) in LB medium and then centrifuged, washed, and resuspended in phosphate buffer. Cell suspensions ($\text{OD}_{600} \sim 0.2$) were incubated with 1 μ M SYTOX Green (Invitrogen, Carlsbad, CA) for 15 min in the dark prior to the influx assay. At 2-4 min after initiating data collection, 5 μ M peptide was added to the cell suspension, and the increase in SYTOX Green fluorescence was measured (485 and 520 nm excitation and emission wavelengths, respectively) for 40 min in a Cary Eclipse spectrofluorimeter. Maximum fluorescence was that resulting from cell lysis with Triton X-100.

Bacterial cytoplasmic membrane depolarization assay

Membrane depolarization was monitored as described earlier (Torrent et al. 2010a). Briefly, *E. coli* and *S. aureus* strains were grown at 37 $^{\circ}$ C to an OD_{600} of 0.2, centrifuged at 5,000 \times g for 7 min, washed with 5 mM HEPES (pH 7.2) containing 20 mM glucose

and resuspended in 5 mM HEPES-KOH, 20 mM glucose, 100 mM KCl at pH 7.2 to an OD_{600} of 0.05. DiSC3(5) was added to a final concentration of 0.4 μ M, and changes in the fluorescence were continuously recorded after peptide (5 μ M) addition. The concentration required to achieve half of total membrane depolarization was estimated from nonlinear regression analysis.

Table 1. Physicochemical properties of the hcRNase-derived peptides

	Sequence ^a	[M+H] ⁺ ^b		Retention time ^c (min)	Hydrophobicity ^e	pI
		M	T			
1	---KESRAKKFQRQHMDSDSSPSSSSTYS <u>N</u> QMMRRRNMTQGR <u>S</u> KPVNTFVH	5630.45	5628.72	4.93	-1.575	11.40
2	KPPQFTWAQWFETQHINMTSQ-----Q <u>S</u> TNAMQVINNYQRR <u>S</u> KNQNTFLL	5453.32	5452.67	8.56	-1.069	10.28
3	RPPQFTRAQWFQIHISLNPP-----R <u>S</u> TIAMRAINNYRWR <u>S</u> KNQNTFL	5478.34	5478.74 ^d	5.05 ^d	-0.764	11.88
4	--QDGMY-QRFLRQHVHPEET-GGSDRY <u>S</u> NLMMQRRKMTLYH <u>S</u> KRFNTFIH	5812.31	5824.84	6.69	-1.228	10.15
5	--QDNSRYTHFLTQH ^Y DAKPQ-GRDDRY <u>S</u> ESIMRRRGLTS-P <u>S</u> KDINTFIH	5638.15	5635.76	6.43	-1.430	9.40
6	WPKRLTKAHWFEIQHIQPSPL-----Q <u>S</u> NRAMSGINNYTQH <u>S</u> KHQNTFLH	5410.85	5404.74	6.88	-1.096	10.45
7	KPKGMTSSQWFKIQHMQPSPQ-----A <u>S</u> NSAMKNINKHTKR <u>S</u> KDLNTFLH	5206.90	5205.67	6.20	-1.209	10.75
8	KPKDMTSSQWFKTQHVPSPQ-----A <u>S</u> NSAMSI INKYTER <u>S</u> KDLNTFLH	5206.95	5204.59	7.48	-1.044	9.70

^a In every peptide, the underlined serine (S) residues correspond to cysteines in the native protein.

^b Measured (M) and theoretical (T) molecular weights in Da.

^c All peptides except RNase3 analyzed as described in Materials and Methods. For RNase 3, data are from ref. 12 see footnote d.

^d Data from ref. 12; HPLC as described in Materials and Methods here, except that gradient is 20-45%B into A over 15 min.

^e Hydrophobicity computed using the GAVY scale

Table 2. Antimicrobial and hemolytic activities of the hcRNase N-terminal peptides

	Antimicrobial activity						Hemolytic activity	
	MIC ₁₀₀ (μM)						HC ₅₀ (μM)	
	Gram-negative bacteria			Gram-positive bacteria			Protein antimicrobial activity ^a	Sheep red blood cells
	<i>E. coli</i>	<i>P. aeruginosa</i>	<i>A. baumannii</i>	<i>S. aureus</i>	<i>M. luteus</i>	<i>E. faecium</i>		
1	9	9	9	5	9	5	n.r.	11.6
2	>10	>10	>10	>10	>10	10	-	>100
3	0.4	0.4	0.3	0.5	0.6	0.6	+++	9.5
4	0.3	0.4	0.5	0.3	1.2	0.8	n.r.	15.2
5	>10	>10	>10	>10	>10	>10	-	>100
6	1.2	1.2	1.2	5	2.5	2.5	n.r.	17.4
7	1.2	1.2	1.2	10	5	2.5	+++	10.4
8	>10	10	>10	>10	>10	>10	+	15.1

^a Antimicrobial activity of the parental proteins obtained from (Boix et al. 2012). (n.r.: not reported. Antimicrobial activity has not been assayed for some proteins)

Table 3. Depolarization and bacteria leakage IC₅₀ values for hcRNase-derived peptides

	Depolarization		Bacteria leakage	
	(nM)		(nM)	
	<i>E. coli</i>	<i>S. aureus</i>	<i>E. coli</i>	<i>S. aureus</i>
1	150±10	350±13	>10	9.1±1
2	>1000	>1000	>10	>10
3	40±1	50±7	3.8±0.1	4.5±0.5
4	40±3	30±2	3.8±0.2	6.1±0.1
5	>1000	>1000	>10	>10
6	40±4	40±2	5.0±0.3	7.3±0.7
7	40±3	70±1	5.7±0.1	7.3±0.2
8	>1000	>1000	>10	>10

Table 4. LPS affinity, agglutination activity and liposome leakage of hcRNase-derived peptides. Values are expressed as ED₅₀.

	LPS binding (μM)	MAC* (μM)	Liposome Leakage (nM)		
			DOPC	DOPC:DOPG	DOPG
1	5.6 \pm 1.3	5.0 \pm 0.5	>1000	>1000	206 \pm 77
2	7.1 \pm 1.0	n.d.	>1000	>1000	>1000
3	2.9 \pm 0.3	0.9 \pm 0.1	>1000	95 \pm 5	99 \pm 2
4	1.3 \pm 0.2	5.0 \pm 0.5	>1000	580 \pm 10	53 \pm 5
5	n.d.	n.d.	>1000	>1000	>1000
6	1.9 \pm 0.3	1.8 \pm 0.1	>1000	210 \pm 30	86 \pm 10
7	3.2 \pm 1.2	5 \pm 0.5	>1000	180 \pm 20	108 \pm 4
8	n.d.	n.d.	>1000	>1000	>1000

* MAC values obtained with *E. coli* cultures.

n.d. Not detected at the assayed concentration range (0.1-10 μ M).

Figure legends

Figure 1.

Bacterial agglutination measured by fluorescence-assisted cell sorting. *E. coli* cell cultures were incubated with hcRNase-derived peptides at 5 μ M concentration for 4 h and analyzed using a FACSCalibur cytometer. Low-angle forward scattering (FSC-H) is represented in the x-axis and the side scattering (SSC-H) in the y-axis to analyze the size and complexity of the cell cultures. (A) Plots are colored to show cell density. Low (blue) to high (red) cell densities are represented. The percentages of cells belonging to each quadrant are indicated. (B) Plots are colored to show cell viability. Live cells (stained by Syto9, green) and dead cells (stained by propidium iodide, red) are colored in the plot. Control live and dead cells were analyzed as a reference.

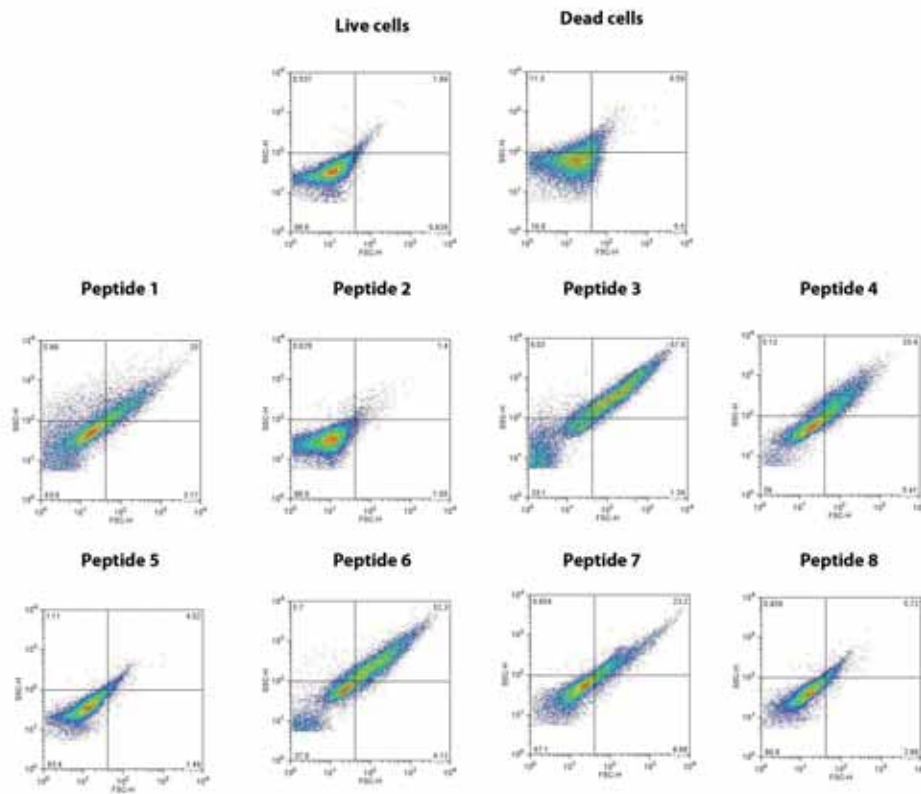
Figure 2.

Liposome aggregation measured by dynamic light scattering. Liposomes containing DOPC (red), DOPG (blue) or a 3:2 molar mixture of DOPC/DOPG (green) were incubated with 5 μ M hcRNase-derived peptides and the size was measured after 15 min by DLS using a Malvern 4700 spectrometer. The plots represent the intensity versus the liposome mean size. For peptides **6** and **7** with DOPG liposomes, large aggregates were observed that made it difficult to determine a defined particle mean size.

Figure 3.

Conservation of the N-terminal antimicrobial domain among vertebrate secreted RNases. The evolutionary history was inferred using the UPGMA method (Sneath, Sokal 1973). The optimal tree is shown. The tree is drawn to scale, with branch lengths in the same units as those of the evolutionary distances used to infer the phylogenetic tree. The evolutionary distances were computed using the Poisson distribution method (Zuckerandl, Pauling 1965) and are in units of number of amino acid substitutions per site. All positions containing gaps and missing data were eliminated. Evolutionary analyses were conducted in MEGA5 (Tamura et al. 2011). All sequences were analyzed using the AMPA algorithm (Torrent et al. 2012); detected antimicrobial regions in the N-terminal domain are depicted in the figure, next to the corresponding tree branch. Each type of RNase family is depicted in a different color.

A



B

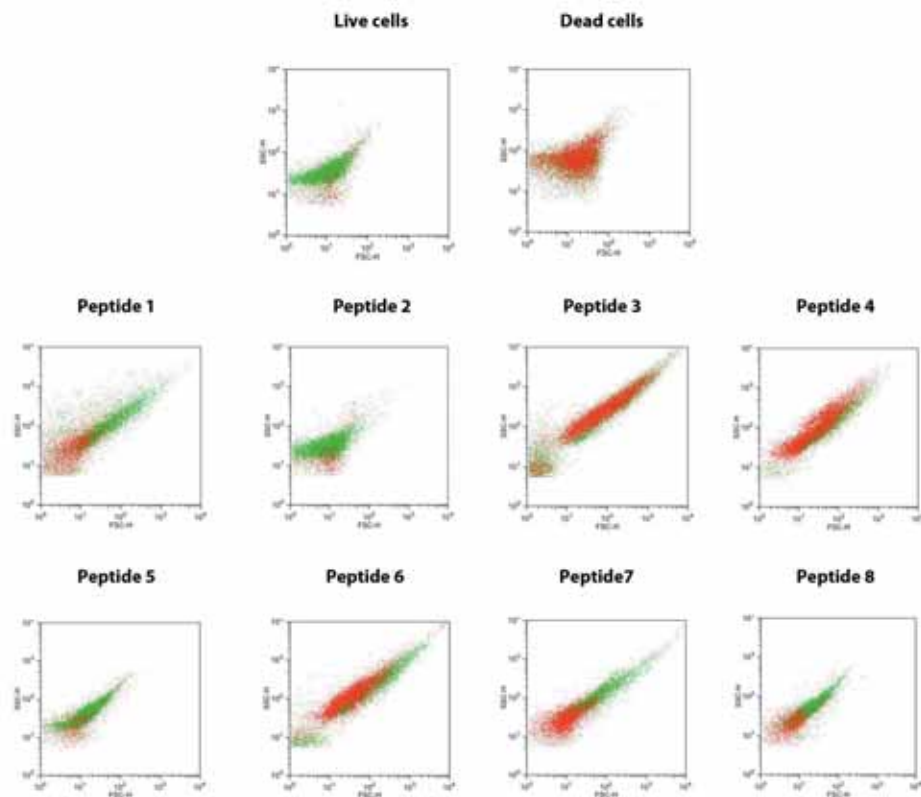


Figure 1

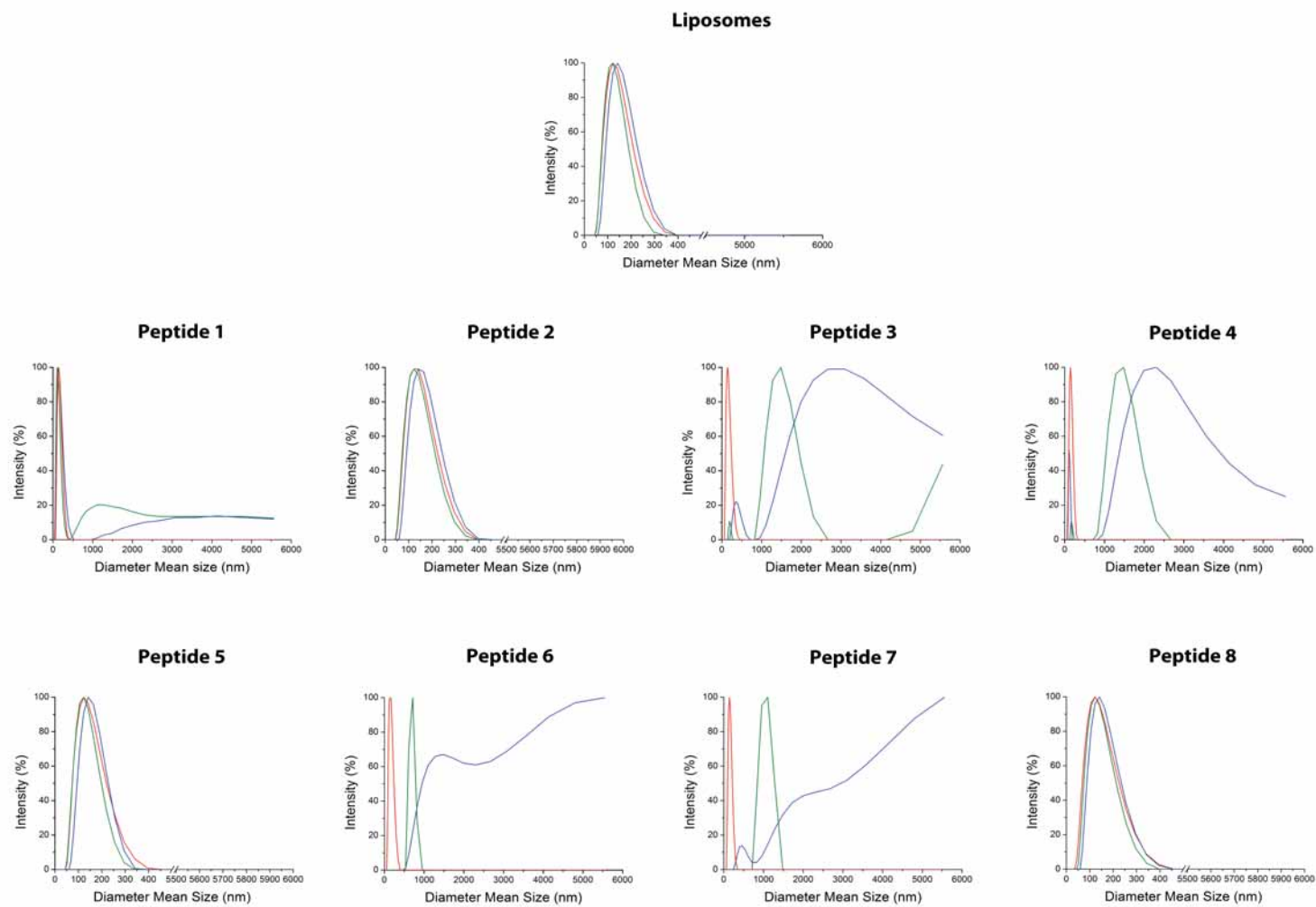


Figure 2

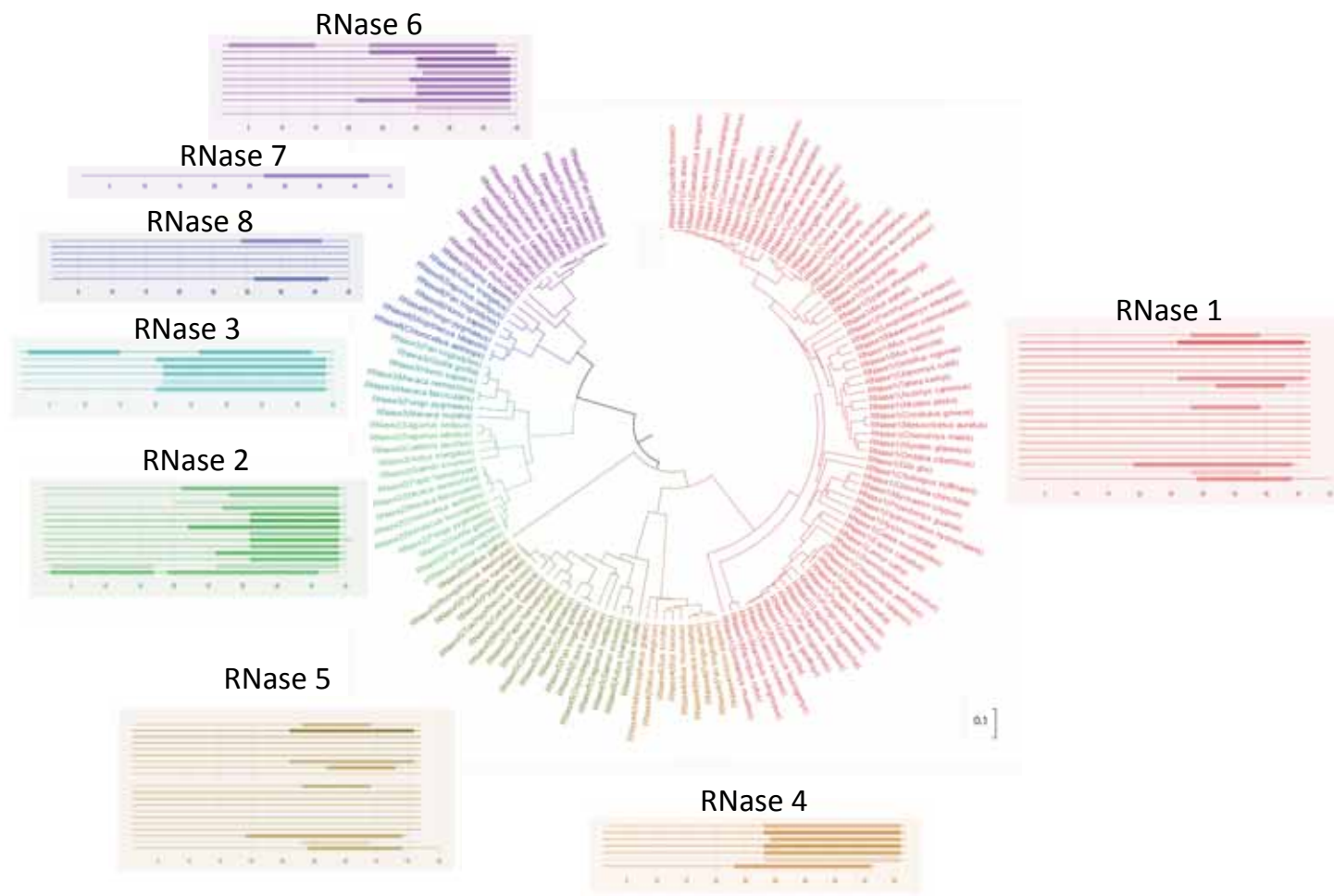


Figure 3

REFERENCES

- Acharya, KR, R Shapiro, SC Allen, JF Riordan, BL Vallee. 1994. Crystal structure of human angiogenin reveals the structural basis for its functional divergence from ribonuclease. *Proc Natl Acad Sci U S A* 91:2915-2919.
- Alvarez-Garcia, E, A Martinez-del-Pozo, JG Gavilanes. 2009. Role of the basic character of alpha-sarcin's NH2-terminal beta-hairpin in ribosome recognition and phospholipid interaction. *Arch Biochem Biophys* 481:37-44.
- Boix, E, MV Nogues. 2007. Mammalian antimicrobial proteins and peptides: overview on the RNase A superfamily members involved in innate host defence. *Mol Biosyst* 3:317-335.
- Boix, E, VA Salazar, M Torrent, D Pulido, MV Nogues, M Moussaoui. 2012. Structural determinants of the eosinophil cationic protein antimicrobial activity. *Biol Chem* 393:801-815.
- Cho, S, JJ Beintema, J Zhang. 2005. The ribonuclease A superfamily of mammals and birds: identifying new members and tracing evolutionary histories. *Genomics* 85:208-220.
- Cho, S, J Zhang. 2007. Zebrafish ribonucleases are bactericidal: implications for the origin of the vertebrate RNase A superfamily. *Mol Biol Evol* 24:1259-1268.
- D'Errico, G, C Ercole, M Lista, E Pizzo, A Falanga, S Galdiero, R Spadaccini, D Picone. 2011. Enforcing the positive charge of N-termini enhances membrane interaction and antitumor activity of bovine seminal ribonuclease. *Biochim Biophys Acta* 1808:3007-3015.
- Dyer, KD, HF Rosenberg. 2006. The RNase a superfamily: generation of diversity and innate host defense. *Mol Divers* 10:585-597.
- Garcia-Mayoral, MF, M Moussaoui, BG de la Torre, D Andreu, E Boix, MV Nogues, M Rico, DV Laurents, M Bruix. 2010. NMR structural determinants of eosinophil cationic protein binding to membrane and heparin mimetics. *Biophys J* 98:2702-2711.
- Huang, YC, YM Lin, TW Chang, SJ Wu, YS Lee, MD Chang, C Chen, SH Wu, YD Liao. 2007. The flexible and clustered lysine residues of human ribonuclease 7 are critical for membrane permeability and antimicrobial activity. *J Biol Chem* 282:4626-4633.
- Kover, KE, M Bruix, J Santoro, G Batta, DV Laurents, M Rico. 2008. The solution structure and dynamics of human pancreatic ribonuclease determined by NMR spectroscopy provide insight into its remarkable biological activities and inhibition. *J Mol Biol* 379:953-965.
- Laurents, DV, M Bruix, MA Jimenez, J Santoro, E Boix, M Moussaoui, MV Nogues, M Rico. 2009. The (1)H, (13)C, (15)N resonance assignment, solution structure, and residue level stability of eosinophil cationic protein/RNase 3 determined by NMR spectroscopy. *Biopolymers* 91:1018-1028.
- Mosimann, SC, DL Newton, RJ Youle, MN James. 1996. X-ray crystallographic structure of recombinant eosinophil-derived neurotoxin at 1.83 Å resolution. *J Mol Biol* 260:540-552.
- Nguyen, LT, EF Haney, HJ Vogel. 2011. The expanding scope of antimicrobial peptide structures and their modes of action. *Trends Biotechnol* 29:464-472.
- Nitto, T, KD Dyer, M Czapiga, HF Rosenberg. 2006. Evolution and function of leukocyte RNase A ribonucleases of the avian species, *Gallus gallus*. *J Biol Chem* 281:25622-25634.

- Pizzo, E, M Varcamonti, A Di Maro, A Zanfardino, C Giancola, G D'Alessio. 2008. Ribonucleases with angiogenic and bactericidal activities from the Atlantic salmon. *FEBS J* 275:1283-1295.
- Rosenberg, HF. 1995. Recombinant human eosinophil cationic protein. Ribonuclease activity is not essential for cytotoxicity. *J Biol Chem* 270:7876-7881.
- Rudolph, B, R Podschun, H Sahly, S Schubert, JM Schroder, J Harder. 2006. Identification of RNase 8 as a novel human antimicrobial protein. *Antimicrob Agents Chemother* 50:3194-3196.
- Sanchez, D, M Moussaoui, E Carreras, M Torrent, V Nogues, E Boix. 2011. Mapping the eosinophil cationic protein antimicrobial activity by chemical and enzymatic cleavage. *Biochimie* 93:331-338.
- Sneath, PHA, RR Sokal. 1973. *Numerical Taxonomy*. San Francisco: Freeman.
- Sorrentino, S. 2010. The eight human "canonical" ribonucleases: molecular diversity, catalytic properties, and special biological actions of the enzyme proteins. *FEBS Lett* 584:2194-2200.
- Sorrentino, S, M Libonati. 1997. Structure-function relationships in human ribonucleases: main distinctive features of the major RNase types. *FEBS Lett* 404:1-5.
- Tamura, K, D Peterson, N Peterson, G Stecher, M Nei, S Kumar. 2011. MEGA5: molecular evolutionary genetics analysis using maximum likelihood, evolutionary distance, and maximum parsimony methods. *Mol Biol Evol* 28:2731-2739.
- Terzyan, SS, R Peracaula, R de Llorens, Y Tsushima, H Yamada, M Seno, FX Gomis-Ruth, M Coll. 1999. The three-dimensional structure of human RNase 4, unliganded and complexed with d(U)p, reveals the basis for its uridine selectivity. *J Mol Biol* 285:205-214.
- Torrent, M, D Andreu, VM Nogues, E Boix. 2011a. Connecting peptide physicochemical and antimicrobial properties by a rational prediction model. *PLoS One* 6:e16968.
- Torrent, M, M Badia, M Moussaoui, D Sanchez, MV Nogues, E Boix. 2010a. Comparison of human RNase 3 and RNase 7 bactericidal action at the Gram-negative and Gram-positive bacterial cell wall. *FEBS J* 277:1713-1725.
- Torrent, M, E Cuyas, E Carreras, S Navarro, O Lopez, A de la Maza, MV Nogues, YK Reshetnyak, E Boix. 2007. Topography studies on the membrane interaction mechanism of the eosinophil cationic protein. *Biochemistry* 46:720-733.
- Torrent, M, BG de la Torre, VM Nogues, D Andreu, E Boix. 2009a. Bactericidal and membrane disruption activities of the eosinophil cationic protein are largely retained in an N-terminal fragment. *Biochem J* 421:425-434.
- Torrent, M, P Di Tommaso, D Pulido, MV Nogues, C Notredame, E Boix, D Andreu. 2012. AMPA: an automated web server for prediction of protein antimicrobial regions. *Bioinformatics* 28:130-131.
- Torrent, M, S Navarro, M Moussaoui, MV Nogues, E Boix. 2008. Eosinophil cationic protein high-affinity binding to bacteria-wall lipopolysaccharides and peptidoglycans. *Biochemistry* 47:3544-3555.
- Torrent, M, MV Nogues, E Boix. 2012. Discovering new in silico tools for antimicrobial peptide prediction. *Curr Drug Targets* 13:1148-1157.
- Torrent, M, MV Nogues, E Boix. 2009. A theoretical approach to spot active regions in antimicrobial proteins. *BMC Bioinformatics* 10:373.
- Torrent, M, F Odorizzi, MV Nogues, E Boix. 2010b. Eosinophil cationic protein aggregation: identification of an N-terminus amyloid prone region. *Biomacromolecules* 11:1983-1990.
- Torrent, M, D Pulido, BG de la Torre, MF Garcia-Mayoral, MV Nogues, M Bruix, D Andreu, E Boix. 2011b. Refining the eosinophil cationic protein antibacterial pharmacophore by rational structure minimization. *J Med Chem* 54:5237-5244.

- Torrent, M, D Sanchez, V Buzon, MV Nogues, J Cladera, E Boix. 2009b. Comparison of the membrane interaction mechanism of two antimicrobial RNases: RNase 3/ECP and RNase 7. *Biochim Biophys Acta* 1788:1116-1125.
- Yeung, AT, SL Gellatly, RE Hancock. 2011. Multifunctional cationic host defence peptides and their clinical applications. *Cell Mol Life Sci* 68:2161-2176.
- Zuckerandl, E, L Pauling. 1965. *Evolutionary divergence and convergence in proteins*. New York: Academic Press.

CHAPTER V

Towards the rational design of antimicrobial proteins: single point mutations can switch on bactericidal and agglutinating activities on the RNase A superfamily lineage

David Pulido¹, Mohammed Moussaoui¹, M. Victòria Nogués¹, Marc Torrent^{1,2*} and Ester Boix^{1*}

¹ Universitat Autònoma de Barcelona, Department of Biochemistry and Molecular Biology, Biosciences Faculty, 08193 Cerdanyola del Vallès, Spain.

² MRC Laboratory of Molecular Biology, Francis Crick Avenue, Cambridge Biomedical Campus, Cambridge CB2 0QH, U.K.

*Corresponding author:

Marc Torrent: marc.torrent@uab.cat

Ester Boix: ester.boix@uab.cat

Running title:

Keywords: Eosinophil cationic protein, Eosinophil derived neurotoxin, ribonuclease, antimicrobial peptides, protein evolution.

Introduction

RNase A was the first ribonuclease discovered and is the eponym of the vertebrate RNase A superfamily (1, 2), which groups together all the vertebrate RNases homologous to RNase A. In humans, eight functional members have been ascribed to the RNase superfamily and are known as “canonical RNases” (3). All of them share common features such as the catalytic triad, composed by two histidines and one lysine, the ability to hydrolyze polymeric RNA substrates, and a specific tertiary structure stabilized by a unique disulfide-bond pattern (4). Notwithstanding, a variety of biological functions have been characterized that are independent from the RNase activity. Specially, several studies have reported significant antimicrobial activity in some family members, thereby suggesting that RNases could have an ancestral host-defense function (4-7).

The eosinophil ribonucleases, eosinophil-derived neurotoxin (EDN or RNase 2) and eosinophil cationic protein (ECP or RNase 3) are two main secretory components in the secondary granules of eosinophils. Since around 50 million years ago, EDN and ECP genes have diverged after gene duplication and have rapidly accumulated non-silent mutations under positive selection pressure while retaining their folding, cysteine pattern and the catalytic triad essential for ribonuclease activity (8-12). The antimicrobial and catalytic properties of both proteins have been extensively studied and characterized (13). EDN was isolated at the beginning of the 80's as an eosinophil protein of 18.4 kDa able to reproduce the Gordon phenomenon when injected intrathecally into rabbits (14). Further investigations revealed an intimate relation of EDN with the host immune system by showing that EDN was active against rhinovirus, adenovirus and, most notably, against the respiratory syncytial virus (RSV) in a ribonuclease activity dependent manner (15-17). However, EDN displays non significant antibacterial and very low antiparasitical activity even at high concentrations (18). Besides, EDN also acts as a modulator of the host immune system leading immature dendritic cells (DCs) chemotaxis both *in vitro* and *in vivo* (18-21). Therefore, EDN has been classified as an alarmin, a protein capable of activating and modulating the host immune system (21, 22).

On the other hand, ECP was firstly isolated at the beginning of 70's, from the secondary granules of human eosinophils as a highly cationic arginine-rich protein. Human ECP is secreted in response to either infection or inflammation processes (23, 24) and displays a highly antimicrobial activity against bacteria (25, 26), and many parasites, such as helminths and protozoa (27-32). In fact, the antimicrobial mechanism of ECP has been extensively studied and, in contrast to EDN, its antimicrobial properties are not dependent on the ribonuclease activity (33).

In spite of all the studies carried out before, little is known about the molecular determinants that conferred so distinct properties to two proteins that share 65% of sequence identity. Despite ECP being more cationic than EDN (pI 10.3 versus 8.6), cationic content by itself is not sufficient to explain the

differences observed, as other antimicrobial RNases display pI values close to EDN though retaining antimicrobial activities similar to ECP.

In the present study we have investigated the minimal molecular determinants that confer to ECP its unique antimicrobial properties that distinguish it from EDN. Here we show that mutating only two residues on EDN, Q34 to R and R35 to W, we can provide EDN with an antimicrobial activity similar to ECP. Even more interestingly, we also show that a third mutation, T13 to I, can give to EDN agglutinating properties intrinsically associated to protein self-aggregation in ECP. In summary, we show in this study that single-point mutation on ribonucleases can dramatically enhance antimicrobial properties and even generate new activities suggesting that the structure and sequence of RNases may have been evolutionary designed to embody antimicrobial activity.

Experimental procedures

Materials and strains

DOPC (dioleoyl phosphatidylcholine) and DOPG (dioleoyl phosphatidylglycerol) were from Avanti Polar Lipids (Alabaster, AL). ANTS (8-aminonaphthalene-1,3,6-trisulfonic acid disodium salt), DPX (p-xylylenebispyridinium bromide), and BC (BODIPY-TR cadaverine, where BODIPY is boron dipyrromethane (4,4-difluoro-4-bora-3a,4a-diaza-s-indacene) were purchased from Invitrogen (Carlsbad, CA). LT (lipoteichoic acids) from *Staphylococcus aureus* and LPS (lipopolysaccharides) from *Escherichia coli* serotype 0111:B4 were purchased from Sigma-Aldrich (St. Louis, MO). PD-10 desalting columns with Sephadex G-25 were from GE Healthcare (Waukesha, WI). Strains used were *Escherichia coli* (BL21, Novagen), *Staphylococcus aureus* (ATCC 502A), *Acinetobacter baumannii* (ATCC 15308), *Pseudomonas sp* (ATCC 15915), *Micrococcus luteus* (ATCC 7468), and *Enterococcus faecium* (ATCC 19434).

Expression and Purification of recombinant proteins.

Wild type ECP and EDN were obtained from human synthetic genes. All mutations were incorporated using the Quick-change mutagenesis kit from Invitrogen (Carlsbad, CA) and sequenced before expression. Protein expression in the *E. coli* BL21DE3 strain, folding of the protein from inclusion bodies, and purification were carried out as previously described (34, 35). Protein identity was checked by MALDI-TOF mass spectrometry. Circular dichroism spectra were recorded to confirm that the introduced mutations did not perturb the native protein overall three dimensional structure.

MIC (Minimal Inhibitory Concentration)

Antimicrobial activity was calculated as the minimal inhibitory concentration (MIC), defined as the lowest protein concentration that completely inhibits microbial growth. MIC of each protein was determined from two independent experiments performed in triplicate for each concentration. Proteins were dissolved in 10 mM sodium phosphate buffer, pH 7.5, and serially diluted from 10 to 0.2 μM . Bacteria were incubated at 37 °C overnight in Luria-Bertani broth and diluted to give approximately 5×10^5 CFU/mL. In each assay protein solutions were added to each bacteria dilution and incubated for 4 h, and samples were plated onto Petri dishes and incubated at 37 °C overnight.

Minimal Agglutination Activity (MAC)

Bacterial cells were grown at 37 °C to an $\text{OD}_{600}=0.2$, centrifuged at 5000 $\times g$ for 2 min and resuspended in 10mM Tris-HCl buffer, 0.1 M NaCl, pH 7.5. An aliquot of 100 μl of the bacteria suspension was treated with increasing protein concentrations (from 0.01 to 10 μM) and incubated at room temperature for 1h. The aggregation behavior was observed by visual inspection and the agglutinating activity is expressed as the minimum agglutinating concentration of the sample tested, as previously described (36).

Bacteria Cytoplasmic Membrane Depolarization Assay.

Membrane depolarization was followed using the method described earlier [33]. Briefly, bacteria strains were grown at 37 °C to an $\text{OD}_{600}= 0.2$, centrifuged at 5000 $\times g$ for 7 min, washed with 5 mM Hepes at pH 7.2 containing 20 mM glucose, and resuspended in 5 mM Hepes-KOH, 20 mM glucose, and 100 mM KCl at pH 7.2 to an $\text{OD}_{600}=0.05$ and 200 μl were transferred to a microtiter plate. DiSC3(5) was added to a final concentration of 0.4 μM and changes in the fluorescence were continuously recorded after addition of protein (5 μM) in a Victor3 plate reader (PerkinElmer, Waltham, MA). The time required to achieve total membrane depolarization and half membrane depolarization (IC_{50}) was estimated from nonlinear regression analysis as previously described (37). Lysis of the cells with the detergent Triton X-100 gives maximum membrane depolarization.

SEM (Scanning electron microscopy)

Cultures of *E. coli* and *S. aureus* (1 mL) were grown at 37 °C to mid-exponential phase (OD₆₀₀ ~0.4) and incubated with proteins (5 μM) in PBS at room temperature. Sample aliquots (500 μl) were taken after up to 4 h of incubation and prepared for SEM analysis as described in (36). The micrographs were viewed at a 15 kV accelerating voltage on a Hitachi S-570 scanning electron microscope, and a secondary electron image of the cells for topography contrast was collected at several magnifications.

Fluorescent Probe Displacement Assay for LPS and Lipid A Binding to ECP.

LPS binding was assessed using the fluorescent probe BODIPY-TR cadaverine (BC) as previously described (38). BC binds strongly to native LPSs, specifically recognizing the lipid A portion. When a protein that interacts with LPSs is added, BC is displaced from the complex and its fluorescence is increased, decreasing its occupancy factor. LPS-binding assays were carried out in a 5 mM HEPES buffer at pH 7.5. The displacement assay was performed in a microtiter plate containing a stirred mixture of both LPS (10 μg/mL) and BC (10 μM). Proteins were serially diluted from 10 to 0.1 μM. Fluorescence measurements were performed on a Victor3 plate reader. The concentration required to achieve half lipopolysaccharide binding (ED₅₀) was estimated from nonlinear regression analysis as previously described (37).

Hemolytic Activity.

Fresh human red blood cells (RBCs) were washed 3 times with PBS (35 mM phosphate buffer, 0.15 M NaCl, pH 7.4) by centrifugation for 5 min at 3000g and resuspended in PBS at $2 \cdot 10^7$ cells/mL. RBCs were incubated with proteins at 37 °C for 4 h and centrifuged at 13000g for 5 min. The supernatant was separated from the pellet and its absorbance measured at 570 nm. The 100% hemolysis was defined as the absorbance obtained by sonicating RBCs for 10 s. HC₅₀ was calculated by fitting the data to a sigmoidal function.

Liposome Preparation.

LUVs (large unilamellar vesicles) of ~100 nm diameter were prepared from a chloroform solution of DOPC, DOPG or a DOPC/DOPG mixture (3:2 molar ratio). After vacuum-drying, the lipid film was suspended in 10mM Tris/HCl, 0.1M NaCl, pH 7.4 buffer to give a 1 mM solution, then frozen and thawed several times prior to extrusion through polycarbonate membranes as previously described (39).

Fluorescence Measurements.

Tryptophan fluorescence emission spectra were recorded using a 280 nm excitation wavelength. Slits were set at 2 nm for excitation and 5-10 nm for emission. Emission spectra were recorded from 300-400 nm at a scan rate of 60 nm/min in a 10 mm x 10 mm cuvette, with stirring immediately after sample mixing. Protein spectra at 0.5 μ M in 10 mM Hepes buffer, pH 7.4, were obtained at 25 $^{\circ}$ C in the absence or presence of 200 μ M liposome suspension, 1mM SDS micelles or 100 μ M LPS micelles. Fluorescence measurements were performed on a Cary Eclipse spectrofluorimeter (Agilent Technologies, Bath, UK). Spectra in the presence of liposomes were corrected for light scattering by subtracting the corresponding LUV background. For each condition three spectra were averaged. The maximum of the fluorescence spectra was calculated by fitting the data to a log-normal distribution function as previously detailed (39).

ANTS/DPX Liposome Leakage Assay.

The ANTS/DPX liposome leakage fluorescence assay was performed as described (39). Briefly, a unique population of LUVs was prepared to encapsulate a solution containing 12.5 mM ANTS, 45 mM DPX, 20 mM NaCl, and 10 mM Tris/HCl, pH 7.5. The ANTS/DPX liposome stock suspension was diluted to 30 μ M and incubated at 25 $^{\circ}$ C with proteins, serially diluted from 10 to 0.1 μ M in a microtiter plate. Fluorescence measurements were performed on a Victor3 plate reader. IC₅₀ values were calculated by fitting the data to a dose-response curve.

Results

Design of EDN mutants

With the aim to study the molecular determinants of antimicrobial activity in the EDN/ECP lineage, we designed and constructed two EDN mutant proteins by rational mutagenesis. Previous results in our laboratory showed that two regions in the N-terminus of ECP are responsible for the antimicrobial properties: one segment encompassing residues 34-45, responsible for bacteria leakage and membrane permeation and another segment located in residues 8-16 responsible for protein self-aggregation and bacteria agglutination (13, 40, 41). Among the former region, it is described that residues R34 and W35 are important for ECP membrane disruptive activity (42) while in the later region I13 is required for bacteria self-aggregation (43, 44).

To understand whether these residues could have a distinctive role in the origin of antimicrobial activity in the ECP lineage, two EDN mutants were obtained: EDN-Q34R/R35W and EDN-T13I/Q34R/R35W. The first mutant incorporates a Trp residue in EDN to generate a RWR membrane permeabilizing tag similar as the one observed in ECP (Figure 1). The second mutant was designed to include a hydrophobic residue and generate an exposed hydrophobic patch at the surface of the protein that can drive protein self-aggregation and trigger bacteria agglutination (Figure 1). The parental proteins and the mutants were assayed by a wide battery of assays to determine the individual contribution of these mutations and infer the molecular determinants of antimicrobial activity.

Antimicrobial and cytotoxic activities

ECP, EDN and the two mutants were tested by MIC assay for antimicrobial activity against three representatives Gram-negative (*E. coli*, *A. baumannii* and *Pseudomonas sp.*) and Gram-positive (*S. aureus*, *M. luteus* and *E. faecium*) species (Table 1). ECP, as previously described (45), displayed a high antimicrobial activity in a submicromolar range against both Gram-positive and Gram-negative bacteria. On the other hand, EDN showed only a minor or undetectable antimicrobial activity for the bacterial species tested. In contrast, both EDN mutants Q34R/R35W and T13I/Q34R/R35W displayed antimicrobial activity on all strains and enhanced the antimicrobial activity up to 20 fold with respect to EDN. More interestingly, mutation of EDN Thr13 to Ile enhanced even more the antimicrobial activity, thus reflecting the contribution of the aggregation region to the protein antimicrobial mechanism.

Further investigations on the bactericidal properties of the EDN mutants were compared with ECP by assaying the membrane depolarization activity against two bacterial model strains *E. coli* and *S. aureus* (Table 2). ECP, as previously described (37), is able to interact with the bacteria Gram-negative and Gram-positive envelope, and can perturb the cell cytoplasmic membrane producing half of the total membranes depolarization at concentrations of 0.04 μM on *E. coli* and 0.05 μM on *S. aureus*. On the contrary, its homolog protein EDN did not show any depolarization activity neither on *E. coli* nor on *S. aureus* under the concentrations assayed. However, Q34R/R35W and T13I/Q34R/R35W EDN mutants displayed a high depolarization activity against both Gram-positive and Gram-negative strains, showing an effect similar to ECP.

Cytotoxicity against eukaryotic cell was tested by the hemolytic assay by incubating erythrocytes with serially diluted concentrations of ECP, EDN, and the corresponding mutants (Table 1). Notably, none of the four proteins tested displayed any hemolytic activity below 25 μM , suggesting that the mutations increased specifically the antimicrobial activity of the protein.

Lipopolysaccharide binding affinity and cell agglutinating activity.

Lipopolysaccharide binding affinity was monitored using cadaverine [BODIPY-TR cadaverine (BC)] fluorescent probe, which measures the competitive displacement of BC by the proteins tested. Lipopolysaccharide binding affinity of ECP, EDN and the corresponding mutants were tested by comparing their ED₅₀ values, defined as the concentration for which half BC displacement occurs (Table 3). EDN LPS-binding was reduced 10-fold respect to ECP. However, EDN mutants Q34R/R35W and T13I/Q34R/R35W showed an enhanced LPS-binding affinity between 4 and 5 times higher than their parental protein EDN. It is interesting to note that after protein addition at 5 μM concentration, BC was completely displaced by ECP while EDN reduced the occupancy by only 20% at the same concentration. More significantly, both EDN mutants decreased the occupancy by about 70%, approaching ECP effect (Table 3). EDN mutants binding to LPS was also confirmed using LPS micelles by recording the Trp fluorescence emission (Table 4), suggesting that only ECP and EDN mutants were able to interact with the Gram-negative outer membrane molecule. Besides, the registered wavelength shifts for ECP and the two mutants pointed to the direct contribution of W35 residue in the LPS interaction.

Previous results in our group described that LPS binding is required to agglutinate bacteria (46). In order to quantify the agglutinating activity, we determined the minimal concentration of protein that was able to agglutinate bacterial cell, defined as the minimal agglutination concentration (MAC). ECP, EDN and their derived mutants were evaluated after incubation with all strains tested for antimicrobial activity (Table 3). Neither EDN nor EDN-Q34R/R35W were able to agglutinate bacteria under the concentrations tested. However, EDN mutant carrying the I13A mutation was the only mutant able to trigger bacteria agglutination in Gram-negative cells. These results suggest that agglutination can only be triggered when an exposed hydrophobic patch is present.

To further investigate the agglutinating activity of the EDN mutants, we analyzed bacteria cultures by scanning electron microscopy to evaluate cell surface morphology and aggregate size and density (Figure 2). As expected, after incubation of *E. coli* with EDN, cells retain their baton-shaped morphology and do not display significant damage. In its turn, both EDN mutants promote severe envelope damage but only the mutant that carries T13I mutation shows bacteria agglutination, registered as dense aggregates with an average size of 10 μm length.

Interaction with model membranes.

To further characterize the antimicrobial mechanism of action of the designed mutants, we have tested their ability to interact with lipid vesicles and disrupt their structure.

To monitor protein-lipid interaction, we monitored the intrinsic tryptophan fluorescence signal, and the λ_{\max} shift displacement induced by changes on the residue microenvironment. We recorded the protein tryptophan fluorescence spectrum before and after incubation with charged (DOPG), neutral (DOPC) and a mixture of charged and neutral (DOPC/DOPG) liposomes and also in the presence of SDS micelles (Table 4). When the spectrum was recorded in the presence of liposomes containing negatively charged phospholipids or SDS micelles a significant blue shift was observed for both ECP and EDN mutants, but no appreciable shift was detected for EDN. Previous characterization of both ECP Trp structural properties revealed that while W10 is mostly embedded inside the protein core, W35 is hyperexposed to the solvent and can partially insert into lipid bilayers (Torrent et al., 2007). On its side, EDN shares with ECP the buried W10 but lacks W35, showing an additional Trp at the N-terminus, W7, which is mainly exposed to the solvent. Calculated surface accessible areas using AREAIMOL (CCP4i) were: W7 (132 Å²) W10 (9 Å²) for EDN and W10 (30 Å²) and W35 (252 Å²) for ECP. Therefore, the experimental data indicate that EDN Trp residues are not involved in membrane binding, while insertion of a Trp at position 35 is enhancing the protein lipid interaction (47).

Finally, to characterize the lipid bilayer destabilization properties of EDN and its mutants we assayed the disruption of ANTS/DPX containing LUVs, where an increase in fluorescence can be recorded as the vesicle leakage proceeds (Table 5). On the one hand, EDN did not promote leakage in the presence of either charged or neutral lipid vesicles at the concentrations tested. However, EDN mutants were able to induce high leakage activity on DOPG containing vesicles, with IC₅₀ values similar to ECP. It is also worth noticing that no leakage was recorded for DOPC micelles either for ECP or EDN derived mutants under 10 μM, showing again that electrostatic interactions drive the protein-lipid interaction process.

Discussion

Eosinophil ribonucleases, eosinophil-derived neurotoxin (EDN) and eosinophil cationic protein (ECP) are two secretory proteins from secondary granules of eosinophils. Date back to 50 million years ago, after the divergence of Old World from New World monkeys, a gene duplication event originated ECP and EDN precursors, that have been accumulating non-silent mutations until now (8, 11). Non-silent mutations rate of EDN/ECP accumulated faster than all the other known functional coding sequences among primates, probably due to a positive selection pressure (12, 48). Many mutations, specially those increasing the cationic nature of ECP, have been linked to its increased antimicrobial action but we cannot ascertain which substitutions on the ancestral precursor were key in ECP to develop antimicrobial activity.

By peptide synthesis approaches, we have proven that the entire protein is not required to display high antimicrobial activity (40, 41). In this context, we found that a protein N-terminal fragment conserves both the antimicrobial and agglutinating properties of ECP. These findings allowed us to locate specific properties to particular regions of the protein (13). Concretely, we identified a key antimicrobial region (residues 24-45) that is essential for membrane leakage, depolarization and LPS binding. Recent work on ECP binding domains also highlighted the involvement of the 34-38 stretch for both heterosaccharide and lipid binding (49, 50). A second region, close to the N-terminus of the protein (residues 8-16) was found essential for bacteria agglutination (44).

When these regions are examined for sequence conservation (Figure 3), we observe that the antimicrobial region in both proteins is fairly well conserved excluding a highly surface exposed group of amino acids (34-36). Therefore, this region may have been selected by evolution to explore a potential antimicrobial domain in ribonucleases. If we compare the chemical properties of the residues in the aforementioned region (Figure 3), we can see a distinct pattern for EDN and ECP. Whereas EDN has a clear charge and hydrophobic segregation, ECP has scrambled both residue types along this region. This observation is in agreement with the interfacial activity model (51), where a limited rather than an accurate amphipathicity in proteins and peptides would confer them antimicrobial capacity. When we mutate residues Q34 to R and R35 to W, we generate a similar charge and hydrophobic distribution in EDN as observed in ECP, giving to this mutant an activity similar to ECP (Table 1).

If this is the case, we can then compare different antimicrobial ribonucleases and check for analogous distributions (13). In the RNase A superfamily, we can see then that antimicrobial RNases (1,3,4,6,7) show an imperfect distribution of hydrophobic and charged residues (Supplementary file 1). However, non-antimicrobial RNases (2,5,8) do not show this pattern and/or accumulate negatively charged residues that mask positive charges. This is also the case of non-mammalian antimicrobial ribonucleases that belong to the RNase A superfamily, like onconase).

The fact that only one or two mutations are needed to change this pattern shows that ribonucleases have a suitable scaffold to become antimicrobial proteins suggesting that this may not be a collateral product of evolution but a true original function of ribonucleases. Indeed a close inspection of the conserved sequence pattern in eosinophil RNases (Supplementary file 2) highlight the unambiguously divergence at the selected mutated residues.

Similar conclusions apply when we analyze the agglutinating properties of the EDN/ECP lineage. A closer look to the chemical properties of these regions evidences that ECP has a more hydrophobic region than EDN (Figure 3), which may explain why only ECP has agglutinating activity. In fact, in our results only one single point mutation T13 to I was enough to develop agglutinating properties in EDN (Table 3). We propose that this is due to the generation of a potent exposed hydrophobic patch near the N-terminus

of the protein. The conservation analysis of these regions shows that, as with the antimicrobial segment, the amino acid residues are overall well conserved (Figure 3; Supplementary file 2). Nonetheless, the T13 by I substitution, which increases considerably the hydrophobic character of the region, is enough to provide an agglutinating activity to EDN, though it cannot fully reproduce ECP action (Table 3). This could be explained because EDN has an glutamic residue in position 12 that may hinder the protein-protein interaction process required for bacteria agglutination.

Indeed, comparing this region among antimicrobial ribonucleases of the RNase superfamily members, we identify a positive correlation between agglutinating activity and hydrophobicity of the aforementioned patch (Supplementary file 3). Henceforth, we observe again a structural pattern in ribonucleases to display antimicrobial related properties, reinforcing the idea that ribonucleases are a suitable molecular scaffold to develop antimicrobial proteins.

Ribonucleases are not an exception among antimicrobial proteins. Other proteins with activities unrelated to antimicrobials were also reported in the bibliography and a similar behavior could be observed, where targeted point mutations triggered or abolished the antimicrobial activity (52). However, this report evidences that evolution does not need to shape an entire protein or even a full domain for developing antimicrobials but single substitutions in suitable exposed regions, or even selected post-translational modifications, can modulate the antimicrobial properties (53). It should then not be surprising that a growing number of proteins not even closely related to host defense mechanisms could display antimicrobial activity, as it has been found for some apolipoproteins (54) or for the Alzheimer beta peptide (55).

It is therefore of general interest to pursue the investigation on the RNase A family lineage, that can assist us to unravel the protein structural and sequence requirements to become antimicrobial.

Acknowledgements

Transmission and scanning electron microscopy were performed at the Servei de Microscopia of the Universitat Autònoma de Barcelona (UAB). Spectrofluorescence assays were performed at the Laboratori d'Anàlisi i Fotodocumentació, UAB. We thank Vivian A. Salazar for her contribution in the preparation of the graphical material. EDN plasmid for recombinant protein expression was kindly provided by Richard J. Youle (NINDS, NIH, Bethesda, MD). The work was supported by the *Ministerio de Educación y Cultura* (grant number BFU2009-09371) and *Ministerio de Economía y Competitividad* (BFU2012-38965), co-financed by *FEDER* funds and by the *Generalitat de Catalunya* (2009 SGR 795). DP

is a recipient of a *FPU* predoctoral fellowship (*Ministerio de Educación y Cultura*) and *MT* is a recipient of a *Beatriu de Pinós* fellowship (*Generalitat de Catalunya*).

References

1. Beintema JJ, Kleineidam RG. The ribonuclease A superfamily: general discussion. *Cell Mol Life Sci.* 1998 Aug;54(8):825-32.
2. Cuchillo CM, Nogues MV, Raines RT. Bovine pancreatic ribonuclease: fifty years of the first enzymatic reaction mechanism. *Biochemistry.* Sep 20;50(37):7835-41.
3. Sorrentino S. The eight human "canonical" ribonucleases: molecular diversity, catalytic properties, and special biological actions of the enzyme proteins. *FEBS Lett.* Jun 3;584(11):2194-200.
4. Boix E, Salazar VA, Torrent M, Pulido D, Nogues MV, Moussaoui M. Structural determinants of the eosinophil cationic protein antimicrobial activity. *Biol Chem.* Aug;393(8):801-15.
5. Cho S, Zhang J. Zebrafish ribonucleases are bactericidal: implications for the origin of the vertebrate RNase A superfamily. *Molecular biology and evolution.* [Research Support, N.I.H., Extramural]. 2007 May;24(5):1259-68.
6. Pizzo E, D'Alessio G. The success of the RNase scaffold in the advance of biosciences and in evolution. *Gene.* 2007 Dec 30;406(1-2):8-12.
7. Rosenberg HF. RNase A ribonucleases and host defense: an evolving story. *J Leukoc Biol.* 2008 May;83(5):1079-87.
8. Rosenberg HF, Dyer KD, Tiffany HL, Gonzalez M. Rapid evolution of a unique family of primate ribonuclease genes. *Nat Genet.* 1995 Jun;10(2):219-23.
9. Zhang J, Rosenberg HF, Nei M. Positive Darwinian selection after gene duplication in primate ribonuclease genes. *Proc Natl Acad Sci U S A.* 1998 Mar 31;95(7):3708-13.
10. Hamann KJ, Ten RM, Loegering DA, Jenkins RB, Heise MT, Schad CR, et al. Structure and chromosome localization of the human eosinophil-derived neurotoxin and eosinophil cationic protein genes: evidence for intronless coding sequences in the ribonuclease gene superfamily. *Genomics.* 1990 Aug;7(4):535-46.
11. Zhang J, Rosenberg HF. Complementary advantageous substitutions in the evolution of an antiviral RNase of higher primates. *Proc Natl Acad Sci U S A.* 2002 Apr 16;99(8):5486-91.
12. Dyer KD, Rosenberg HF. The RNase a superfamily: generation of diversity and innate host defense. *Molecular diversity.* [Research Support, N.I.H., Intramural Review]. 2006 Nov;10(4):585-97.
13. Boix E, Salazar VA, Torrent M, Pulido D, Nogues MV, Moussaoui M. Structural determinants of the eosinophil cationic protein antimicrobial activity. *Biological chemistry.* 2012 Aug 1;393(8):801-15.
14. Durack DT, Ackerman SJ, Loegering DA, Gleich GJ. Purification of human eosinophil-derived neurotoxin. *Proc Natl Acad Sci U S A.* 1981 Aug;78(8):5165-9.
15. Garofalo R, Kimpen JL, Welliver RC, Ogra PL. Eosinophil degranulation in the respiratory tract during naturally acquired respiratory syncytial virus infection. *J Pediatr.* 1992 Jan;120(1):28-32.

16. Harrison AM, Bonville CA, Rosenberg HF, Domachowske JB. Respiratory syncytial virus-induced chemokine expression in the lower airways: eosinophil recruitment and degranulation. *Am J Respir Crit Care Med.* 1999 Jun;159(6):1918-24.
17. Domachowske JB, Dyer KD, Bonville CA, Rosenberg HF. Recombinant human eosinophil-derived neurotoxin/RNase 2 functions as an effective antiviral agent against respiratory syncytial virus. *J Infect Dis.* 1998 Jun;177(6):1458-64.
18. Yang D, Rosenberg HF, Chen Q, Dyer KD, Kurosaka K, Oppenheim JJ. Eosinophil-derived neurotoxin (EDN), an antimicrobial protein with chemotactic activities for dendritic cells. *Blood.* 2003 Nov 1;102(9):3396-403.
19. Rosenberg HF. Eosinophil-derived neurotoxin / RNase 2: connecting the past, the present and the future. *Curr Pharm Biotechnol.* 2008 Jun;9(3):135-40.
20. Yang D, Chen Q, Rosenberg HF, Rybak SM, Newton DL, Wang ZY, et al. Human ribonuclease A superfamily members, eosinophil-derived neurotoxin and pancreatic ribonuclease, induce dendritic cell maturation and activation. *J Immunol.* 2004 Nov 15;173(10):6134-42.
21. Yang D, Chen Q, Su SB, Zhang P, Kurosaka K, Caspi RR, et al. Eosinophil-derived neurotoxin acts as an alarmin to activate the TLR2-MyD88 signal pathway in dendritic cells and enhances Th2 immune responses. *J Exp Med.* 2008 Jan 21;205(1):79-90.
22. Oppenheim JJ, Tewary P, de la Rosa G, Yang D. Alarmins initiate host defense. *Adv Exp Med Biol.* 2007;601:185-94.
23. Venge P, Bystrom J, Carlson M, Hakansson L, Karawaczyk M, Peterson C, et al. Eosinophil cationic protein (ECP): molecular and biological properties and the use of ECP as a marker of eosinophil activation in disease. *Clin Exp Allergy.* 1999 Sep;29(9):1172-86.
24. Bystrom J, Amin K, Bishop-Bailey D. Analysing the eosinophil cationic protein--a clue to the function of the eosinophil granulocyte. *Respir Res.*12:10.
25. Lehrer RI, Szklarek D, Barton A, Ganz T, Hamann KJ, Gleich GJ. Antibacterial properties of eosinophil major basic protein and eosinophil cationic protein. *J Immunol.* 1989 Jun 15;142(12):4428-34.
26. Carreras E, Boix E, Rosenberg HF, Cuchillo CM, Nogues MV. Both aromatic and cationic residues contribute to the membrane-lytic and bactericidal activity of eosinophil cationic protein. *Biochemistry.* 2003 Jun 10;42(22):6636-44.
27. McLaren DJ, Peterson CG, Venge P. *Schistosoma mansoni*: further studies of the interaction between schistosomula and granulocyte-derived cationic proteins in vitro. *Parasitology.* 1984 Jun;88 (Pt 3):491-503.
28. Hamann KJ, Gleich GJ, Checkel JL, Loegering DA, McCall JW, Barker RL. In vitro killing of microfilariae of *Brugia pahangi* and *Brugia malayi* by eosinophil granule proteins. *J Immunol.* 1990 Apr 15;144(8):3166-73.
29. Singh A, Batra JK. Role of unique basic residues in cytotoxic, antibacterial and antiparasitic activities of human eosinophil cationic protein. *Biol Chem.* Apr;392(4):337-46.

30. Elshafie AI, Hlin E, Hakansson LD, Elghazali G, Safi SH, Ronnelid J, et al. Activity and turnover of eosinophil and neutrophil granulocytes are altered in visceral leishmaniasis. *Int J Parasitol.* Mar;41(3-4):463-9.
31. Kierszenbaum F, Villalta F, Tai PC. Role of inflammatory cells in Chagas' disease. III. Kinetics of human eosinophil activation upon interaction with parasites (*Trypanosoma cruzi*). *J Immunol.* 1986 Jan;136(2):662-6.
32. Waters LS, Taverne J, Tai PC, Spry CJ, Targett GA, Playfair JH. Killing of *Plasmodium falciparum* by eosinophil secretory products. *Infect Immun.* 1987 Apr;55(4):877-81.
33. Rosenberg HF. Recombinant human eosinophil cationic protein. Ribonuclease activity is not essential for cytotoxicity. *The Journal of biological chemistry.* 1995 Apr 7;270(14):7876-81.
34. Boix E, Nikolovski Z, Moiseyev GP, Rosenberg HF, Cuchillo CM, Nogues MV. Kinetic and product distribution analysis of human eosinophil cationic protein indicates a subsite arrangement that favors exonuclease-type activity. *J Biol Chem.* 1999 May 28;274(22):15605-14.
35. Boix E, Wu Y, Vasandani VM, Saxena SK, Ardelt W, Ladner J, et al. Role of the N terminus in RNase A homologues: differences in catalytic activity, ribonuclease inhibitor interaction and cytotoxicity. *J Mol Biol.* 1996 Apr 19;257(5):992-1007.
36. Torrent M, Badia M, Moussaoui M, Sanchez D, Nogues MV, Boix E. Comparison of human RNase 3 and RNase 7 bactericidal action at the Gram-negative and Gram-positive bacterial cell wall. *FEBS J.* Apr;277(7):1713-25.
37. Torrent M, Navarro S, Moussaoui M, Nogues MV, Boix E. Eosinophil cationic protein high-affinity binding to bacteria-wall lipopolysaccharides and peptidoglycans. *Biochemistry.* [Research Support, Non-U.S. Gov't]. 2008 Mar 18;47(11):3544-55.
38. Wood SJ, Miller KA, David SA. Anti-endotoxin agents. 1. Development of a fluorescent probe displacement method optimized for the rapid identification of lipopolysaccharide-binding agents. *Comb Chem High Throughput Screen.* 2004 May;7(3):239-49.
39. Torrent M, Cuyas E, Carreras E, Navarro S, Lopez O, de la Maza A, et al. Topography studies on the membrane interaction mechanism of the eosinophil cationic protein. *Biochemistry.* [Research Support, Non-U.S. Gov't]. 2007 Jan 23;46(3):720-33.
40. Torrent M, de la Torre BG, Nogues VM, Andreu D, Boix E. Bactericidal and membrane disruption activities of the eosinophil cationic protein are largely retained in an N-terminal fragment. *Biochem J.* 2009 Aug 1;421(3):425-34.
41. Torrent M, Pulido D, de la Torre BG, Garcia-Mayoral MF, Nogues MV, Bruix M, et al. Refining the eosinophil cationic protein antibacterial pharmacophore by rational structure minimization. *Journal of medicinal chemistry.* [Research Support, Non-U.S. Gov't]. 2011 Jul 28;54(14):5237-44.
42. Carreras E, Boix E, Navarro S, Rosenberg HF, Cuchillo CM, Nogues MV. Surface-exposed amino acids of eosinophil cationic protein play a critical role in the inhibition of mammalian cell proliferation. *Mol Cell Biochem.* 2005 Apr;272(1-2):1-7.

43. Torrent M, Odorizzi F, Nogues MV, Boix E. Eosinophil cationic protein aggregation: identification of an N-terminus amyloid prone region. *Biomacromolecules*. [Research Support, Non-U.S. Gov't]. 2010 Aug 9;11(8):1983-90.
44. Torrent M, Pulido D, Nogues MV, Boix E. Exploring new biological functions of amyloids: bacteria cell agglutination mediated by host protein aggregation. *PLoS pathogens*. 2012 Nov;8(11):e1003005.
45. Torrent M, Pulido D, de la Torre BG, Garcia-Mayoral MF, Nogues MV, Bruix M, et al. Refining the eosinophil cationic protein antibacterial pharmacophore by rational structure minimization. *J Med Chem*. Jul 28;54(14):5237-44.
46. Pulido D, Moussaoui M, Andreu D, Nogues MV, Torrent M, Boix E. Antimicrobial action and cell agglutination by the eosinophil cationic protein are modulated by the cell wall lipopolysaccharide structure. *Antimicrob Agents Chemother*. May;56(5):2378-85.
47. The CCP4 suite: programs for protein crystallography. *Acta Crystallogr D Biol Crystallogr*. 1994 Sep 1;50(Pt 5):760-3.
48. Rosenberg HF. The eosinophil ribonucleases. *Cell Mol Life Sci*. 1998 Aug;54(8):795-803.
49. Fan TC, Fang SL, Hwang CS, Hsu CY, Lu XA, Hung SC, et al. Characterization of molecular interactions between eosinophil cationic protein and heparin. *J Biol Chem*. 2008 Sep 12;283(37):25468-74.
50. Lien PC, Kuo PH, Chen CJ, Chang HH, Fang SL, Wu WS, et al. In silico prediction and in vitro characterization of multifunctional human RNase3. *Biomed Res Int*. 2013:170398.
51. Wimley WC. Describing the mechanism of antimicrobial peptide action with the interfacial activity model. *ACS chemical biology*. [Research Support, N.I.H., Extramural Research Support, Non-U.S. Gov't Review]. 2010 Oct 15;5(10):905-17.
52. De Samblanx GW, Goderis IJ, Thevissen K, Raemaekers R, Fant F, Borremans F, et al. Mutational analysis of a plant defensin from radish (*Raphanus sativus* L.) reveals two adjacent sites important for antifungal activity. *The Journal of biological chemistry*. [Comparative Study]. 1997 Jan 10;272(2):1171-9.
53. Mukherjee S, Partch CL, Lehotzky RE, Whitham CV, Chu H, Bevins CL, et al. Regulation of C-type lectin antimicrobial activity by a flexible N-terminal prosegment. *The Journal of biological chemistry*. [Research Support, N.I.H., Extramural Research Support, Non-U.S. Gov't]. 2009 Feb 20;284(8):4881-8.
54. Motizuki M, Itoh T, Yamada M, Shimamura S, Tsurugi K. Purification, primary structure, and antimicrobial activities of bovine apolipoprotein A-II. *Journal of biochemistry*. 1998 Apr;123(4):675-9.
55. Soscia SJ, Kirby JE, Washicosky KJ, Tucker SM, Ingelsson M, Hyman B, et al. The Alzheimer's disease-associated amyloid beta-protein is an antimicrobial peptide. *PloS one*. [Research Support, Non-U.S. Gov't]. 2010;5(3):e9505.

Table 1. Bactericidal (MIC₁₀₀) and Hemolytic Activity (HC₅₀) of ECP, EDN and EDN mutants.

	MIC ₁₀₀ (μM)						HC ₅₀ (μM) ^a
	<i>E. coli</i>	<i>Pseudomonas sp.</i>	<i>A. baumannii</i>	<i>S. aureus</i>	<i>M. luteus</i>	<i>E. faecium</i>	
ECP	0.5	0.4	0.3	0.4	0.8	0.6	>25
EDN	>10	10	9	>10	>10	9	>25
EDN-Q34R/R35W	1	0.8	0.5	1.5	1.5	1.5	>25
EDN-T131/Q34R/R35W	0.6	0.5	0.3	0.8	1.5	0.8	>25

^a Hemolytic activity was assayed on Sheep Red Blood Cells.

Table 2. Depolarization activity on *E. coli* and *S. aureus* cells determined by DiSC₃(5) assay for ECP, EDN and EDN mutants.

	Depolarization (μM)			
	<i>E. coli</i>		<i>S. aureus</i>	
	ED ₅₀	Desp _{max} ^a	ED ₅₀	Desp _{max}
ECP	0.040 ± 0.001	1459 ± 308	0.050 ± 0.009	3628 ± 289
EDN	>10	n.d.	>10	n.d.
EDN-Q34R/R35W	0.030 ± 0.004	1218 ± 121	0.030 ± 0.002	2285 ± 289
EDN-T13I/Q34R/R35W	0.030 ± 0.004	1381 ± 155	0.040 ± 0.005	2262 ± 173

n.d. Not detected at the assayed concentration range (0.1-10 μM). ^a Maximum fluorescence value reached at the final incubation time.

Table 3. Minimal Agglutination Activity (MAC) and LPS Binding (ED₅₀) of ECP, EDN and mutants.

	MAC (μM)						LPS binding	
	<i>E.coli</i>	<i>Pseudomonas sp.</i>	<i>A. baumannii</i>	<i>S. aureus</i>	<i>M. luteus</i>	<i>E. faecium</i>	ED ₅₀ (μM)	% _{max} ^a
ECP	0.60 ± 0.05	0.60 ± 0.05	1.50 ± 0.05	n.d.	n.d.	n.d.	0.86 ± 0.13	100
EDN	n.d.	n.d.	n.d.	n.d.	n.d.	n.d.	7.49 ± 1.06	48
EDN-Q34R/R35W	n.d.	n.d.	n.d.	n.d.	n.d.	n.d.	1.76 ± 0.33	74
EDN-T13I/Q34R/R35W	4.50 ± 0.05	4.50 ± 0.05	4.50 ± 0.05	n.d.	n.d.	n.d.	1.82 ± 0.41	65

^a 100% refers to a total displacement whereas 0% is for no displacement of the dye, indicating no binding. N.d., not detected

Table 4. Tryptophan fluorescence in the presence of lipid vesicles, LPS and SDS micelles for ECP, EDN and mutants.

	Trp fluorescence ^a							
	ECP		EDN		EDN-Q34R/R35W		EDN-T13I/Q34R/R35W	
	λ_m (nm)	λ_s (nm)	λ_m (nm)	λ_s (nm)	λ_m (nm)	λ_s (nm)	λ_m (nm)	λ_s (nm)
Buffer	349	-	344	-	346	-	344	-
DOPG	341	8	341	3	341	5	339	5
DOPC	349	0	344	0	346	0	344	0
3:2 DOPC/DOPG	342	7	341	3	341	5	340	4
LPS	344	5	343	1	342	4	340	4
SDS	340	9	343	1	339	7	336	8

^a λ_m represents the wavelength of the maximum and λ_s the shift in the wavelength compared with the buffer.

Table 5. Liposome leakage of ANTS/DPX LUVs by ECP, EDN and EDN mutants.

	Liposome leakage (ED₅₀ in μM)		
	DOPG	3:2 DOPC/DOPG	DOPC
ECP	0.046±0.009	0.14±0.08	>10
EDN	> 10	>10	>10
EDN-Q34R/R35W	0.025±0.006	0.080±0.004	>10
EDN-T13I/Q34R/R35W	0.029±0.008	0.030±0.007	>10

Figure Legends

Figure 1.

Analysis of the chemical properties of ECP/EDN in antimicrobial-related regions. A molecular surface representation shows the amino acid chemical properties of ECP (left) and EDN (right). The highly exposed RWR in the antimicrobial region (residues 34-45) is visible for ECP in this representation. In EDN a QRR region is observed instead, highlighting the absence of a hydrophobic residue in this region. Besides, a clear hydrophobic patch in the aggregation region (residues 8-16) is present in ECP while absent in EDN. Residues were colored according to their chemical properties, cationic residues in blue, non-charged polar residues in green and hydrophobic residues in yellow .

Figure 2.

SEM micrographs for E. coli cultures incubated in the absence and presence of ECP, EDN and EDN mutants Q34R/R35W and T13I/Q34R/R35W). Two magnifications (top and bottom panels) are shown for each condition to visualize the extent of bacteria aggregates and cell morphology.

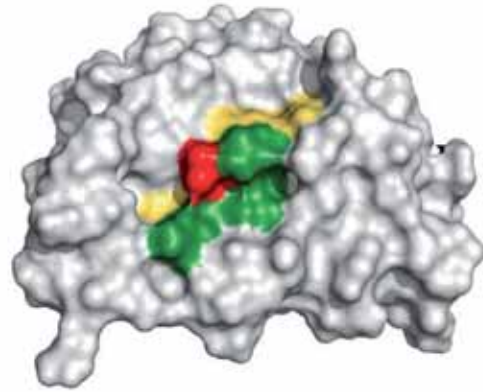
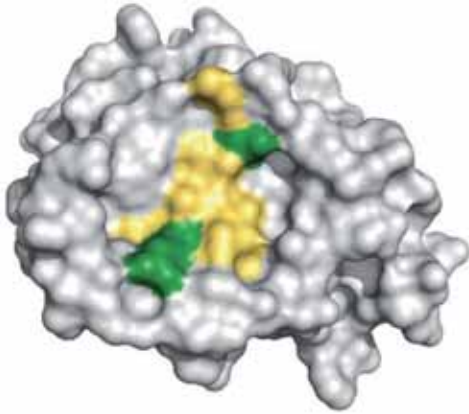
Figure 3.

Conservational analysis of EDN/ECP. A molecular representation of ECP (left) and EDN (right) shows the amino acid conservation score during evolution (top) and the chemical properties (bottom) of the antimicrobial region. The picture shows a backbone of conserved residues both for ECP and EDN. Residues displaying high sequence variability that correspond to the amino acids analyzed in the present study are drawn in CPK space filling representation. Interestingly, the latter residues can change the vectorial chemical properties of the protein. By breaking down the highly segregated properties of EDN into a more scrambled structure, we could efficiently generate antimicrobial activity in EDN. Conservation scores were calculated using *Consurf* and colored according to the conservation score: very high (purple), high (pink), low (dark blue) or very low (light blue) degree of conservation. For chemical representation, cysteines (yellow), cationic (blue), non-charged polar (green) and hydrophobic (red) amino acids were colored.

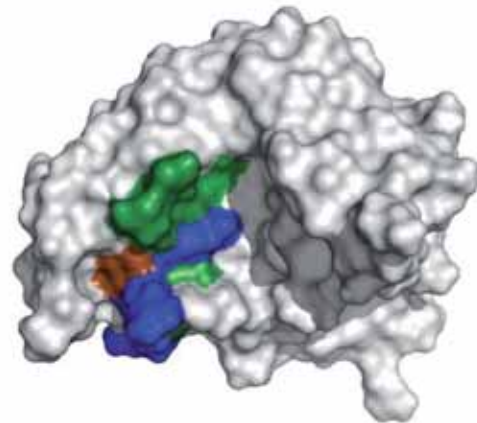
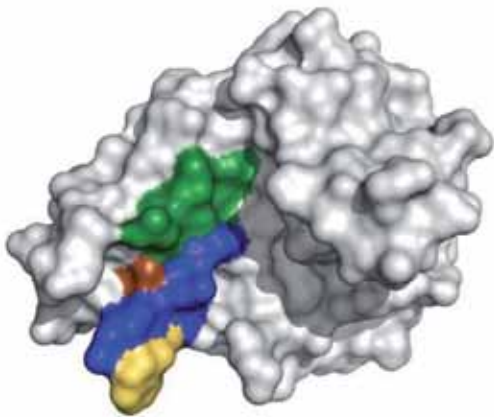
Ancestor
(Gene duplication)

ECP

EDN



Aggregation region



Antimicrobial region

Figure 1

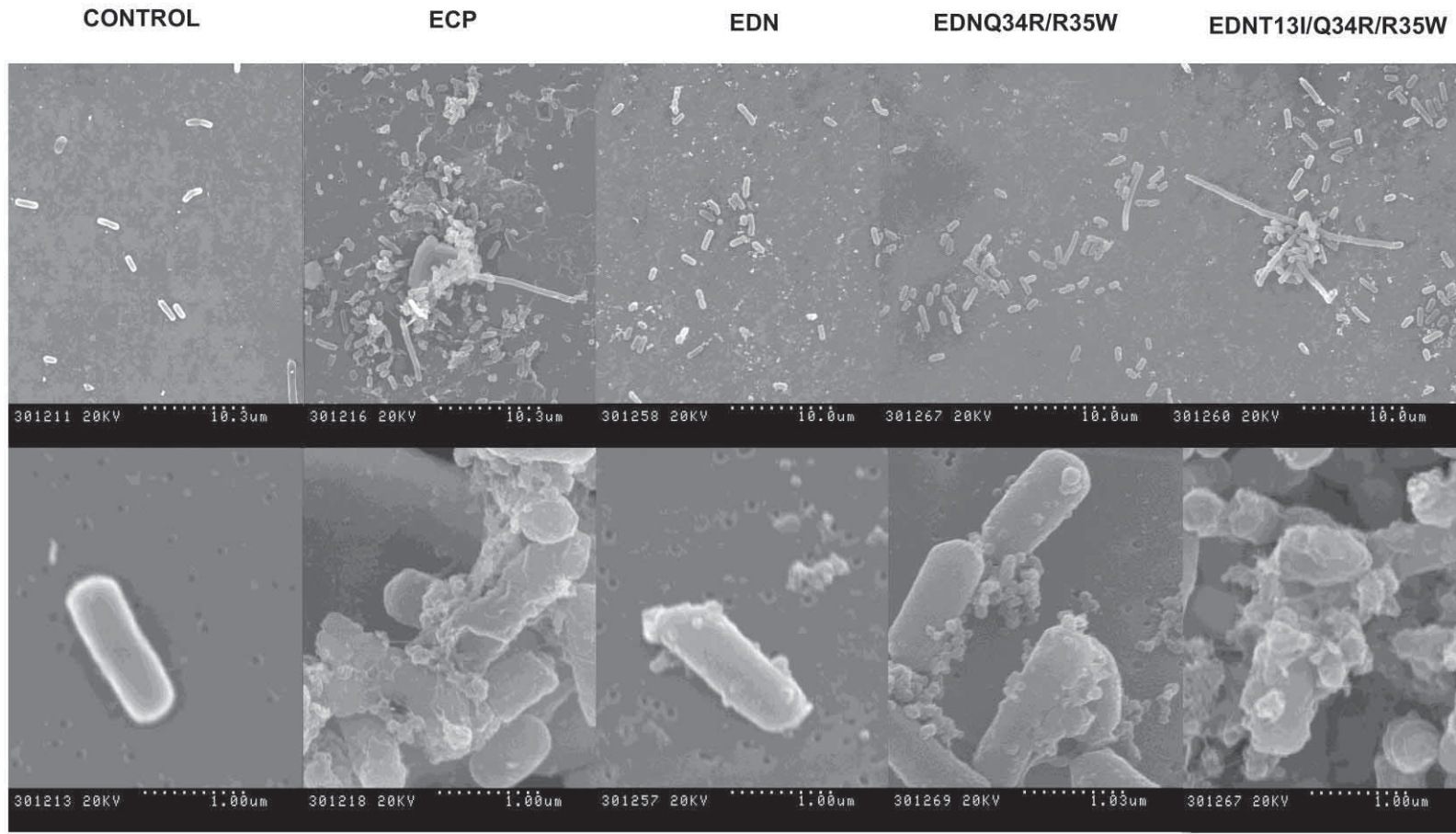


Figure 2

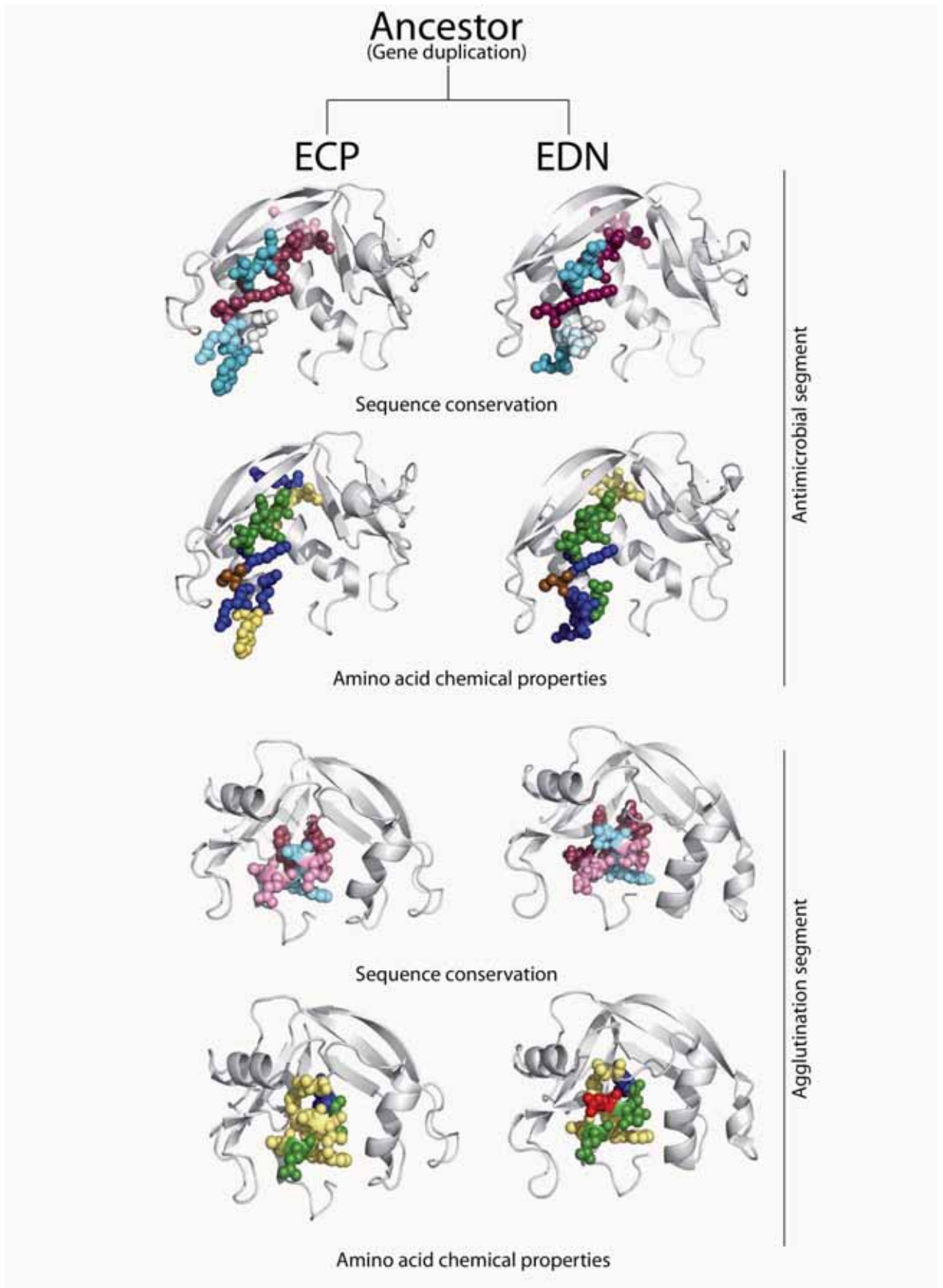


Figure 3

CHAPTER VI

Two human host defense ribonucleases against mycobacteria: the eosinophil cationic protein (ECP/RNase 3) and RNase 7.

David Pulido¹, Marc Torrent^{1,2}, David Andreu³, M. Victoria Nogués¹ and Ester Boix^{1#}

¹Department of Biochemistry and Molecular Biology, Biosciences Faculty, Universitat Autònoma de Barcelona, Cerdanyola del Vallès, Spain

² Present address: Regulatory Genomics and Systems Biology, MRC Laboratory of Molecular Biology, Cambridge, United Kingdom

³ Department of Experimental and Health Sciences, Universitat Pompeu Fabra, Barcelona Biomedical Research Park, Barcelona, Spain

#Corresponding author:

Ester Boix

Dpt. Biochemistry and Molecular Biology

Fac. Biosciences

Universitat Autònoma de Barcelona

08193 Cerdanyola del Vallès, Spain

Tf.: 34-935814147

Fax: 34-935811264

E.mail: Ester. Boix@uab.cat

RUNNING TITLE: Antimycobacterial RNases

Abstract

There is an urgent need to develop new agents against mycobacterial infections, such as tuberculosis and other respiratory tract or skin affections. In this work, we have tested two human antimicrobial RNases against mycobacteria. RNase 3, also called the eosinophil cationic protein, and RNase 7 are two small cationic proteins secreted by innate cells during host defense. Both proteins are induced upon infection displaying a wide range of antipathogen activities. In particular, they are released by leukocytes and epithelial cells, contributing to tissue protection. Here, the two RNases have been proven effective against *Mycobacterium vaccae* at a low micromolar level. High bactericidal activity correlated with their bacteria membrane depolarization and permeabilization activities. Further analysis on both protein-derived peptides identified for RNase 3 an N-terminus fragment even more active than the parental protein. Also, a potent bacteria agglutinating activity was unique to RNase 3 and its derived peptide. The particular biophysical properties of the RNase 3 active peptide are envisaged as a suitable reference for the development of novel antimycobacterial drugs. The results support the contribution of secreted RNases to the host immune response against mycobacteria.

Introduction

Tuberculosis is still a global threat and one of the main infectious diseases, causing about 2 million deaths per year (1). Nowadays the risk has further been increased by the emergence of multidrug resistant strains in hospitals, and the growing population affected by the acquired immune deficiency syndrome (1-3). Tuberculosis is indeed an ancient plague and there is even fossil evidence of hominid infection. Although only 10% of infected individuals do develop the disease, about one third of the world's population is estimated to be latently infected (4, 5).

Most of the species of *Mycobacterium* genera are environmental and non-pathogenic, whilst others, as *M. tuberculosis*, are the cause of severe pulmonary diseases (6, 7). Not to neglect are also skin affections as leprosy, or other cutaneous infections caused by *M. haemophilum*, *M. chelonae* or *M. kansasii* among others, that threaten immunocompromised patients (8). Pathogenic mycobacteria invade and dwell inside human host targets, such as macrophages, successfully replicating inside the cells (9, 10). The final outcome of the host-pathogen first encounter is dependent on the host immune response and a variety of antimicrobial proteins and peptides (AMPs) secreted by innate cells are contributing to fight the intruder. Expression of antimycobacterial peptides is induced during the host response by a variety of innate cells, from blood to epithelial cells (4, 11). In particular, eosinophil and neutrophil granules are engulfed by infected macrophages (12-15). Following, the secreted AMPs and potential proteolytic products could target the macrophage intracellular dwelling pathogens (9, 12). Human-derived AMPs showing high targeted cytotoxicity but low immunogenicity are therefore promising antimycobacterial therapeutic agents (16). However, research on innate immunity during mycobacterial infection is still scarce, and only few examples of characterized AMPs are available (11, 17). In particular, upon mycobacterial infection high levels of cathelicidin, defensin and hepcidin are reported in macrophages and

correlated to microbe growth inhibition (11, 18, 19). Upregulation in tuberculosis patients is observed for α -defensins in eosinophils and β -defensins secretion is triggered at airway epithelial cells (11, 15, 20). Both active cathelicidins and defensins can be released from precursors by *in vivo* proteolysis at the infection site (21-23).

Mycobacteria are also characterized by their unusual lipid-rich cell wall, composed of a variety of unique glycoconjugates and intercalating complex lipids, offering a highly impermeable barrier for common antibiotics. Noteworthy, the mycolic acids outer layer provides a wax-like architecture to the cell wall that can hinder the uptake of many antimycobacterial drugs (24). Specific features of the antimicrobial peptides and proteins (AMPs), as low molecular weight, high cationicity, amphipatic structure, selective affinity to prokaryotic negatively charged cell envelope, together with their immunomodulatory effects and diverse modes of action (25), make them an interesting source of novel antimycobacterial agents (11, 26).

In our laboratory, we are working on the mechanism of action of two human RNases that are secreted by key effector innate cells, which are known to contribute to the host response to mycobacterial infection (12, 15, 27, 28), and therefore envisaged to test their potential antimycobacterial activity. RNase 3 and RNase 7 (Figure 1) are two representative members of the vertebrate secreted RNase superfamily with a well characterized cytotoxic action against a variety of pathogens (29-33). RNase 3, also called the eosinophil cationic protein (ECP), is a small highly cationic protein secreted by eosinophil secondary granules with potent antibacterial and antiparasitic activities (34, 35). Secondly, the RNase 3 protein expression has also been reported in stimulated neutrophils (36). We previously studied the RNase 3 antimicrobial mechanism of action against a wide range of Gram positive and Gram negative strains (37, 38) and designed peptide-derived pharmacophores (39, 40). As eosinophils and neutrophils are potent host defense effector cells activated by mycobacterial

infection (31, 41, 42) and RNase 3 was found to contribute to mycobacterial growth inhibition (15) we committed ourselves to characterize the protein activity. When eosinophilia was first linked to tuberculosis (43), eosinophils were regarded as mere offenders, exacerbating pulmonary inflammation. Notwithstanding, later bibliography evidenced their protective role contributing to bacterial clearance at the infection focus (28, 44). Eosinophils together with neutrophils are recruited in lung granulomas (15, 45), releasing their granule content into macrophages, where they can target intracellular pathogens (4, 13). Leukocyte granule proteins are therefore suitable weapons to eradicate the macrophage resident bacteria.

Complementarily we have analysed RNase 7, as an antimicrobial protein secreted by a variety of epithelial tissues (32, 33, 46-49). In particular, RNase 7 is abundantly secreted by keratinocytes and mainly contributes to the skin barrier protection (49, 50). Indeed, keratinocyte secreted proteins are mostly involved in the skin defense against infective microorganisms, like *M. leprae* (51).

Finally, as a first approach to understand the underlying mechanism of action of both RNases, synthetic derived peptides have been characterized. Scarce experimental work has been applied so far to enhance the antimycobacterial properties of natural compounds and very few examples of *de novo* designed peptides are currently available, as cathelicidin or magainin analogs (19, 52). Here, we have analyzed an N-terminus RNase 3 derived peptide as a suitable template towards further structure-based drug design applied therapy to mycobacterial diseases.

Materials and Methods

Materials

E. coli BL21(DE3) cells and the pET11 expression vector were from Novagen, (Madison,WI). *LIVE/DEAD* bacterial viability kit was purchased from Molecular Probes (Eugene, OR). The *BacTiter-Glo* assay kit was from Promega (Madison, WI). *SYTOX Green* and DiSC3(5) (3,3-dipropylthiacarbocyanine) were purchased from *Invitrogen* (Carlsbad, CA). Microplates 96-well type were from Greiner, Wemmel, Belgium. Strain used, *Mycobacterium vaccae* (ATCC 15483; CECT-3019T) (53, 54), was purchased at the *Colección Española de Cultivo (CECT)*, Universidad de Valencia. Fmoc-protected amino acids and 2-(1H-benzotriazol-1-yl)-1,1,3,3-tetramethyluronium hexafluorophosphate (HBTU) were obtained from *Iris Biotech* (Marktredwitz, Germany). Fmoc-Rink-amide (MBHA) resin was from *Novabiochem* (Laüfelfingen, Switzerland). HPLC-grade acetonitrile (ACN) and peptide synthesis-grade N,N-dimethylformamide (DMF), N,N-diisopropylethylamine (DIEA), and trifluoroacetic acid (TFA) were from *Carlo Erba-SDS* (Peypin, France). The cecropin A –melittin (CA-M) hybrid peptide, CA(1-8)-M(1-18): (KWKLFKKIGIGAVLKVLTTGLPALIS-NH₂) was used as a control antimicrobial peptide.

Protein expression and purification

Recombinant RNase 3 was expressed from a human synthetic gene (55). The cDNA from RNase 7 was a gift from Prof. Helene Rosenberg (NIAID, NIH, Bethesda). Genes were cloned in pET11c. Protein expression in the *E. coli* BL21DE3 strain, folding of the protein from inclusion bodies, and purification were carried out as previously described (55).

Peptide synthesis and purification

Peptides were designed based on the 1-45 N-terminus sequences of RNase 3, peptide RN3(1-45), and RNase 7, peptide RN7(1-45) (Figure 1). Cys residues were substituted by Ser to avoid potential intra and intermolecular disulfide bridges. Ser residue was chosen as the best isosteric substitute for Cys. Peptides were synthesized as previously described (40). Briefly, solid phase peptide synthesis was done by Fmoc-based chemistry on Fmoc-Rink-amide (MBHA) resin (0.1 mmol) in a model 433 synthesizer running FastMoc protocols. Couplings used 8-fold molar excess each of Fmoc-amino acid and HBTU and 16-fold molar excess of DIEA. Side chains of trifunctional residues were protected with tert-butyl (Ser, Thr, Tyr), tert-butyloxycarbonyl (Lys, Trp), 2,2,4,6,7 pentamethyldihydrobenzofuran-5- sulfonyl (Arg), and trityl (Asn, Gln, His) groups. After chain assembly, full deprotection and cleavage were carried out with TFA-water-triisopropylsilane (95:2.5:2.5 v/v, 90 min, at room temperature). Peptides were isolated by precipitation with cold diethyl ether and separated by centrifugation, dissolved in 0.1M acetic acid, and lyophilized. Analytical reversed-phase HPLC was performed on a Luna C18 column. Linear gradients of solvent B (0.036% TFA in ACN) into A (0.045% TFA in H₂O) were used for elution at a flow rate of 1 mL/min and with UV detection at 220 nm. Preparative HPLC runs were performed on a Luna C18 column, using linear gradients of solvent (0.1% in ACN) into A (0.1% TFA in H₂O), as required, with a flow rate of 25 mL/min. MALDI-TOF mass spectra were recorded in the reflector or linear mode in a Voyager DE-STR workstation using R-hydroxycinnamic acid matrix. Fractions of adequate (>90%) HPLC homogeneity and with the expected mass were pooled, lyophilized, and used in subsequent experiments. Peptide secondary structure and biophysical properties were predicted using the *PSIPRED* server (56).

Minimal Inhibitory Concentration (MIC)

Antimicrobial activity was calculated as the minimal inhibitory concentration (MIC₁₀₀), defined as the lowest peptide concentration that completely inhibits microbial growth. MIC of each protein and peptide (RNase 3, RNase 7, RN3(1-45) and RN7(1-45)) was determined from two independent experiments performed in triplicate for each concentration. A dilution of *M. vaccae* stock culture was plated onto agar Petri dishes. A smooth colony was selected and bacteria were incubated at 37°C in *Corynebacterium* Broth (CB) medium and diluted to give approximately 5x10⁵ CFU/mL. Bacterial suspension was incubated with proteins or peptides serially diluted from 50 to 0.1 µM at 37°C for 4 h in PBS. Samples were plated onto Petri dishes and incubated at 37°C for 48 h and colonies were counted.

Alternatively, MIC₁₀₀ of each protein and peptide was determined using the microdilution broth method according to NCCLS guidelines (57). Briefly, bacteria were incubated at 37°C in CB and diluted to give approximately 5x10⁵ CFU/mL. MICs were performed in 96-well microplates. Bacterial suspension was incubated with proteins or peptides at various concentrations (0.1–50 µM) at 37°C in CB. Bacteria growth was recorded by optical density at λ= 550 nm after incubation at 37°C for 48 h.

Bacterial viability assays

Bacterial viability was assayed using the *BacTiter-Glo* microbial cell viability kit as described (38). Briefly, proteins or peptides were dissolved in PBS, serially diluted from 50 to 0.1 µM, and tested against *M. vaccae* (optical density at 600 nm [OD₆₀₀] ~ 0.2) for 4 h of incubation time. An aliquot of 50 µl of culture was mixed with 50 µl of *BacTiter-Glo* reagent in a microtiter plate according to the manufacturer's instructions and incubated at 25°C for 15 min. Luminescence was read on a Victor3 plate reader (Perkin-Elmer, Waltham, MA) with a 1-s integration time.

Fifty percent inhibitory concentrations (IC_{50}) were calculated by fitting the data to a dose-response curve.

Kinetics of bacterial survival were determined using the *LIVE/DEAD* bacterial viability kit in accordance with the manufacturer's instructions as described (58). *LIVE/DEAD* bacterial viability kit is composed by the nucleic acid dyes Syto9, which can cross intact cell membranes, and propidium iodide (PI), which can only bind DNA and displace Syto 9 when the cytoplasmic membrane is permeabilized. *M. vaccae* was grown at 37°C to an OD_{600} of 0.2, centrifuged at 5,000x *g* for 5 min, and stained in a 0.85% NaCl solution containing the probes. Fluorescence intensity was continuously measured after protein or peptide addition (10 μ M). To calculate bacterial viability, the signal in the range of 510 to 540 nm was integrated to obtain the Syto 9 signal (live bacteria) and that in the range of 620 to 650 nm was integrated to obtain the propidium iodide (PI) signal (dead bacteria). Percentage of live bacteria was calculated at final incubation time.

Bacteria Cytoplasmic Membrane Depolarization Assay

Membrane depolarization was followed using the sensitive membrane potential DiSC3(5) fluorescent probe as described (58). After interaction with intact cytoplasmic membrane, the fluorescent probe DiSC3(5) is quenched. Following incubation with the antimicrobial protein or peptide, the membrane potential is lost and the probe is released to the medium ensuing in an increase of fluorescence that can be quantified and monitored as a function of time. Bacteria cultures were grown at 37 °C to an OD_{600} of 0.2, centrifuged at 5000x *g* for 7 min, washed with 5 mM HEPES-KOH, 20 mM glucose, pH 7.2, and resuspended in 5 mM HEPES-KOH, 20 mM glucose, and 100 mM KCl, pH 7.2 to an OD_{600} of 0.05. DiSC3(5) was added to a final concentration of 0.4 μ M and changes in the fluorescence were continuously recorded after addition of protein (10 μ M) in a Victor3 plate reader (PerkinElmer, Waltham, MA). The time

required to achieve maximum membrane depolarization was estimated from nonlinear regression analysis.

Bacteria cytoplasmic membrane permeation

Bacteria cytoplasmic membrane permeation was followed by the *SYTOX Green* uptake assay.

SYTOX Green is a cationic cyanine dye (~900 Da) that is not membrane permeable. When a cell's plasma membrane integrity is compromised, influx of the dye and subsequent binding to DNA causes a large increase in fluorescence. For *SYTOX Green* assays, *M. vaccae* bacterial cells were grown to mid-exponential growth phase (OD₆₀₀ of 0.6) and then centrifuged, washed, and resuspended in PBS. Cell suspensions in PBS (OD₆₀₀ of 0.2) were incubated with 1 μM *SYTOX Green* for 15 min in the dark prior to the influx assay. At 2-4 min after initiating data collection, 10 μM of proteins or peptides was added to the cell suspension, and the increase in *SYTOX Green* fluorescence was measured (excitation wavelength at 485 nm and emission at 520 nm) for 40 min in a Cary Eclipse spectrofluorimeter. Bacteria cells lysis with 10% Triton X-100 gives the maximum fluorescence reference value.

Minimal Agglutination Activity (MAC)

Bacterial cells were grown at 37 °C to an OD₆₀₀ of 0.2, centrifuged at 5000x *g* for 2 min and resuspended either in PBS or CB media. An aliquot of 100 μl of the bacteria suspension was treated with increasing protein/peptide concentrations (from 0.01 to 50 μM) and incubated at 25°C for 1h. The aggregation behavior was observed by visual inspection and the agglutinating activity is expressed as the minimum agglutinating concentration of the sample tested, as previously described (38).

Transmission electron microscopy (TEM)

TEM samples were prepared as previously described (59). *M. vaccae* was grown to an OD₆₀₀ of 0.2 and incubated at 37°C with 10 µM proteins or peptides in PBS for 4h. After treatment, bacterial pellets were prefixed with 2.5% glutaraldehyde and 2% paraformaldehyde in 0.1M cacodylate buffer at pH 7.4 for 2 h at 4°C and postfixed in 1% osmium tetroxide buffered in 0.1M cacodylate at pH 7.4 for 2 h at 4°C. The samples were dehydrated in acetone (50, 70, 90, 95, and 100%). The cells were immersed in Epon resin, and ultrathin sections were examined in a Jeol JEM 2011 instrument (Jeol Ltd., Tokyo, Japan).

SEM (Scanning electron microscopy)

SEM samples were prepared as previously described (59). Bacterial culture of *M. vaccae* were grown at 37 °C to mid-exponential phase (OD₆₀₀ ~ 0.2) and incubated with proteins or peptides (10 µM) in PBS at 37°C. Sample aliquots (500 µl) were taken after up to 4 h of incubation and prepared for SEM analysis. The micrographs were viewed at a 15 kV accelerating voltage on a Hitachi S-570 scanning electron microscope, and a secondary electron image of the cells for topography contrast was collected at several magnifications.

Results and Discussion

A better understanding on the mechanism of action of AMPs effective against mycobacterial infection is a promising approach to develop alternative drugs, such as anti-tuberculosis agents. Current treatments against tuberculosis are expensive, mostly long and cumbersome, and even occasionally ineffective (1). Unfortunately, only few insights have been done to apply peptide based drugs in mycobacterial diseases therapies (19). In the present study we have considered two human antimicrobial RNases, secreted by innate cells, as

eosinophils, neutrophils and keratinocytes, which mostly contribute to fight mycobacterial infections.

Human host defense RNases against mycobacteria

Bactericidal activity of RNase 3 and RNase 7 has been extensively documented against a wide range of Gram-negative and Gram-positive bacteria (30, 33, 38, 60). Here, both the eosinophil secreted RNase 3 and the skin derived RNase 7 were envisaged as good candidates to contribute to the host defense against mycobacterial infections. In order to assess their potential antimycobacterial activity we evaluated the protein effect on bacteria viability. *Mycobacterium vaccae* was chosen as a rapid growing non-virulent and suitable working specie model (61). Although the specie infects cattle (62) and is generally considered nonpathogenic to humans, few cases of cutaneous and pulmonary infection in farm workers have also been reported (63).

Interestingly, experimental data indicated that RNase 3 and RNase 7 were indeed able to totally inhibit mycobacterial growth in a low micromolar range, showing MIC₁₀₀ values from 10 to 20 μ M (Table 1). The same results were reproduced when tested in both PBS and CB broth, either plated in Petri dishes or incubated in microtiter plates (results not shown). Following, the microbial cell viability was assayed using the *BacTiter-Glo* luminiscent approach. Mycobacterial cells metabolically active, and thus viable, were measured by ATP quantification using a coupled luciferin/oxy luciferin in the presence of luciferase, where luminescence is proportional to ATP and hence to the number of viable cells in the culture. Comparison of IC₅₀ values for RNase 3 and RNase 7 showed comparable results (Table 1). Therefore the assays confirmed the antimycobacterial activity of the two tested human ribonucleases; both being able to totally inhibit bacterial viability in a low micromolar range as depicted by the MIC and IC₅₀ values. This is the first characterization of the antimycobacterial activity of human secreted RNases. The results reinforce the previous preliminary studies on the eosinophil role during

mycobacteria infection and in particular on the contribution of eosinophil secretion proteins (15).

Active N-terminal derived Peptides

Following, we envisaged the identification of the proteins' functional domain. Both RNases, sharing a low sequence identity (~40%), adopt the same three dimensional overall fold, where nonconserved residues are mostly surface exposed (Figure 1C). Previous works have outlined that the main determinants for the human RNases antimicrobial action are clustered at the N-terminus region and derived peptides were designed as potential lead pharmacophores (39, 40, 64, 65). Accordingly, synthetic peptides corresponding to the first 45 residues of both RNases, encompassing the first α 1- α 3 helices (Figure 1), were tested against *M.vaccae*. Experimental data indicated that the peptides RN3(1-45) and RN7(1-45) retained most of the full protein antimicrobial properties. Interestingly, the RNase 3 derived peptide was even more effective than the parental protein, showing a very promising behavior.

While the RN7(1-45) peptide emulated the MIC value of the whole protein, RN3(1-45) achieved MIC values at half peptide concentrations, leading to mycobacteria total lethality at 10 μ M. Cell viability assay corroborated that RN7(1-45) displayed the same effectiveness than the parental RNase 7 and RN3(1-45) produced 50% of mortality at a lower concentration, below 5 μ M. The peptide was even more active than the tested cecropin A-Mellitin (CA-M) control peptide, a potent antimicrobial peptide with pore forming ability, effective against a wide range of bacterial strains (66, 67).

The RN3(1-45) peptide was previously proven to display a high antimicrobial on a wide range of Gram negative and Gram positive strains (40). To better interpret the particularly high bactericidal propensity of the RN3(1-45) peptide, its biophysical properties were analyzed in relation to its counterparts (Figure 1). The peptide was observed to be mostly unstructured on aqueous solution and adopt a defined α -helix secondary structure on a lipid environment, as

deduced from previous circular dichroism (CD) analysis (40) and NMR studies (68). NMR spectroscopy identified a first α -helix matching the protein α 1 and a second α -helix covering the protein α 2- α 3 region (Figure 1A) and expanding to the C-terminus (68). Prediction of RNase 7 peptide secondary structure also suggested equivalent matching helical structures. Moreover, the CD spectrum of the RN7 (1-45) peptide corroborated that its structuration is promoted by a lipid environment. A high affinity of both peptides for anionic phospholipids and a lipid bilayer disruption activity was registered when working on lipid vesicles as model membranes (40). Side by side comparison of both peptides mechanism of action on liposomes also supported a distinct behavior. In particular, a high lipid vesicles agglutination activity for the RN3(1-45) peptide, not shared by the RN7(1-45) peptide, was observed (38) (M. Torrent, D. Pulido, J. Valle, M.V. Nogués, D. Andreu and E. Boix, submitted for publication). A hydrophobic patch, identified as an aggregation prone region, unique to the RNase 3 N-terminus (Figure 1B) could also facilitate its action at the lipid rich mycobacterial wall level. Comparison of the two peptides physicochemical properties highlights the RNase 3 peptide amphipatic and cationic character, showing a higher pI (pI =12.61 versus 10.94) and positive net charge (+8 versus +7). The RN3(1-45) peptide amphipatic character is mostly enhanced by a pronounced alternating profile of cationic and hydrophobic residues (Figure 1B). Moreover, when scanning both peptide sequences using the *AMPA* antimicrobial server (69) a wider propensity stretch is identified in RNase 3. A closer look at the respective amino acid composition reveals the presence of an unfavored anionic residue at the RNase 7 N-terminus (Asp39), which would disrupt the antimicrobial region. Besides, the RNase 3 N-terminus includes an hyperexposed Trp residue (Trp35), which was proven to directly contribute to the protein membrane destabilization (70). On the other hand, we cannot discard that the higher efficiency of the RNase 3 N-terminus peptide in relation to the parental protein is indicative of a physiological role where the eosinophil granule protein once engulfed by macrophages can undergo proteolysis (9).

Bacteria viability assays

The promising preliminary results encouraged us to further investigate the protein and peptides mechanism of action at the bacteria cell level. Based on our previous characterization work on the RNases peptides action on Gram negative and Gram positive bacteria (40, 64), we have analyzed here the peptide cytotoxic mechanism on mycobacterial cells. We first compared the proteins and N-terminus peptides ability to depolarize the mycobacterial cell membrane. Maximum depolarization values working at the IC_{50} concentration were calculated. Comparative analysis showed a poor depolarization effect for both RNases (Table 2). The corresponding RNase 7 peptide, RN7(1-45), also depolarized as poorly as its parental protein, with only a 6.5% of the maximum reference value, suggesting a non-traditional pore forming mechanism of action. On its turn, the RN3(1-45) peptide was able to depolarize at values over 60% (Table 2), significantly increasing its permeabilizing ability on mycobacterial cells in comparison with the parental protein. The RN3(1-45) effectiveness was even higher than the antimicrobial control peptide CA-M, with a high membrane depolarization activity against a wide range of Gram-positive and Gram-negative (67, 71). We suggest that the particular biophysical properties of the RNase 3 peptide can better overcome the complexity of the mycobacterial wall barrier, reaching more easily the cytoplasmic membrane.

Further insight into the membrane permeabilizing effect of both proteins and their derived peptides was performed using the *SYTOX Green* assay. *SYTOX Green* uptake/fluorescence was monitored as a function of time after adding 10 μ M of protein and peptides (Figure 2). Total permeabilizing effect was calculated after 40 min incubation (Table 2) showing that the RN3(1-45) peptide presented the best permeabilizing effect with a 50% value, whereas both RNases achieved a lower permeabilizing value (around 30%) and the RNase 7 peptide only permeabilized the 20% of the total cell population. On the other hand,

the membrane permeabilization time course profile indicated a similar timing for all the tested samples, confirming that the protein interaction with cell membrane and subsequent permeabilizing effect is a rapid event, taking less than 5 minutes to produce half of the maximum membrane depolarization value.

Following, in order to analyze the kinetics of the tested peptides on mycobacterial population, we used the *LIVE/DEAD* bacterial viability kit. Live bacteria population was estimated from the Syto 9 fluorescence dye, which can cross intact cell membranes, while dead bacteria, with damaged membranes, were stained with the PI fluorescent marker. By the integration of Syto 9 and PI fluorescence we determined the viability percentage as a function of the incubation time upon addition of 10 μ M of proteins and peptides, monitoring the bacteria killing process. The viability percentage was calculated at the final incubation time. Similar reduction percentages of the mycobacterial population viability were registered for both RNases, the RN7(1-45) and CA-M peptides (Table 2). Again, the RN3(1-45) peptide displayed a higher performance, and was able to almost abolish the mycobacterial population within the registered time, with only a 6 % of final survival; the results being consistent with the aforementioned MIC values and IC₅₀ values (Table 1).

Bacteria agglutination assays

Another key antimicrobial property thoroughly studied in our laboratory is the capacity of human RNase 3 to induce bacterial cell agglutination (37, 58, 59). The RNase 3 agglutinating activity, not shared with RNase 7, is specific towards Gram-negative bacteria and is dependent on the protein primary structure (37, 38). A sequence stretch responsible for the protein self aggregation was spotted at the RNase 3 N-terminus (72) and the N-terminal derived peptides partially retained the bacteria agglutinating ability (38, 40). In order to assess the agglutinating activity on *M.vaccae* cultures we determined the minimal agglutination concentration (MAC), defined as the minimal concentration able to induce agglutination. Only RNase 3 and the

corresponding RN3(1-45) peptide were able to induce mycobacterial cells to agglutinate at a 1 μ M concentration in both PBS and CB broth media (Table 1). No agglutination was observed for RNase 7 and its derived peptide RN7(1-45), neither for the CA-M reference peptide, even at the maximum concentration range tested. Complementary work on the peptides behavior on model membranes also revealed a specific vesicle agglutinating ability for the RNase 3 peptide, not shared by the RNase 7 counterpart (M. Torrent, D. Pulido, J. Valle, M.V. Nogués, D. Andreu and E. Boix, submitted for publication). Comparison of the peptides hydrophobicity and aggregation prone profiles within the RNase A family context corroborated that the active segment is unique to the RNase 3 N-terminus, explaining its cell agglutination properties (Figure 1B). Moreover, the enhanced membrane destabilization activity of the RN3(1-45) peptide (Table 2) may partly rely on its aggregation propensity, where a local peptide self-aggregation at the mycobacterial surface could promote the membrane damage. We can also hypothesize that the induction of bacteria cell agglutination by the eosinophil granule protein self-aggregation may trigger *in vivo* the autophagy path contributing to the mycobacteria clearance inside macrophages (73, 74).

Ultrastructural analysis of damage at the mycobacteria cell envelope

Finally, to better characterize the protein and peptide action at the mycobacterial cell envelope electron microscopy techniques were applied. Treated cells were visualized by electron transmission microscopy (TEM) and scanning electron microscopy (SEM). *M. vaccae* cells were micrographied by TEM after 4 h incubation with 10 μ M of both RNases and the RN3(1-45), RN7(1-45) and CA-M peptides (Figure 3). All proteins and peptides at the assayed conditions produced a complete disruption of the cell integrity, bacteria swelling, intracellular material spillage, bacterial cell wall layer detachment and alteration of cell morphology. Finally, we applied electron scanning microscopy (SEM) with the purpose to visualize the cell surface and the cell population behavior (Figure 4). The methodology also proved useful to

assess the agglutination activity by evaluating simultaneously the size and density of the bacteria aggregates. Upon RNase 3 incubation big dense bacterial aggregates were observed, where cells were badly damaged, showing frequent blebs and partial loss of their baton shape morphology. Cultures treated with the RN3(1-45) peptide also presented tight-dense aggregates with visible loss of membrane integrity and cell morphology. On their side, RNase 7 and its derived peptide RN7(1-45) displayed similar damage on mycobacterial cultures but without visible agglutination. Likewise, the CA-M antimicrobial peptide showed no mycobacterial agglutination, but severe cell damage, with blebbing and partial loss of cell content.

The high antimycobacterial and cell agglutinating activity of the RN3(1-45) peptide opens a new research field to explore its particular mechanism of action at the mycobacterial wall at the molecular level. Additionally, considering our previous observation of amyloid-like aggregates at the bacterial surface (37) and the location of an amyloid prone region at its N-terminus (72), we are also planning to inspect in a mycobacterial infection model whether the eosinophil granule protein can undergo *in vivo* an ordered self-assembly process, as recently nicely reported for another human antimicrobial peptide contributing to innate immunity(75).

Conclusions

Little is known about the mechanism of action of antimicrobial peptides against *Mycobacterium* species. In this work we have assessed the antimycobacterial activity of two human RNases that are secreted by innate cells during respiratory tract and skin infection. The eosinophil RNase 3 and skin RNase 7, together with their synthetic N-terminus peptides, were assayed against *Mycobacterium vaccae* to characterize their underlying mechanism of action. The results represent the first characterization of the cytotoxicity of two RNase A family

members towards mycobacteria. In particular, the RN3(1-45) peptide, showing both a high antimicrobial activity and agglutinating properties, offers new perspectives to develop antimycobacterial agents. Further work on other mycobacteria species with a more clinical approach is envisaged. We hypothesize that both innate cells secretion proteins may target *in vivo* the mycobacteria dwelling inside macrophages or other host cell types.

Acknowledgements

Transmission and scanning electron microscopy were performed at the Servei de Microscopia of the Universitat Autònoma de Barcelona (UAB). Spectrofluorescence assays were performed at the Laboratori d'Anàlisi i Fotodocumentació, UAB. The work was supported by the *Ministerio de Educación y Cultura* (grant number BFU2009-09371) and *Ministerio de Economía y Competitividad* (BFU2012-38965), co-financed by *FEDER* funds and by the *Generalitat de Catalunya* (2009 SGR 795). DP is a recipient of a *FPU* predoctoral fellowship (*Ministerio de Educación y Cultura*).

References

1. Dye C, Glaziou P, Floyd K, Raviglione M. 2012. Prospects for Tuberculosis Elimination. *Annu Rev Public Health*. **14**:3-16.
2. Martinson NA, Hoffmann CJ, Chaisson RE. 2011. Epidemiology of tuberculosis and HIV: recent advances in understanding and responses. *Proc Am Thorac Soc*. **8**:288.
3. Chiang CY, Yew WW. 2009. Multidrug-resistant and extensively drug-resistant tuberculosis. *International Journal of Tuberculosis and Lung Disease* **13**:304-311.
4. Saiga H, Shimada Y, Takeda K. 2011. Innate Immune Effectors in Mycobacterial Infection. *Clinical & Developmental Immunology* **2011**:347594.
5. Janssen S, Jayachandran R, Khathi L, Zinsstag J, Grobusch MP, Pieters J. 2012. Exploring prospects of novel drugs for tuberculosis. *Drug Design Development and Therapy* **6**:217-224.
6. De Groot MA, Huitt G. 2006. Infections due to rapidly growing mycobacteria. *Clinical Infectious Diseases* **42**:1756-1763.
7. Brown-Elliott BA, Nash KA, Wallace RJ. 2012. Antimicrobial Susceptibility Testing, Drug Resistance Mechanisms, and Therapy of Infections with Nontuberculous Mycobacteria. *Clinical Microbiology Reviews* **25**:721-721.
8. Elston D. 2009. Nontuberculous Mycobacterial Skin Infections Recognition and Management. *American Journal of Clinical Dermatology* **10**:281-285.
9. Liu PT, Modlin RL. 2008. Human macrophage host defense against Mycobacterium tuberculosis. *Current Opinion in Immunology* **20**:371-376.
10. Pinheiro RO, Salles JD, Sarno EN, Sampaio EP. 2011. Mycobacterium leprae-host-cell interactions and genetic determinants in leprosy: an overview. *Future Microbiology* **6**:217-230.
11. Shin D-M, Jo E-K. 2011. Antimicrobial peptides in innate immunity against mycobacteria. *Immune Network* **11**:245-252.
12. Tan BH, Meinken C, Bastian M, Bruns H, Legaspi A, Ochoa MT, Krutzik SR, Bloom BR, Ganz T, Modlin RL, Stenger S. 2006. Macrophages acquire neutrophil granules for antimicrobial activity against intracellular pathogens. *Journal of Immunology* **177**:1864-1871.
13. Soehnlein O. 2009. Direct and alternative antimicrobial mechanisms of neutrophil-derived granule proteins. *Journal of Molecular Medicine-Jmm* **87**:1157-1164.
14. Lasco TM, Turner OC, Cassone L, Sugawara I, Yamada H, McMurray DN, Orme IM. 2004. Rapid accumulation of eosinophils in lung lesions in guinea pigs infected with Mycobacterium tuberculosis. *Infection and Immunity* **72**:1147-1149.

15. Driss V, Legrand F, Hermann E, Loiseau S, Guerardel Y, Kremer L, Adam E, Woerly G, Dombrowicz D, Capron M. 2009. TLR2-dependent eosinophil interactions with mycobacteria: role of alpha-defensins. *Blood* **113**:3235-3244.
16. Mendez-Samperio P. 2008. Role of antimicrobial peptides in host defense against mycobacterial infections. *Peptides* **29**:1836-1841.
17. Mendez-Samperio P. 2010. The human cathelicidin hCAP18/LL-37: A multifunctional peptide involved in mycobacterial infections. *Peptides* **31**:1791-1798.
18. Sow FB, Florence WC, Satoskar AR, Schlesinger LS, Zwilling BS, Lafuse WP. 2007. Expression and localization of hepcidin in macrophages: a role in host defense against tuberculosis. *Journal of Leukocyte Biology* **82**:934-945.
19. Sonawane A, Santos JC, Mishra BB, Jena P, Progidia C, Sorensen OE, Gallo R, Appelberg R, Griffiths G. 2011. Cathelicidin is involved in the intracellular killing of mycobacteria in macrophages. *Cellular Microbiology* **13**:1601-1617.
20. Mendez-Samperio P, Miranda E, Trejo A. 2006. Mycobacterium bovis Bacillus Calmette-Guerin (BCG) stimulates human beta-defensin-2 gene transcription in human epithelial cells. *Cellular Immunology* **239**:61-66.
21. Lehrer RI, Ganz T. 2002. Cathelicidins: a family of endogenous antimicrobial peptides. *Current Opinion in Hematology* **9**:18-22.
22. Zanetti M. 2004. Cathelicidins, multifunctional peptides of the innate immunity. *Journal of Leukocyte Biology* **75**:39-48.
23. Wilson CL, Ouellette AJ, Satchell DP, Ayabe T, Lopez-Boado YS, Stratman JL, Hultgren SJ, Matrisian LM, Parks WC. 1999. Regulation of intestinal alpha-defensin activation by the metalloproteinase matrilysin in innate host defense. *Science* **286**:113-117.
24. Mishra AK, Driessen NN, Appelmelk BJ, Besra GS. 2011. Lipoarabinomannan and related glycoconjugates: structure, biogenesis and role in Mycobacterium tuberculosis physiology and host-pathogen interaction. *Fems Microbiology Reviews* **35**:1126-1157.
25. Fjell CD, Hiss JA, Hancock REW, Schneider G. 2012. Designing antimicrobial peptides: form follows function. *Nature Reviews Drug Discovery* **11**:37-51.
26. Kapoor R, Eimerman PR, Hardy JW, Cirillo JD, Contag CH, Barron AE. 2011. Efficacy of Antimicrobial Peptoids against Mycobacterium tuberculosis. *Antimicrobial Agents and Chemotherapy* **55**:3058-3062.
27. Martineau AR, Newton SM, Wilkinson KA, Kampmann B, Hall BM, Nawroly N, Packe GE, Davidson RN, Griffiths CJ, Wilkinson RJ. 2007. Neutrophil-mediated innate immune resistance to mycobacteria. *Journal of Clinical Investigation* **117**:1988-1994.
28. Akuthota P, Xenakis JJ, Weller PF. 2011. Eosinophils: Offenders or General Bystanders in Allergic Airway Disease and Pulmonary Immunity? *Journal of Innate Immunity* **3**:113-119.

29. Boix E, Torrent M, Sánchez D, Nogués MV. 2008. The Antipathogen Activities of Eosinophil Cationic Protein. *Current Pharm Biotec.* **9**:141-152.
30. Boix E, Salazar VA, Torrent M, Pulido D, Nogués MV, Moussaoui M. 2012. Structural determinants of the eosinophil cationic protein antimicrobial activity. *Biol Chem* **393**:801-815.
31. Malik A, Batra JK. 2012. Antimicrobial activity of human eosinophil granule proteins: Involvement in host defence against pathogens. *Crit Rev Microbiol* **38**:168-181.
32. Spencer JD, Schwaderer AL, DiRosario JD, McHugh KM, McGillivray G, Justice SS, Carpenter AR, Baker PB, Harder J, Hains DS. 2011. Ribonuclease 7 is a potent antimicrobial peptide within the human urinary tract. *Kidney International* **80**:175-181.
33. Koten B, Simanski M, Glaser R, Podschun R, Schroder JM, Harder J. 2009. RNase 7 Contributes to the Cutaneous Defense against *Enterococcus faecium*. *Plos One* **4**:e6424.
34. Venge P, Bystrom J, Carlson M, Hakansson L, Karawacjzyk M, Peterson C, Seveus L, Trulsson A. 1999. Eosinophil cationic protein (ECP): molecular and biological properties and the use of ECP as a marker of eosinophil activation in disease. *Clin Exp Allergy* **29**:1172-1186.
35. Bystrom J, Amin K, Bishop-Bailey D. 2011. Analysing the eosinophil cationic protein - a clue to the function of the eosinophil granulocyte. *Respiratory Research* **12**:10.
36. Monteseirin J, Vega A, Chacon P, Camacho MJ, El Bekay R, Asturias JA, Martinez A, Guardia P, Perez-Cano R, Conde J. 2007. Neutrophils as a novel source of eosinophil cationic protein in IgE-mediated processes. *J Immunol* **179**:2634-2641.
37. Torrent M, Pulido D, Nogués MV, Boix E. 2012. Exploring new biological functions of amyloids: bacteria cell agglutination mediated by host protein aggregation. *Plos Pathogens* **8**:e1003005.
38. Pulido D, Moussaoui M, Andreu D, Nogues MV, Torrent M, Boix E. 2012. Antimicrobial Action and Cell Agglutination by the Eosinophil Cationic Protein Are Modulated by the Cell Wall Lipopolysaccharide Structure. *Antimicrobial Agents and Chemotherapy* **56**:2378-2385.
39. Torrent M, de la Torre BG, Nogues VM, Andreu D, Boix E. 2009. Bactericidal and membrane disruption activities of the eosinophil cationic protein are largely retained in an N-terminal fragment. *Biochem J* **421**:425-434.
40. Torrent M, Pulido D, De la Torre BG, Garcia-Mayoral MF, Nogues MV, Bruix M, Andreu D, Boix E. 2011. Refining the Eosinophil Cationic Protein Antibacterial Pharmacophore by Rational Structure Minimization. *Journal of Medicinal Chemistry* **54**:7.

41. Borelli V, Vita F, Shankar S, Soranzo MR, Banfi E, Scialino G, Brochetta C, Zabucchi G. 2003. Human eosinophil peroxidase induces surface alteration, killing, and lysis of *Mycobacterium tuberculosis*. *Infection and Immunity* **71**:605-613.
42. Driss V, Hermann E, Legrand F, Loiseau S, Delbeke M, Kremer L, Guerardel Y, Dombrowicz D, Capron M. 2012. CR3-dependent negative regulation of human eosinophils by *Mycobacterium bovis* BCG lipoarabinomannan. *Immunology Letters* **143**:202-207.
43. Vijayan VK, Reetha AM, Jawahar MS, Sankaran K, Prabhakar R. 1992. Pulmonary Eosinophilia in Pulmonary Tuberculosis. *Chest* **101**:1708-1709.
44. Kita H. 2011. Eosinophils: multifaceted biological properties and roles in health and disease. *Immunological Reviews* **242**:161-177.
45. Castro AG, Esaguy N, Macedo PM, Aguas AP, Silva MT. 1991. Live but Not Heat-Killed *Mycobacteria* Cause Rapid Chemotaxis of Large Numbers of Eosinophils *In Vivo* and Are Ingested by the Attracted Granulocytes. *Infection and Immunity* **59**:3009-3014.
46. Harder J, Schroder JM. 2002. RNase 7, a novel innate immune defense antimicrobial protein of healthy human skin. *J Biol Chem* **277**:46779-46784.
47. Zhang J, Dyer KD, Rosenberg HF. 2003. Human RNase 7: a new cationic ribonuclease of the RNase A superfamily. *Nucleic Acids Res* **31**:602-607.
48. Zanger P, Holzer J, Schleucher R, Steffen H, Schitteck B, Gabrysch S. 2009. Constitutive Expression of the Antimicrobial Peptide RNase 7 Is Associated with *Staphylococcus aureus* Infection of the Skin. *Journal of Infectious Diseases* **200**:1907-1915.
49. Simanski M, Köten B, Schröder JM, Gläser R, Harder J. 2012. Antimicrobial RNases in Cutaneous Defense. *Journal of Innate Immunity* **4**:241-247.
50. Bernard JJ, Gallo RL. 2011. Protecting the boundary: the sentinel role of host defense peptides in the skin. *Cell Mol Life Sci* **68**:2189-2199.
51. Casanova JL, Abel L. 2002. Genetic dissection of immunity to mycobacteria: The human model. *Annual Review of Immunology* **20**:581-620.
52. Jiang ZQ, Higgins MP, Whitehurst J, Kisich KO, Voskuil MI, Hodges RS. 2011. Anti-Tuberculosis Activity of alpha-Helical Antimicrobial Peptides: De Novo Designed L- and D-Enantiomers Versus L- and D-LL37. *Protein and Peptide Letters* **18**:241-252.
53. Boenickse R, Juhasz E. 1964. Description of the new species *Mycobacterium Vaccae* n. sp. *Zentralbl Bakteriolog Orig* **192**:133-135.
54. Skerman VBD, McGowan V, Sneath PHA. 1980. Approved lists of bacterial names. *Int. J. Syst. Bacteriol.* **30**:225-420.
55. Boix E, Nikolovski Z, Moiseyev GP, Rosenberg HF, Cuchillo CM, Nogues MV. 1999. Kinetic and product distribution analysis of human eosinophil cationic protein indicates

- a subsite arrangement that favors exonuclease-type activity. *J Biol Chem* **274**:15605-15614.
56. Buchan DWA, Ward SM, Lobley AE, Nugent TCO, Bryson K, Jones DT. 2010. Protein annotation and modelling servers at University College London. *Nucleic Acids Research* **38**:W563-W568.
 57. NCCLS. 2003. Methods for dilution antimicrobial susceptibility tests for bacteria that grow aerobically, 6th ed. ed. National Committee for Clinical Laboratory Standards.
 58. Torrent M, Badia M, Moussaoui M, Sanchez D, Nogues MV, Boix E. 2010. Comparison of human RNase 3 and RNase 7 bactericidal action at the Gram-negative and Gram-positive bacterial cell wall. *Febs J* **277**:1713-1725.
 59. Torrent M, Navarro S, Moussaoui M, Nogues MV, Boix E. 2008. Eosinophil cationic protein high-affinity binding to bacteria-wall lipopolysaccharides and peptidoglycans. *Biochemistry* **47**:3544-3555.
 60. Singh A, Batra JK. 2011. Role of unique basic residues in cytotoxic, antibacterial and antiparasitic activities of human eosinophil cationic protein. *Biol Chem* **392**:337-346.
 61. Ho YS, Adroub SA, Abadi M, Al Alwan B, Alkhateeb R, Gao G, Ragab A, Ali S, van Soolingen D, Bitter W, Pain A, Abdallah AM. 2012. Complete Genome Sequence of *Mycobacterium vaccae* Type Strain ATCC 25954. *Journal of Bacteriology* **194**:6339-6340.
 62. Koehne G, Maddux R, Britt J. 1981. Rapidly Growing *Mycobacteria* Associated with Bovine Mastitis. *American Journal of Veterinary Research* **42**:1238-1239.
 63. Hachem R, Raad I, Rolston KVI, Whimbey E, Katz R, Tarrand J, Libshitz H. 1996. Cutaneous and pulmonary infections caused by *Mycobacterium vaccae*. *Clinical Infectious Diseases* **23**:173-175.
 64. Sanchez D, Moussaoui M, Carreras E, Torrent M, Nogues V, Boix E. 2011. Mapping the eosinophil cationic protein antimicrobial activity by chemical and enzymatic cleavage. *Biochimie* **93**:331-338.
 65. Wang H, Schwaderer AL, Kline J, Spencer JD, Kline D, Hains DS. 2012. Contribution of Structural Domains to Ribonuclease 7's Activity Against Uropathogenic Bacteria. *Antimicrob Agents Chemother.* in press.
 66. Andreu D, Ubach J, Boman A, Wahlin B, Wade D, Merrifield RB, Boman HG. 1992. Shortened Cecropin-a Melittin Hybrids - Significant Size-Reduction Retains Potent Antibiotic-Activity. *Febs Letters* **296**:190-194.
 67. Milani A, Benedusi M, Aquila M, Rispoli G. 2009. Pore Forming Properties of Cecropin-Melittin Hybrid Peptide in a Natural Membrane. *Molecules* **14**:5179-5188.

68. García-Mayoral MFM, M.; de la Torre, B.G.; Andreu, D.; Boix, E.; Nogués, M.V.; Rico, M. Laurents, D.V. and Bruix, M. 2010. NMR structural determinants of eosinophil cationic protein binding to membrane and heparin mimetics. *Biophys J* **98**:2702-2711.
69. Torrent M, Di Tommaso P, Pulido D, Nogués M, Notredame C, Boix E, Andreu D. 2012. AMPA: an automated web server for prediction of protein antimicrobial regions. *Bioinformatics* **28**:130-131.
70. Torrent M, Cuyas E, Carreras E, Navarro S, Lopez O, de la Maza A, Nogues MV, Reshetnyak YK, Boix E. 2007. Topography studies on the membrane interaction mechanism of the eosinophil cationic protein. *Biochemistry* **46**:720-733.
71. Saugar JM, Rodriguez-Hernandez MJ, de la Torre BG, Pachon-Ibanez ME, Fernandez-Reyes M, Andreu D, Pachon J, Rivas L. 2006. Activity of cecropin A-melittin hybrid peptides against colistin-resistant clinical strains of *Acinetobacter baumannii*: Molecular basis for the differential mechanisms of action. *Antimicrobial Agents and Chemotherapy* **50**:1251-1256.
72. Torrent M, Odorizzi F, Nogues MV, Boix E. 2010. Eosinophil Cationic Protein Aggregation: Identification of an N-Terminus Amyloid Prone Region. *Biomacromolecules* **11**:1983-1990.
73. Cemma M, Brumell JH. 2012. Interactions of Pathogenic Bacteria with Autophagy Systems. *Current Biology* **22**:R540-R545.
74. Mostowy S, Cossart P. 2012. Bacterial autophagy: restriction or promotion of bacterial replication? *Trends in Cell Biology* **22**:283-291.
75. Chu HT, Pazgier M, Jung G, Nuccio SP, Castillo PA, de Jong MF, Winter MG, Winter SE, Wehkamp J, Shen B, Salzman NH, Underwood MA, Tsolis RM, Young GM, Lu WY, Lehrer RI, Baumler AJ, Bevins CL. 2012. Human alpha-Defensin 6 Promotes Mucosal Innate Immunity Through Self-Assembled Peptide Nanonets. *Science* **337**:477-481.
76. Boix E, Pulido D, Moussaoui M, Nogues MV, Russi S. 2012. The sulfate-binding site structure of the human eosinophil cationic protein as revealed by a new crystal form. *Journal of Structural Biology* **179**:1-9.
77. Gouet P, Courcelle E, Stuart DI, Metz F. 1999. ESPript: analysis of multiple sequence alignments in PostScript. *Bioinformatics* **15**:305-308.
78. Waterhouse AM, Procter JB, Martin DMA, Clamp M, Barton GJ. 2009. Jalview Version 2-a multiple sequence alignment editor and analysis workbench. *Bioinformatics* **25**:1189-1191.
79. Conchillo-Sole O, de Groot NS, Aviles FX, Vendrell J, Daura X, Ventura S. 2007. AGGRESKAN: a server for the prediction and evaluation of "hot spots" of aggregation in polypeptides. *BMC Bioinformatics* **8**:65.

80. Maurer-Stroh S, Debulpaep M, Kuemmerer N, de la Paz ML, Martins IC, Reumers J, Morris KL, Copland A, Serpell L, Serrano L, Schymkowitz JWH, Rousseau F. 2010. Exploring the sequence determinants of amyloid structure using position-specific scoring matrices. *Nature Methods* 7:237-U109.
81. Huang YC, Lin YM, Chang TW, Wu SJ, Lee YS, Chang MD, Chen C, Wu SH, Liao YD. 2007. The flexible and clustered lysine residues of human ribonuclease 7 are critical for membrane permeability and antimicrobial activity. *J Biol Chem* 282:4626-4633.

Table 1. Antimicrobial and agglutinating activities of RNase 3, RNase 7, and their corresponding N-terminal derived peptides on *M. vaccae*^a.

Protein/peptide	MIC ₁₀₀ (μ M)	IC ₅₀ (μ M)	MAC (μ M)
RNase 3	20.0 \pm 1.0	11.6 \pm 0.2	1.0 \pm 0.1
RNase 7	20.0 \pm 0.5	9.3 \pm 1.2	>50
RN3(1-45)	10.0 \pm 0.5	4.2 \pm 0.2	1.0 \pm 0.1
RN7(1-45)	20.0 \pm 0.8	9.5 \pm 0.3	>50
CA-M ^b	20.0 \pm 1.0	10.3 \pm 0.3	>50

^a Minimal Antimicrobial Concentration (MIC₁₀₀), bacteria viability (IC₅₀) and Minimal Agglutinating Activity (MAC) were calculated as described in *Materials and Methods*. MIC₁₀₀ values were calculated by CFUs counting on plated Petri dishes. Mean values \pm SEM are indicated. All values are averaged from three replicates of two independent experiments. The standard error of the mean is indicated.

^bThe cecropin A-melittin hybrid peptide (CA-M) was used as a control.

Table 2. Percentage of viability, membrane permeabilization and membrane depolarization activities of RNase 3, RNase 7 and their N-terminus derived-peptides on *M. vaccae*^a.

Protein/peptide	Bacteria Viability (%)	Membrane permeabilization (%) ^c	Membrane depolarization (%) ^c
RNase 3	55.1 ± 0.6	35.9 ± 0.1	8.8 ± 0.1
RNase 7	48.7 ± 1.8	28.8 ± 0.1	4.1 ± 0.2
RN3(1-45)	6.8 ± 0.8	50.0 ± 1.2	63.2 ± 1.8
RN7(1-45)	55.1 ± 1.5	19.3 ± 0.1	6.5 ± 0.2
CA-M ^b	44.8 ± 1.6	27.3 ± 0.1	44.7 ± 1.3

^aBacteria viability was determined using the *LIVE/DEAD* kit; membrane permeabilization using the *SYTOX Green* assay and membrane depolarization activity using the DiSC3(5) probe, as described in *Materials and Methods*. Mean values ± SEM are indicated. All values are averaged from three replicates of two independent experiments.

^bThe cecropin A-melittin hybrid peptide (CA-M) was used as a control.

^cPercentages were calculated referred to the maximum value corresponding to the positive control (10% Triton X-100).

FIGURE LEGENDS

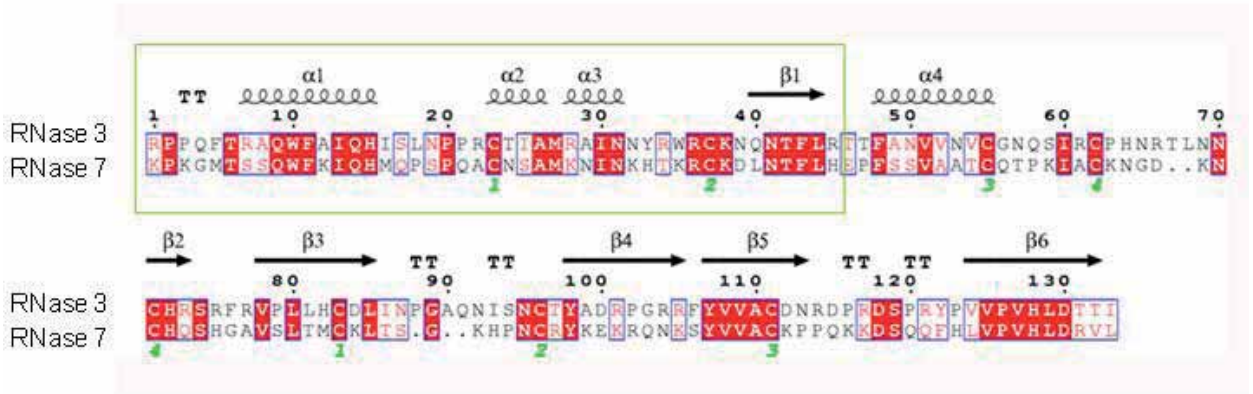
Figure 1. A) Comparison of the blast alignment of RNase 3 and RNase 7 primary sequences. Secondary structure of RNase 3 is depicted (4A2O PDB, (76)). Strictly conserved residues are boxed in red and conserved residues, as calculated by a similarity score, are boxed in white. The first 45 residues corresponding to RNase 3 and RNase 7 peptides are green boxed. Cysteine pairings for disulfide bridges are numbered below. The figure was created using the *ESPrpt* software (77). B) Sequence alignment of RN3(1-45) and RN7(1-45) peptides. Residues are coloured according to their hydrophobicity using the sequence alignment editor *Jalview* (78) and the aggregation prone regions predicted by both *Aggregscan* (79) and WALTZ (80) are boxed in white. C) Graphical representation of RNase 3 and 7 three dimensional structures. Coordinates were taken from the 4A2O PDB ((76)) and 2HKY PDB ((81)) respectively. The surface representation was colored using the CONSURF web server (<http://consurf.tau.ac.il/>) featuring the relationships among the evolutionary conservation of amino acid positions inside the RNase A family. Residues were colored by their conservation score using the color-coding bar at the bottom image. Residues were colored in yellow when not enough information was available.

Figure 2. Membrane permeabilization was determined by *SYTOX Green* uptake after incubation of *M. vaccae* culture cells with 10 μ M of proteins and peptides: RNase 3(■), RNase 7(●), RN3(1-45)(▲), RN7(1-45)(▼), or CA-M(◆) are depicted as a function of time. Maximum fluorescence reference value of 64 ± 0.4 was achieved for 10% Triton X-100.

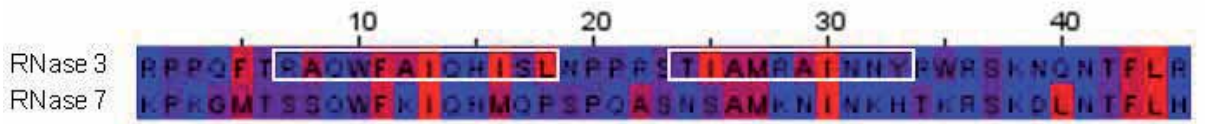
Figure 3. Transmission electron micrographs of *M. vaccae* incubated for 4 h in the presence of 10 μ M of proteins and peptides. (A) Control cells, (B) RNase 3, (C) RN3(1-45), (D) CA-M, (E) RNase 7, and (F) RN7(1-45). The magnification scale is indicated at the bottom of each micrograph.

Figure 4. Scanning electron micrographs of *M. vaccae* incubated for 4 h in the presence of 10 μ M of proteins and peptides. (A) Control cells, (B) RNase 3, (C)RN3(1-45), (D)CA-M, (E) RNase 7, and (F) RN7(1-45). The magnification scale is indicated at the bottom of each micrograph.

A



B



C

